2011

Aspects of Film Formation from Bimodal Latexes

Lili Liu
Lehigh University

Aspects of Film Formation from Bimodal Latexes

by

Lili Liu

A Dissertation

Presented to the Graduate and Research Committee

of Lehigh University

in Candidacy for the Degree of

Doctor of Philosophy

in

Chemistry

Lehigh University

May, 2011

Approved and recommended for acceptance as a dissertation in partial fulfillment of the requirements for the degree of Doctor of Philosophy

Lili Liu
Aspects of Film Formation from Bimodal Latexes

_____
Defense Date

_____
Dr. Andrew Klein
Dissertation Director and Advisor

_____
Approved Date

Committee Members:

_____
Dr. Eric S. Daniels
Co-advisor

_____
Dr. James E. Roberts

_____
Dr. Tianbo Liu

_____
Dr. Natalie M. Foster

_____
Dr. James F. Gilchrist
External member

_____
Dr. E. David Sudol
External member

DEDICATION

to My Dear Parents:

Guodong Liu & Aimin Ang

ACKNOWLEDGEMENTS

This doctoral dissertation would not have been possible without the support and advice of my committee members, colleagues and friends.

First and foremost, I would like to express my greatest appreciation to my advisor Professor Andrew Klein. Without his guidance, understanding and tremendous support both in my research and life, I probably would not see the completion of this project. Thank you, my admired academic grandfather!

I would like to thank my co-advisor Dr. Eric S. Daniels for his interest and help in this project, especially for his patience and efforts in correcting my reports.

I would also like to give my sincere thanks to Dr. E. David Sudol. He always gave me hope and support when I was frustrated during my Ph.D study.

I remain grateful to Professor Natalie M. Foster, Professor James E. Roberts, Professor James F. Gilchrist, and Professor Tianbo Liu for their interest in this project and serving on my committee. Particularly, I want to thank Professor Foster and Professor Roberts for their great patience and very careful corrections on my dissertation draft.

I want to thank Professor Mohamed El-Aasser for his help and suggestions in my study, and for his hospitality during the Thanksgiving days in his house.

I also give my sincere appreciation to Professor Do Ik Lee and Professor Ray Pearson for their suggestions and help on developing the modified high temperature tensile testing method. I would be remiss if I did not mention Dr. Irina Kobylanska,

Professor Donard Sundberg, Dr. Stuart Thickett and Professor Mitchell Winnik for their suggestions on synthesizing functionalized polystyrene latex particles.

I am very thankful to get to know Dr. Victoria Dimonie. Her very positive life attitude impresses me a lot and is exactly what I am pursuing.

My colleagues in EPI and many of my friends in Chemistry department gave me a home-like feeling here at Lehigh. Their friendship made my life much easier during the past five years.

I would also like to thank my dear English professor Carolyn Maraist for her encouragements all along the way. We have kept a very strong friendship since we got to know each other during my undergraduate study in Zhejiang University in China.

Last but not least, I would like to express my heartfelt thanks to my family. My fiancé, Lixiang Luo, is the 'superman' to me, because he not only helped me in this project on making Aluminum molds as a mechanical engineer and drawing contour graphs as a programmer, but also gave me tremendous love and support in my life. My parents, Guodong Liu and Aimin Ang, are the meaning of my life. I am so lucky to have them and cannot express enough my appreciation for their understanding, love, and support in my life.

TABLE OF CONTENTS

LIST OF TABLES

LIST OF FIGURES

ABSTRACT

The main goal of this work is to further the molecular level understanding of the film formation process, employing a model system of bimodal latexes. The properties of the two latexes, such as particle sizes, molecular weights, crosslinking densities as well as the functional components, are varied independently.

A self-assembled close-packed morphology was observed in bimodal polystyrene latex blends at an optimum blend ratio, which can be calculated as a function of particle size ratio based on the theory of continuity. It has been found that bimodal particle packing can greatly reduce the void content inside latex films. The film formation process required much less time to complete in a well-blended film than in an unblended film.

Polystyrene particles with different molecular weights were synthesized, and the tensile strengths of films made from these latexes were compared. It was found that the tensile strength increased with molecular weight until it reached a maximum, and then it became independent of molecular weight. The molecular weight (weight-average), rather than the particle size, was the dominant factor in determining a film's mechanical strength.

Crosslinked latexes were mixed together with non-crosslinked latex particles. The corresponding blended film exhibited clear improvements in strength over the unblended

non-crosslinked latex films, when the non-crosslinked polymer chains were not long enough to make sufficient entanglements by themselves at the interface.

The experimental results were compared to the theoretical models to examine the competition between polymer interdiffusion and a crosslinking reaction in films comprised of polystyrene reactive latex blends, in which the reactive groups (carboxylic acid and primary amine) were incorporated in separate latex particles. By controlling the molecular parameters we were able to design the film formation process to be reaction controlled, so that the corresponding mechanical properties of the films, such as film modulus, tensile strength and toughness, could be enhanced. A model based on theories and verified against the experimental data was established, which could provide useful guidelines for film interface strengthening with potential applications in the coatings industry.

CHAPTER 1

Introduction

1.1 Background

Natural latex, known for its origin—the natural liquid extracted from rubber trees, consists of a suspension of rubber particles with sizes ranging from 0.1 to 1 μm in a buffered aqueous medium. Synthetic latex, therefore, is defined as a suspension of polymer microparticles (not only rubber particles) in an aqueous medium prepared by emulsion polymerization, which is a type of free radical polymerizations that usually starts with an emulsion incorporating water, monomer, surfactants and initiators.

One of the major applications of latexes is in paints and coatings. Nowadays, water-borne latex coatings are more accepted than solvent borne products, due to their eco-friendly characteristic of less use of volatile organic compounds (VOCs). In the United States and around the world, there is a rising concern in coating technology about the emission of VOCs, which serve as promoters of coalescence and film formation, but are toxic to humans and the environments. Therefore, this environmental issue has forced a reduction of solvent levels in coatings and required designers of coatings to reconsider and improve coating materials and processes. Because of these concerns, industry is pursuing more green chemistry technologies, such as developing alternative water-based

latex products. But even for latex coatings, achieving zero or low VOCs is still a big challenge. Unlike solvent-based products, which are basically homogenous in nature (because polymers are dissolved in the solvent), water-borne polymers are present in a compartmentalized manner in the medium, which means the entire coating body is heterogeneous. To prepare continuous and coherent coating films, VOCs are still essential in the coating process, which is also known as the film formation process. The film formation process can be broken down into three stages[1]. In the first stage, the continuous phase (water) evaporates and adjacent particles come into close contact. The second stage begins when particle coalescence occurs. When the temperature is above the minimum film formation temperature (MFFT), interparticle diffusion occurs which leads to film integrity in the third stage and the film develops its mechanical strength.

VOCs are needed to solve the problem in the second stage of film formation process. On one hand, films are required to be continuous and void-free. To achieve this state, it is better to use polymers with low glass transition temperatures (T_g), so that the particles deform easily and become space-filling as water evaporates. On the other hand, films have to be strong, i.e., they should have good mechanical performance. However, film formation from low T_g particles results in the formation of weak and tacky films. Therefore, high T_g particles are needed to increase the hardness of the film and other desirable properties, such as block resistance and scratch resistance. However, the compliance of high T_g latexes is so small that forces much larger than those of low T_g particles are needed to deform the particles, which requires energy. The traditional way to overcome this limitation is to add a VOC or coalescing agent to help decrease the

minimum film formation temperature. The coalescing aid then evaporates during the drying process, leaving only high T_g particles in place so that the film remains hard. This has proven to be a very useful solution, but it has the disadvantage of polluting the environment.

Fortunately, strategies may be applied to minimize the usage of VOCs in the coating process. Powder coatings are good for preparing thick and texture-free coatings, but not as good at applying smooth thin films. The use of latex blends or core-shell particles becomes a more promising way to solve this problem in the absence of organic solvents. Latex blends are more flexible than core-shell particles, not only because blending has the ability to generate complex systems without utilizing multiple reactors and complicated particles, but also because one can obtain properties different from the blends other than the individual latex components, and under some circumstances, one might even get unique properties.

Aqueous dispersions provide great design flexibility for latex blends, because of their ability to combine multiple polymer particles in one system, such as large/small latex particle blending, hard/soft latex blending, and blending cross-linked gel particles together with linear polymer particles. These strategies can generally be divided into four categories. The first one is to blend particles of different sizes to reduce the amount of continuous aqueous phase, so that the drying rate can be greatly increased. The second is to blend latexes with different molecular weights, because the physical entanglements at the particle-particle interfaces (which play an important role in building up film interfacial strength) is highly dependent on the polymer molecular weights. The third

strategy is to add crosslinked latexes to the system so that the film's "bulk-related" properties, such as film stiffness and water resistance, can be enhanced. The fourth approach is to induce chemical crosslinks at the particle-particle interface so that the film interfaces is more quickly (less interpenetration depth is needed) and strongly (more effective crossings) formed, which leads to an improvement in film "interface-related" properties, such as strength and toughness.

These strategies are used in industry on a daily basis. However, since these approaches are primarily empirical in nature, a large number of bench-trial experiments are needed to determine one single parameter, which is very time consuming. If these strategies can be quantified in terms of the relationship between the molecular parameters and the resulting film performance, the overall properties of the latex films will be able to be controlled. Therefore, the goal of my research is to determine the relationship between microscopic molecular parameters (such as particle size, molecular weight, crosslinking density and functionality) and macroscopic film mechanical properties (such as tensile strength and toughness), and to use a knowledge of those relationships to design a better film system.

1.2 Current Status in the Literature

1.2.1 Latex Blending

Most latex blending studies in the past decades can be categorized into two types: those evaluating blends of different size particles, and those evaluating blends of hard and

soft polymer particles (including blends of natural rubber with synthetic polymer particles).

Polymeric dispersions can achieve a very high solids content (70 wt% or higher[2]), which decreases the drying time and impacts the rheological properties such as brush flow out. Comparing polymeric dispersions, the maximum solids for latex dispersions with monodisperse particles are around 50 wt% due to the effect of the electrical double layer on the hydrodynamic volume fractions of dispersions. Overbeek in his recent review paper[3] also pointed out the undesirability of high solids monodisperse particle systems, because of the phase transition from random packing to crystalline packing, which leads to coexisting phases with different packing densities. This phase transition does not take place with polydisperse particle systems.

Other groups are focusing on developing ways to achieve *in situ* multimodal latexes[4,56,7,8,9]. Among the methods, two common ones are: (a) adding surfactants and monomers in the middle of the polymerization to generate secondary nucleation, and (b) introducing seed particles of different sizes to prepare multiple size distributions *in situ*.

Some groups focus on studying the packing morphology specifically in latex blends[10,11,12,13,14]. One of the studies done in Keddie's group may be cited as an example. They have examined blends with latex particles of various sizes and hardness[15].They found that in the case where large soft particles were mixed with either small soft or small hard particles, surface roughness and void volume concentration of the film reaches a minimum by applying blends with a blending ratio of 18 (small): 82 (large). When large

hard particles were blended with small soft particles, film formation was hindered by the clustering of the large particles and subsequent creation of voids.

Few groups have investigated the influence of latex blends with different sizes on the resulting film mechanical performance. Peters [16], however, found that blending different size particles (~50 and ~350 nm with T_g around 20 °C) at an 80 (large)/ 20(small) blend ratio reduces the minimum film formation temperature and increases water resistance as well as tensile strength.

In contrast, many studies have investigated the effect of hard and soft latex blends on film mechanical properties[17,18,19,20,21]. When soft particles are the continuous phase with hard particles dispersed in the soft matrix, films can be formed at a low temperature, but with improved film mechanical properties, such as block resistance, scratch resistance, and film hardness. When the hard particles constitute the continuous matrix and soft particles are presented in the dispersed phase, the corresponding films may have enhanced resistance to crack propagation. While the latter is rarely used in the coatings industry, it is quite common in the plastics industry, such as in the design of impact modifiers[2].

Although from a practical point of view, blending hard and soft latex particles is more helpful to achieve systems with zero-VOC and satisfying film performance, these hard/soft latex blends are more complicated from theoretical prospectives, because of the uncontrollable film formation process. A fundamental study of the film formation process requires precise control of the experimental conditions, including temperature and pressure. This requirement allows one to control the latex film forming time and to

monitor the progress of polymer chain interdiffusion. As a result, in this thesis, focus is on the study of hard particle blends to understand the relationship between fundamental parameters and the film properties.

1.2.2 Chain Diffusion at Polymer Interface

1.2.2.1 The Reptation Theory

Rouse[22] and Zimm[23] described the motions of a single polymeric chain in the relaxed state, such as in a good solvent. de Gennes[24] extended this study to polymer chain movements in a more concentrated state (such as a melted state or in a crosslinked polymer gel network), and this work has become known as the reptation theory, one of the most important theories in polymer physics. The reptation theory describes how the polymer chain performs "worm-like" displacement in a restricted imaginary tube within an entangled gel network; the time required for complete renewal of chain conformation is defined as the reptation time. de Gennes also concluded that the polymer chain mobility and the diffusion coefficient are proportional to the reciprocal of the squared mass of the polymer chain.

Based on the repation theory, Wool[25,26] specifically adapted the minor chain model for the description of chain reptation at a polymer-polymer interface. The minor chain, which is defined as the portion of the polymer chain that no longer has its initial chain conformation, grows with time and is able to cross an interface many times to strengthen the interface by physical entanglements. Therefore, Wool proposed that a film's interfacial strength depends only on the one-half power of the chain molecular weight after the reptation time.

1.2.2.2 The Role of Molecular Weight

Theories of interface healing have all pointed out that the diffusion of polymer chains across an interface is highly dependent on molecular weights[24, 27, 28]. This molecular weight dependence has also been substantiated by experiments. Adolf *et al.* compared theoretical results of healing and fracture behavior with experimental data for glassy polymers[29]. They found that both molecular weight and molecular weight distribution are important in determining the value where fracture stress plateaus. In polydisperse samples, interface healing occurred faster due to quick diffusion of short polymer chains. However, bulk strength was achieved at a much later time, which they explained in terms of effective crossings at the interface.

Using small angle neutron scattering (SANS), Yoo *et al*. studied polymer chain interdiffusion in blends of protonated and deuterated polystyrene latexes with a broad molecular weight distribution[30,31]. They reported the same trend, that lower molecular weight polymers diffuse faster than higher molecular weight chains. But they also found that short chains diffuse farther (about one radius of gyration of the whole chain) than longer chains. The short chains need only to reach approximately the depth of the radius of gyration of the critical entanglement molecular weight, which is the minimum molecular weight required for effective entanglements. Therefore, they proposed two critical parameters for the interdiffusion of film formation (see Figure 1.1): the first is the location of polymer chain ends that determines the direction towards which polymer chains move; the second is the dimensionless ratio of the polymer chain length to the particle size, which determines the chain conformation state (constrained or relaxed).

However, good mixing is not formed because of the thermodynamics of mixing of protonated and deuterated latexes. The versatility of this theory is somewhat restricted because only two molecular weights with broad distributions were investigated.

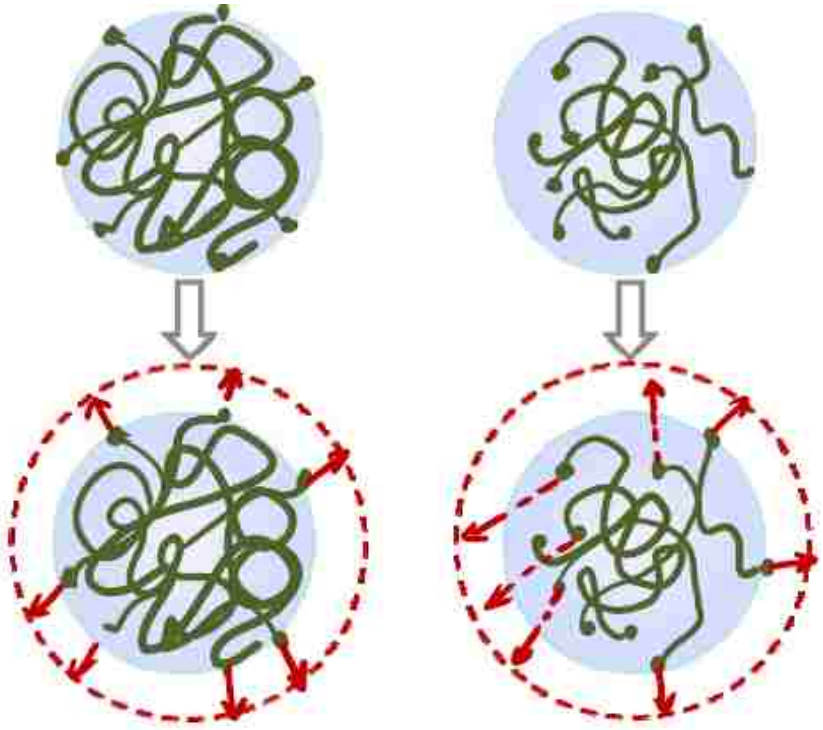

Figure 1.1: Model showing the effect of chain conformation and chain end location. On the left hand side is the high molecular weight case; on the right hand side is the low molecular weight case.

Kim *et al*. overcame this problem of broad molecular weight distributions by using the direct emulsification method to create particles (artificial latex) with polymer chain molecular weights having low polydispersity[32]. They studied the chain self-

diffusion coefficient and the effect of sulfonate end groups on diffusion *via* small angle neutron scattering.

Besides SANS, Winnik's group utilized a direct nonradiative energy transfer technique (DET) to carry out studies investigating chain interdiffusion at the latex particle-particle interfaces[33,34,35,36]. Mohamadi *et al.* developed a dental burr grinding instrument[37], and Sambasviam used this instrument for a study of the role of molecular weights on the fracture of PS films by calculating the number of chain scissions and chain pull-outs[38]. Based on the study of a series of latexes with a very narrow molecular weight distribution, he found that at the low end of the molecular weight spectrum (around the entanglement molecular weight), chain pull-out is dominant and the fracture energy of the film is not improved during annealing, while at the high end, chain scission dominates. In the intermediate range, the energies for both motions are comparable. Sambasviam also concluded that the film strength reaches a plateau value, which should represent the strength of a film with infinite MW. This plateau value is close to the strength of the film with M_n around 420,000 g/mol, when 90% of the fracture energy is contributed by the chain scission process. Because the molecular weight plays a very important role in the film interfacial strength build-up, further study of the molecular weight effect on bimodal latex films is worthwhile for a comparison with monodal latex systems and various studies in the literature.

1.2.3 Chemical Crosslinking at an Interface

When films form in a reactive system, chemical crosslinking and film coalescence should be well controlled and balanced, because chain interdiffusion and entanglements

are responsible for the generation of latex film strength. However, up until now, most of the chemical crosslinking reactions introduced into latex film systems (either with different functional group combinations or with addition of external crosslinkers) are room temperature reactions, which means that the chemical reactions cannot be monitored in the time domain, but instead, can only be characterized when the reaction is complete [39, 40, 41, 42]. Although parameters (such as the reaction temperature, the concentration of reactive groups) can be adjusted to make latex films with better properties, it is still an empirical process and not suitable for a fundamental study of these two competitive processes. A well-controlled system with careful system designs is essential to predict the film properties.

Tronc *et al*, took into account the control of crosslinking reactions when they studied the competition between interdiffusion and crosslinking in films formed from two pairs of epoxy latexes in the presence of a diamine crosslinking agent[43]. In their study, they observed a crossover from a diffusion dominant regime to a chemical reaction dominant regime in the film curing process. There is no obvious improvement of film tensile strength and fracture toughness in the presence of external crosslinker, which means that the film curing process was still not reaction controlled. Besides, they did not calculate the ratio of interdiffusion time to crosslinking time to clearly differentiate between the fast (reaction rate is faster than diffusion rate) and slow (reaction rate is slower than diffusion rate) reaction regimes. Better controllable and more systematic work on the effect of interface-related chemical crosslinking on latex film performance is therefore highly desirable.

1.3 Selection of Model System

Styrene was chosen to be the backbone monomer in this work for two reasons. First, it has been widely studied and well-documented in the literature, so that it provides a good reference for comparison. Secondly, it has a high glass transition temperature T_g (105 °C), so that it is easier to control the film formation process by controlling the annealing temperature. Once the backbone monomer was selected, the functional components for designing a reactive film system needed to be selected. The reaction pair of carboxyl group and primary amine group was chosen, because an even higher reaction temperature (compared to the minimum film formation temperature) is needed to induce the reaction. Therefore, the film formation process and the chemical reaction process will be controlled separately by controlling the temperature, which provides a solid basis for a fundamental study of the competition between polymer chain interdiffusion and chemical crosslinking in a reactive latex film.

1.4 Objectives and Scope of this Research

The main goal of this research is to further the molecular-level understanding of the film formation process by a parametric study of film performance, employing a model system of bimodal latexes where the properties of the two latexes, such as particle size, molecular weight, gel content, and functionality, are varied independently.

The arrangement of this thesis is as follows:

Chapter 2 introduces all of the characterization methods and techniques used in this study, and Chapter 3 discusses the synthesis of latex particles with different physical (such as particle size, molecular weight) and chemical properties (such as functionality).

Chapter 4 focuses on the effect of bimodal particle packing on the film mechanical performance, which is later combined with the study of the molecular weight effect. Film tensile strength, as representative of film interface-related properties, is investigated and compared.

With an understanding of particle packing effects and molecular weight effects discussed in Chapter 4, the effects of crosslinking, in terms of both bulk crosslinking by addition of external crosslinker, DVB, and interface crosslinking by initiation of internal $COOH/NH_2$ chemical reaction, is explored in Chapter 5.

By applying the scaling theory and shrinking core model (a kinetic model designed for a solid-gas reactive system which will be discussed later in Chapter 6) with suitable adjustments to the polystyrene reactive film system, Chapter 6 analyzes the experimental results and presents a practical guideline towards the film interface strengthening strategy, which directly relates microscopic molecular parameters to the macroscopic mechanical performance of the film.

1.5 References

1. Keddie, J. *Mater. Sci. Eng.* **1997**, *21*, 101
2. Lee, D.I. *Advances in Emulsion Polymerization and Latex Technology*, **2010**
3. Overbeek, A. *J. Coat. Technol. Res.*, **2010,** *7(1)*, 1
4. Schneider, M.; Graillat, C.; Guyot, A.; McKenna, T. F. *J. Appl. Polym. Sci.,* **2002**, *84*, 1916;
5. Schneider, M.; Graillat, C.; Guyot, A.; McKenna, T. F. *J. Appl. Polym. Sci.,* **2002**, *84*, 1897
6. Guyot, A.; Chu, F.; Schneider, M.; Graillat, C.; McKenna, T.F. *Prog. Polym. Sci.*, **2002**, *27*, 1573
7. Ai, Z.; Deng, R.; Zhou, Q.; Liao, S.; Zhang, H. *Adv. Colloid Interface Sci.*, **2010**, *159*, 45
8. Zhao, C.; Li, X. *J. Polym. Mate.*, **2006**, *23*, 197
9. Boutti, S.; Graillat, C.; McKenna, T.F. *Polymer*, **2005**, *46*, 1211
10. Wang, T.; Keddie, J. *Adv. Colloid Interface Sci.*, **2009**, *147-148*, 319
11. Wang, L.; Wan, Y.; Li, Y.; Cai, Z.; Li, H.; Zhao, X.; Li, Q. *Langmuir*, **2009**, *25*, 6753
12. Winnik, M. A.; Feng, J. *J. Coat. Tech.* **1996**, *68*, 39
13. Bartlett, P.; Ottewill, R.H.; *J. Chem. Phys.* **1992**, *96 (4)*, 3306
14. Bartlett, P.; Ottewill, R.H.; Pusey, P.N. *Phys. Rev. Lett.* **1992**, *68*, 3801
15. Tzitzinou. J.; Keddie, A. *Macromolecules*, **2000**, *33*

16. Peters, A.C.I.A; Overbeek, G.C.; Buckmann, A.J.P.; Padget, J.C.; Annable, T.; *Prog. Org. Coat.*,**1996**, *29*, 183

17. Eckersley, S.T.; Helmer, B.J. *J. Coat. Tech.* **1997**, *69*, 97

18. Feng, J.; Winnik, M. A. *Macromolecules* **1995**, *28*, 7671

19. Vidovska, D.; Maurer, F.H.J. *Composite Interfaces* **2006**, *13*, 819

20. Geurts, J.; Bouman, J.; Overbeek, A. *J. Coat. Tech. Res.* **2008**, *5*, 57

21. Tang, J. *Ph. D Dissertation*, **2000**, Lehigh University

22. Rouse, P.E. *J. Chem. Phys.* **1953**, *21*, 1272

23. Zimm, B.H. *J. Chem. Phys.* **1956**, *24*, 269

24. de Gennes, P.G. *J. Chem. Phys.* **1971**, *55*, 572

25. Wool, R. P.; Connor, K. M. *J. Appl. Phys.* **1981**, *52*, 5953

26. Kim, Y.; Wool, R. *Macromolecules*, **1983**, *16*. 1115

27. de Gennes, P.G. *C.R. Acad. Sci. Paris*, **1980**, *B291*. 219.; Williams J. et al., *J. Mater. Sci*, **1981**, *16*. 204S

28. Prager, M.; Tirrell, J. *J. Chem. Phys*, **1981**, *75*. 5194

29. Adolf, D.; Tirrell, M.; Prager, S. *J. Polym. Sci. Phys.Ed.*, **1985**, *23*. 413

30. Yoo, J.; Sperling, L.; Glinka, C.; Klein, A. *Macromolecules*, **1990**, *23*. 3962.

31. Yoo, J.; Sperling, L.; Glinka, C.; Klein, A. *Macromolecules*, **1991**, *24*. 2868.

32. Kim, D.; Klein, A.; Sperling, L.H.; Boczar, E.M.; Bauer, B.J. *Macromolecules*, **2000,** *33*, 8334

33. Spiro, J.G.; Farinha, J.P.S.; Winnik, M.A. *Macromolecules*, **2003**, *36*, 7791

34. Yang, J.; Lu, J.; Rharbi, Y.; Cao, L.; Winnik, M.A. *Macromolecules*, **2003**, *36*, 4485

35. Pham, H.H.; Farinha, J.P.S.; Winnik, M.A. *Macromolecules*, **2000**, *33*, 5850

36. Feng, J.; Pham, H.; Stoeva, V.; Winnik, M.A. *J. Polym. Sci. Part B: Polym. Phys.*, **1998**, *36*, 1129

37. Mohammadi, N.; Klein, A.; Sperling, L.H. *Macromolecules*, **1993**, 26 (5), 1019

38. Sambasivam, M. *Ph. D Dissertation*, **1995**, Lehigh University

39. Kessel, N.; Illsley, D.R.; Keddie, J.L. *J. Coat. Tech. Res.*, **2008**, *5*, 285

40. Zhang, J.; Yang, M.; Yang, H.; Zhu, Y. *Acta. Polym. Sinica*, **2006**, *55*, 951

41. Pham, H.H.; Winnik, M.A. *J. Polym. Sci. Part A: Polym. Chem.*, **2000**, *38*, 855

42. Clemens, R.J.; Rector, F.D. *J. Coat. Technol*, **1989**, *61*, 83

43. Tronc, F.; Chen, W.; Winnik, M.A.; Eckersley, S.T.; Rose, G.D.; Weishuhn, J.M.; Meunier, D.M. *J.Polym.Sci. Part A: Polym. Chem.*, **2002**, *40*, 4098

CHAPTER 2

Characterization Methods and Film Formation Techniques

2.1 Introduction

Because the subjects of this study cover microscopic latex particles as well as macroscopic latex films, a broad scope of characterization methods and techniques are used in this work, some of which also required modifications for specific tests. Therefore, this chapter summarizes all the characterization methods as well as film-making techniques. Polystyrene (PS) latexes that have a high glass transition temperature (T_g) cannot form films at room temperature in the absence of solvents. Therefore, transparent and coherent PS films are formed from dried latex powders at higher temperatures by pressure molding, instead of being cast into films at ambient conditions as is the case for most low T_g latexes.

2.2 Latex Particle Characterization Methods

2.2.1 Particle Size Characterization

There are several instruments used for measuring latex particle sizes and size distributions:

1) Capillary Hydrodynamic Fractionation (CHDF)

Capillary hydrodynamic fractionation is a very powerful method for measuring particle size within a range from 20 nm to 2 μm. Because of the size exclusion effect, larger particles have a faster average velocity than smaller particles and will elute from the CHDF sooner than the smaller. Particles are detected by a UV detector as they elute, and the elution time is compared with the calibration curve developed from size standards.

However, because CHDF is able to detect small molecules including monomers, if the latexes contain dissolved portions of unpolymerized monomers or water-soluble polymer chains, these monomers and chains will also be detected and will be considered as small size particles with diameters around 30 nm (see Figure 2.1a). The existence of small molecules does not affect the determination of latex particle sizes larger than 100 nm, but will affect the result if the latex particle size is small, due to overlapping of the absorbance peaks (Figure 2.1b). This problem can be solved by cleaning the latex particles before testing, when smaller size particles (less than 100 nm) need to be measured.

2) Dynamic Light Scattering (DLS, Nicomp)

Dynamic light scattering is the fastest way to obtain a general idea about latex particle sizes and size distributions. Samples are diluted with DI water until the reading of the intensity falls into the range of 300~ 400 counts.

However, because the Nicomp result is a statistical value, to get a more accurate result, a certain time is required before the dilute latex being tested becomes homogenous *via* Brownian motion. However, the waiting time cannot be too long (around 20 minutes),

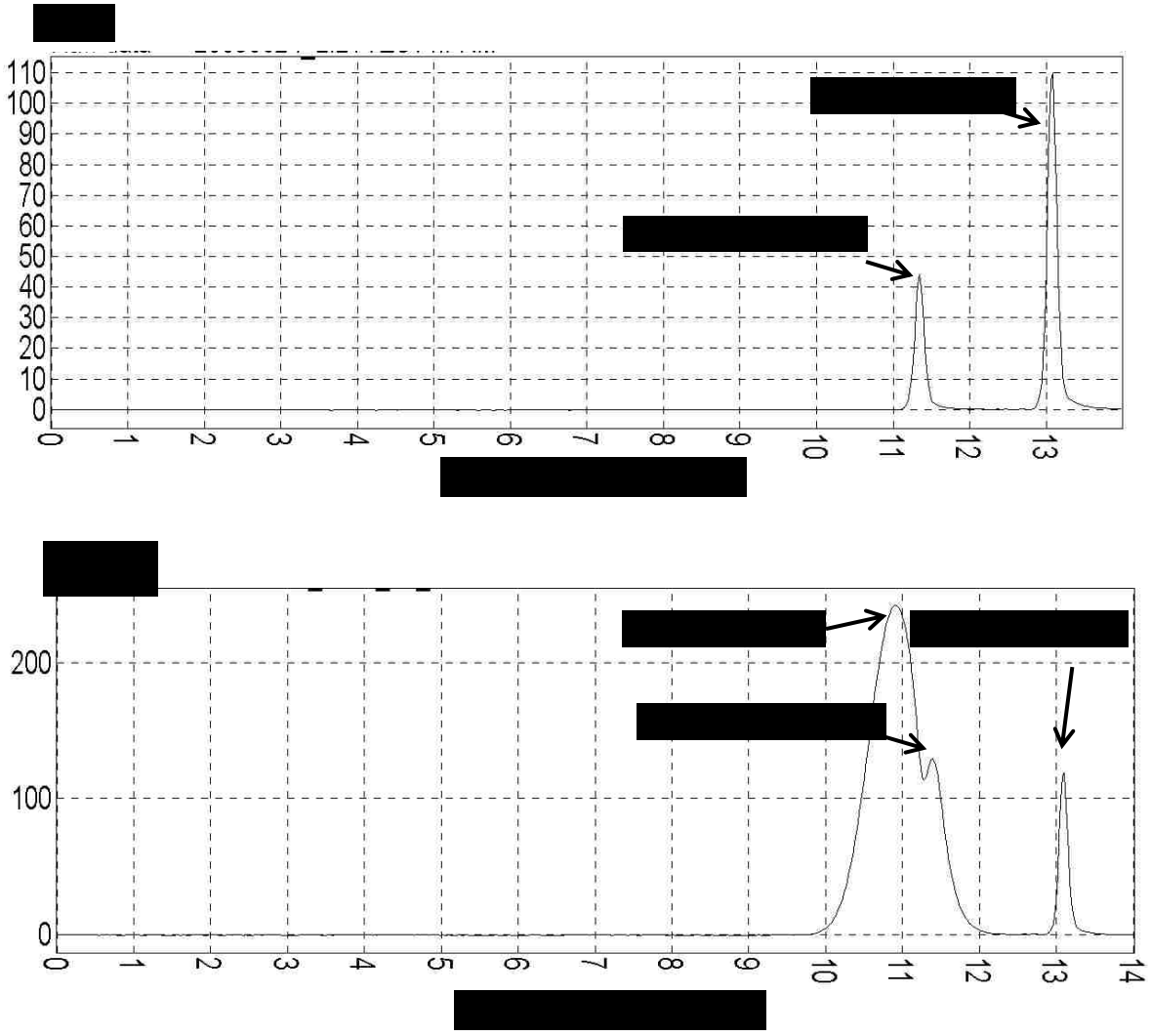

Figure 2.1: Raw data from CHDF absorption intensity with elution time. a) Small marker molecule was injected as the sample; b) Uncleaned small latex particles were used as the sample. The small molecule peak overlapped with the sample peak.

also because of the Brownian motion of the particles. Larger particles tend to settle out much quicker than smaller particles. Especially, for latexes with a broad particle size distribution, the composition within the channel area being tested changes overtime, and the changing composition affects the value of the final particle size.

2.2.2 Particle Morphology Characterization

The scanning electron microscope (SEM) and transmission electron microscope (TEM) are both used for characterizing particles in the dried state. Usually, the results from TEM are several to tens of nanometers smaller than the value measured by SEM. The resolution of TEM is higher than SEM, due to the much higher electron beam. The voltage normally used for TEM is 180 kV to 200 kV, while the voltage for SEM is normally around 3 kV to 20 kV. Therefore, TEM is a much better way to measure smaller latex particles (less than 50 nm). In addition, TEM has an advantage of detecting the composition of the latex particles using chemical staining techniques.

On the other hand, SEM is one of the most powerful tools for studying the morphology of both latex particles and the latex films. The samples are given an Iridium coating to dissipate charging of particles. The 30-second coating time can make a coat 3~5 nm thick. The beam voltage generally used for polymers is 3 kV. However, since polystyrene is a hard polymer (high T_g), 10 kV has been used for a better resolution without deforming the particles. Figure 2.2.2 shows different surface morphologies of polystyrene latexes.

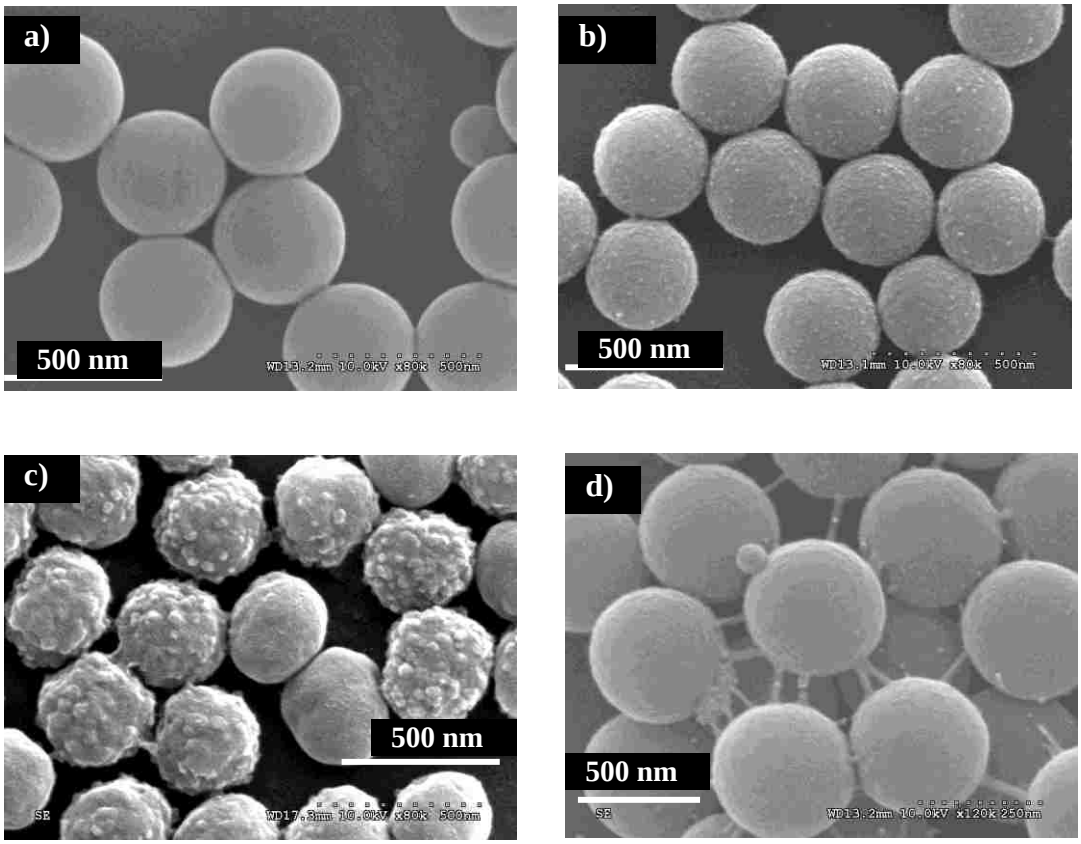

Figure 2.2: SEM images of different morphologies of PS latex particles with similar particle sizes. a) Smooth surface were observed on pure PS particles; b) rough surface of carboxylated PS particles were observed; c) irregular shapes of crosslinked PS particles were observed due to phase separations; d) bridges between carboxylated PS particles were observed, which may be attributed to the water-soluble poly (methylacrylic acid).

2.2.3 Latex Polymer Molecular Weight Characterization

For polymers, the molecular weight is a fundamental determinant of many physical properties including stiffness, strength, viscoelasticity, and toughness.

1) Gel Permeation Chromatography (GPC)

Gel permeation chromatography is the most common way to determine molecular weight and molecular weight distributions of latex polymers. Linear polymer in a latex particle is obtained by drying the latex and then dissolving it in THF (about 1 wt %) until a clear solution is formed. However, GPC is not able to differentiate the highly branched polymer chains from linear polymer chains. Therefore, in order to check if the chains are highly branched, viscosity measurements *via* solution viscometry could be used for comparison of the viscosity-average molecular weights measured by GPC.

2) Swelling Measurement

Swelling measurements are a direct method used to determine the average molecular weight between crosslink points, M_c. The Flory-Rehner equation (eq 2.1), which assumes a uniform distribution of crosslinking throughout the particle, can be used to quantify the extent of crosslinking[1]. Thus, the crosslinking density, ρ_c, is calculated according to eq 2.2:

$$M_c = \frac{V_1 \rho_c \left[\phi^{1/3} - \phi/2\right]}{-\left[\ln(1-\phi) + \phi + \chi\phi^2\right]} \tag{2.1}$$

$$\rho_c = \frac{\rho_p}{M_c} \tag{2.2}$$

where V_1 is the molar volume of toluene and ρ_p is the density of dry polymer. The polymer-solvent interaction parameter, χ, and volume fraction of polymer, ϕ, in the solvent are calculated as:

$$\chi = 0.34 + \frac{V_1}{RT}(\delta_1 - \delta_2)^2 \tag{2.3}$$

$$\phi = \frac{W_p \rho_s}{W_p \rho_s + W_s \rho_p} \tag{2.4}$$

where δ_1 and δ_2 are the solubility parameters of the polymer and solvent, W_p and W_s are the weight fractions of polymer and solvent, ρ_p and ρ_s are the densities of the polymer and the solvent, respectively. The constant 0.34 is the entropic term that compensates for the relatively large difference in free volume between the polymer and the solvent[2,3,4]. Because the molar volume of toluene, V_1, is 106.3 cm^3/mol, the solubility parameter of polystyrene, δ_1, is 9.3, and the solubility parameter of toluene, δ_2, is 8.9, the polymer-solvent interaction parameter, χ, is calculated to be 0.37 at room temperature, according to eq 2.3.

The major step in this method is the process of experimentally determining the volume fraction of polymer ϕ. The dried latex sample is weighed (m_0). If the dried sample is comprised of dried latex particles, it is usually put into a bag made of filter paper, and then immersed in THF solvent at room temperature for two days to remove the soluble polymer fraction from the sample. If the dried sample is a coherent latex film, there is no need of using filter paper bags. The amount of solvent is usually 100 times more than the

weight of the dried sample. This step is important, because it prevents the non-crosslinked polymers from contributing to the total crosslinking density. Then the swollen sample is dried in a 40 °C ~ 50 °C oven more than 12 hours. The temperature cannot be too high, or this may induce additional crosslinking during the drying process. The dried portion is weighed again (m_1) and then tumbled in toluene , which is 60 times more than the weight of dried portion at room temperature for 24 hours. The ratio of m_1 to m_0 is the sample gel content, which can also be used to characterize the extent of crosslinking in the sample. The swollen portion is then blotted dry (surface dried) and quickly weighed (m_2) when the last digit of the balance reading remains unchanged for at least 10 seconds. The volume fraction of polymer (ϕ) can be calculated using eq 2.4 and the weight fraction of polymers (ratio of m_0 to m_2).

2.2.4 Functional Groups and Functionality Distribution Characterization

This section covers the characterizations of small molecules, polymers, and small molecule reactions as well as reactions in polymers.

1) Fourier Transform Infrared Spectroscopy (FT-IR)

Fourier transform infrared spectroscopy is one of the most efficient techniques to provide the qualitative information of functional groups in small molecules as well as latex particles. However, if a calibration curve can be properly made, a quantitative measurement can also be achieved (see Chapter 3 for examples).

Two basic setups of FT-IR are used in measuring functionalities in latex particles. The most common method is to mix a trace amount of dried latex sample with anhydrous potassium bromide, and then press the mixture into a transparent film for testing. Another way is to make the latex solution using THF solvent, and then dry the solution on a slide of silicon single crystal; germanium single crystal can also be used. Since the concern is more about the total functionality within the latex particles including surface and bulk, the transmittance (or absorbance) mode is used instead of the reflection mode used in attenuated total reflectance (ATR). Hence, a latex film dried on a single crystal should be as thin and transparent as possible to maintain good light transmittance. Figure 2.3 compares IR results for pure polystyrene particles, carboxylated polystyrene particles, and isocyanate functionalized polystyrene particles.

Regarding the characterization of small molecules and small molecule reactions, normally a drop or two of the liquid sample is placed between two transparent sodium chloride salt plates and is then squeezed into a very thin liquid film between the two plates. If a solvent is used in the samples, the solvent must be used for the background scan as well.

2) Nuclear Magnetic Resonance (NMR)

Nuclear magnetic resonance (NMR) is well known for its high sensitivity and resolution for analyzing molecule structures. Specifically, in this work, it is used to characterize the extent of purification of the synthesized monomers and to investigate the chemical reactions between small molecules. In most cases, chloroform-d was used as the

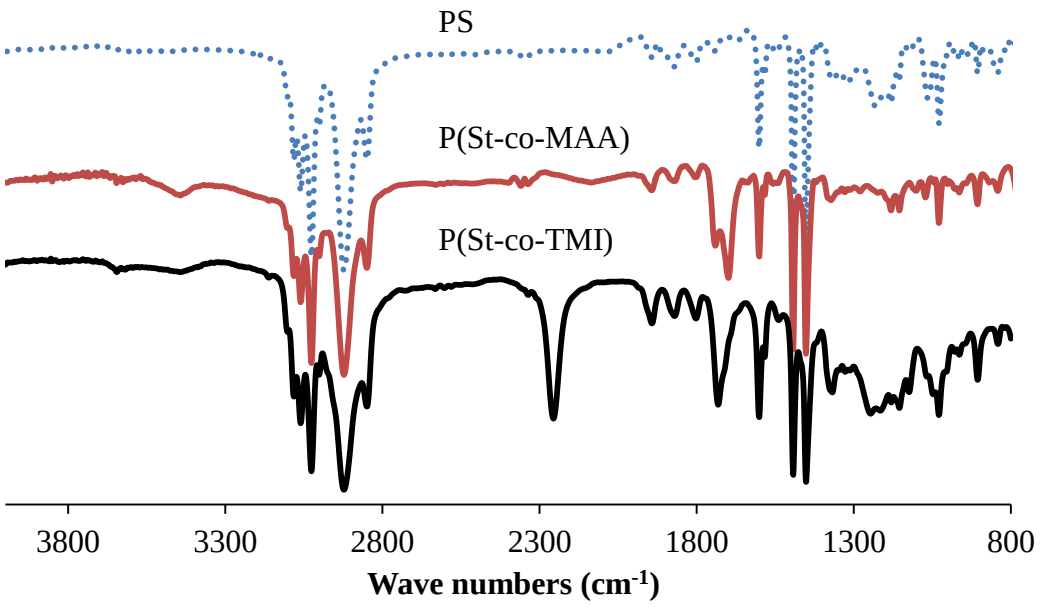

Figure 2.3: Infrared spectroscopy (IR) comparison result of polystyrene, carboxylated polystyrene, and isocyanate-functionalized polystyrene latex particles.

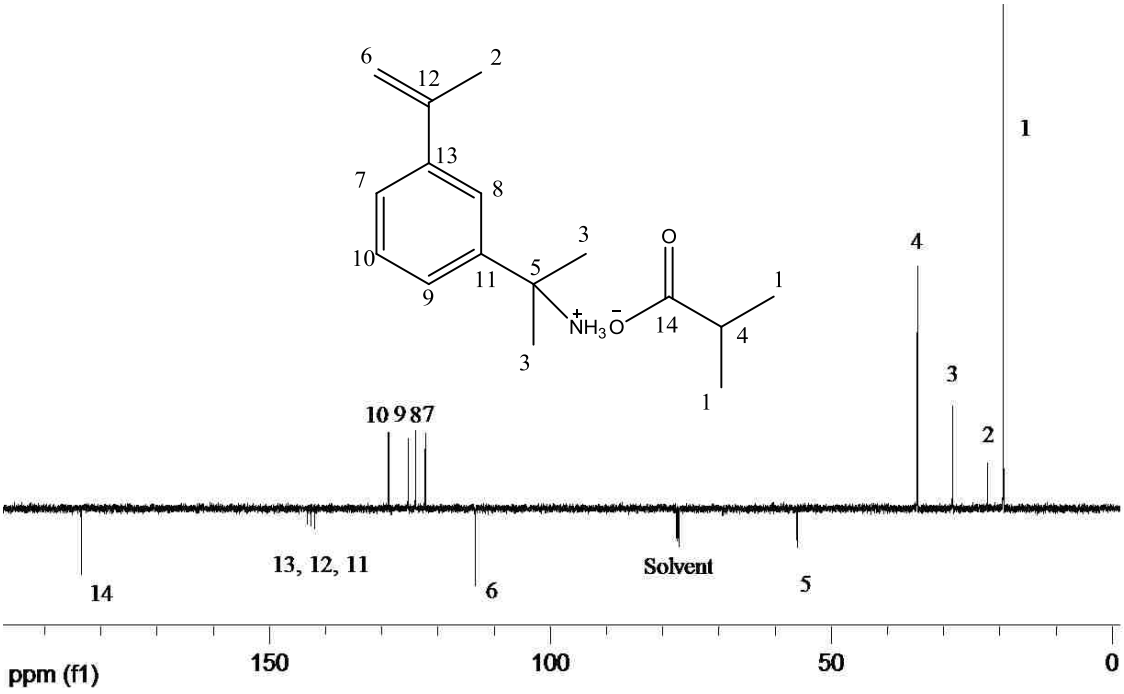

Figure 2.4: Nuclear magnetic resonance result of a mixture of TMA (isopropenyl dimethylbenzyl amine) with isobutylic acid at room temperature.

solvent; however, d6-dimethylsulfoxide (DMSO) and d5-pyridine have also been used in some cases for characterizing latex films.

The characterization of the progress of chemical reactions between small molecules is as follows: one drop of liquid sample is taken from the reactor at different reaction times and dissolved in a deuterated solvent for both ^{1}H and ^{13}C NMR analysis. The ^{13}C NMR analysis in this work is based on the distortionless enhancement by polarization transfer (DEPT) experiments. With this method, the CH, CH_2, and CH_3 groups can be differentiated by varying the selection angle parameter. Here, we use 135° angle to separate all CH and CH_3 from CH_2 and quaternary C (see Figure 2.4 for examples).

3) Conductometric Titration

This measurement is used for the determination of the carboxyl group distribution within latex particles. Unlike a regular weak acid/strong base titration in which all the functional groups are homogenously distributed and available for titration, the carboxyl groups are distributed throughout the latex particle non-uniformly and cannot be titrated at the same time. Therefore, when the cleaned particles are directly titrated with 0.0200 N standard NaOH solution, there is not be a sharp end point but a gradually changing curve (see Figure 2.5a), because the NaOH molecules move into the inner layers of the particle sphere and react with the existing COOH groups present there as they diffuse deeper.

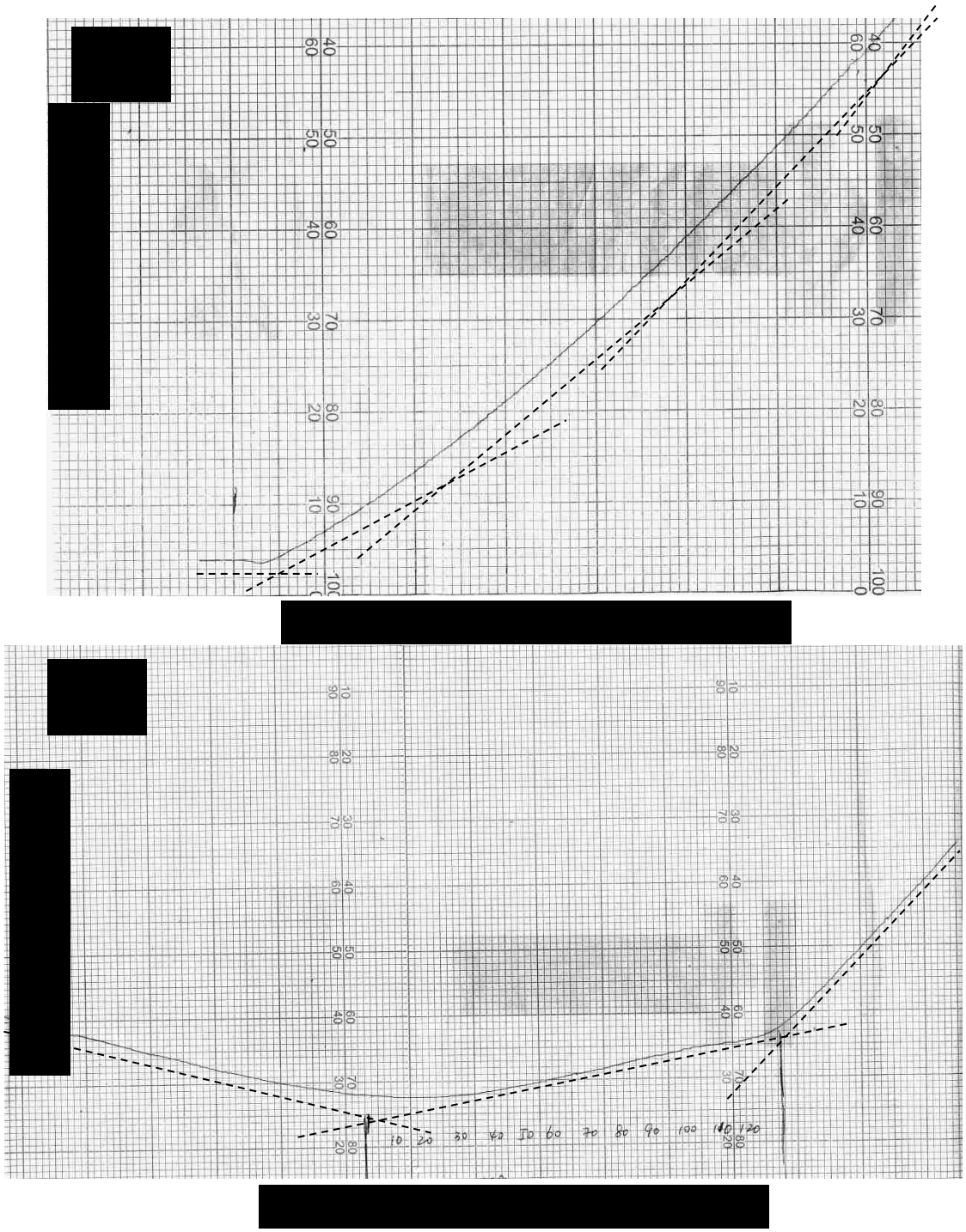

Figure 2.5: Conductometric titration results by a) directly titrating the cleaned polymer latex with 0.0200N NaOH standard solution; b) back titrating 0.0200N HCl solution after adding excess NaOH to the cleaned polymer latex. The black dotted lines describe the changing slopes of the titration curve. The change of slope is not obvious in (a), but very evident in (b).

Therefore, a titration method is applied which is similar to a back titration method. Excess NaOH is added to the diluted latex samples, and then titrated back with standard HCl solution after several time periods: immediately (0 min), 15 min later and one day (24 hour) later. Consequently, the functionality distribution within different layers of particles can be estimated in this way.

The amount of carboxyl groups located in the aqueous phase of latex system can be also determined by directly titrating the serum (the supernatant separated from the uncleaned latex) with the standard NaOH solution. The amount of carboxyl groups located in the core of the latex particles can be considered as the untitrated fraction of the functional groups, which is calculated by subtracting the amount that is titrated from the total amount that is charged in the recipe.

4) Ultraviolet-Visible Spectometer

Ultraviolet-visible spectometer is used to characterize the surface amine functionality of the PS particles using the N-succinimidyl 3-(2-pyridyldithio)-propionate (SPDP) / dithiothreitol (DTT) pair in a reduction-oxidation titration. The solution used for diluting samples is a 0.05 M $NaHCO_3$ buffer solution with a pH of 8.2. The optical density is read at a wavelength of 345 nm. The details of the titration are presented in Chapter 3.

2.2.5 Glass Transition Temperature Characterizations

Differential Scanning Calorimetry (DSC) is the major technique to measure the change of glass transition temperatures (T_g) of copolymers with different compositions. A

sample of dried latexes (10 mg) is sealed in a DSC pan and the test is performed from 80°C to 200 °C at a heating rate of 4°C/ min. Each sample is tested at least twice. The dried sample is ground as fine as possible before being sealed in the aluminum pan. The powder is then heated at an initial temperature 80 °C for a relatively long equilibrium time (15 min) to make sure the sample is heated more uniformly afterwards. As a result, the value of T_g is much more reliable and the turning curve is much smoother. Dynamic mechanical analysis (DMA) can also be used for T_g measurements, but the T_g obtained from DMA (tan δ peak) is generally larger than that from DSC.

2.3 Latex Film Characterization Methods

In this section, characterization methods for latex films from morphology tests to mechanical property tests are discussed in detail.

2.3.1 Film Formation Technique

Because the backbone polymer is polystyrene, the films cannot be cast at room temperature without solvents. Therefore, films are made by compression-molding the dried powder under a higher temperature but below the melting point until the particles adhere to each other; this is called the sintering process. In the sintering process, pre-made dumbbell and rectangular molds are used for compression molding (Figure 2.6). Both film shapes result in very similar film strengths, but the results from the dumbbell-shaped films are more scattered than those obtained from the rectangular latex films. The internal stress induced at the curved “ear part” of the dumbbell shape leads to more

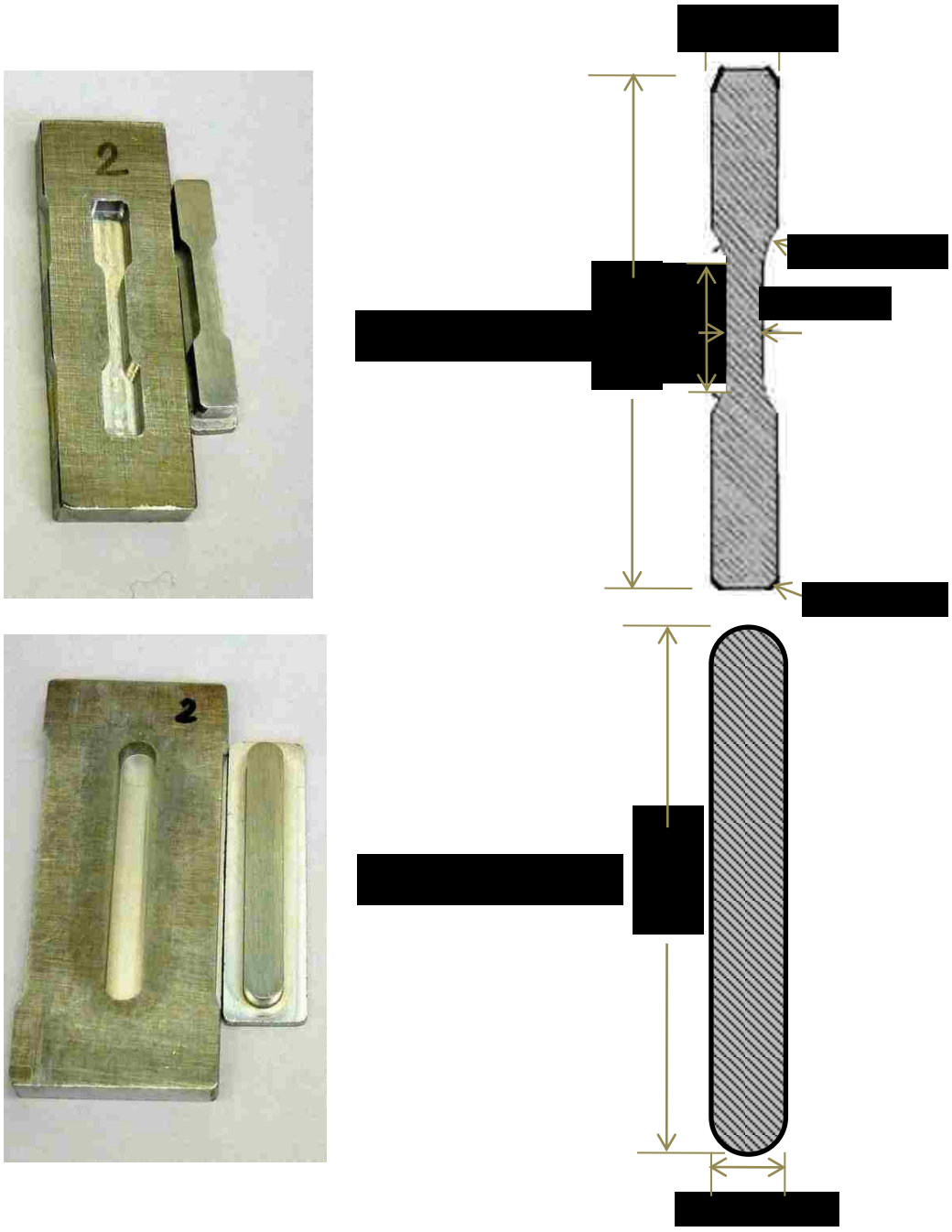

Figure 2.6: Pictures and sketches of two aluminum molds used for sintering latex powders into films (Since relative comparisons of the film strengths were of interest, the molds were not manufactured strictly based on ASTM standards).

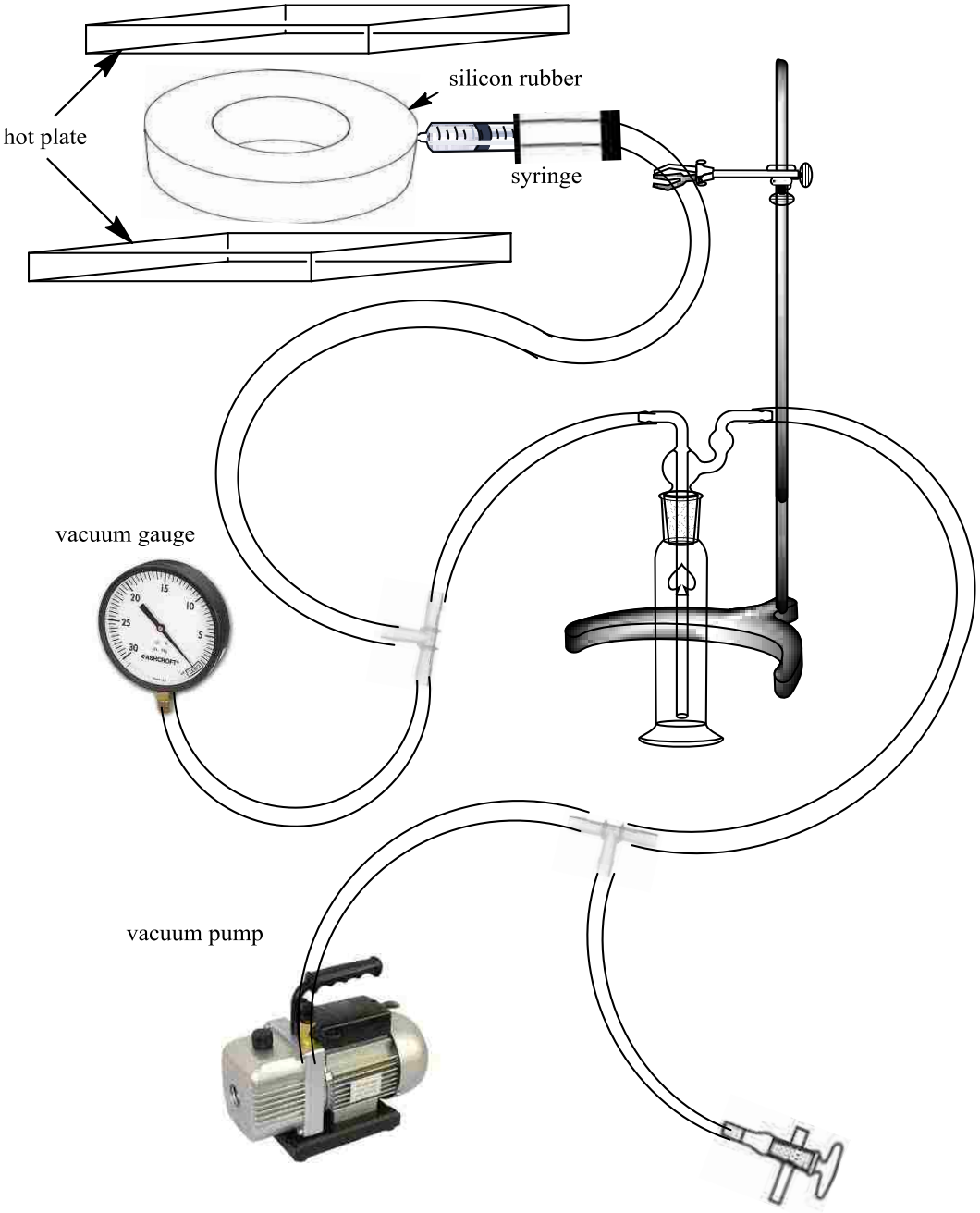

Figure 2.7: Sketch of the homemade vacuum hot press setup. The ring between the two hot plates is made of silicon rubber. The thickness of the ring is about ½ inch. When a vacuum is applied, the vacuum created within this silicon rubber ring is approximately 25- 30 mm Hg.

defects in the film. As a result, most film strength tests were done using rectangular-shaped latex film samples.

The dried polystyrene particles are sintered for 35 min by using a vacuum hot press (Carver hydraulic press) at 110~ 120 ℃ (slightly higher than the T_g of PS) and a pressure of around 11 MPa under vacuum. If the particles are carboxyl functionalized, the sintering temperature are around 120~ 130 ℃. To apply vacuum to the hydraulic press machine, a homemade vacuum setup is used (see Figure 2.7). The sintering condition is just sufficient to form a dense film that is free of visible flaws, scratches, or imperfections. The resulting bulk films are then annealed at different temperatures, which is higher than the sintering temperature but far lower than the melting temperature of polystyrene around 250 ℃, for various times to build film interfacial strength. To prevent sample distortion during the annealing process, the polystyrene films are left in the molds and placed directly into a convection oven after sintering. If the films are reactive, the sintered films are placed between two aluminum plates clamped together in the oven. In this way, the reaction product water is able to escape from the film without distorting the sample during the annealing process. A 10 min period is allowed for the temperature to equilibrate before the annealing time begins. As soon as the samples are taken out of the oven, they are quenched in a tap water bath (approximately 15 °C) to inhibit any further polymer chain interdiffusion.

2.3.2 Film Morphology Characterization

The term ‘film morphology’ is not accurate, but really represents the macroscopic dried latex chunks; when polystyrene latexes are dried at 40°C, they only form brittle

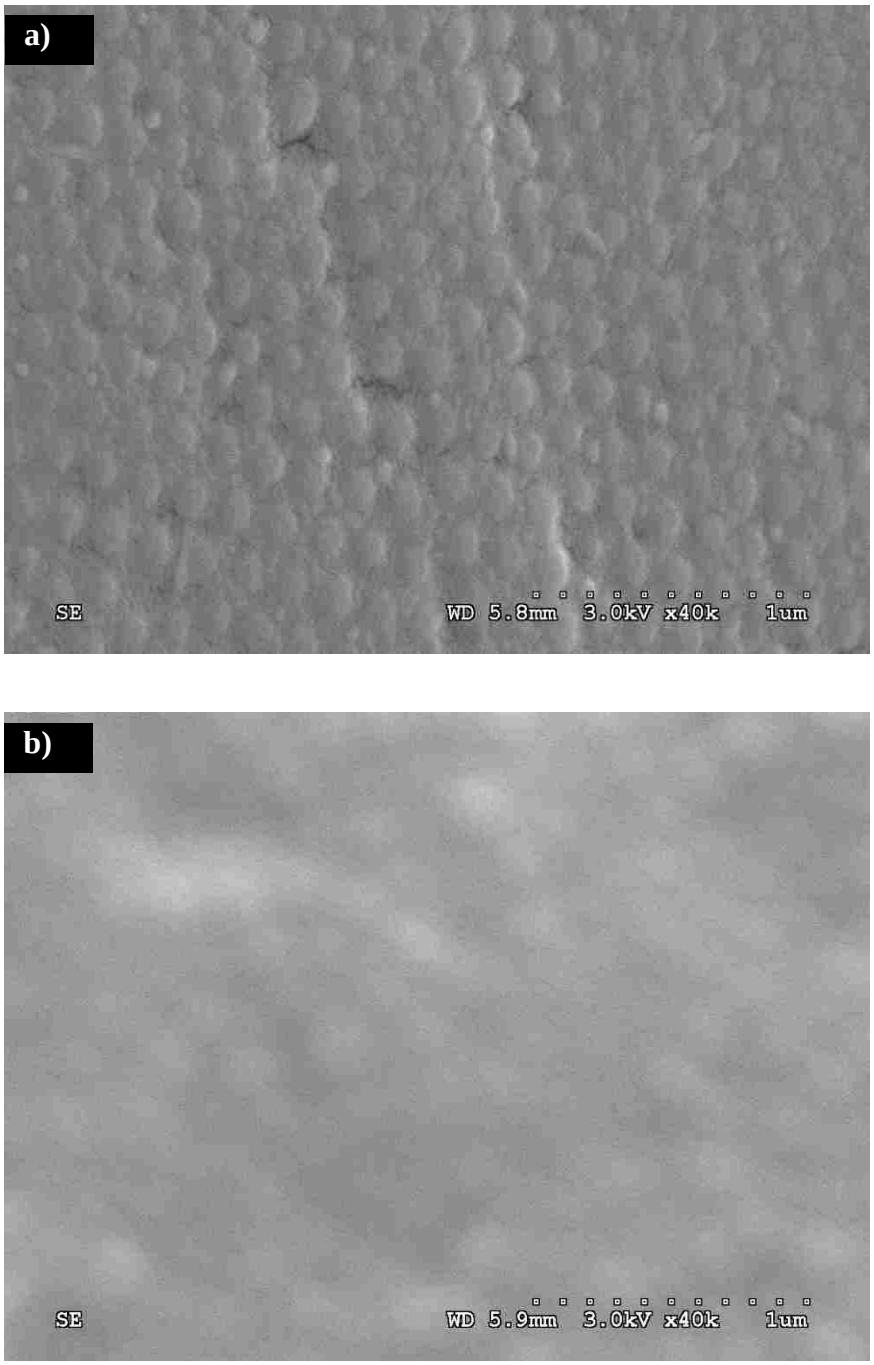

Figure 2.8: Scanning Electron Microscope (SEM) images of the surface morphology of: a) dried PS latex blends that have been sintered for only 10 minutes (the small particles are almost indistinguishable); b) dried large PS latexes that have been sintered for 25 minutes (the large particles become indistinguishable). The typical sintering time to produce a transparent film is 35 minutes.

chunks without building any internal strength due to its much higher T_g. When a coherent latex film has been formed, the boundary between particles is no longer distinguishable due to the interpenetration of the polymer chains at the particle-particle interface. Figure 2.8 shows the surface of two incompletely sintered film samples, which show some interpenetration between particles, but the interface healing is still not complete. This can be considered a transition state between the dried latex state and the fully formed film state. After this transition state, no individual particles can be observed. In water-borne latex coatings, particle morphologies are the basis for film morphology; thus it is reasonable to study the packing effect on the latex chunks.

For the characterization of the blend morphology, one drop of each latex sample is put onto a freshly peeled mica surface and left at room temperature until totally dried. Scanning electron microscopy (SEM) and atomic force microscopy (AFM) are two techniques used to study packing morphology. Regarding AFM, the advantage of this technique is the ability to distinguish intrinsic differences in the material. Although in the system the large and small particles are both made of the same materials so that a phase difference cannot be detected, AFM is a very useful tool if the blend particles are made of different materials, such as hard and soft particles. The evidence can be found in Figure 2.9, which shows the topographic and phase profiles of the same sample. Most particles (both large and small) have light colors in the phase profile, while some of the small particles surfaces appear darker (little black dots) possibly because of the unremoved Triton X-100 existing on the particle surface, which is much softer than the particle itself.

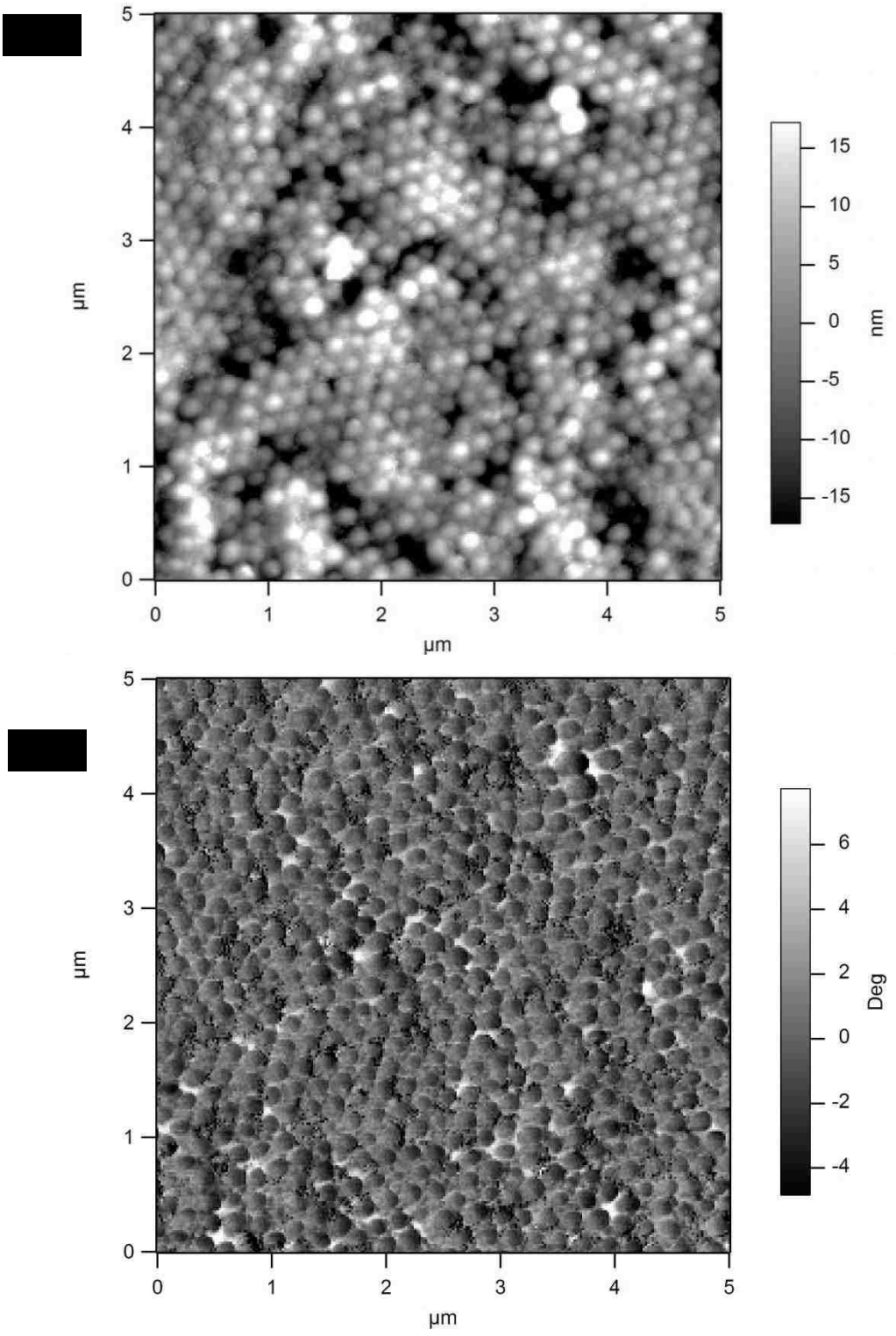

Figure 2.9: a) Atomic force microscopy (AFM) topographical profile, and b) phase profile of a polystyrene latex blend with a composition of 31 (small): 1(large) on average.

In addition, the simplicity of the sample preparation is another great advantage of the AFM. Unlike SEM, for which the sample needs to be coated by iridium, there is no damage or contamination of the samples in AFM. However, its drawback is contamination of the AFM tip when using the tapping or contact mode. Especially for soft materials, such as polymers, the probe tip is easily contaminated. As a result, the feedback force from the sample surface to the cantilever can be affected, which leads to unreliable scanning images, such as distorted shapes or overestimated heights.

2.3.3 Film Mechanical Performance Characterization

1) Instron Universal Testing Measurements

The characterization of the strength of unreactive films is carried out by tensile strength measurements on an Instron 5567 universal testing machine at room temperature. The load cell is 500 N. The grip separation distance is 12.5 mm and the separation rate is 25.4 mm/min. At least 3 specimens are tested for each sample depending on the consistency of the data, and the values are averaged. However, the tensile test taken at room temperature cannot characterize the film strength built by the additional crosslinking at the film interface. Because at room temperature polystyrene chains are still frozen in their glassy state, there will be no difference between breaking the free mobile chains and breaking the chain crosslinking network. Therefore, a modified film strength measurement *via* advanced rheometric expansion system (ARES) is developed so that the tensile tests can be done at a testing temperature close to the T_g of styrene.

2) Advanced Rheometric Expansion System (ARES)

Advanced rheometric expansion system is well known for measuring sample modulus. In our study, it is not only used for the modulus test but it is also modified for film strength tests at high test temperatures. For the modulus, the experiments are performed *via* dynamic temperature step test. Basically, the test takes successive measurements at selected temperatures while mantaining a constant frequency and strain. The condition used in this test is 0.2 % ~0.4 % test strain, 1 Hz frequency, and the temperature ranges from 80 °C to 180 °C at 2 °C increments.

For the film tensile strength part, a multi-extension mode test has been used. The mode of extension is controlled by the linear rate, which in our case is 0.333 mm/s, which is converted from the separation rate used in the Instron. The sample specimen is much smaller than the one used in the Instron, because the maximum load for the ARES transducer is much smaller (around 2000 g). Dremel tools were used to grind the rectangular film samples into the dumbbell-shaped micro-specimens, with the smallest neck area around 1.10 mm× 0.35 mm. Raw data from a sample test run is shown in Figure 2.10.

Because the test instrument was changed from the Instron to the ARES, it was necessary to check if the results from these two instruments are comparable and if the increased operating temperature changed the trend of tensile strength with annealing time. Table 2.1 shows a comparison of tensile tests between these two machines. For the same batch samples and the same operating temperature (room temperature), the ARES tensile strength results are higher than the ones from the Instron. However, the use of ARES

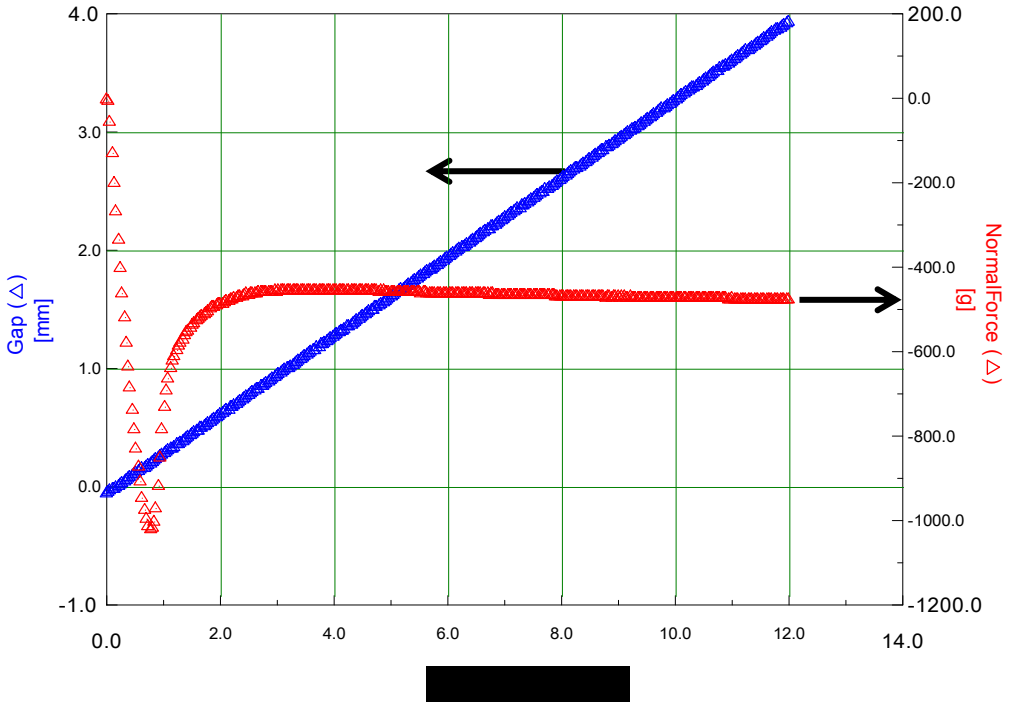

Figure 2.10: A typical sample test run *via* the modified ARES strength measurement.

Table 2.1: Comparison of TS Results via Instron and ARES

	Instron (MPa)	**ARES (MPa)**
S_l3-1*	24.91	32.31
S_l3-2*	31.10	40.66
S_l3-3*	29.13	34.03
Average	28.38	35.60

*S_l3-1, S_l3-2, S_l3-3 are the same sample films comprised of only the small latex particles with linear polymer chains but different specimens, which are annealed at 144 °C for 30 min.

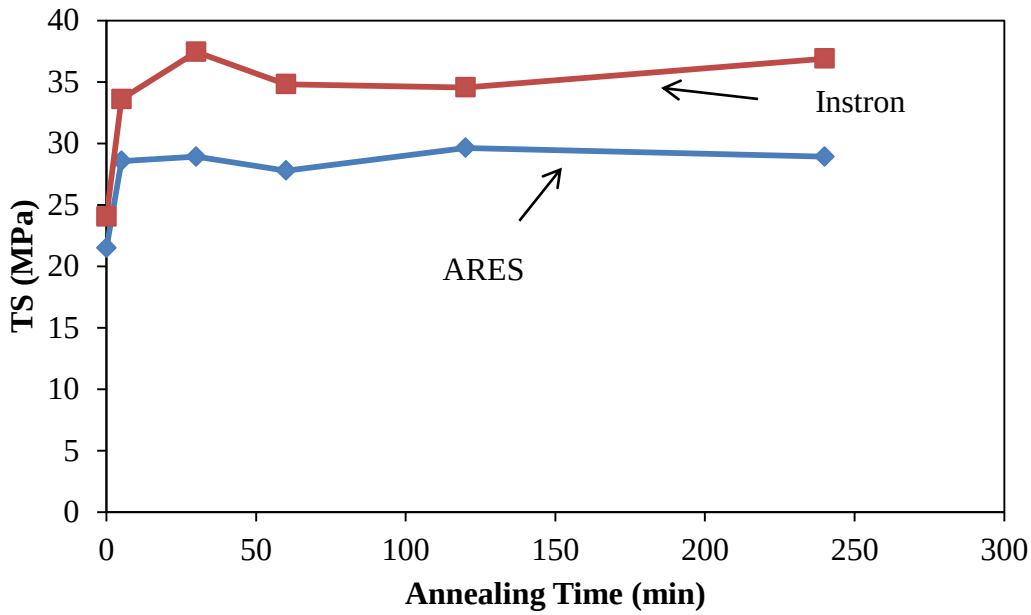

Figure 2.11: Tensile strength *vs* annealing time for the S_l3 sample with the same composition via Instron at room temperature (RT) and ARES at 90 °C.

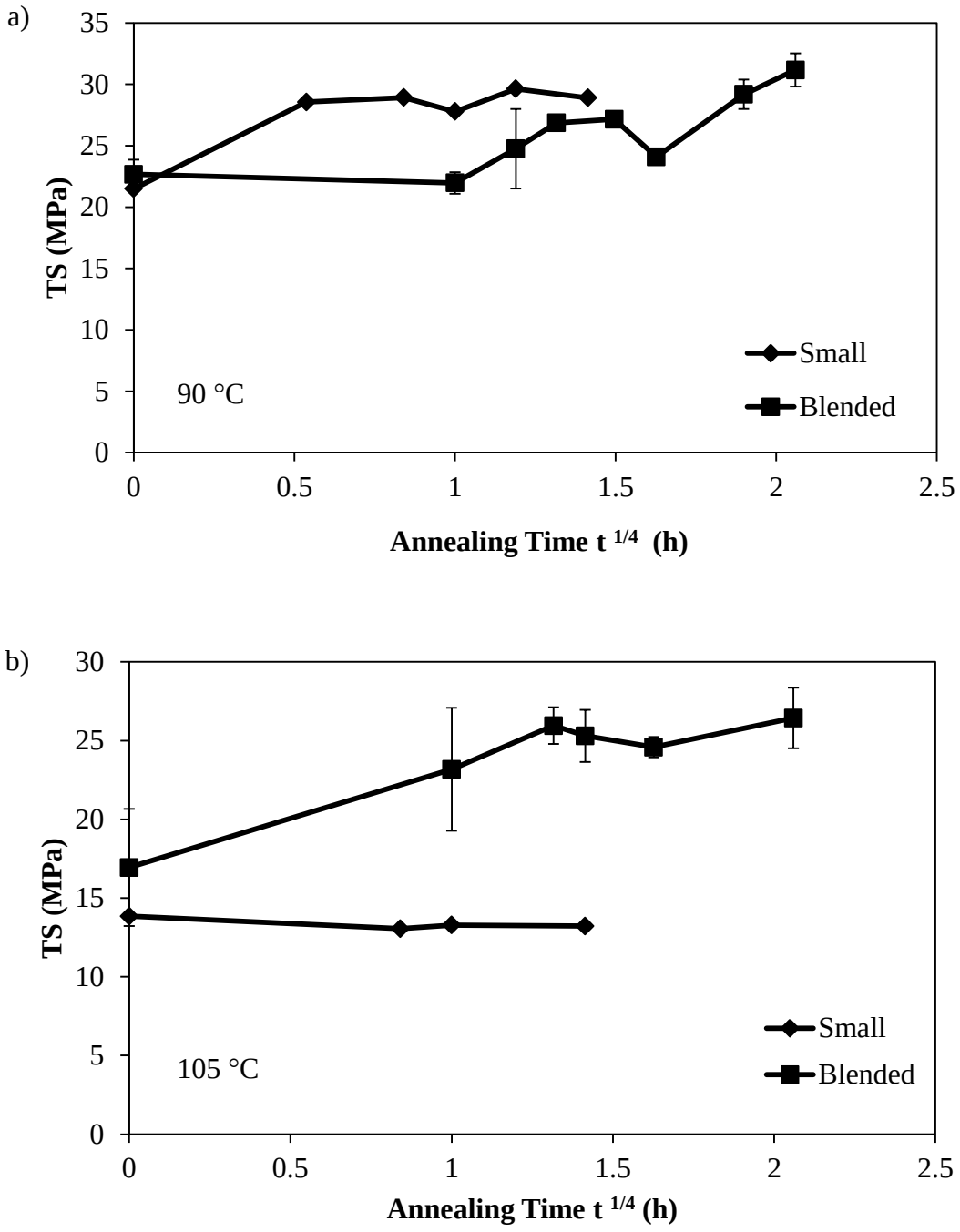

Figure 2.12: a) Tensile strength at 90 °C vs (annealing time)$^{1/4}$ for films comprised of large/small latex particles with a blend ratio of 76: 24 by weight, annealed at 165 °C. b) tensile strength at 105 °C *vs* annealing time for the same blended films annealed at 165 °C.

does not change the trend of the tensile strength *vs.* annealing time when the operating temperature increases (Figure 2.11). The increase in operating temperature decreases the film tensile strength, because the tensile strength obtained from the ARES at 90 °C is lower than that from the Instron at room temperature. At a higher temperature, polymer chains move more easily and rearrange themselves so that more chain pullouts take place upon film fracture.

In addition, Figure 2.12 shows that only when the testing temperature is increased to approximately T_g (105 °C) of polystyrene can the crosslinking effect be recognized. Under such conditions almost all free non-crosslinked chains are movable and rearrange to align along the stress direction, leaving the crosslinked chains fixed in their position to increase the macroscopic film strength. This is a condition similar to the strength test taken at room temperature for the low T_g films (T_g is close or lower than room temperature), in which low T_g polymer chains are free to move and able to rearrange themselves.

2.4 References

1. Flory, P.J.; Rehner, J.; *J.Chem.Phys.;* **1943**, *11*, 521
2. Coleman, M. M.; Graf, J. F.; Painter, P. C. *Specific Interactions And the Miscibility of Polymer Blends*, Technomic Publishing Company, Inc. **1991**, Page 17
3. Van Krevelen, D. W.; *Properties of Polymers, Correlations with Chemical Structure 2nd ed*. Elsevier Amsterdam, **1976**
4. Tobing, S.; Klein, A. *J. Appl. Polym. Science*; **2001**, *79*, 2230.

CHAPTER 3

Synthesis and Characterization of Model Large and Small Polystyrene Latex Particles

Abstract

In this chapter, the synthesis of carboxylated crosslinked large polystyrene (PS) latex particles with different carboxyl functionality distributions as well as different crosslinking density distributions was investigated using different polymerization methods, such as batch, semi-batch and seeded-batch polymerization. All of the polymerization methods resulted in mono-disperse particles. However, due to the hydrophilicity of the carboxyl group the semi-batch polymerization method proved to be not a very successful method to provide a uniform distribution of carboxyl functionalities with a high percentage of incorporation in the PS particles. An amino-functionalized methylstyrene monomer derivative was synthesized to copolymerize with styrene to provide amine functionality to the polystyrene particles. Only batch polymerization was used to make the small PS particles. Polystyrene particles with different molecular weights was also synthesized and characterized for the study of molecular weight effects on film performance.

3.1 Introduction

To do a fundamental study on the influence of molecular parameters on latex film performance, each parameter (such as particle size, molecular weight, crosslinking density, and concentration of functional groups) should be able to be independently controlled and individually taken into account. A model latex particle should have at least the following requirements: 1) the particle size should be monodisperse; 2) a range of particle sizes should be available; 3) polymer molecular weight, crosslinking density, and concentration of functional groups should each be controllable and not affect the particle sizes. A successful preparation of model latex particles is crucial to the study of film formation and for achieving reliable conclusions.

Specifically, concerning the particle packing effect, non-crosslinked large and small polystyrene particles with monodisperse size distributions and similar molecular weights were prepared; regarding the molecular weight effect, linear polystyrene particles with controllable molecular weights and controllable particle sizes have been prepared. In terms of the crosslinking effect, it is the aim to apply the optimum packing ratio and optimum molecular weights in the study of crosslinking based on the study of the previous two effects. Therefore, the preparation of two functionalized polystyrene particles is required with controllable particle size, functional group concentration, crosslinking density (for the crosslinked ones) and molecular weights (for the noncrosslinked ones).

Regarding the pair of functional groups selected for the chemical crosslinking study, acrylic acid (AA) or its derivatives is chosen to be one of the two functional

moieties, such as methacrylic acid (MAA), because the C=C bond can be used to copolymerize with styrene monomer and the carboxyl group is capable of reacting with various functional groups. Among all acrylic monomers, MAA is primarily considered because it is the most common derivative of AA and more hydrophobic than AA itself. Its relatively higher oil-solubility and higher reactivity with styrene reduce its tendency to form homopolymers in the aqueous phase, thus it will give a relatively higher level of incorporation of carboxyl groups into the latex particles.

Concerning the other functionality, the amino moiety was the choice. The main reason to choose the carboxyl-amine reaction over other reactions is that this acid-base reaction will not easily happen in the absence of catalysts, unless heat is applied. Therefore, the chemical crosslinking reaction can be controlled by controlling temperature to prevent any premature cross-linking during film sintering process. More analysis details of this acid-base reaction can be found in Chapter 5.

3.2 Experimental

3.2.1 Materials

Styrene (J.T. Baker) monomer was distilled at 50 ℃ and a reduced pressure of 40 mm Hg to remove the inhibitor and any oligomers. Sodium lauryl sulfate (SLS; MP Biomedicals, Inc.), Aerosol MA-80 (AMA, sodium di-hexyl sulphosuccinate; Cytec Industries), Triton X-100 (nonionic, octylphenol ethoxylate (9.5EO); Dow Chemical), potassium persulfate (KPS; Fisher Scientific), azobisisobutyronitrile (AIBN, Aldrich) and

sodium bicarbonate ($NaHCO_3$; Mallinckrodt Baker) were used as received. Potassium hydroxide (KOH; Fisher Scientific) was ground into powder from pellets. Carbon tetrachloride (CCl_4; Fisher Scientific), 0.02N standard sodium hydroxide solution (NaOH; J.T. Baker) and 0.0200N standard hydrochloric acid (HCl; J.T. Baker) were also used as received, as well as isopropenyl dimethyl benzyl isocyanate (TMI, Cytec Industies), dibutyltin dilaurate (Aldrich) , butyl cellosolve (Alfa Aesar), isobutyric acid (Aldrich), heptanoic acid (Aldrich), hydroxyl propyl methacrylate (HPMA, Polysciences Inc.), N-succinimidyl 3-(2-pyridyldithio)-propionate SPDP, VWR), D,L-dithiothreitol (DTT, Aldrich) and 4-Dimethylaminopyridine (DMAP, Aldrich).

3.2.2 Latex Cleaning

Some of the small latex particles were synthesized using the non-ionic surfactant Triton X-100, and thus these latexes were cleaned by using methanol and hot water[1]. However, this caused instability of the latexes. This was acceptable for latex films comprised of only one kind particle, but was not acceptable for films made of latex blends, which requires stable cleaned latexes for blending. Therefore, most of the latex preparations avoided using Triton X-100 in the recipes and only used ionic surfactants instead. The latexes were then cleaned by the serum replacement when clean latexes were needed. Deionized water was pumped through the serum replacement cell until the outlet serum conductivity became approximately equal to the conductivity of the inlet stream of the serum replacement cell.

3.2.3 Characterizations

The particle size and the particle size distribution were measured by dynamic light scattering (Nicomp Submicron Particle Sizer; Model 370, Pacific Scientific), and Scanning electron microscope (SEM; Model 4300, Hitachi). Gel permeation chromatography (GPC; Waters 515 HPLC pump/ Waters 201 differential refractometer) was employed to measure the molecular weight of the latex polymers. Fourier transform infrared spectroscopy (FT-IR, Satellite) and nuclear magnetic resonance (NMR, Bruker 500 MHz) were used to characterize the extent of purification of the synthesized monomers. FT-IR and conductometric titration were utilized together for the determination of carboxyl functionality distribution, while UV-vis was used for the determination of surface amine functionality.

Differential scanning calorimetry (DSC, Model 2920, TA instruments) was used to obtain the T_g of copolymers. Molecular weights between crosslinking points, M_c (or ρ_c, the crosslinking density, $\rho_c = \rho_p / M_c$, ρ_p is the density of the polymer) were obtained by direct swelling measurements and indirectly calculated based on the film shear modulus, which was measured using the advanced Rheometric Expansion System (ARES, Rheometric Scientific).

Chapter 2 has included the details for every characterization method.

3.3 Results and Discussion

3.3.1 Preparation of Large and Small Non-functionalized Linear PS Particles

3.3.1.1 Particle Size Control

The particle size was the first molecular parameter that was studied in this work, because it was the basis for studies of any other molecular effects.

Controlling the surfactant and initiator concentration as well as the reaction temperature is the general means to control the particle size *via* emulsion polymerization. Other strategies may also apply, such as the use of seeded batch or seeded semi-continuous polymerization, the use of the mixed surfactants, the change of the solid contents, and the change of the pH or salt concentration. There are a variety of methods available at hand, and combining and adjusting these parameters are part of the fine art in emulsion polymerization. In this section, the purpose is to produce non-functionalized PS latex particles with relatively large sizes in the range from 200 to 400 nm and small sizes in the range from 50 to 100 nm.

Recipes used to prepare large and small polystyrene latex particles are shown in Table 3.1 and Table 3.2. Batch bottle polymerization (everything placed into a tumbled bottle at one time) was used in all cases.

In most cases, the ionic surfactant Aerosol MA-80 was preferred over SLS, because unlike SLS (films turn yellowish), it does not change the color of the latex films during the high temperature annealing process and most importantly, Aerosol MA-80 can provide a more uniform particle size distribution than SLS. On the other hand, SLS

generally provides smaller sized particles than Aerosol MA-80. So if smaller size particles near 50 nm or less are needed, SLS should be chosen as the surfactant instead of Aerosol MA-80 (the minimum particle size the Aerosol MA-80 can produce is approximately 80 nm when the surfactant concentration is far beyond its critical micelle concentration, CMC). Concerning the non-ionic surfactant Triton X-100, it is primarily used to increase the stability of latexes, but the stability is not a problem in the polystyrene system. Besides, it was found that the latex cleaning was more difficult if Triton X-100 was brought into the system. Thus, Triton X-100 is not preferred over the above two ionic surfactants, Aerosol MA-80 and SLS.

Table 3.1: Typical Recipe for Preparation of Large PS Particles and Characterization Results

Ingredient	**Amount (g)**	
Styrene	20.0	8.0
KPS	0.10 (4.63 mM*)	0.04 (9.26 mM*)
Aerosol MA-80	0.940 (30.28 mM*)	0.128 (20.62 mM*)
$NaHCO_3$	0.125 (18.6 mM*)	0.024 (17.8 mM*)
Deionized water	80.0[a]	16.0[b]
Solids	20.9 %	33.6 %
D_N (nm)	211.3	440.8
PDI	1.01	1.01
M_W (g/mol)	1.1×10^6	6.6×10^5
PDI_{MW}	2.1	2.7

* based on water; a: at 50 ℃ for 24h; b: at 60 ℃ for 24h

Table 3.2: Typical Recipe for Preparation of Small PS Particles with Various Surfactants at 60 °C and Characterization Results

Ingredient	**Amount (g)**		
Styrene	16.0	20.0	8.0
KPS	0.90 (10.28 mM*)	0.90 (16.7 mM*)	0.10 (23.1 mM*)
Aerosol MA-80	-	-	0.90 (145 mM*)
$NaHCO_3$	-	-	0.06 or less (44.6 mM*)
SLS	0.54 (5.78 mM*)	2.70 (46.8 mM*)	-
Triton X-100	5.40 (1.67 wt%*)	-	-
KOH	0.13 (7.44 mM*)	0.12 (10.7 mM*)	-
Deionized water	324.0	200.0	16.0
Solids	5.10 %	10.6 %	36.1 %
D_N ** (nm)	49	55	79
PDI	1.06	1.14	1.05
M_W (g/mol)	1.2×10^6	8.4×10^5	1.6×10^6
PDI_{MW}	2.1	2.7	2.1

* based on water;

** D_N: number-average particle size

3.3.1.2 Molecular Weight Control

To study the molecular weight effect on the corresponding film properties, latexes with similar particle sizes and a good control of molecular weight are needed. A number of novel techniques have been reported to control molecular weights and molecular weight distributions of polystyrene, such as electrochemical control by changing the

electric current density[2], control by the addition of polyfunctional monomer[3], atom transfer radical polymerization with activators regenerated by electron transfer[4], and catalytic chain transfer polymerization[5]. However, all of these methods introduce additives into the model system. Varying experimental conditions (e.g., reaction temperature, initiator concentration) or direct emulsification of commercial polymers with narrow disperse molecular weight are able to solve this problem, but the latex particle size is likely to change along with changes in the molecular weight.

Addition of chain transfer agents (CTAs) will provide good control on the average MW and not necessarily change the latex particle size. Table 3.3 shows the sequential recipe used for controlling the MW of PS latex particles with the addition of a chain transfer agent (CCl_4) by batch bottle polymerization.

The characterizations of corresponding latex particle sizes and molecular weights are shown in Table 3.4. The results prove that batch polymerization with the addition of chain transfer agent can modify polymer molecular weights (MWs) and has little effect on particle sizes, but the molecular weight distributions are relatively broad using this synthesis route. However, this is typical for emulsion polymerizations compared to living free radical polymerizations. Since all of the particles used in the present study are emulsion polymerized, this relatively broad distribution is representative. Nevertheless, the amount of CTA cannot be used too much, or it can significantly broaden the distribution of both the particle size and the molecular weight. This effect has been observed when the amount of CTA was charged at a level of more than 10 wt% based on styrene monomer.

Table 3.3: Recipe for Preparation of Polystyrene Latex Particles with Controlled Molecular Weights *via* Batch Bottle Polymerization

Series / Ingredients	CTA-0	CTA-1	CTA-2	CTA-3	CTA-4	CTA-5	CTA-6
St (g)	8.0						
MA-80 (g)	0.9 (145 mM, based on water)						
KPS (g)	0.1 (23.1 mM, based on water)						
$NaHCO_3$ (g)	0.06 (44.6 mM, based on water)						
H_2O (g)	16.0						
CCl_4 *(g)	0 0.0 wt%	0.02 0.2 wt%	0.04 0.5 wt%	0.08 1.0 wt%	0.16 2.0 wt%	0.32 4.0 wt%	0.5 6.3 wt%

* based on styrene monomer

Table 3.4: Particle Size and Molecular Weight of PS Latexes Prepared with Different Amounts of Chain Transfer Agents

	CTA-0	CTA-1	CTA-2	CTA-3	CTA-4	CTA-5	CTA-6
D_N (nm)	79	74	72	74	77	73	81
PDI	1.04	1.08	1.06	1.06	1.05	1.09	1.09
M_N (g/mol)	7.5×10^5	7.1×10^5	5.9×10^5	2.7×10^5	1.8×10^5	1.1×10^5	0.72×10^5
M_W (g/mol)	1.6×10^6	1.8×10^6	1.3×10^6	5.7×10^5	3.6×10^5	2.4×10^5	1.4×10^5
PDI_{MW}	2.1	2.5	2.2	2.1	2.0	2.2	2.0

According to the MW results shown above, a linear trend line can be drawn in the graph (see Figure 3.1) of the inverse number-average degree of polymerization ($1/\overline{X_n}$) *vs.* the amount of chain transfer agent based on monomer concentration ($[CTA]/[M]$),

$$\frac{1}{\overline{X_n}} = \frac{1}{\overline{X_{n0}}} + C_{CTA}\frac{[CTA]}{[M]} \qquad (3.1)$$

in which $\overline{X_n}$ and $\overline{X_{n0}}$ are the degree of polymerization with and without chain transfer agent, respectively; C_{CTA} is the chain transfer constant for CTA. $[M]$ is monomer concentration, while $[CTA]$ is the concentration of chain transfer agent.

According to the experimental data, the chain transfer constant (C_{CTA}) was calculated to be 0.0213, which provided the experimental prediction for the molecular weight control of PS particles by CCl_4. The extension of this relationship was validated using higher amounts of chain transfer agent in the system. Specifically, 8 wt% and 10 wt% of CCl_4 based on styrene monomer were charged. Based on eq 3.1, the predicted number-average molecular weights were 5.8 $\times 10^4$ g/mol (for 8 wt%) and 4.6 $\times 10^4$ g/mol (for 10 wt%), which were very close to the measured values (6.1 $\times 10^4$ g/mol for 8 wt% and 4.2 $\times 10^4$ g/mol for 10 wt%).

Therefore, by using chain transfer agents, a broad range of molecular weights with similar sized latex particles can be produced, which is essential to the study of the molecular weight effect on the film performance.

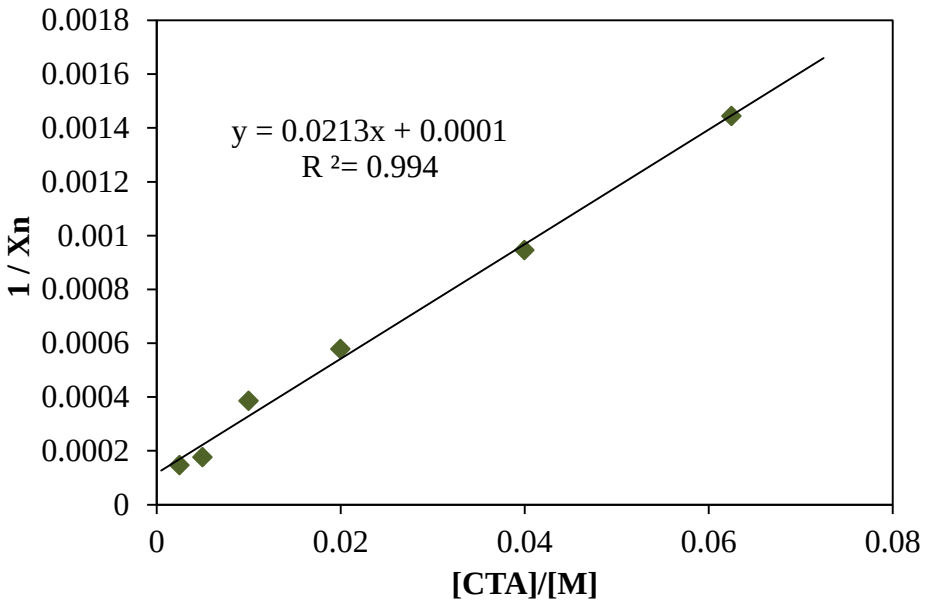

Figure 3.1: Relationship between inverse degree of polymerization and chain transfer agent amount based on the monomer concentration.

Another interesting parameter of particles with linear polymer chains is the entanglement molecular weight, M_e, of the polymer chains, which determines the lower bound above which the polymer chains can be entangled. There are two techniques that can be used to calculate M_e: one is based on a dynamic mechanical measurement and the other is the plasticizer model.

In terms of dynamic mechanical measurement, M_e can be estimated from the rubbery plateau modulus (G_n^0) as follows[6]:

$$M_e = \frac{\rho RT}{G_n^0} \tag{3.2}$$

in which ρ is the density of the polymers, R is the gas constant, T is the temperature in Kelvin in which G_n^0 is located, and G_n^0 is determined from the storage modulus G' at the onset of the rubbery region.

Figure 3.2 shows a typical DMA modulus data of a sintered polystyrene sample film (see Chapter 2 for more details on the setup of the DMA measurement). The rubbery plateau modulus is approximately 1.84×10^5 Pa, therefore, the entanglement molecular weight of the sintered PS film was calculated to be 2.0×10^4 g/mol.

On the other hand, analogous to the plasticizer model designed for compatible rubber / tackifier or rubber / oil blends[7], the low molecular weight components in polymer chains can act as plasticizers. Therefore, by making comparison with the monodisperse polystyrene $M_{e,monodisperse}$, M_e for the polydisperse sample would follow the relationship:

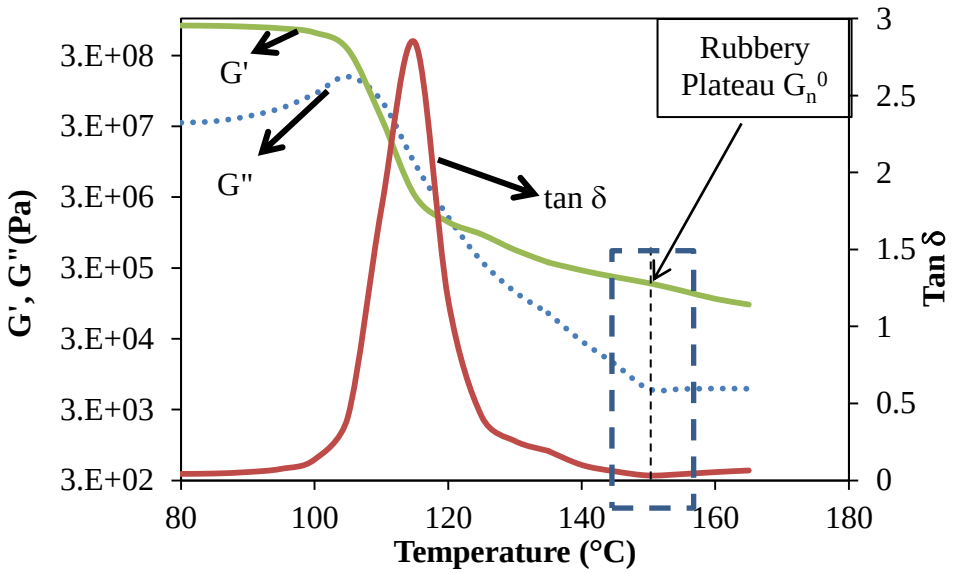

Figure 3.2: Temperature sweep DMA modulus results of a sintered latex film comprised of linear polystyrene particles with M_W=8.2 × 10^5 g/mol, M_N=4.5 × 10^5 g/mol. G': storage modulus; G": loss modulus; tan δ: phase angle.

$$M_{e,polydisperse} = \frac{M_{e,monodisperse}}{\varphi^{2.3}} \quad (3.3)$$

in which φ, for the gel-free polydisperse sample, is considered to be the weight fraction of polymer chains that have the molecular weight greater than monodisperse M_e. φ can be determined by GPC cumulative molecular weight distribution (see Figure 3.3).

Figure 3.3 shows two typical GPC results of the synthesized PS samples. If the molecular weight of the polymers is large enough, the value of φ is 100%, because all of the polymer chains have molecular weights larger than $M_{e,monodisperse}$ (Figure 3.3a). The M_e of the sample is equivalent to the M_e in monodisperse polystyrene which is close to 32,000 g/mol[8]. If the molecular weight is smaller, there will be some fraction of chains that contribute as a plasticizer to the system, which will therefore increase the M_e of the samples (Figure 3.3b).

Comparing the values obtained from the above two methods, the DMA estimated value is generally smaller than the one calculated from the plasticizer model.

3.3.2 Preparation of Carboxylated Crosslinked Large PS Particles

To create a design for the synthesis of poly(St-co-MAA) latex particles, two aspects need to be taken into consideration: 1) particle size control is needed; and 2) there is a strong dependence on functional group concentrations in the chemical cross-linking mechanism, so functional group distribution control is also needed. On the other hand, in preparing crosslinked gel particles, the amount of crosslinking as well as the distribution of the crosslinking should be considered. In this work, divinylbenzene (DVB) was chosen

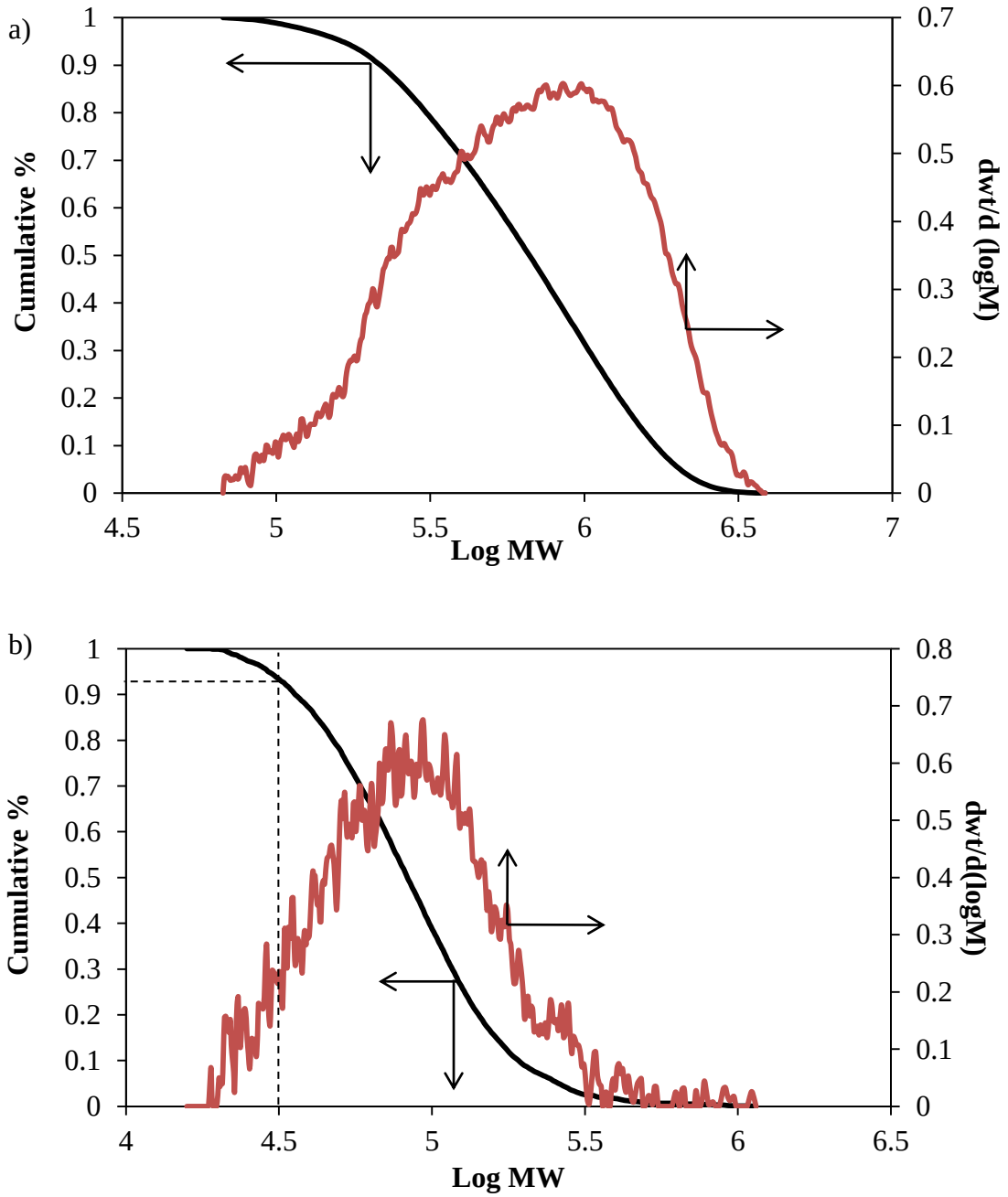

Figure 3.3: GPC data of a) THF dissolved polystyrene latex samples with Mw = 8.2 × 10^5 g/mol; b) THF dissolved polystyrene latex samples with Mw = 1.1 × 10^5 g/mol. The calculated M_e in (a) is 32,000 g/mol, and the M_e in (b) is 36,000 g/mol.

to be the primary control of the crosslinking density in the system, which is the external crosslinker that has been widely used for crosslinking styrene monomer. However, there is another influence on the crosslinking density, which is the hydrogen bonding within the carboxylic acid dimers (Scheme 3.1). This partially reversible contribution is more significant at room temperature than at higher temperatures, because it is found that the intensity of carbonyl C=O stretching in the acid dimer decreases as the temperature increases[9]. Therefore, the crosslinking density of carboxylated crosslinked PS particles measured by the swelling measurement at room temperature is a contribution of two interlinkings: permanent DVB covalent bonding and partially reversible carboxylic acid hydrogen bonding.

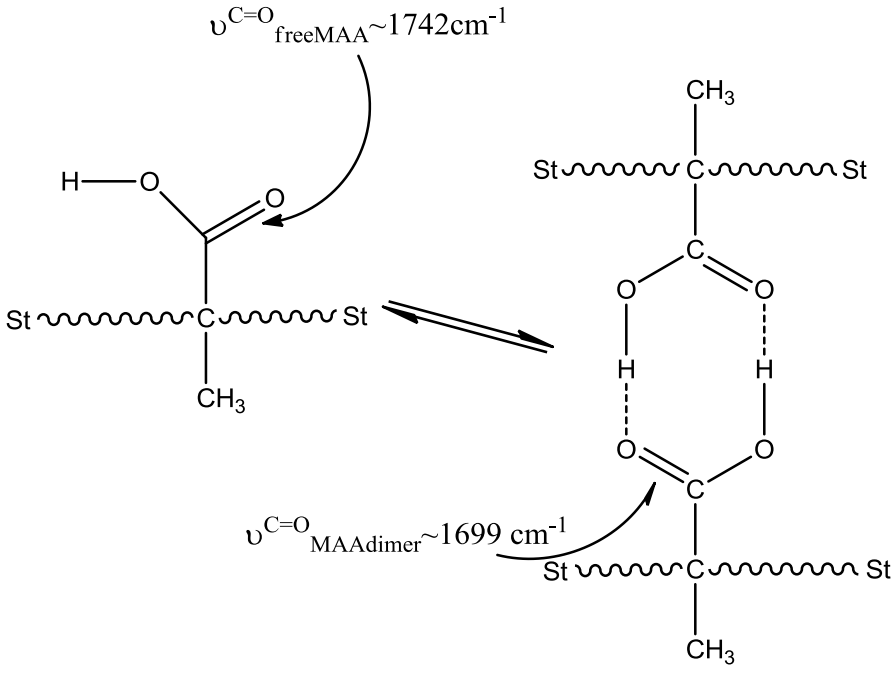

Scheme 3.1: The free MAA and MAA dimer transformation[9].

3.3.2.1 Synthesis *via* Batch Polymerization

The batch polymerization of St-co-MAA was first tried without the external crosslinker DVB, to see to what extent crosslinking by hydrogen bonding could be provide. Table 3.5 shows the recipe for copolymerization of St and MAA by batch bottle polymerization. The increased glass transition temperature indicates the incorporation of MAA into the PS particles, which can be further confirmed by the FT-IR spectrum of cleaned and dried latex (Figure 3.4).

However, based on the results for the gel content, only at higher MAA amounts (more than 40 wt%) could the gel content due to hydrogen bonding be precisely detected. Because a higher amount of MAA incorporation will change the PS latex properties dramatically, to maintain the properties of polystyrene, adding DVB into copolymer systems to obtain a reasonable amount of crosslinking is preferred.

Table 3.6 gives the recipe for the copolymerization of styrene and methacrylic acid in the presence of DVB as the crosslinker, as well as the resulting particle size and the gel content.

From the results, the gel contents of the samples with the amount of DVB varied from 0.1 wt% to 2.0 wt% are all close to 90%, which indicates that 0.1 wt% DVB is sufficient to give a tightly crosslinked network. Considering that tight crosslinking would have the chance to distort the particle morphology due to phase separation (see comparison in Figure 3.5), later in the following preparations of crosslinked particles, the DVB amount was kept under 0.1 wt%.

Table 3.5: Recipes and Characterization for the Bottle Batch Copolymerization of Styrene and Methacrylic Acid 60 °C

Series / Ingredients	Co-1	Co-2	Co-3	Co-4	Co-5
St (g)	9.00	8.00	7.00	6.00	5.00
MAA (g)	1.00 10 wt%*	2.00 20 wt%	3.00 30 wt%	4.00 40 wt%	5.00 50 wt%
KPS (g)	0.03 (1.23 mM**)				
MA-80 (g)	0.04 (1.15 mM**)				
H_2O (g)	90.0				
T_g (℃)	123.19	142.25	157.34	160.87	165.72
Gel content in THF	-(1)	-(1)	-(1)	20.4%	21.3%

*: based on the total monomer weight; **: based on water. (1): gel content is too small to be measured.

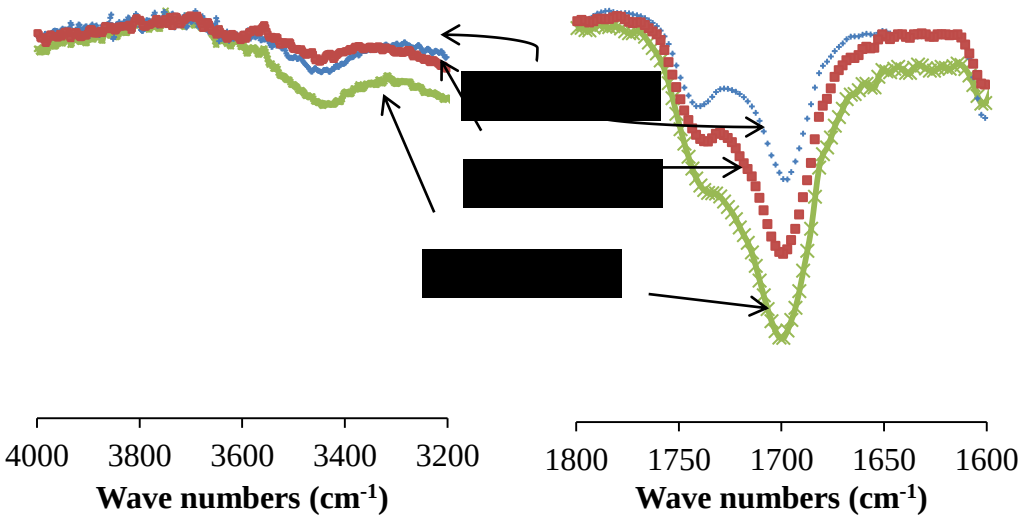

Figure 3.4: FT-IR spectra of poly(St-co-MAA) copolymers with different MAA amounts in the initial preparation recipe were compared. The higher the initial amount of MAA, the higher intensity the carbonyl peak is in final latex polymers.

Table 3.6: Recipes for Batch Bottle Polymerization of Styrene and MAA Using DVB as Crosslinker & Characterization Results

Series / Ingredients	Cro-1	Cro-2	Cro-3	Cro-4
St (g)	8.80	8.97	8.98	8.99
DVB (g)	0.200 (2.0 wt%*)	0.035 (0.35 wt%)	0.02 (0.2 wt%)	0.01 (0.1 wt%)
MAA (g)	1.07 (10 wt%*)	1.00 (10 wt%)	1.00 (10 wt%)	1.00 (10 wt%)
KPS (g)	0.03 (1.39 mM**)	0.03 (1.85 mM)	0.03	0.03
MA-80 (g)	0.04 (1.29 mM**)	0.04 (1.72 mM)	0.04	0.04
H_2O (g)	90	60	60	60
Gel content in THF	88.1%	85.6%	87.0%	86.6%
D_N (nm) by SEM	173	230	233	178
PDI	1.121	1.004	1.004	1.006

* based on styrene monomer; ** based on water

To make large carboxylated crosslinked particles with a range of particle sizes, decreasing surfactant or initiator concentrations was found to be insufficient. Therefore, surfactant free batch polymerization was used to make larger latex particles (monodisperse with size range from 280 nm~ 400 nm) (Figure 3.6).

Table 3.7 presents the recipe for the surfactant free emulsion polymerization with various MAA and DVB amounts. Although the FT-IR spectra (Figure 3.7) show the incorporation of MAA into the latex particles by detecting the typical carbonyl peak at approximately 1700 cm^{-1}, it shows almost no peak in the hydroxyl group stretching area (3300 ~ 3500 cm^{-1}), compared to Figure 3.4. A possible reason may be attributed to the formation of carboxylic acid anhydride among surface carboxylic acid groups[10]. The absence of hydroxyl group peaks indicates that more COOH groups are present on the surface of latex particles adjacent to each other, stabilizing the particles in the absence of the surfactant Aerosol MA-80. Figure 3.4 does show some OH stretching peak. The presence of OH peak is probably due to the existence of hydrophilic groups from the surfactant on the particle surface, which helps to prevent the two carboxyl groups from reacting with each other and losing water.

3.3.2.2 Synthesis *via* Other Polymerization Methods

Since batch polymerization only produces one kind of carboxylated crosslinked particles, the purpose of applying other polymerization methods is to intentionally design the particle structure with a controllable carboxyl group distribution as well as various crosslinking density distributions. It is worth mentioning that only batch polymerized particles were used as the large carboxylated crosslinked particles for blended film studies. The particles produced by the next two polymerization methods brought more complexities to the latex film system. However, hopefully by introducing them here, a useful reference is provided for further related studies.

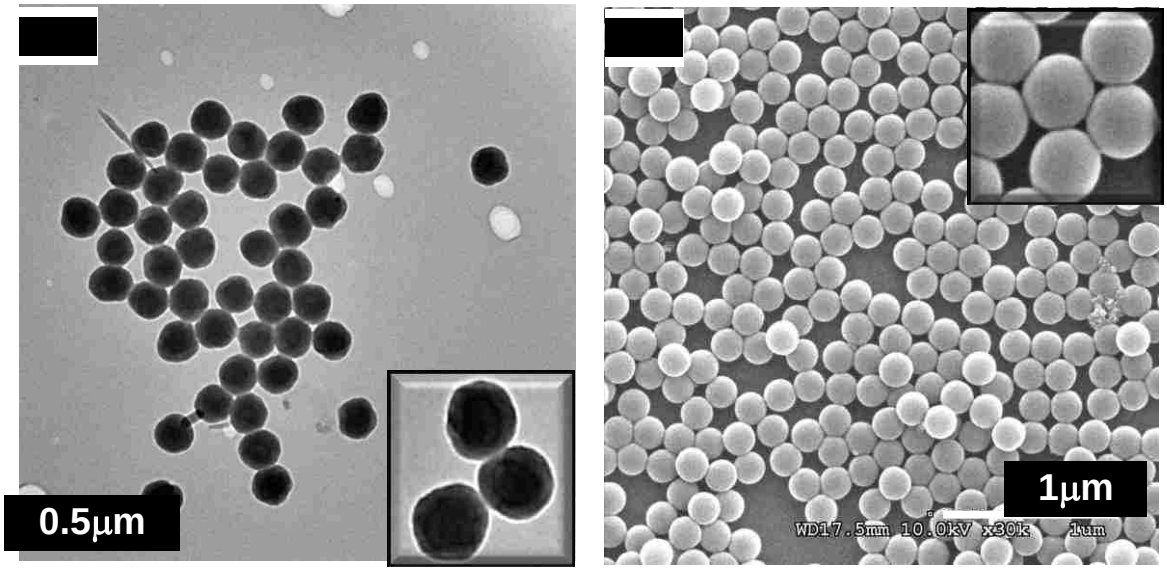

Figure 3.5: a) TEM image of poly(St-co-MAA) copolymer particles with 2 wt% DVB; b) SEM image of Poly(St-co-MAA) copolymers with 0.2 wt% DVB.

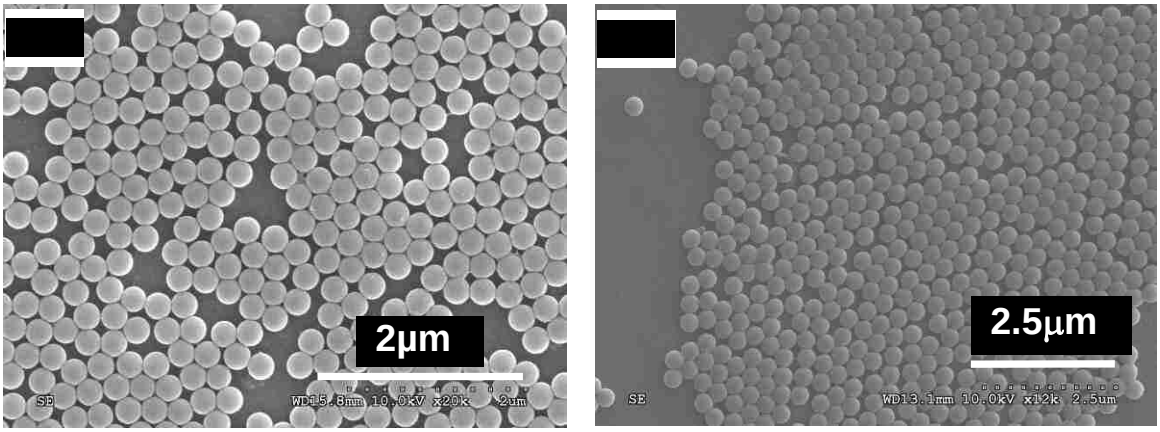

Figure 3.6: SEM images of monodisperse latex particles *via* surfactant free batch polymerization of Styrene and MAA with presence of a) 0.1 wt% (based on the total monomer), and b) 0.05 wt% DVB.

Table 3.7: Recipes for Surfactant Free Batch Polymerization of Styrene and MAA with Various Amount of DVB & Characterization Results

Series / Ingredients	SF-1	SF-2	SF-3	SF-4
St	7.98	7.99	7.99	8.00
DVB(g)	0.0205 (0.2 wt%*)	0.0126 (0.1 wt%)	0.0045 (0.05 wt%)	0.0084 (0.1 wt%)
MAA(g)	0.80 (9.1 wt%*)	0.80 (9.1 wt%)	0.80 (9.1 wt%)	0.40 (4.8 wt%)
KPS(g)	0.04 (0.926 mM**)	0.04 (0.903mM)	0.04 (0.897 mM)	0.05 (1.157 mM)
H_2O(g)	160	164	160	160
D_N (nm) by SEM	291	251	279	293
PDI	1.003	1.004	1.007	1.003
ϕ ***	26.13%	18.89%	14.02%	9.86%
M_c ***	4.2×10^3	9.2×10^3	1.8×10^4	3.8×10^4

* based on monomer; ** based on water; *** ϕ is the volume fraction of polymer in the solvent; M_c is the average molecular weight between crosslink points

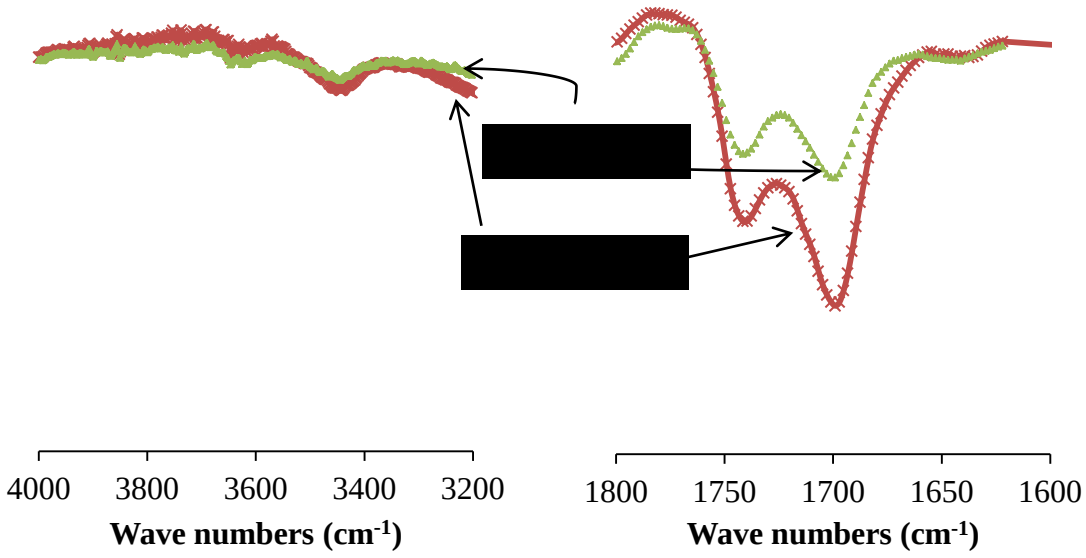

Figure 3.7: FT-IR spectra of poly(St-co-MAA-DVB) with two MAA incorporation amounts in the initial recipes (SF-3 and SF-4) by surfactant free batch polymerization were compared

3.3.2.2.1 Synthesis *via* Seeded Batch Polymerization

As the name suggests, seeded batch is to grow polymer particles from the prepared seeds. By varying the properties of the seed, as well as controlling the feed properties, particles comprised of layers with different properties can be produced.

Here, loosely, tightly, and no crosslinked PS seed particles were parepared and then swollen with the feed monomers for 4 hours. The initiator AIBN was added to initiate the polymerization. Table 3.8 shows the basic recipe variations for the seeded batch polymerization with different crosslinking distribution designs. Figure 8a shows the particle morphology with AIBN as the initiator *via* SEM.

The reason AIBN was used as the initiator, instead of KPS, is because of its hydrophobicity. Oil soluble initiator AIBN has a preference to partition inside the seed particles to initiate the polymerization, so that more uniform particles can be generated; while water soluble initiator KPS prefers to stay in the aqueous phase, so that the secondary nucleation is more likely to be occurred (see Figure 3.8b for comparison. Except for the initiator, all parameters are the same for each sample preparation: SB-H, SB-L, SB-N).

Although it has been shown that monodisperse particles can be made via seeded batch polymerization, it remains a significant challenge to characterize the distribution of various crosslinking densities. Up until now, there is no direct way to measure the crosslinking density distribution within the particles, but some indirect measurements may provide help in the characterization, such as detecting the diffusion coefficient *via*

Table 3.8: Recipes for Seeded Bottle Polymerization with various DVB amounts at 70 °C

	Seed	Momomer for swelling			One shot feed	
		St (g)	MAA(g)	DVB(g)	AIBN(g)	H_2O(g)
SB-H	M_c =1.6×10^4 g/mol Solids:3.73 % 50g St-MAA-DVB	1.87	0.1	-	0.0045 (0.69 mM)	48.0
SB-L	M_c >>1×10^5 g/mol Solids:11.94 % 20g St-MAA-DVB	2.39	0.12	-	0.0055 (0.45 mM)	75.0
SB-N	Solids:2.67 % 50 g St-MAA	1.34	0.07	0.0013	0.0030 (0.91 mM)	20.0

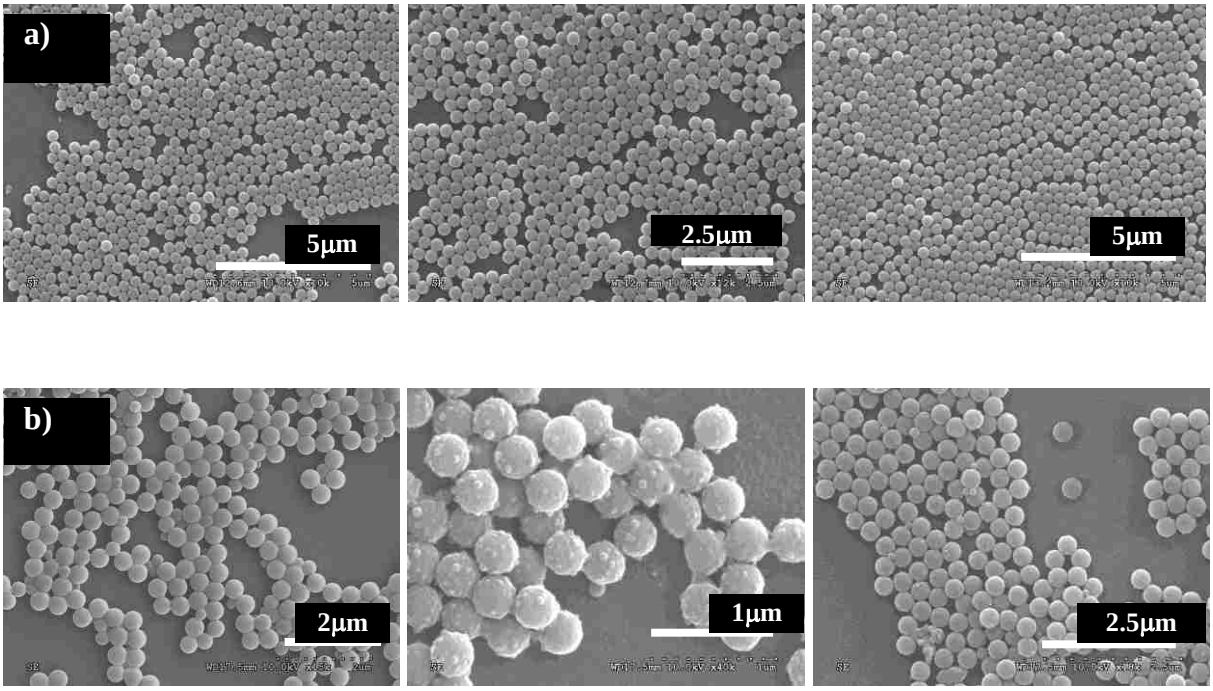

Figure 3.8: SEM images of latex particles of sample SB-H, SB-L, SB-N with a) AIBN as the initiator; b) KPS as the initiator.

small angle neutron scattering and introducing a labeled crosslinker. Due to lack of reliable characterization methods, it is only provided here the potential synthesis route that can be used to design particles with various distributions of crosslinking density.

3.3.2.2.2 Synthesis *via* Semi-continuous Polymerization

In Section 3.3.2.1, it was already shown that batch polymerization is sufficient to prepare polystyrene latexes with narrow particle size distributions, but it is not able to control the carboxyl group distribution within the particles. Semi-continuous polymerization is well known for its ability to prepare structured latex particles. The motivation driving the development of a semi-continuous process is to make monodisperse large particles with a uniform distribution of carboxyl functionalities.

Tang reported in his dissertation[11] a well-designed semi-continuous process to prepare carboxylated PS latexes with monodisperse particle sizes. However, he only made the core-shell structure with a very thin 3nm copolymer layer by adding the styrene and MAA monomer mixture at the end of the feeding stage, thus he was only able to control the surface concentration of the carboxyl groups in the particles.

However, for MAA evenly distributed throughout the PS particles, applying a starved semi-continuous copolymerization can help but will be faced with several challenges: 1) styrene (St) polymerizes so slowly, such that a true starved condition is hard to be achieved; 2) MAA is more hydrophilic and has a much higher propagation rate than St, which means there is little driving force for MAA to be located inside the PS particles and thus MAA prefers to quickly polymerize in the aqueous phase; 3) to prepare larger latex particles (larger than 300 nm), larger seeds are needed. The larger the seed

size, the slower the polymerization rate will be, which can make the feed rate too low to be feasible.

To make the starved feed rate feasible, raising the reaction temperature to increase the styrene polymerization propagation rate constant is primarily considered. 85°C was chosen to be the reaction temperature, which is a reasonably high temperature without a compensation of losing too much water medium by evaporation.

For the experimental design, there are several things worth considering:

1) The decomposition rate constant of the initiator KPS.

   According to the Arrhenius equation:

$$k_d = k_0 e^{\frac{-\Delta E}{RT}} \tag{3.4}$$

   in which k_d is the decomposition rate constant, k_0 is pre-exponential factor. ΔE is the activation energy, R is the gas constant and T is the temperature in degree Kelvin.

   The decomposition rate constant for KPS at 85 °C is calculated to be close to 6.65 $\times 10^{-5}$ s^{-1}. Therefore, the half-life of KPS at 85 °C is then calculated to be 3 hours.

   It is decided not to charge too much KPS in the initial seed preparation step, otherwise a small seed will be produced for the later polymerization and the final particle size will be smaller. On the other hand, the concentration of KPS in the system should be sufficient during the polymerization process to provide a high conversion. By monitoring the batch polymerizations, the minimum concentration

of KPS needed in the system can be estimated without affecting the conversion, which is approximately 0.5 mM. With this value and the half-life of KPS at hand, the time and the amount of KPS needed to be fed into the system during polymerization process can be estimated.

2) The feeding rate towards "monomer-starved" condition

Because monomer-starved conditions are hard to achieve for styrene polymerizations, the feed rate can only be slowed close to the styrene polymerization rate. MAA has a much higher polymerization rate than styrene, thus only the styrene polymerization rate needs to be considered. Based on the classic reaction rate equation:

$$R_p = k_p[St][R\cdot] \tag{3.5}$$

in which [R·] is the radical concentration.

At a quasi-monomer-starved condition, the monomer is assumed to be consumed fast enough such that there will be no monomer droplets in the aqueous phase. Then the feed rate is determined by the polymerization rate inside the particles. Based on a reasonable assumption for the monomer partition in polymer particles (20 % volume based[12]) for a monomer starved condition, the ideal feed rate can be calculated at 85 °C.

3) Surfactant concentration

Since large particles need to be produced, the surfactant concentration in the aqueous phase should be kept as low as possible. Besides, the MAA can also

serve as a stabilizer at the PS particles surface. The surfactant concentration was kept low at 1.2 mM (an empirical number based on batch polymerization results), just enough to prevent coagulation during the polymerization process.

Here a typical recipe was used for preparing carboxylated crosslinked particles *via* semi-continuous polymerization (see Table 3.9). The particle sizes obtained under these conditions are monodisperse with a range from 200 to 250 nm and the polydispersity index (PDI) is less than 1.02.

3.3.2.3 Characterization of Carboxyl Functionality

The two techniques for the characterization of carboxyl functionality distributions were combined: FTIR for detecting the total MAA incorporation and conductometric titration for detecting the MAA distribution within the particles (see Chapter 2 for more details of the characterization methods themselves).

For the quantitative IR analysis, a calibration curve of various known MAA incorporation amounts needed to be built. Bulk copolymerizations (with AIBN as the initiator) of styrene and MAA with the amount varying from 1 wt % to 10 wt% were performed. The solid products were totally dissolved in THF solvent before the IR test. Cleaned THF was used as the background scan. Since the relative molar concentrations of two species are directly proportional to the amount of infrared energy that absorbs at their characteristic wavelengths, the absorbance ratio between the peak at 1497 cm^{-1} for styrene and the peak at 1700 cm^{-1} for methacrylic acid was measured. The calibration curve is shown in Figure 3.9.

Table 3.9: Recipe for Semi-continuous Polymerization of Carboxylated Crosslinked PS

	Monomer Mixture 5 g total amount			KPS (g)	SLS (g)	H_2O (g)	Reaction Time (h)	Feeding Rate (mL/h)	
	St 4.75 (g)	MAA 0.25 (g)	DVB 4.75e-3 (g)					Ideal	Real
Seed *in situ*	20% monomer			0.05 2.06 mM	0.03 1.16mM	90	2	-	-
Feed	80% monomer			3.3e-8[(1)] mol/s after 6h feeding	-	-	9	0.022	0.5[(2)]

(1) After the 2 h seed preparation step and 6 h feed time, the KPS solution was fed into the system for 1 h to ensure enough initiator for the polymerization.
(2) Real feed rate is 2 times faster than the ideal case, but no obvious secondary nucleation was observed.

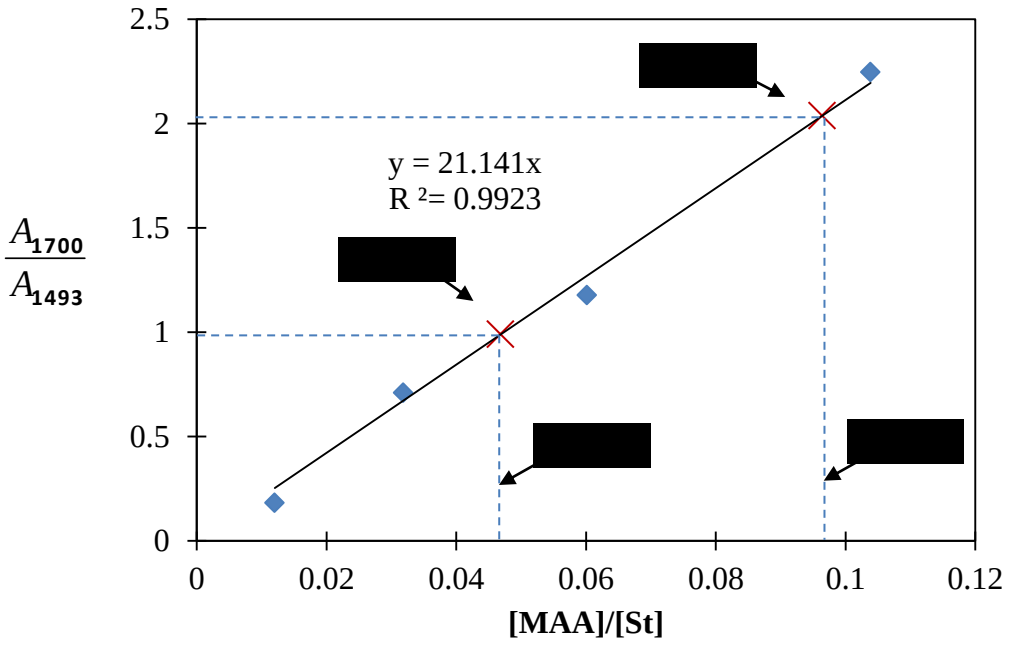

Figure 3.9: Calibration of FT-IR absorbance ratio of peak at 1700 cm^{-1} and peak at 1493 cm^{-1} *vs.* MAA concentration based on styrene monomer.

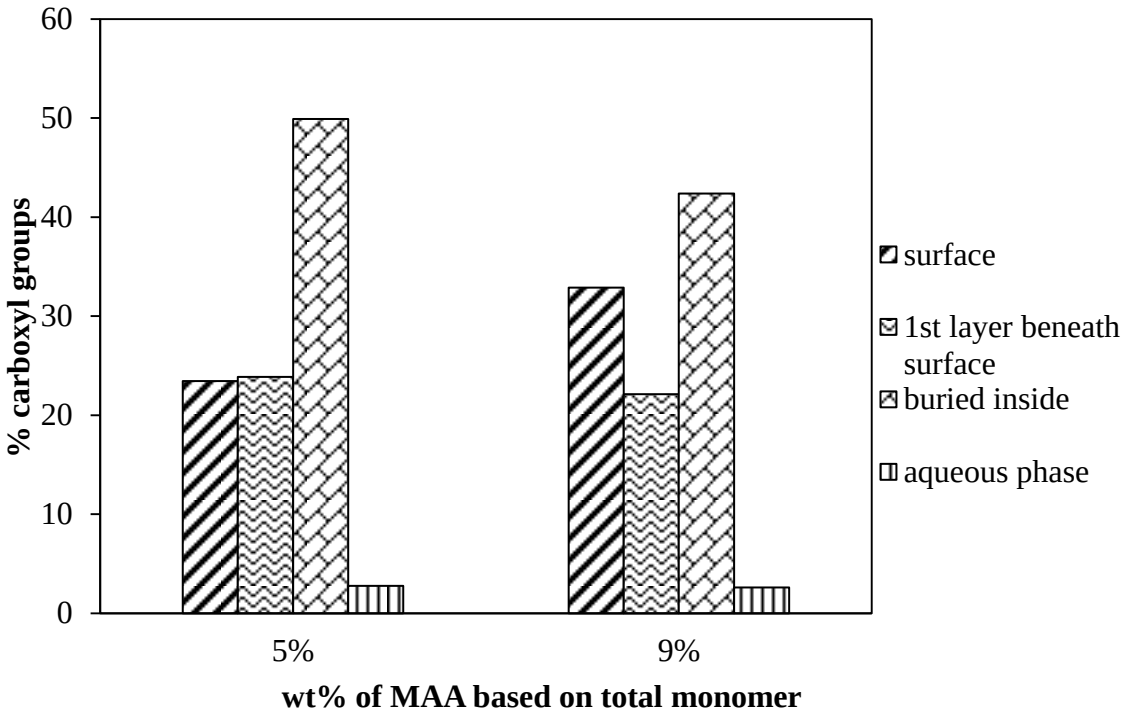

Figure 3.10: Carboxyl group distribution for surfactant free batch polymerization of St/MAA latexes *vs.* wt% MAA in total monomers. The "1st layer" is the portion of functional groups back titrated 5 minutes after adding excess NaOH solution.

Cleaned latex samples SF-3 and SF-4 prepared *via* surfactant free batch polymerization are used as examples. Based on the curve, it was determined that the 93.4% of the MAA was incorporated inside the SF-3 latex particles (with 5 wt% MAA on monomer), and 96.7% of the MAA was incorporated in the SF-4 sample (with 9 wt% MAA monomer). The greater the initial amount of MAA, the larger the amount of carboxyl groups incorporated into the latex particles.

The quantitative distribution of carboxyl groups on the surface and inside the particles of Samples SF-3 and SF-4 sample were determined by back conductometric titration, as shown in Figure 3.10. The greater the initial amount of MAA, the more the carboxyl groups stay on the surface of the particles than are buried inside. The different surface concentrations of carboxyl groups indicates that simply by batch polymerization method, the particle surface coverage by the carboxyl groups can be controlled.

Concerning the particles produced by semi-continuous polymerization, the results showed that the carboxyl groups have a relatively more uniform distribution within the particles; however, a large amount of carboxyl groups were formed in the aqueous phase (25~30% of total MAA amount), which indicates that the semi-continuous polymerization is still not suitable for monomers with very different propagation rates and very different aqueous phase solubilities. Starved-feed dispersion polymerization might be a better choice in this case.

3.3.3 Preparation of Amine Functionalized Noncrosslinked Small PS Particles

3.3.3.1 Synthesis of Amine Functionalized α-methylstyrene Monomer

There are some amino-functional styrene monomers commercially available, but these functional monomers are either not suitable for copolymerization or are very expensive. Synthesis of amino functional styrene monomer derivatives is the practical alternative. The synthesis route of producing 3-isopropenyl-α, α-dimethylbenzylamine (TMA) from 3-isopropenyl-α,α-dimethylbenzyl isocyanate (TMI)[13] are chosen, because TMI is a commercially available styrene monomer derivative with a reasonable price and the isocyanate group can be hydrolyzed into a primary amine group in a good yield. But the most important reason is the α-methyl group adjacent to the vinyl group can prevent the product TMA from homopolymerizing, which is preferred in the copolymerization with styrene.

In this synthesis route, the isocyanate group in TMI is reacted with the hydroxyl functional groups to form a urethane linkage in the presence of dibutyltin dilaurate as a catalyst. This intermediate product (3-isopropenyl-α,α-dimethylbenzyl urethane, TMU) then decomposes under basic conditions to obtain the amine-functionalized styrene (TMA). The yield is close to 50 % after purification *via* high vacuum distillation (see Appendix I for more experimental details of this organic synthesis as well as the purification parameters).

The chemical equation of this synthesis route is shown as follows:

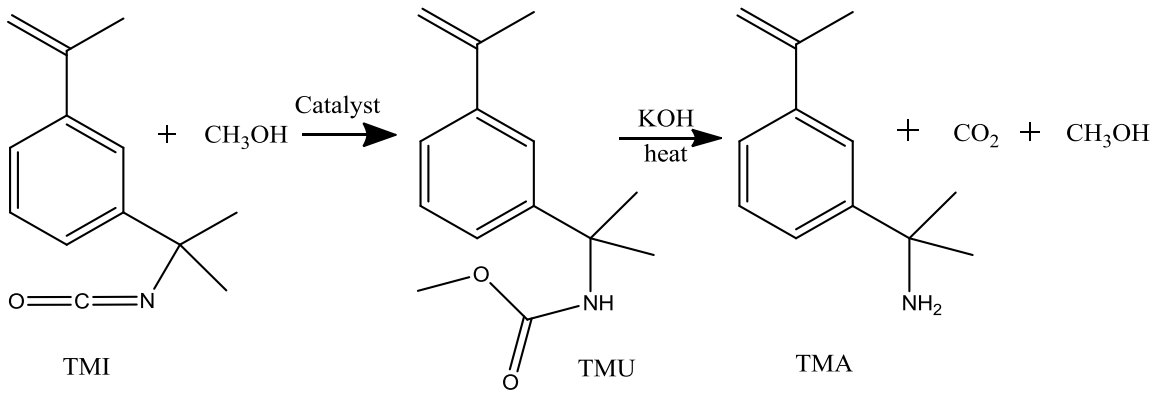

(3.6)

Both FTIR and NMR confirmed the existence and purity of the final TMA product (see Figure 3.11).

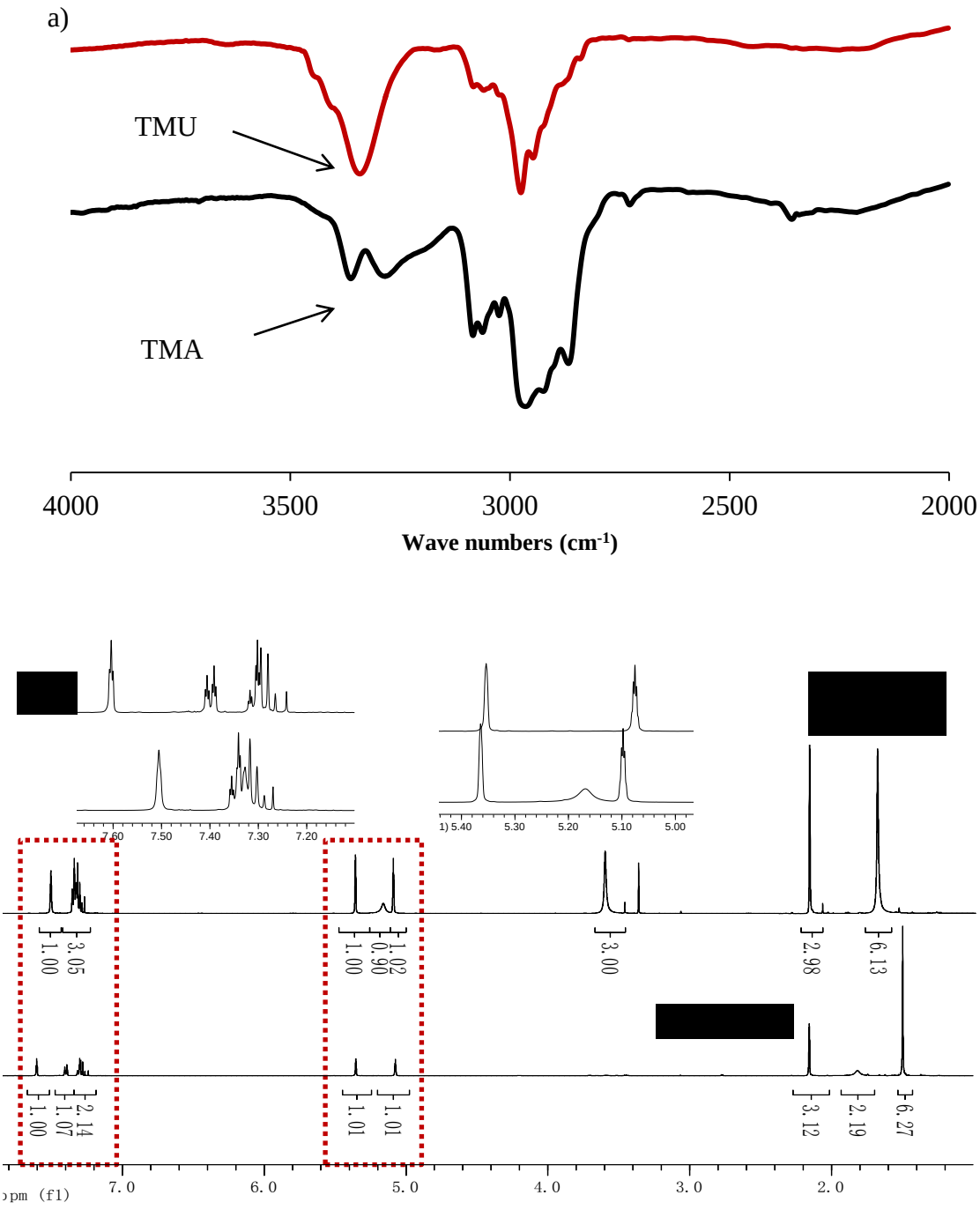

Figure 3.11: a) FTIR comparison results show the one N-H stretching peak in TMU and two N-H stretching peaks in TMA. b)^{1}H NMR comparison between TMU and TMA. The peak integration of the chemical shifts is provided as well.

3.3.3.2 Synthesis and Characterization of Amine Functionalized Latex Particles

Batch bottle polymerization was applied to prepare the amine functionalized PS particles, and the basic recipe is shown in Table 3.10. Typically, the particle size of the synthesized latexes based on this recipe is 70~ 90 nm based on SEM results.

Table 3.10: Basic Recipe for Bottle Polymerization of Various Functionalized Styrene*

Ingredient	**Parts by Weight (g)**
Styrene	8.0
TMA**	0.4
KPS or APS	0.05
Aerosol MA-80***	0.9
Deionized H_2O	27

* The reaction temperature was varied from 60 to 80°C, depending on the molecular weight desired. **TMA can be changed to other monomers, like TMI, if other functionalities are needed. *** SLS surfactant is not used in this recipe, because the resulting latexes cannot dissolve in THF solvent, which is probably due to SLS generating more $SO_3^-NH_3^+$ ionic bonding on the particle surfaces that affects the solubility of polymers in THF.

Comparing these results to the non-functionalized small linear polystyrene particles, the amine functionalized particles have two unique properties: 1) the weight-average molecular weight is almost 10 times smaller than that of the non-functionalized or other functionalized ones (like the TMI or TMU functionalized), which is approximately 1×10^5 g/mol to 3×10^5 g/mol based on different reaction temperatures, and the polydispersity index is fairly small (PDI=1.5~1.6); 2) the hydrogen bonding between

amine groups is so strong that it can both turn uncleaned latexes (in the presence of surfactants) totally into solid gels within several months and make cleaned latexes precipitate out within weeks. Due to this strong hydrogen bonding, a precaution needs to be taken into account in the latex cleaning process. The latexes cannot be too dilute or 'too clean', which means that a certain amount of surfaants needed to be present on the surface of the amine functionalized latexes to help separate adjacent amine groups from bonding with each other.

Regarding the characterization of amine functionality, the titration methods that apply to the titration of carboxyl groups cannot be directly used, such as pH titration and conductometric titration. The most important reason for the inapplicability of those *in situ* techniques is the stability issue. The amine functionalized latex particles are neither stable when diluted with DI water (or tap water) nor stable when titrated with addition of standard HCl solution. Therefore, the amine titration is performed by applying an oxidation-reduction titration that does not require an all-time stability of the latexes throughout the process. Figure 3.12a shows the procedure used to detect the surface amine concentration on latex particles [14]. The latexes are all diluted by using $NaHCO_3$ buffer solution (pH=8.2) to ensure the stability of the latexes for the first SPDP reaction. The stability of latexes for the first step is needed, because the first step is to convert all the amine groups on the surface of the particles and several layers beneath surface into the amide groups using an excess of SPDP. Then the stability of the latexes is not as important for the reduction reaction step, because the unreacted SPDP will be washed out leaving only amide in the system, which is the product of the surface reaction with SPDP.

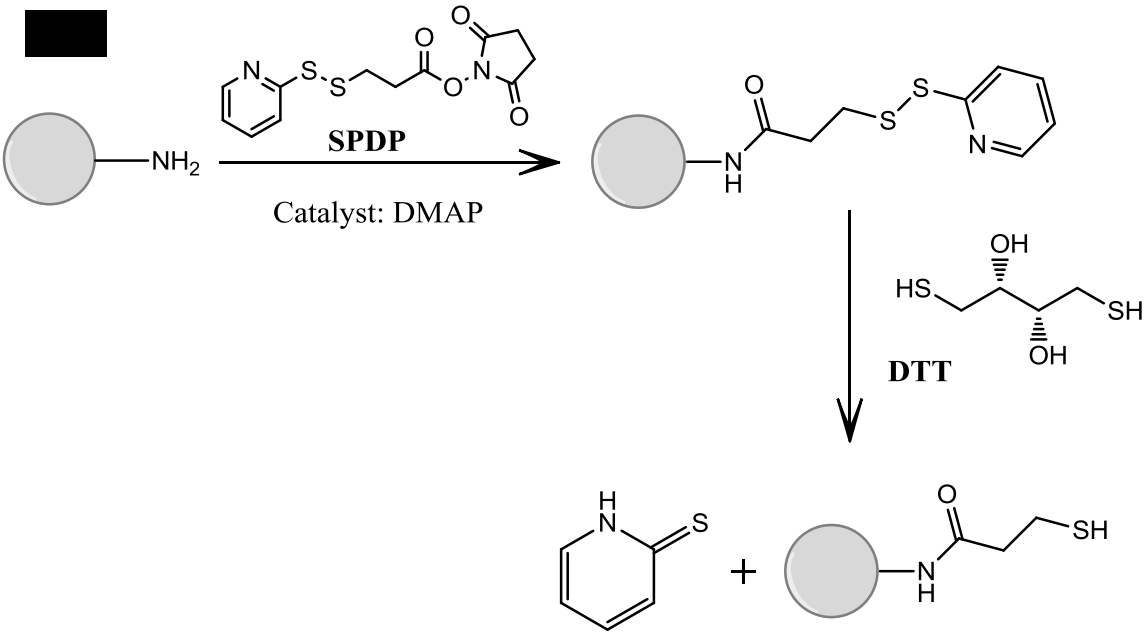

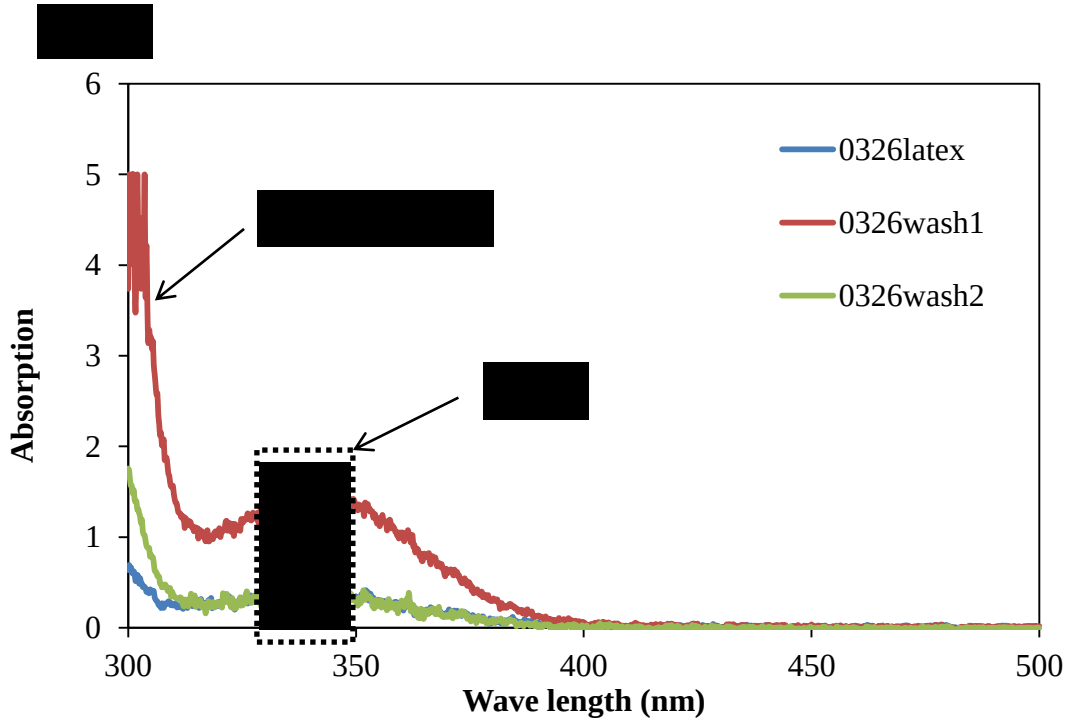

Figure 3.12: a) Chemical reactions occurred in the surface amine titration process; b) UV spectrum of C=S optical density *vs.* wavelength for sample 0326.

Thus, after adding excess DTT, the optical density detected is only contributed by the SPDP coupling with the surface amine of the latexes. Figure 3.12b shows an example of the titration for one of the latex samples (sample 0326). Y_{coupling} is estimated:

$$Y_{coupling} = \frac{A_{Latex}}{A_{wash1} + A_{wash2} + A_{Latex}}$$

$$[\text{Amine}]\ (\mu\text{eq/g latex}) = Y_{\text{coupling}}[\text{SPDP}]_{\text{initial}}\text{P}^{-1} \qquad (3.7)$$

in which A is the optical density read at 345 nm, with the subscripts wash1, wash2 and latex representing the first wash, second wash separated from the latex solution and the latex supernatant itself after reacting with DTT. $[\text{SPDP}]_{\text{initial}}$ is the initial amount of SPDP charged to the latex system. P represents the total amount of latex solids.

The percentage of surface amine is estimated to be 33.8 %, based on the total amine. Amine groups in the aqueous phase of the latexes are not detectable, which indicates a high incorporation of TMA in the PS particles. These results also indicate the same trend as the carboxyl functionality incorporation, which shows that by increasing the initial charged concentration of amine functionality, the surface concentration of amine groups that can be incorporated into the latex particles increases.

3.4 Conclusions

In this chapter, the preparations of different kinds of monodisperse latex particles were introduced and discussed. These latexes, such as PS particles with different particle sizes but similar molecular weights, PS particles with different molecular weights but

similar particle sizes, PS particles with different functional groups and crosslinking densities, are the basis for the study of the influence of latex molecular parameters on the latex film formation. Most of the particles were generated by batch polymerization. It was already proved that batch polymerization can prepare mono-dispersed particles with controllable surface functionality concentrations. Some other polymerization methods, such as seeded batch polymerization and semi-continuous polymerization, were also introduced, which provide more potential options for making structured particles. However, to avoid bringing more complexity to the model system, only batch polymerized latex particles were used for the following studies of film formation.

3.5 References

1. Yoo, J.N.; Sperling, L.H.; Glinka, C.J.; Klein, A. *Macromolecules*, **1990**, *23*, 3962.
2. Mdtrquez, J.; Lopez, F.; Marquez, O.; Parra, H. *Polymer Bulletin*, **1990**, *24*, 451
3. Myers, C. *United States Patent*, **1989**, 4833223
4. Jakubowski, W.; Kirci-Denizli, B.; Gil, R. *Macromol Chem. and Phys.*, **2007**, *209*, 32
5. Gall, B.; Pelascini, F.; Ebeling, H.; Beckerle, K.; Okuda, J.; Mlhaupt, R.; *Macromolecules*, **2008**, ***41***, 1627
6. Menard, K.P. *Dynamic Mechanical Analysis*, Taylor & Francis Group, LLC, 2008
7. Wool, R.P. *Polymer Interfaces Structure and Strength*; Hanser/Gardner Publications, 1995.
8. Wool, R.P. *Macromolecules* **1993**, *26*, 1564
9. Motzer, H.R.; Painter, P.C.; Coleman, M.M. *Macromolecules* **2001,** *34*, 8390

10. Cleveland C.S.; Fearnley S.P.; Hu, Y.; Wagman, M.E.; Painter, P.C.; Coleman M.M. *J. Macromol. Sci-Phys*, **2000**, *B39(2)*, 197

11. J. Tang, *Ph.D Dissertation*, Lehigh University, **2000**.

12. Sajjadi, S. *Polymer*, **2003**, *44*, 223

13. D. L. Trumbo, B. E. Mote, A.S. Trevino and M. Van Den Brink, *J. Appl. Poly. Sci*, **82**, 1030 (2001)

14. T. Delair, V. Marguet, C. Pichot, B. Mandrand *Colloid Polym. Sci.* **1994**, 272, 962

CHAPTER 4

Effect of Latex Particle Packing and Molecular Weight of Polymers

Abstract

Bimodal latexes have a pronounced effect on dispersion rheology as well as the film formation characteristics. The particle packing greatly reduced the void content inside latex films, and most importantly it provided system self-assembly to selectively arrange particles of one type to be surrounded by other particles with different properties. To achieve optimum packing, the latexes were blended at an optimal ratio, V_c, according to the theory of critical volume percent of dispersed material required for continuity. At V_c, large particles was isolated by small particles which tend to form a continuous phase.

For films comprised of latex particles with different molecular weights, it was found in the work that tensile strength increased with molecular weight until it reached a maximum, and then it became independent of the molecular weight. Polymer molecular weight, instead of the particle size, was the dominant factor for the film strength development if there were only physical entanglements of polymer chains interlinking the particle-particle interface.

4.1 Introduction

4.1.1 Particle Packing

When one dispersion is mixed into another, the packing morphology is influenced by the particle size ratio and volume fraction. Based on a study of polyethylene-nickel (large/small) blending mixtures, Kusy suggested that optimal packing could be achieved when the small particles form a continuous phase around the large particles[1]. He proposed a theory describing the critical volume percentage of small particles required for phase continuity, V_c (see Figure 4.1).

Based on cubic packing, V_c has been calculated as a function of the particle size ratio both in the ideal case (i.e, small particles fill in all the voids produced by close-packing of large particles, eq 4.1) and real cases (i.e., not all interstices are completely filled, eq 4.2):

$$V_C = 100\left(1 + 1.515 \times \left(\frac{R_l}{R_s}\right)\right)^{-1} \qquad \text{Ideal} \qquad (4.1)$$

$$V_C = 100\left(1 + 0.756 \times \left(\frac{R_l}{R_s}\right)\right)^{-1} \qquad \text{Real} \qquad (4.2)$$

in which R_l and R_s represent the large particle size and small particle size. Therefore, given a certain particle size ratio in a blended system, the minimum volume percentage of small particles needed to form a continuous phase can be estimated. It can be expected that efficient particle packing will lead to optimal film formation and low permeability in the latex films.

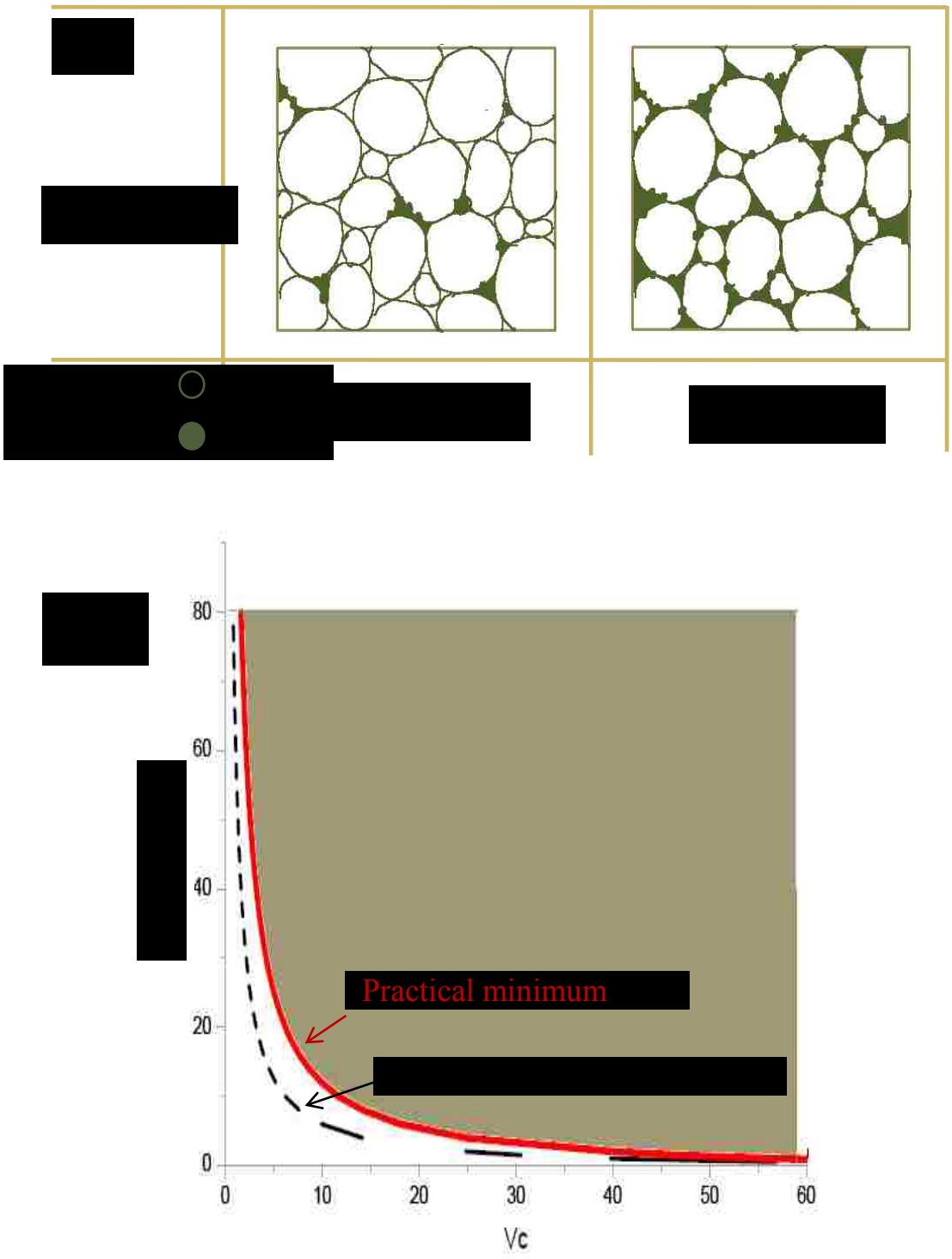

Figure 4.1: a) The scheme of Kusy's theory[1] in terms of V_c, the small particle volume percentage for an optimum blend; b) Particle size ratio *vs.* V_c based on the cubic packing calculation.

4.1.2 Polymer Chain Interdiffusion

Polymer chain interdiffusion increases the interpenetration depth and the amount of physical entanglements at the particle-particle interface, which builds up the interfacial strength and leads to mechanical integrity of the film. This film formation process is analogous to the healing process in bulk polymers, in which the interface between the two surfaces is bridged by chain reptation and subsequently formed entanglements. Therefore, the study of chain interdiffusion during latex film formation can be related to the interface healing problems.

Four important theoretical models have been proposed to describe the time and molecular weight dependence of strength development during interface healing.

1) de Gennes' Model[2]

de Gennes assumed that the fracture energy, G_{IC} *is* proportional to the number of bridges across the interface, *p*, and consequently, G_{IC} is related to the square root of time, which leads to the fracture stress, K_{IC} increasing with one quarter power of time before complete healing.

$$K_{IC} \propto t^{1/4} \qquad t < \tau \qquad (4.3)$$

$$K_{IC} \propto M^{0.0} \qquad t > \tau \qquad (4.4)$$

in which τ is the reptation time or full annealing time, M is polymer molecular weight.

2) Jud, Kausch, William's Model[3]

In this model, the contact surface area ratio, A / A_0 (A_0 is the total cross-sectional area of the interfacial bond) and the proportion of the links formed across that area, N / N_0 (N_0 is the concentration of links at full strength) are primarily considered. The described relationships for K_{IC} are as follows:

$$K_{IC} \propto t^{1/4} M^{-1/2} \qquad t < \tau \qquad (4.5)$$

$$K_{IC} \propto M^{1/4} \qquad t > \tau \qquad (4.6)$$

where τ is the reptation time or full annealing time, M is polymer molecular weight.

3) Prager and Tirrell's Model[4]

Because Prager and Tirrell found distinct differences in the time dependence of the crosslink densities for the interface, the molecular crossing density (ρ) at the interface is predicted to be the controlling factor in their model. Accordingly, K_{IC} has the following relationships:

$$K_{IC} \propto t^{1/4} M^{-3/4} \qquad t < \tau \qquad (4.7)$$

$$K_{IC} \propto M^{0.0} \qquad t > \tau \qquad (4.8)$$

4) Kim and Wool's Model[5]

Kim and Wool's minor chain model is based on the assumption that fracture stress depends on the monomer segment interpenetration distance χ, resulting in:

$$K_{IC} \propto t^{1/4} M^{-1/4} \qquad t < \tau \qquad (4.9)$$

$$K_{IC} \propto M^{1/2} \qquad t > \tau \qquad (4.10)$$

Although these four theories are based on different assumptions indicating differences in the relationship between fracture stress and molecular weight, they are all in agreement that K_{IC} is dependent on time to the one quarter power. They all describe the same physical phenomenon that the interdiffusion results in the formation of entanglements on both sides of the healing interface. Therefore, one can expect that efficient interfacial entanglements will lead to better interface-related film properties, such as film strength.

In this chapter, the theories discussed above and the experimental data will be combined and used to study the effect of bimodal particle packing and polymer molecular weights on the film mechanical performance, in terms of film strength.

4.2 Experimental

4.2.1 Materials

Styrene (J.T. Baker) monomer was distilled at 50 ℃ and a reduced pressure of 40 mm Hg to remove inhibitor and any oligomers. Sodium lauryl sulfate (SLS; MP Biomedicals, Inc.), Aerosol MA-80 (AMA, sodium di-hexyl sulphosuccinate; Cytec Industries), Triton X-100 (nonionic, octylphenol ethoxylate (9.5EO); Dow Chemical), potassium persulfate (KPS; Fisher Scientific), and sodium bicarbonate ($NaHCO_3$; Mallinckrodt Baker) were used as received. Potassium hydroxide (KOH; Fisher Scientific)

was ground into powder from pellets. Recipes used to prepare large and small polystyrene latex particles are found in Chapter 3.

4.2.2 Latex Particles and Blends

Blends of large and small non-functionalized linear PS latex particles were used for the study of the packing effects. These latexes all have similar molecular weights, which help to simplify the analysis with only the particle size being a variable. Table 4.1 shows the three sets of latex blends used in this work. There were some other blends used as controls, whose parameters are shown within the related paragraphs.

Table 4.1: Characteristics of PS Latex Blends used in the Packing Effect Study

	Sample	D_N* **(nm)**	D_W/D_N*	M_W **(g/mol)**	M_W/M_N	V_c**
Blend1	Large	203	1.105	1.1×10^5	2.1	21.0%
	Small	42	1.763	1.2×10^6	2.4	
Blend2	Large	179	1.120	1.1×10^6	2.5	23.2%
	Small	41	1.824	1.1×10^6	2.1	
Blend3	Large	306	1.031	3.7×10^5	2.1	20.3%
	Small	60	1.308	7.3×10^5	1.8	

* D_N: Number-average particle size, measured by CHDF. The polydispersity is usually larger than the one measured by electron microscope. Although the individual values are slightly different using different characterization methods, the particle size ratio is similiar as long as the characterization for the pair of large and small particles is consistent. Therefore, V_c will not be affected.

**Although V_c is the volume percentage of small particles, it is equal to the weight percentage since both large and small particles are made of the same PS material.

Latexes with similar particle sizes but different molecular weights were used for the study of the molecular weight effect (Table 4.2). It was found that by using chain transfer agents (CTA), a broad range of molecular weights with similar size latex particles was able to be produced, which was essential to the study of the molecular weight effect on the film performance. However, the amount of CTA charged could not be too much, or it would begin to broaden the distribution of both particle size and molecular weight (See samples CTA-7 and CTA-8, for which the amount of CTA charged was 8~ 10 wt% based on styrene monomer).

Table 4.2: Particle Size and Molecular Weight of PS Latexes Prepared with Different Amounts of Chain Transfer Agents

	CTA-0	**CTA-1**	**CTA-2**	**CTA-3**	**CTA-4**	**CTA-5**	**CTA-6**	**CTA-7**	**CTA-8**
D_N **(nm)**	79	74	72	74	77	73	81	86	96
D_W/D_N	1.04	1.08	1.06	1.06	1.05	1.09	1.09	1.13	1.09
M_N **(10^5g/mol)**	7.5	7.1	5.9	2.7	1.8	1.1	0.72	0.61	0.42
M_W/M_N	2.1	2.5	2.2	2.1	2.0	2.2	2.0	2.6	2.7

* D_N: The number-average particle diameter, measured by SEM

4.2.3 Characterization Methods

The particle packing has been characterized by SEM in terms of the surface and bulk morphology. Atomic force microscopy (AFM) was used for film surface characterization in terms of topograph and phase profile. The molecular weight and weight distribution were measured by GPC. The film strength was measured using an Instron Universal Testing machine. At least 3 specimens were tested for each sample.

4.3 Results and Discussion

4.3.1 Bimodal Particle Packing

Based on Kusy's theory, bimodal latexes were blended at V_c, the optimum blending ratio to achieve system close packing. To check if the theory of continuity also applies to hard particle latex blends, the surface and bulk morphology of dried latex blends were characterized by SEM (Figure 4.2). Both at the surface and within the bulk phase, the special close-packed morphology was found where the large particles were surrounded by the small particles and the small particles formed the continuous phase right at V_c. AFM profiles also showed a similar morphology (Figure 4.3) in a different batch of PS blends. However, from a practical point of view, if having large particles isolated without touching each other by small particles (such as in the reactive system where the large and small particles have two different reactive groups) is of more interest, the volume percentage of small particles should be larger than V_c, because V_c is the theoretical minimum amount for the small particles to surround the large particles and fill the void space between them. To totally separate the large particles, the volume of small particles should be slightly higher than this critical point. Taking Figure 4.2a for example, the large particles are actually touching each other and the small particles only occupy the interstices created by the close-packed large particles. Therefore, a volume percentage of small particles slightly higher than V_c is needed to separate the large particles from each other. By doing this, the large particles can become well separated in a continuous network formed by small particles, even though they may not appear to be very ordered on the surface.

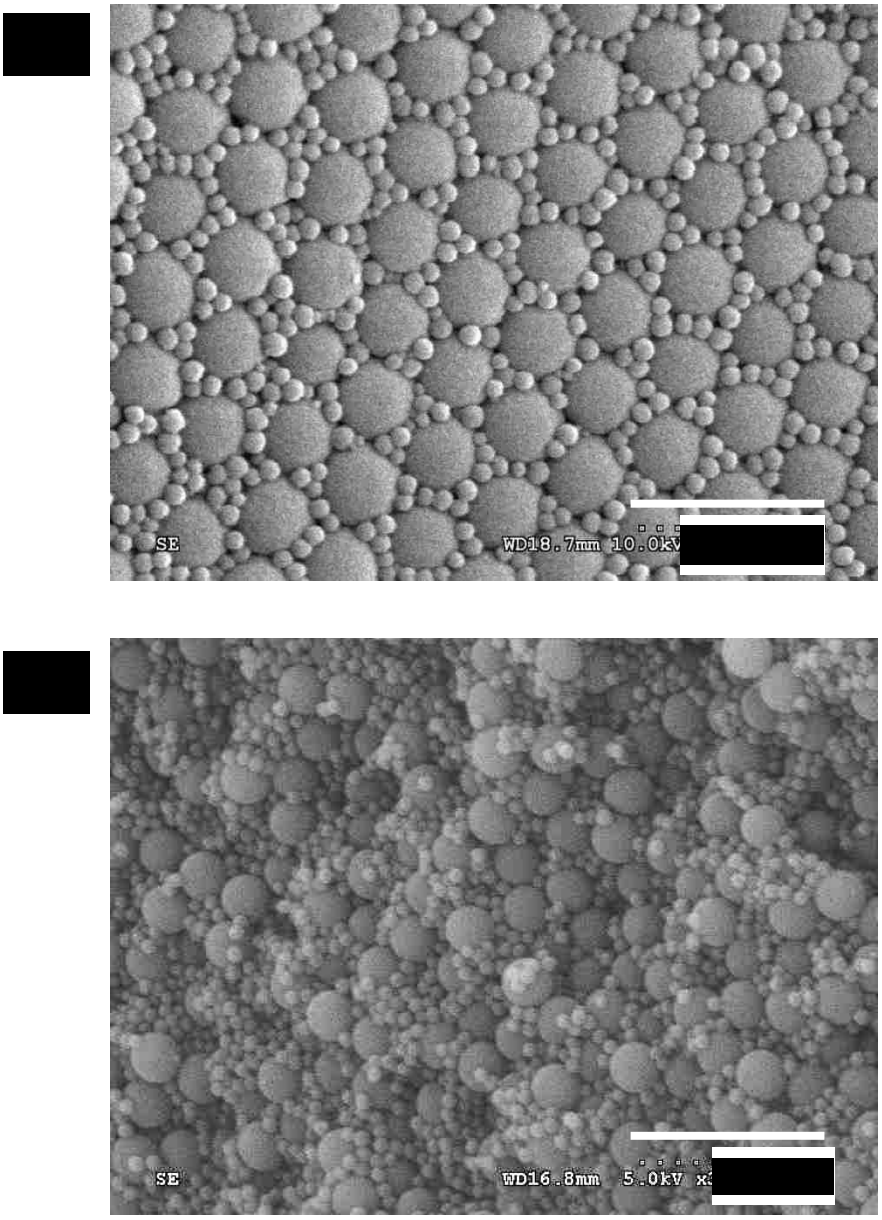

Figure 4.2: Scanning electron microscopy (SEM) images for a) surface and b) bulk phase morphology of Blend 1 sample.

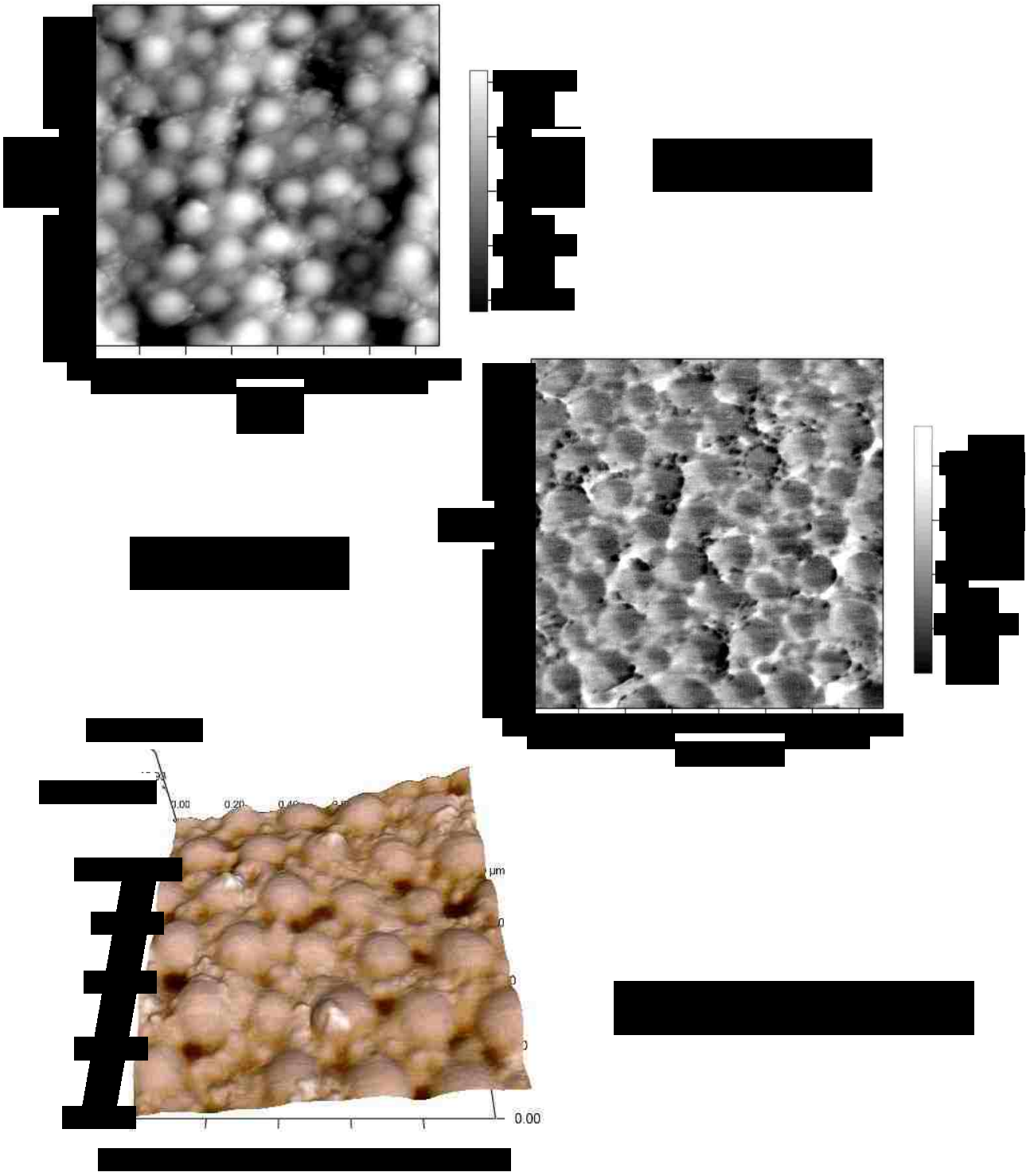

Figure 4.3: Atomic force microscopy (AFM) 2D and 3D profiles reconstructing the surface morphology of Blend 2 sample. The black dots in the phase diagram indicate soft materials, such as surfactant.

To check if V_c is really the critical point for obtaining continuity in the bimodal system, the same pair of large and small particles used in the Blend 1 were used. Instead of being blended at V_c= 21.0 %, it was blended at V'= 13.5 %. At the optimal blend ratio, one large particle was surrounded by 33 small particles on average, while Figure 4.4 shows the surface morphology when one large particle was surrounded by only 18 small particles on average. The small particles could hardly be observed neither through SEM or AFM, which proves that it is not possible to obtain film morphology with large particles surrounded by a matrix of small particles at a blend ratio less than V_c.

A number of factors, besides the critical volume percentage V_c, may affect particle packing as well, such as the particle size ratio (the internal factor), which determines whether the bimodal packing structure is random close packed (if the small particles are larger than the interstitial volume created by the close pack of large particles) or ordered close-packed (if the small particles can fit in the interstices created by the close-packing of large particles); and drying conditions (the external factor), which can be affected in many ways, such as the influence of meniscus shape, the latex solid contents, the drying rate, and the pH. Since the uniformity of the packing, not the order of packing, is the major concern, the external drying conditions are more important in this study.

1) Influence of meniscus shape

Since the drying rate along the drying front is usually much faster than the rate from the body of the latex pool, an uneven and non-uniform drying behavior usually occurs over the liquid film surface. Latex particles in the dispersions are transported to

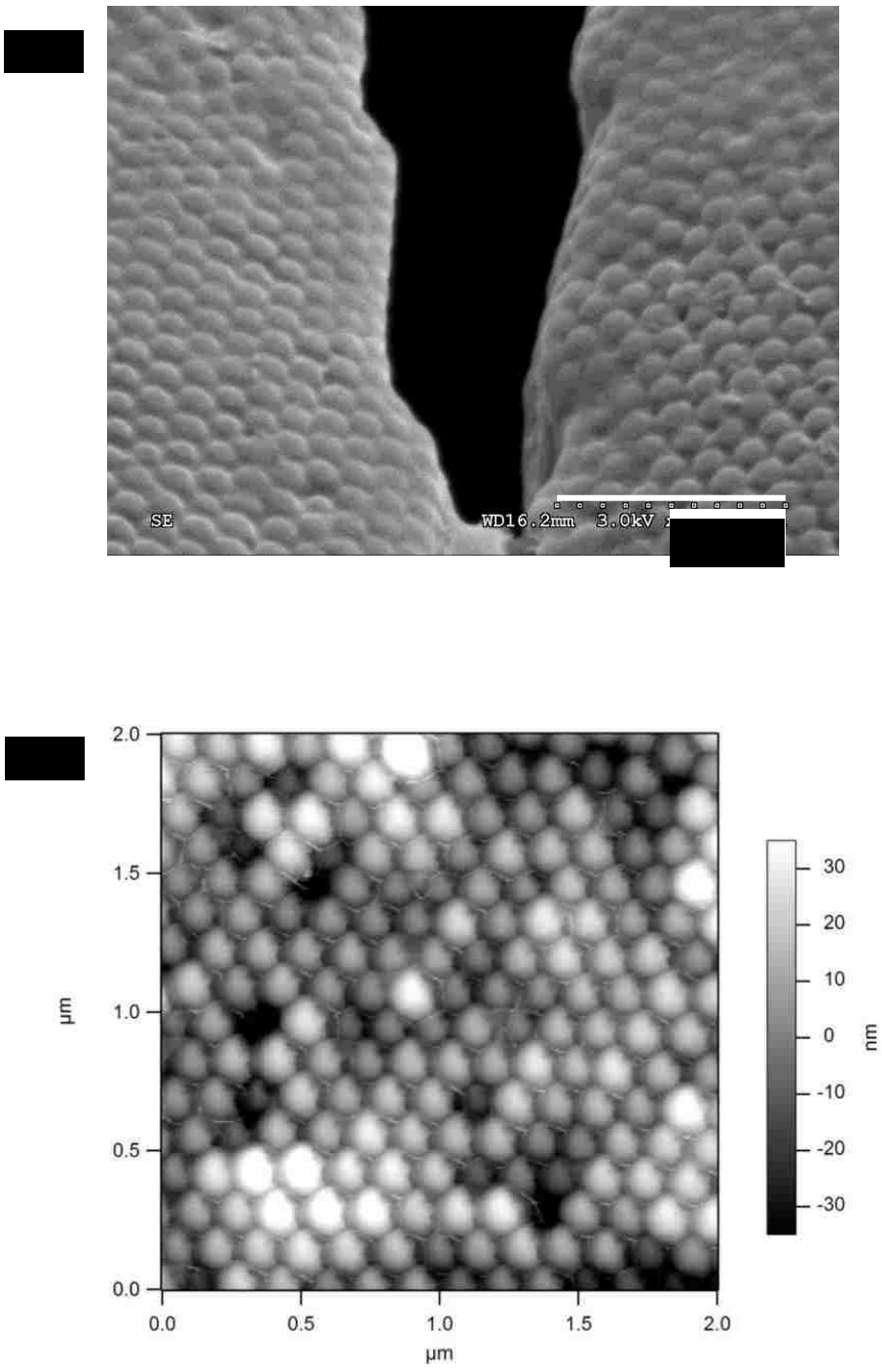

Figure 4.4: a) Scanning electron microscopy (SEM) image and b) atomic force microscopy (AFM) topographic profile of the sample Blend 1 at a blend ratio of 13.5 %, which is smaller than the optimum ratio of 21.0 %.

the drying edge by the water flux formed in the liquid phase. If the contact angle of the drop on the substrate is larger than 90 °, the liquid meniscus becomes concave[6]. As the evaporation proceeds, the thinnest part of the liquid is the center meniscus, where particles tend to contact each other to be ordered by the force of the strong water flux. However, in most cases of latex drying, the contact angle is smaller than 90 ° and the liquid surface will be convex. Then the driving front is the edge of the liquid meniscus, which moves inward resulting in particles moving from the center to the edge. This has been described as the "coffee ring" phenomenon[7] as theoretically analyzed by Larson *et al.*[8] (see Figure 4.5).

Figure 4.6 shows the effect of the drying front on latex packing as characterized by SEM. The meniscus has a 1~2 mm thickness with around 10 % initial solids content. Because of the convective flow from the low evaporation rate area (center) to the high evaporation rate area (edge), fewer particles and more voids occurred in the center of the dried latex chunk, while more ordered packing showed up in the edge areas. Therefore, to obtain much more uniform latex packing, a flatter air/latex interface is preferred, such that there will be little tendency to form a ridge at the edge and possible voids in the center. Dispersions with smaller amounts of surfactants (cleaned latex or surfactant-free latex) and a much thinner and larger surface are needed to form a flatter meniscus with a contact angle close to 90 ° at the interface. As long as the latex is dried uniformly, it can be considered that almost every fraction of the dried latex bulk phase contains the same large/small particle number ratio and the same close-packing arrangement.

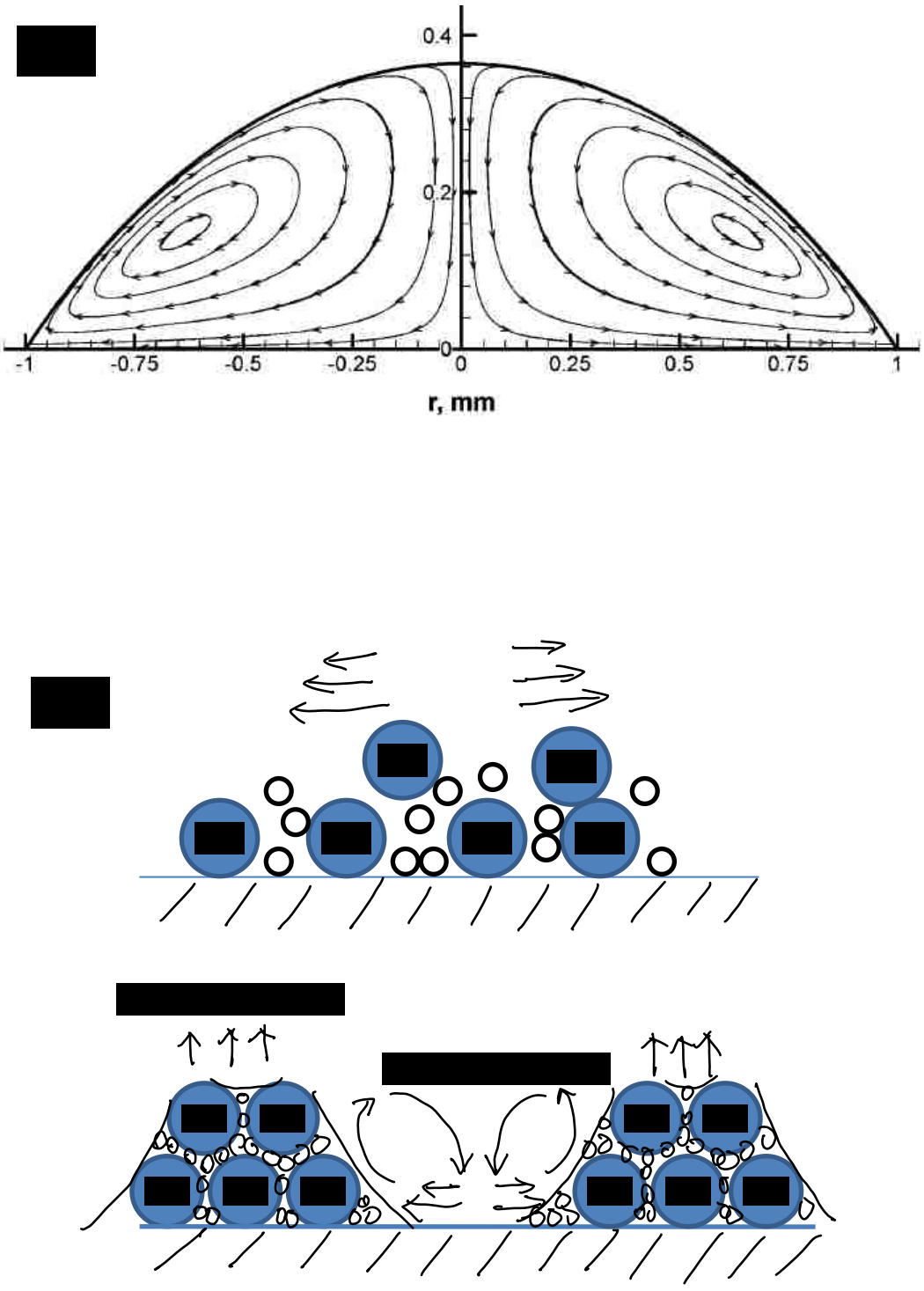

Figure 4.5: a) Reprint of streamline plots of the flow field for the Marangoni-stress boundary condition at contact angle of 40 ° from Larson's paper[8]; b) the scheme of water driven transportation of bimodal particles.

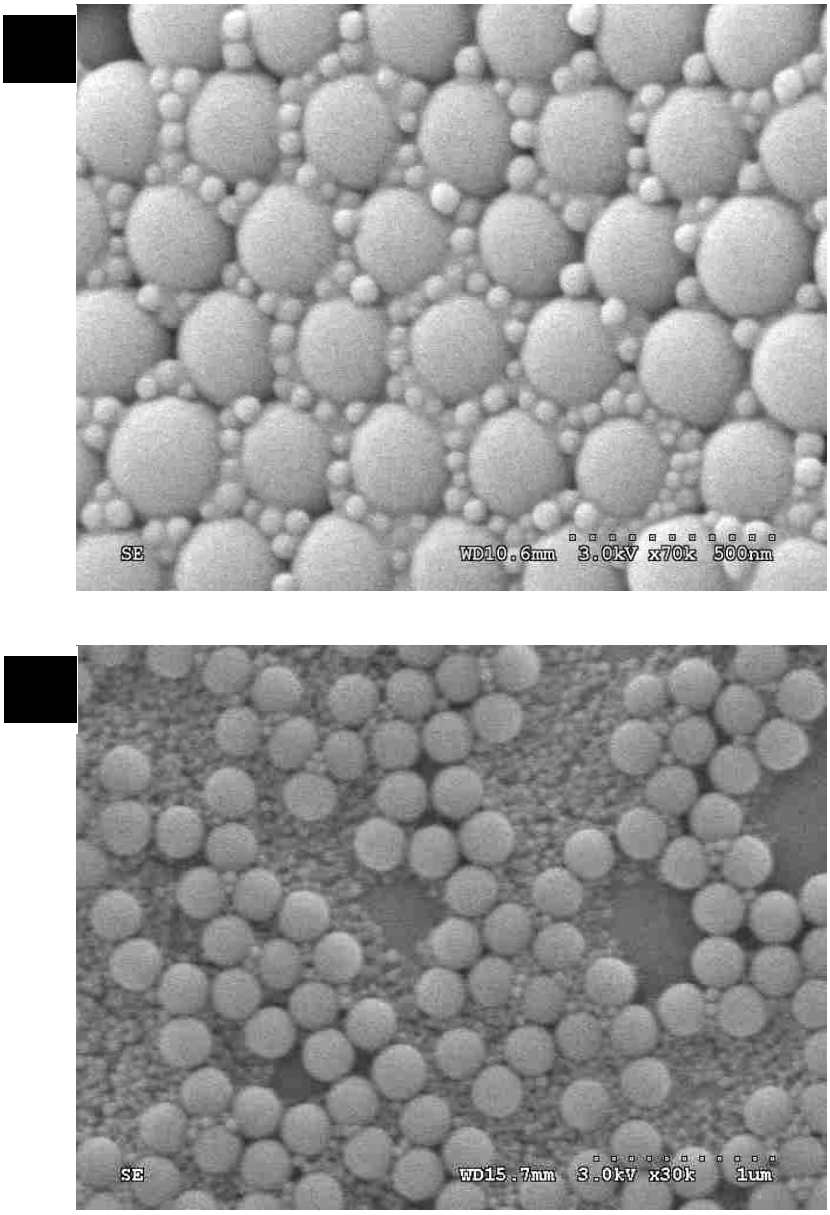

Figure 4.6: Scanning electron microscopy (SEM) images of: a) the edge and b) the center of the dried latex Blend 3.

2) Influence of solids content

The solids content directly affects the volume percentage of the continuous phase in the liquid film. In the case of latexes the continuous phase is water, so decreasing the solids level increases the water content and decreases the drying time, which will enhance the internal particle transportation driven by the water flux. Therefore, the solids content should be as high as possible to minimize water driven particle transportation.

3) Influence of the drying rate

Many groups have done research on the influence of drying rate. Winnik[9] suggested macroscopic ordering was promoted by slow drying of the dispersion and disrupted by rapid drying. Lang and Juhue[10] reported much more regular arrangements at higher T under vacuum than at ambient condition *via* AFM images. Luo *et al.*[11] showed coffee-ring like structures in the center and irregular interstitial filling with small particles at the edge at room temperature, while good packing was obtained at 60 °C. To investigate the influence of the drying rate specifically in the PS bimodal latex systems, the water evaporation rates of the latex blends that comprise of 440 nm large PS particles and 79 nm small PS particles at 19.2 % volume based blend ratio under three different drying conditions were measured in terms of the amount of water loss *vs.* time by gravimetric analysis (see Figure 4.7). Figure 4.8 depicts that different drying rates lead to different packing patterns.

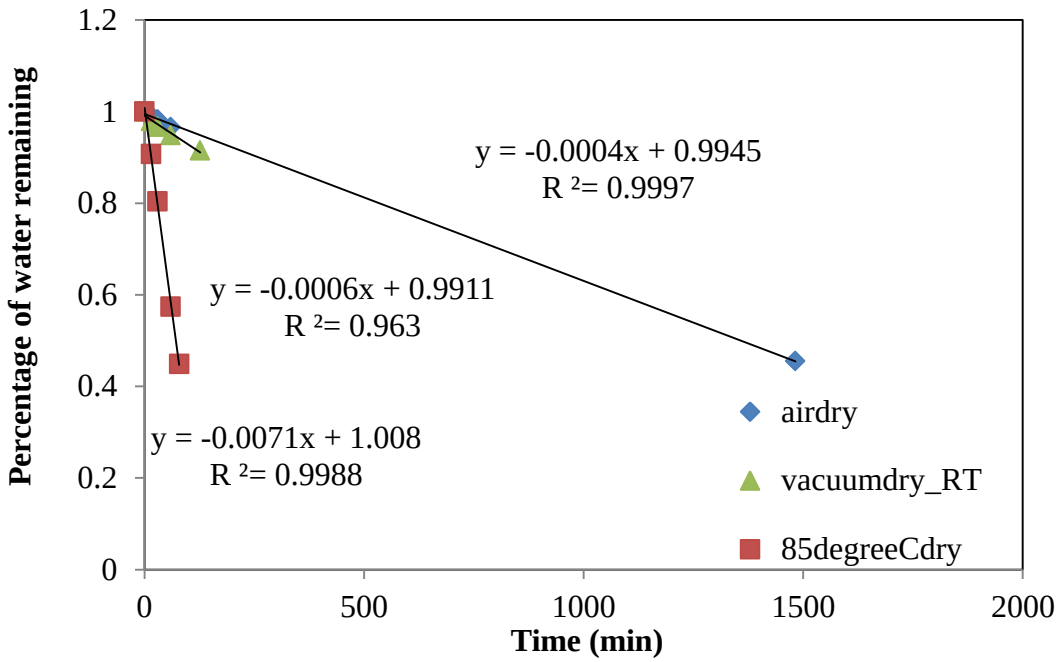

Figure 4.7: Water weight loss *vs.* the drying time under different drying conditions: (◆)ambient conditions, (▲)room temperature with vacuum (25 mm Hg) and (■) 85°C.

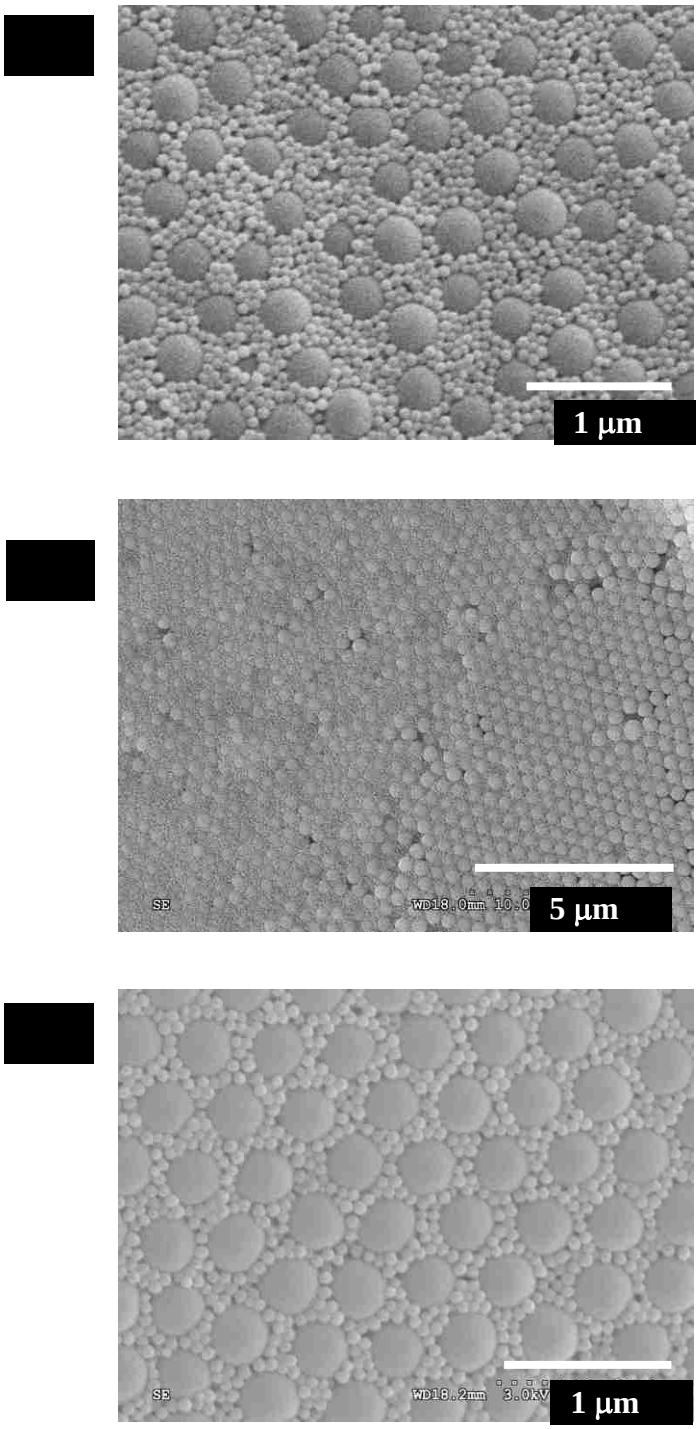

Figure 4.8: Scanning electron microscopy (SEM) images of the surface morphology from the same latex blend dried at a) 85°C; b) room temperature under vacuum; and c) ambient conditions. Image b) has a different magnification to show the transition area between random packing and close packing.

When the drying temperature is high (at 85 °C), the water evaporates so fast that the large particles do not have enough time to self-arrange into close-packed patterns. Therefore, more randomly packed morphology of large particles and more non-uniformly distributed small particles are observed at the 85 °C drying conditions. When the drying temperature is low, at ambient temperature, the water evaporates much slower, which provides more time for the large particles to equilibrate and form entropy favored ordered packing, and also gives more time for the small particles to rearrange inside the interstices created by large particles. The room temperature, vacuum drying has a drying rate in between 85 °C and room temperature, close to the ambient conditions. As a result, most of the packing patterns are ordered packing, while there are some transition regions where random packing and ordered packing morphologies coexist. Therefore, the drying temperature should be as low as possible to enable ordered close packing to occur during the drying process. However, to shorten the drying time, in practice, the drying rate should be kept as slow as possible at first and then increased when the viscosity of the latex solution is thick enough (> 60% solids content).

4) Influence of pH

When two latexes with different pH values are blended together, the pH of the mixture can be neutral, basic or acidic depending on the pH strength of each of the latexes and the amounts in the blend. Changing pH may greatly affect the stability of the latexes and lead to particle aggregation and a non-uniform packing morphology. Since in this chapter, the focus is the non-functionalized latex particle packing, more details

concerning the pH influence on reactive latex blends can be seen in the experimental part of Chapter 5.

4.3.2 Bimodal Packing Effect on Film Strength

In terms of the effect of latex particle packing on the film mechanical performance, film strengths were compared for the non-functionalized polystyrene blended films comprised of the latex Blend 2 (large and small particles blended at V_c) and the unblended films made of individual component particles (i.e., large-only and small-only PS latex films) for example.

Figure 4.9a plots the development of tensile strength (TS) of unblended latex films *vs.* the annealing time. The latex film made from the small particles presented higher film strengths at early annealing times than the latex film comprised of large particles. There are two reasons for this: First, the interfacial contact area is greater for small particles packing which leads to a quicker interface healing process; Second, considering the chain end distribution within the particles, for similar molecular weights, polymer chains are more restricted in small particles. Therefore, polymer chains tend to have more chain ends on the surface of small particles than on large particles. Since the chain end determines the direction towards which the polymer chain moves, more chain ends on the surface leads to shorter interpenetration depth across the interface and thus the time for building film interfacial strength will be shorter[12].

According to the theories introduced at the beginning of this chapter, the fracture strength is proportional to the one quarter power of the annealing time before the

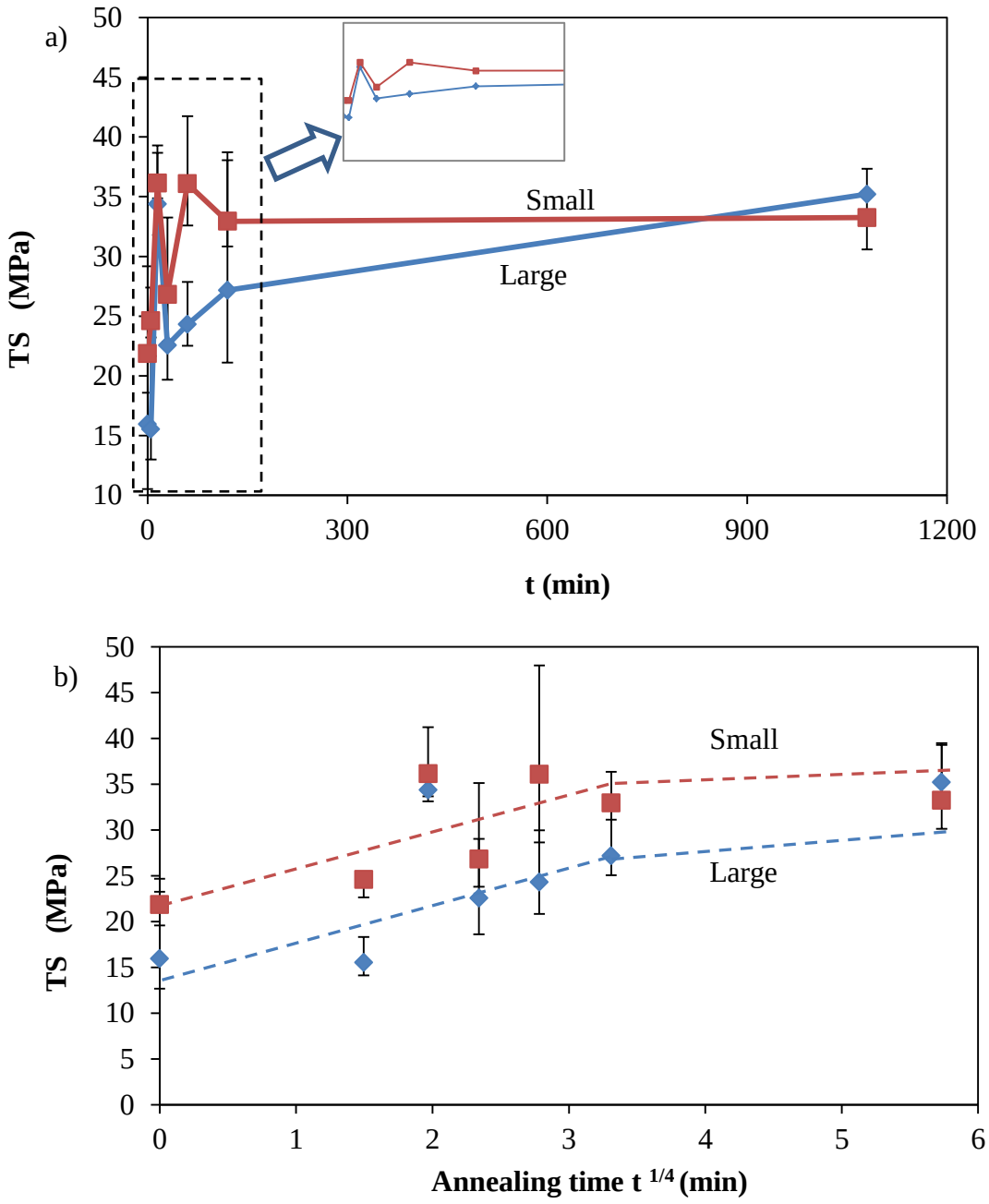

Figure 4.9: (a) Tensile strength (TS) of PS films made of large and small particles individuals (the components of Blend 2) *vs.* annealing time. The inset is the expansion of the dashed box. (b) Tensile strength *vs.* one quarter power of annealing time. The last data point (when t=1440 min) of plot (a) is not included in plot (b). The error bars show the whole range of data gained from specimens for each sample.

reptation time (when the interface is fully healed), and then after the reptation time, the fracture strength is independent of time. Based on the experimental data, the tensile strength *vs.* one quarter power of the annealing time was plotted (Figure 4.9b), which shows a good agreement with the theories. The film tensile strength first increases proportionally with one fourth order of the time, and then the strength reaches a plateau value in both cases. By applying the minor chain model, the theoretical reptation time needed for the two latex films was calculated as follows.

For polystyrene random coils, it is known that in the relaxed state, the radius of gyration, R_g, is related to the weight-average molecular weight, M_w, and the end-to-end distance, R, is related to R_g, as described by:

$$R_g = 0.275 \times M_W^{1/2} \tag{4.10}$$

$$R = \sqrt{6} R_g \tag{4.11}$$

The radius of gyration R_g in large and small particles was calculated to be around 290 Å. Therefore, according to eq 4.12:

$$\tau = \frac{R^2}{3\pi^2 D} \tag{4.12}$$

the reptation time τ was calculated to be approximately 200 min, which is right at the onset of the plateaus shown in Figure 4.9b.

It is worthwhile to mention that there is an inconsistency with the theories that a peak exists in the tensile strength at approximately 15 min. Mohammadi *et al*. gave a

possible explanation for this peak[13]. They split the healing process into three regions as shown in Figure 4.10: (1) mixed region, in which polymer chains just start to diffuse through the interface and film strength builds up; (2) after the peak region, in which cracks tend to deviate to the area (e.g., inside particles) with lower entanglement density than the interface because of the chain movement; the mechanical strength, therefore, drops due to the non-equilibrium structure of the entanglement network of the chains inside the particles; and (3) recovery region, in which this non-equilibrium network equilibrates over a long term and mechanical strength recovers.

The tensile strength development of blended films is shown in Figure 4.11 in comparison to the unblended films (films made of large particles only and small particles only). Amazingly, the tensile strength almost reaches the plateau value at the beginning of the annealing process, and therefore the strength does not have a significant increase during annealing compared to that of the unblended films. This result proves that the bimodal latex packing greatly decreases the void content within the film, so that the time to complete the interfacial entanglements is even smaller than the time needed for the film made of small latex particles. In terms of resulting in the same maximum strength, this is understandable. Once the interface is completely healed, there will be no separate particles but only polymer chains entangled in the film, since the molecular weights of both large and small particles are similar, the maximum strength of the blended film is expected to be close to that of the unblended films. This is also supported by the theories, which predict the fracture energy depends only on the molecular weight after the reptation time.

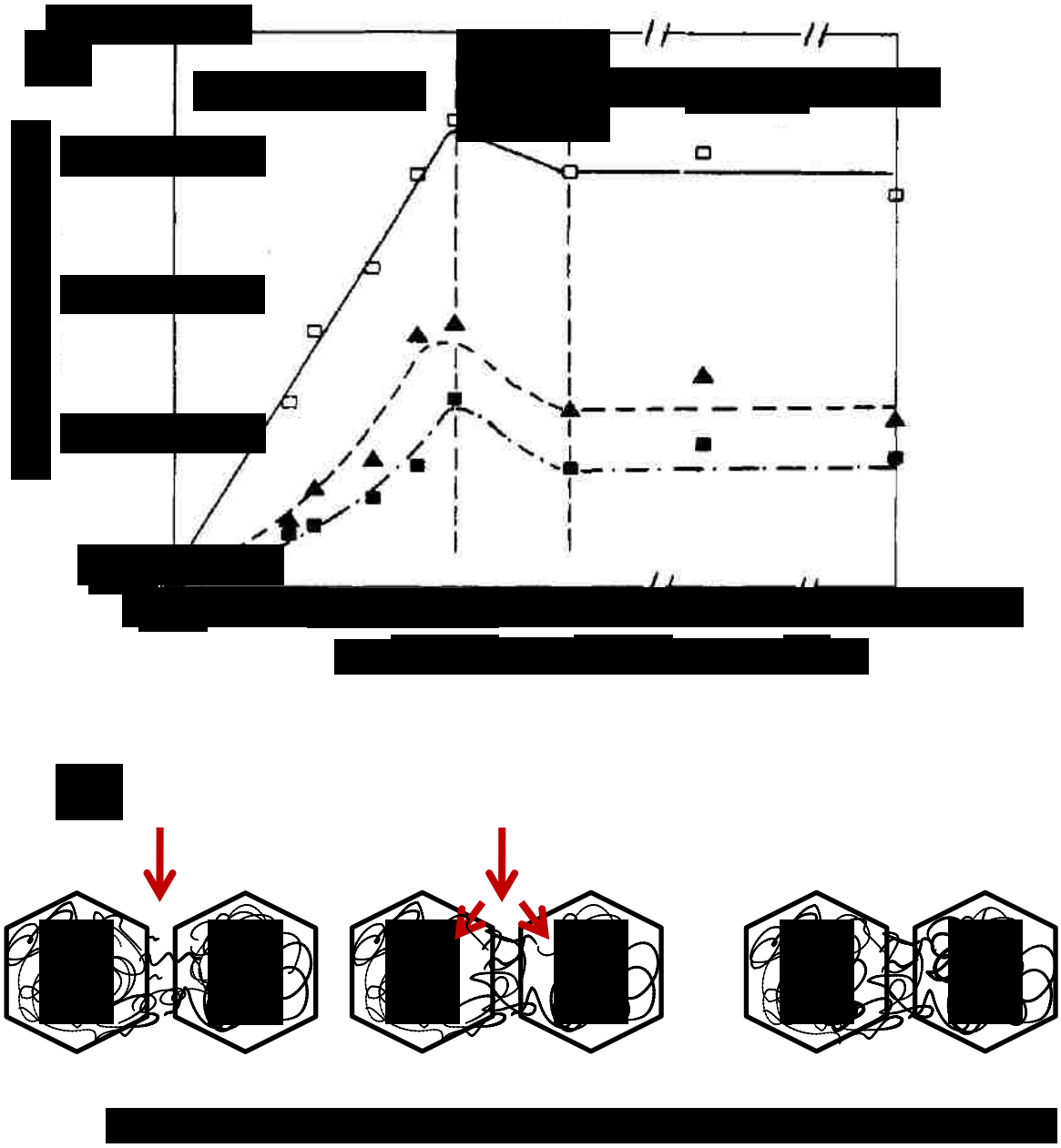

Figure 4.10: a) Fracture energy per unit area at various frequencies characterized by dental burr instrument with three regions defined. (Reproduced from Mohammadi *et al*.'s paper[13]); b) Illustration of the three regions proposed by Mohammadi *et al.*. The arrow indicates the weakest part where the film will break when stress is applied.

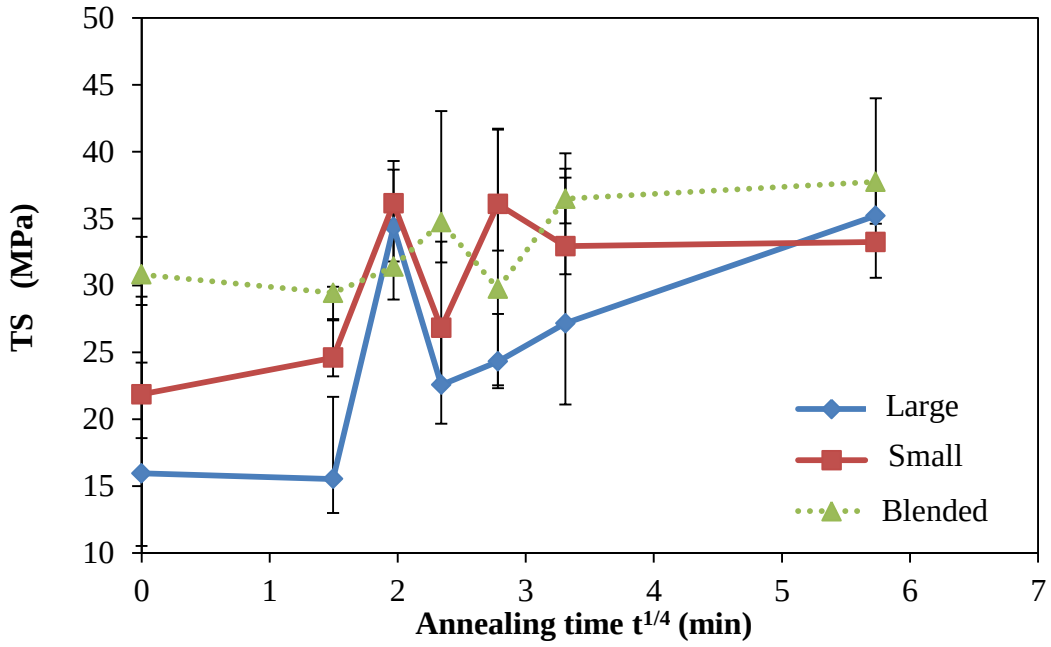

Figure 4.11: Tensile strength development *vs.* one quarter power of the annealing time for the blended (Blend 2) and unblended (components in Blend 2) polystyrene latex films

Thus if the molecular weights are the same, it is expected that the maximum yield strength at the breaking point should be the same.

4.3.3 Molecular Weight Effect on Film Strength

Since by bimodal latex packing latex films can be more quickly formed, how to strongly form latex films needs to be investigated, which is the purpose of the study of the molecular weight effect in this section, because the interfacial strength should be highly dependent on the polymer molecular weight (MW).

Figure 4.12 depicts the tensile strength development of four different latex films *vs.* one quarter power of the annealing time. The four latex films are prepared from high (M_n 710,000 g/mol), medium MW (M_n 450,000 g/mol and M_n 270,000 g/mol) and low MW (M_n 72,000 g/mol) polystyrenes with relatively broad MW distributions (polydispersity close to 2.2), respectively.

It is very clear that the sample with the lowest MW has the lowest tensile strength of the fully annealed film, but the films with medium MW and highest MW have similar tensile strengths after the annealing process is complete. The comparison is a little complicated, but the result is still understandable for those samples which have relatively broad MWs. At the very beginning of the film annealing process, before the film interface becomes fully entangled, lower MW polymer chains inside the particles diffuse faster and farther than higher MW polymer chains at the interface. As a result, there cannot be any comparison in the early stages of the film annealing process due to the broad distribution of molecular weights of the polymer chains. After the sample films

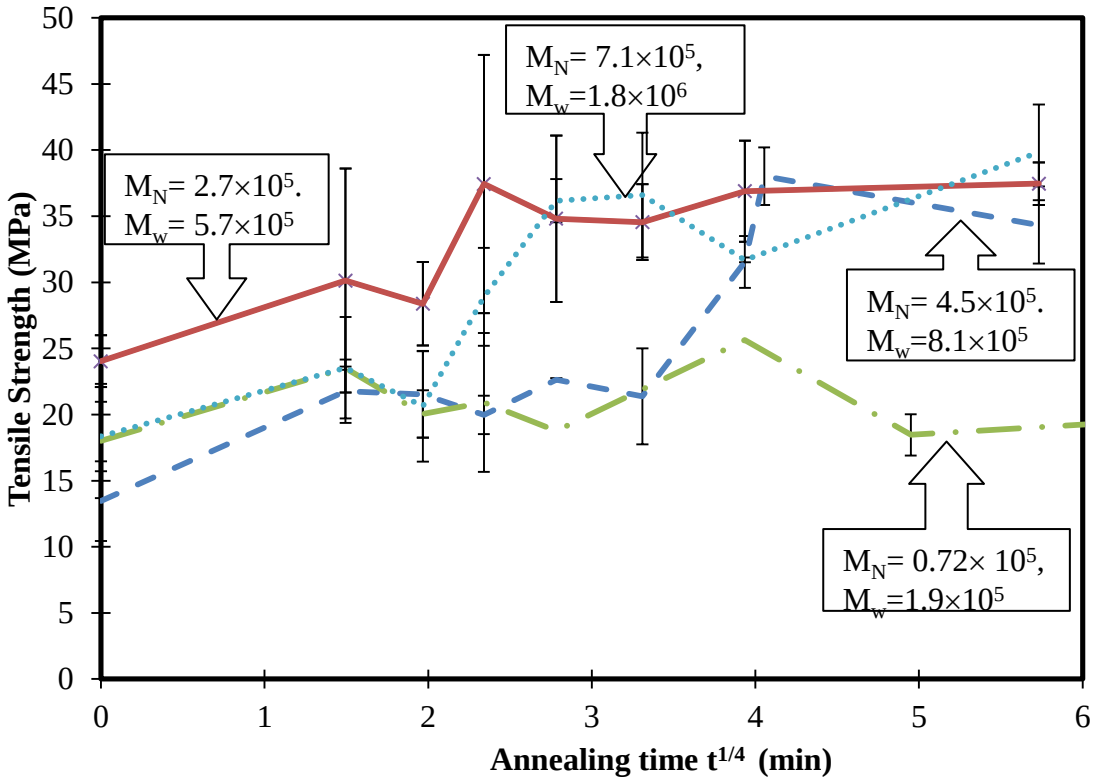

Figure 4.12: Tensile strength development *vs.* one quarter power of the annealing time for the films made of PS particles with four different molecular weights.

reach the strength plateau, which means that the polymer interdiffusion was complete including the high MW polymer chains, their maximum tensile strengths are very close within the error range: 39.8 ± 3.62 MPa for highest MW films, 34.33 ± 2.91 MPa for MW (M_n 450,000 g/mol), and 37.5 ± 1.61 MPa for MW (M_n 270,000 g/mol) films. This result supports Sambasivam *et al.*'s prediction[14] that there is an upper limit for the film total fracture strength. They found the calculated upper limit, which is supposed to be the strength of films with infinite molecular weights, is close to the strength of the film with M_n near 420,000 g/mol.

Therefore, to quickly form stronger films, the polymer chain does not need to be as long as possible, because the film strength after full annealing will reach a plateau value no matter how high the polymer chain molecular weight is. To determine the optimum chain length in the polystyrene system, three more polystyrene films with weight-average molecular weights lower than 570,000 g/mol have been investigated. Figure 4.13a gives the relationship of full film strength with the number of entanglement points per chain. Considering the critical entanglement molecular weight, M_e, to be the lower limit of molecular weight, beyond which effective film interface strength is able to build up, and the upper limit of film strength to be the maximum strength of the film with the highest molecular weight in this studied system (M_w=1.8×10^6 g/mol), the optimal polymer chain length is found to be approximately 3.0 ×10^5 g/mol (weight-average), which is consistent with Adolf and Tirrell's finding[15] based on the study of molecular weight dependence of healing.

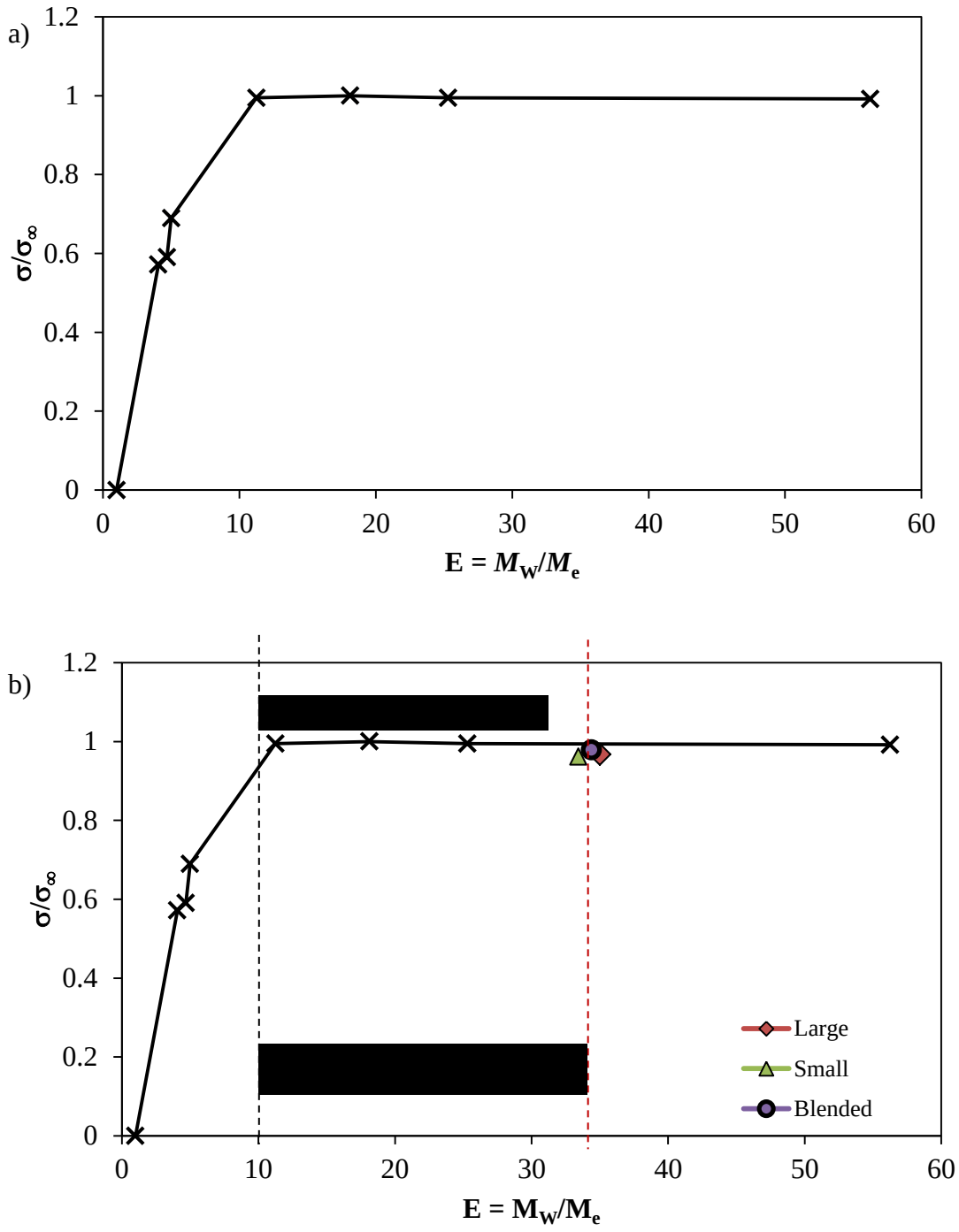

Figure 4.13: a) Ratio of tensile strength of a fully annealed film with molecular weight M_W to the maximum tensile strength that polystyrene film can achieve (here it is considered to be the strength for the polymer with M_w=1.8×10^6 g/mol), *vs.* the number of entanglement points per chain; b) Results from the blended film (Blend 2) included in the curve in plot (a).

Because the above results are based on the films prepared from only one size latex particles, to check if the particle size also plays a role in the final film strength, the previous results obtained from the bimodal polystyrene film system were compared with the result of the monomodal system in this section. The bimodal system had both large and small particle components with a weight-average molecular weight near 1.1×10^6 g/mol. When plugged the tensile strength value into the plot of the relationship between full film strength and the molecular weight, the values were found to be fit the curve quite well in all three cases (two unblended films and one blended film) (Figure 4.13b). This result indicates that only polymer chain length (molecular weight) is the dominant factor responsible for the latex film interfacial strength build-up. It also supports Wool's minor chain model, which predicts the film fracture strength is only proportional to the polymer molecular weight after the reptation time (film complete annealing time).

4.4 Conclusions

In this chapter, the particle packing effect and molecular weight effect on the film mechanical performance in terms of film tensile strength were discussed. Bimodal particle close packing can be achieved at an optimal blend ratio V_c, based on Kusy's theory of continuity. When applied the close packing in film formation, the corresponding film needed a much shorter annealing time to obtain full film strength (after complete interface healing) due to less void content presented in the latex film.

Polymer molecular weight plays an important role in film mechanical strength. In a certain range, the higher molecular weight, the higher the film strength is. The film strength can reach a plateau despite an increasing of molecular weight increasing. Based on the data in the polystyrene system, the optimal weight-average molecular weight was approximately 3.0×10^5 g/mol, with which the strongest polystyrene film could be formed within the shortest annealing time.

It is found that the polymer molecular weight is the dominant factor responsible for the final latex film interfacial strength. The particle size and latex blending do not affect the maximum film strength after the film annealing process is complete.

Therefore, to quickly form stronger latex films, latex blends need to be utilized, which have an optimal blend ratio (at V_c) and a proper molecular weight (close to the optimal molecular weight needed in the monomodal system). The reactive film systems discussed in the next chapter were built on the basis of these two optimized parameters.

4.5 References

1. Kusy, R. *J. Appl. Phys.*, **1977**, *48*. 5301.
2. de Gennes, P.G. *C.R. Acad. Sci. Paris*, **1980**, *B291*. 219.
3. Jud, K.; Kausch, H.; Williams J. *J. Mater. Sci*, **1981**, *16*. 204S.
4. Prager, M.; Tirrell, J. *J. Chem. Phys*, **1981**, *75*. 5194.
5. Kim, Y.; Wool, R. *Macromolecules*, **1983**, *16*. 1115.

6. Denkov, N.; Velev, O.; Kralchevsky, P.; Ivanov, I.; Yoshimura, H.; Nagayama, K. *Langmuir*, **1992**, *8*. 3183

7. Deegan, R.; Bakajin, O.; Dupont, T. *Nature*, **1997**, *389*. 827

8. Hu, H.; Larson, R. *Langmuir*, **2005**, *21*. 3972.

9. Winnik, M. A. *Emulsion Polymerization and Emulsion Polymers*, Lovell, P.A.; El-Aasser, M. S. edited. John Wiley and Sons Ltd, **1997**, Chapter 14

10. Lang, J.; Juhue, D. *Langmuir*, **1993**, *9*, 792

11. Luo. H.; Cardinal, C. M.; Scriven, L. E.; Francis, L. F. *Langmuir*, **2008**, *24*, 5552

12. Yoo, J.N.; Sperling, L.H.; Glinka, C.J.; Klein, A. *Macromolecules*, **1991**, *24*,2868.

13. Mohammadi, N.; Klein, A.; Sperling, L. *Macromolecules*, **1993**, *26*, 1019

14. Sambasivam, M.; Klein, A.; Sperling, L. H. *Macromolecules*, **1995**, *28*, 152

15. Adolf, D.; Tirrell, M. *J. Polym. Sci-Polym Phys. Ed.*, **1985**, *23*, 413.

CHAPTER 5

Effect of Crosslinking on Mechanical Properties of Films

Abstract

The chemical reaction between carboxyl and primary amine functionalities in the absence of catalysts was introduced into the design of the latex film system, in which the functional groups were present in separate latex particles. By investigating the reaction between small molecules, it was found that only a temperature beyond 140 °C could trigger this specific reaction. The kinetics study was undertaken both in the small molecule reaction and the reaction between polymers. It was found that there was a slight difference in the activation energy between the two types of reactions. The chemical reaction in the polymers had a higher activation energy due to the retardation of polymer chain movement in the entangled polymer network.

The mechanical performance of the blended films comprised of carboxylated crosslinked large particles and amine functionalized small particles mixed at the optimal packing ratio V_c was also investigated. The study confirmed that the blended film with a reaction controlled film formation process had a better film performance than that of the non-blended films.

5.1 Introduction

Chemical crosslinks *vs*. physical crosslinks are bonds that link the polymer chains by covalent bonding or ionic bonding. When the term "cross-linking" is used in the synthetic polymer science field, it usually refers to the formation of chemical links between molecular chains to form a three-dimensional polymer network. Polymer crosslinking can be achieved either by addition of a cross-linking agent (which has the ability to promote the intermolecular covalent bonding between polymer chains and link them together) or by directly inducing chemical reactions between functional groups that are attached to the polymer chains *via* heat, pressure, radiation, or changing the pH.

The use of cross-linked latexes can improve film bulk related properties, such as Young's modulus, surface hardness or water resistance, but they will not show any improvement in interfacial energy upon annealing, like film toughness or tensile strength, due to the absence of physical entanglements at the interface. So if there are linear polymer chains that can entangle with the polymer networks, the film strength at the interface will be greatly improved. When the physical entanglement is restricted, like in hard/soft latex blends, the rate of entanglement formation becomes very low, chemical interfacial crosslinking becomes more important to provide a good connection between the continuous and dispersed phases.

Tobing *et al.*[1] in their study introduced a way to increase adhesive performance by interlinking microgels with linear polymers and further initiating chemical reactions in the blends of acrylic pressure sensitive adhesives (PSA), as shown in Figure 5.1.

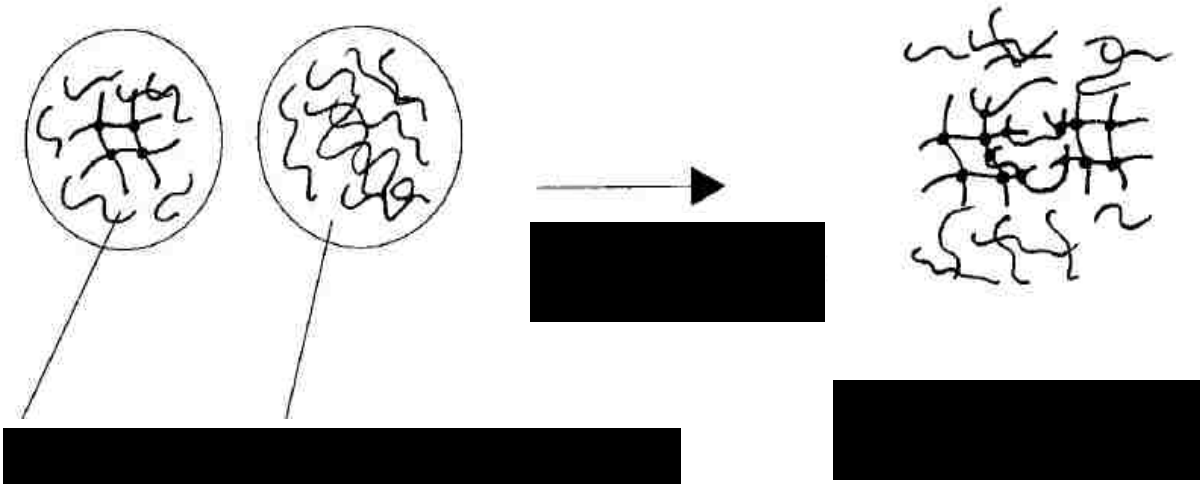

Figure 5.1: Reprint of the scheme of interlinking microgels by linear polymers[1]. After casting the film at room temperature, the film was annealed at 121 °C for 10 min to induce the crosslinking reaction.

As a result, a synergistic effect in shear holding power arose in films prepared with a certain blend ratio, compared to films made of individual latex constituents. They proposed the conditions to obtain this synergism to be: the molecular weight between crosslink points, M_c, of the gel particle is no less than the entanglement molecular weight, M_e, of linear polymer and the molecular weight (M_w) of the linear polymer is greater than $2M_e$.

This present study further expanded Tobing *et al.*'s idea to the high T_g polystyrene system. The film mechanical performance was studied in which gel particles (cross-linked) were interconnected with linear polymers, either by physical entanglements only or by entanglements together with chemical interlinking. Therefore, there are actually two types of crosslinking studied in this work: one is the crosslinking in an existing gel network, which is created during the particle synthesis process by addition of the crosslinking agent, divinylbenzene (DVB); the other is crosslinking created in the film annealing process by initiating a chemical reaction between reactive sites in the gel network and in the mobile polymer chains. To avoid confusion later, the first crosslinking is referred as pre-crosslinking, and the second kind as post-crosslinking.

The pre-crosslinking happens in the particle preparation step before the latex blending and film processing, so it can improve film bulk properties by improving particle properties. But during film annealing, its existence will affect the diffusion of the linear polymer chains in the polymer network. In terms of the post-crosslinking effect, it is more complicated, because it happens together with chain diffusion. Although interdiffusion and cross-linking can both help to strengthen the polymer particle interface,

they are two competitive processes occurring during the film formation. Aradian *et al*. used a scaling approach to build a model presenting this competition and attempted to find some guidelines in optimizing systems in which both interdiffusion and cross-linking (by an external crosslinking agent) exist[2,3]. A control parameter α, which is related to the physicochemical properties of the polymer and the cross-linker, was proposed in their theory and defined as the ratio between the typical interdiffusion time and the typical reaction time. When $\alpha < 1$, the reaction is slow compared to the diffusion, and the polymer chain is able to interpenetrate into the gel network before the reaction takes place; while when $\alpha > 1$, the reaction goes faster than interdiffusion such that the system is frozen before any significant coalescence can occur. A reaction-controlled film formation process ($\alpha < 1$) is needed to enhance the interfacial strength of the film. This control parameter will be discussed more in the next chapter (Chapter 6).

5.2 Experimental

5.2.1 Materials

Methacrylic acid (MAA; Aldrich) monomer was used as received; isopropenyl dimethyl benzyl amine (TMA) was synthesized (see details in Appendix A). Isobutyric acid (Aldrich), heptanoic acid (Aldrich), hydroxyl propyl methacrylate (HPMA, Polysciences Inc.) and glycidyl methacrylate (GMA, Aldrich) were all used as received.

5.2.2 Latex Blends

There are three sets of latex blends used in this study of film mechanical properties in terms of the crosslinking effect: Blend I is the mixture of non-functionalized

crosslinked large particles with non-functionalized non-crosslinked small particles, used for the study of the pre-crosslinking effect; Blend II is the mixture of functionalized non-crosslinked large particles with functionalized non-crosslinked small particles, used for the study of the post-crosslinking effect; Blend III mixes functionalized crosslinked large particles with functionalized non-crosslinked small particles, which combines the two crosslinking effects together. The parameter details of the major latex blends are shown in Table 5.1. Some latex blends were used as controls, the parameters of which will be detailed in the relevant paragraph.

Table 5.1: Characteristics of Latex Blends

	Blend I		**Blend II**		**Blend III**	
Components	Large Particles	Small Particles	Large Particles	Small Particles	Large Particles	Small Particles
D_N **(nm)**	413	81	302	86	351	86
D_w/D_N	1.003	1.106	1.004	1.030	1.003	1.030
V_c	20.6 %		27.4 %		24.5 %	
M_c **(g/mol)**	50,000	-	-	-	54,000	-
M_W **(g/mol)**	-	150,000	290,000	100,000	-	100,000
M_w/M_N	-	2.08	1.90	1.45	-	1.45
M_e **(g/mol)**	-	36,000	32,000	36,000	-	36,000

In the table, D_N is the number-average particle size *via* SEM; V_c is the volume percentage of small particles; M_c is the molecular weight between crosslinking points in the crosslinked large particle; and M_W is the weight- average molecular weight of linear

polymer chains in noncrosslinked particles; The entanglement molecular weight M_e is calculated by applying the plasticize model.

Concerning the reactive latex blends (Blends II and III), there is another parameter (other than the optimum blend ratio V_c) that needs to be considered when blending the latexes, which is the pH. Since the pH of the carboxyl functionalized latex is about 4.5, and the pH of the amine functionalized latex is about 8.5, this large difference in pH causes the blended latex to be unstable without any pH adjustments. Through SEM images (see Figure 5.2b), the reason for the instability of the blends can be found out, which is the coagulation results in the phase separation between the two particles. It is worth mentioning that the latex blends prepared from uncleaned latexes (in the presence of surfactants) were observed to be stable for a short time, but not beyond 12 hours, probably because the surfactant absorbed on the latex surfaces were able to keep the functional groups separated from each other (see Figure 5.2a).

Two different treatments were tested: (1) neutralizing COOH-functionalized latex by adding ammonia solution (~ 0.10 N); (2) neutralizing NH_2-functionalized latex by addition of HCl solution (0.02 N). The ammonia treatment proved to be successful. The blends were stable beyond a week and exhibited a close-packed structure in which large particles were isolated by small particles (see Figure 5.2d). The acid treatment turned out to be unsuccessful. The amine functionalized latex was not stable right after addition of the dilute HCl solution. A possible reason may be that when the pH is low, NH_2 groups attached to the latex particles are protonated into NH_3^+ which then form ionic bonds with

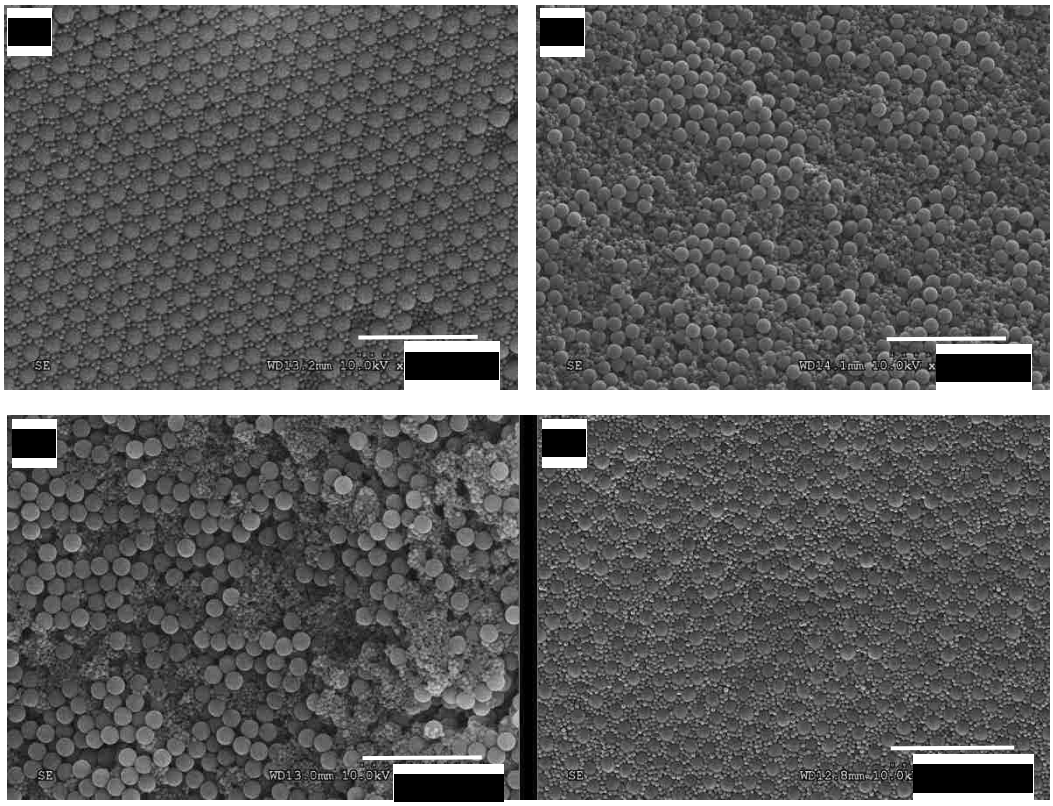

Figure 5.2: (a) Uncleaned latex blends; (b) cleaned latex blends without pH treatment; (c) latex blends after HCl treatment of NH_2 functionalized latex; d) blends after ammonia treatment of COOH functionalized latex.

the SO_3^- groups attached to the Aerosol MA-80 surfactant (see Figure 5.2c). This might also be the reason for the coagulation that occurred in the cleaned latex blends without pH adjustment.

Because of the reversible neutralization reaction, the addition of ammonia to the system does not affect the film properties, once the dried blended latexes are sintered:

$$\text{R-COOH} + NH_4OH \leftrightarrow \text{R-COO}NH_4 + H_2O \quad (5.1)$$

$$\text{R-COO}NH_4 \rightarrow \text{R-COOH} + NH_3 \uparrow \quad (5.2)$$

At the sintering temperature of 120 °C ~ 130 °C, ammonia is able to evaporate from the film, leaving COOH in place to react with NH_2 groups during the annealing process.

After mixing, the blends were then dried, sintered, and annealed according to the procedure detailed in Chapter 2.

5.2.3 Characterization Methods

Infrared spectroscopy (IR) and nuclear magnetic resonance (NMR) were used to investigate the reactivity of different chemical reactions between COOH and NH_2, NCO and OH moieties both within small molecules and in solid polymers.

The chemical kinetics in the COOH/NH_2 small molecule reaction was investigated with the experimental determination of the reaction rates. The reaction rate constant and the activation energy were then calculated by two different methods: one is based on the second-order reaction for the condition that both chemicals have comparable

concentrations; the other one is based on the integrated first-order rate laws on the condition that one chemical is in great excess. Nuclear magnetic resonance (NMR) was used to monitor the amount of TMA decreasing with the reaction time.

The Instron and advanced rheometric expansion system (ARES) were used to test the film tensile strength at room temperature and at elevated temperatures, respectively.

5.3 Results and Discussion

5.3.1 Determination of Reaction Activities

To separately control the film diffusion process and the chemical reaction process, an intermediate temperature region is required, which is not high enough to bring about a significant chemical reaction between the functional moieties but is higher than the glass transition temperature T_g of the blends, such that polymer chain diffusion can proceed in the absence of the chemical reaction. Therefore, a screening test on the reaction kinetics of different small molecule reactions has been done to find out a proper pair of reactive groups that has a minimum reaction temperature beyond 120 °C (the sintering temperature for polystyrene film).

By fixing the carboxyl group COOH as one of the reactive moieties, which can react with a variety of reactive groups, the search range was reduced to the determination of the other proper reactive moiety. Four different reactions were investigated in parallel

between the carboxylic acid group and the hydroxyl, epoxy, isocyanate, and amine groups.

Figure 5.3 compares the NMR results of the four reactions taking place at different temperatures (room temperature, 100 °C and 150 °C). By monitoring the chemical shift change of the carbonyl (C=O) carbon from 180~190 ppm in the carboxylic acid group to 160~170 ppm in the ester or amide group, it was found that COOH/OH and COOH/epoxy reactive pairs could be totally converted to the reaction products at 100 °C. The COOH/NCO reactive pair needed a higher temperature for the initiation, but a partial reaction was still observed at 100 °C. Only the pair of carboxyl and amine reactive groups did not react at 100 °C but did at approximately 150 °C. Therefore, this reactive pair was decide to be introduced the latex film system for the study of crosslinking effect.

Because the T_g of polystyrene is near 105 °C, and based on the preceding results, there existed the possibility that within an approximately 30 °C temperature range (110 ~ 140 °C), only polymer chain diffusion should take place with the absence of significant COOH/NH_2 reaction. However, this prediction from the results of small molecules reaction needs to be validated by the actual polymer reaction at the particle-particle interface inside the film, as will be discussed later in this chapter.

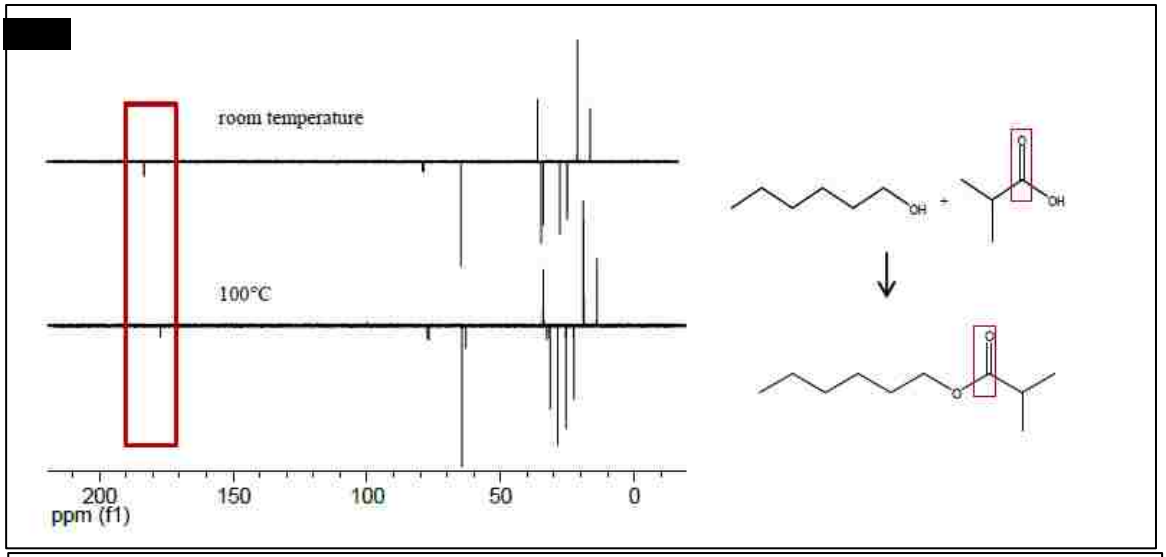
room temperature
100°C
200
150
100
50
0
ppm (f1)
OH
OH
O
O

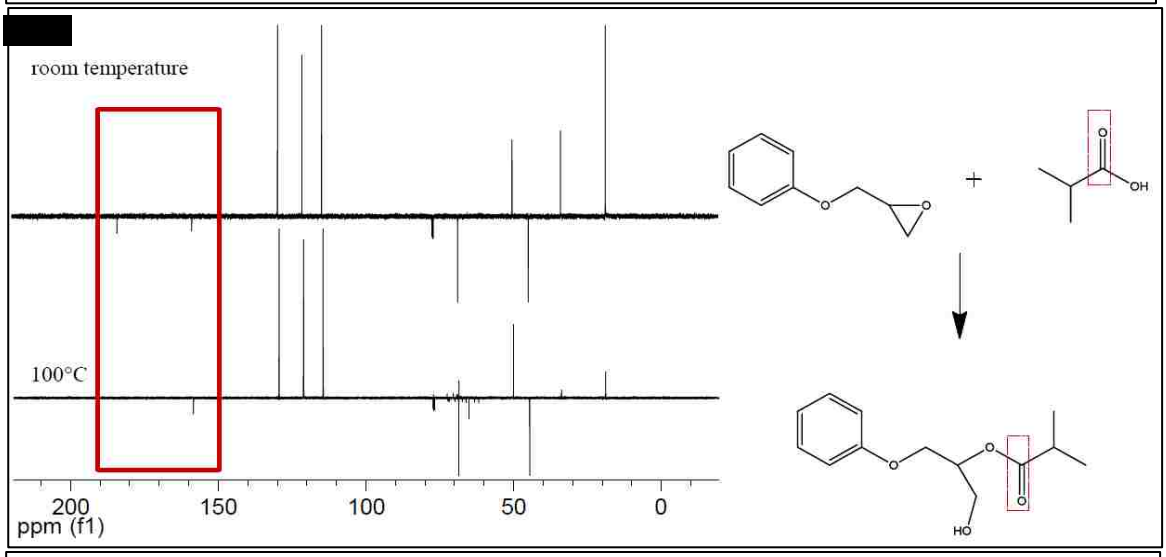
room temperature
100°C
200
150
100
50
0
ppm (f1)
O
OH
HO

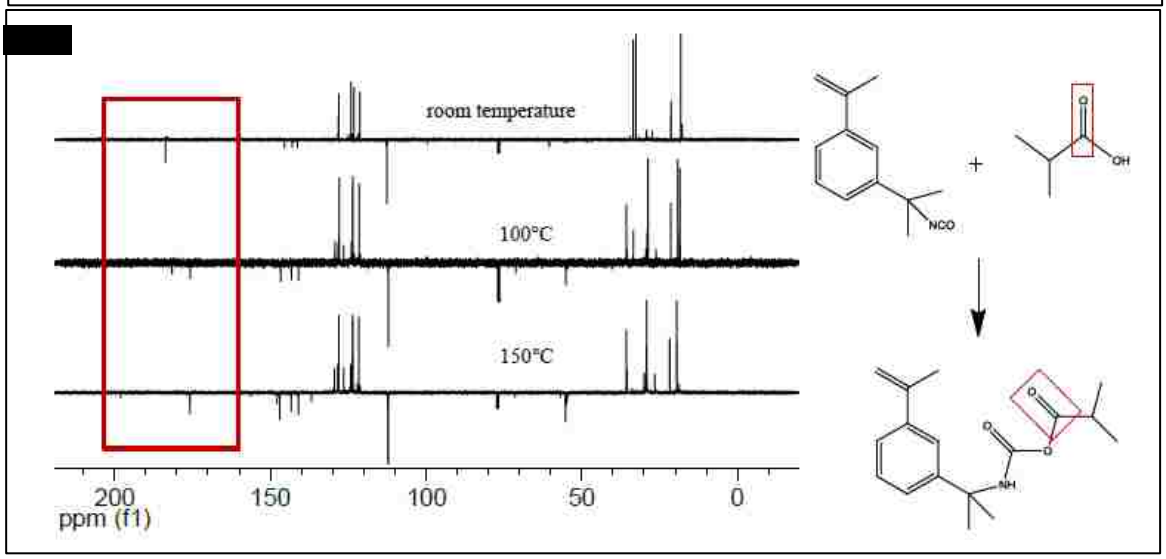
room temperature
100°C
150°C
200
150
100
50
0
ppm (f1)
NCO
OH
NH

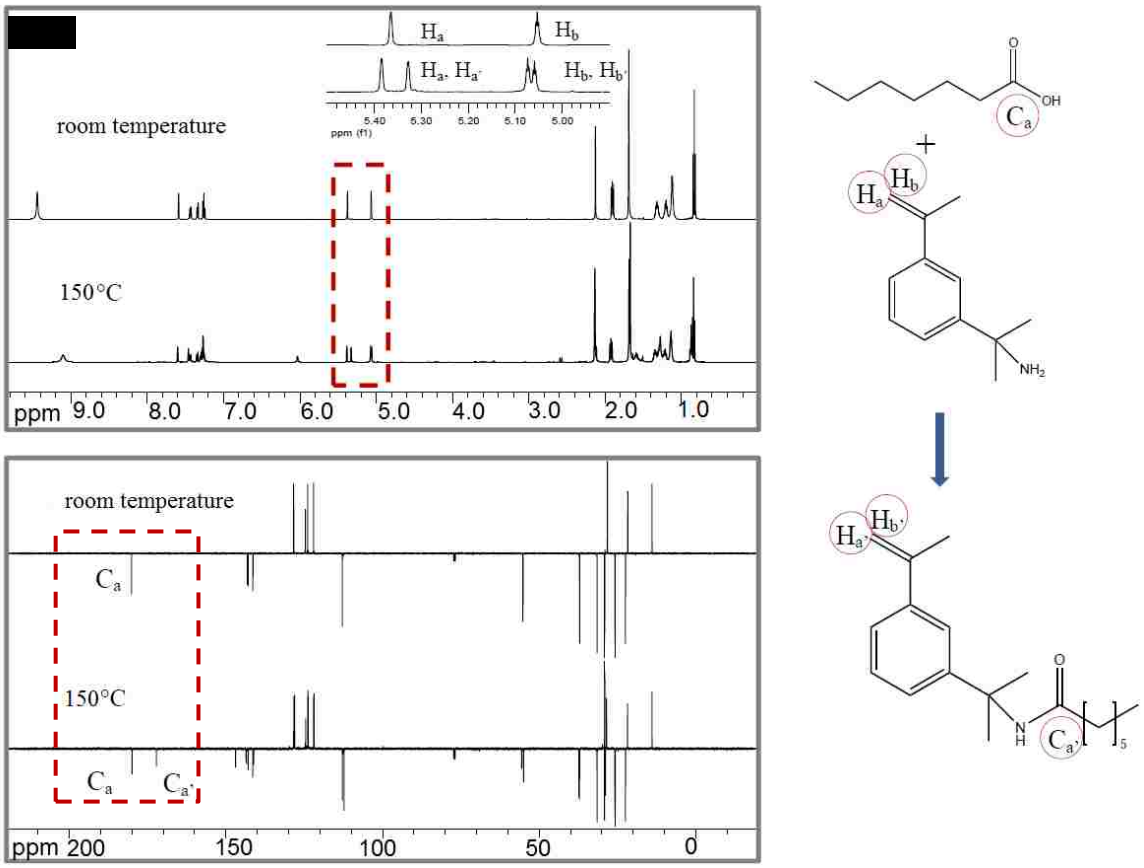

Figure 5.3: Distortionless Enhancement by Polarization Transfer (DEPT, one kind of ^{13}C NMR test) comparison results for: a) the reaction between isobutyric acid and hexanol at room temperature and 100 °C; b) the reaction between isobutyric acid and glycidyl metharylate at room temperature and 100 °C; c) the reaction between isobutyric acid and m-isopropenyl-α,α'-dimethylbenzyl-isocyanate (TMI) at room temperature, 100 °C and 150 °C; d) ^{1}H and ^{13}C NMR comparison results of the reaction between heptanoic acid and isopropenyl dimethylbenzyl amine (TMA) at room temperature and 150 °C. All the reaction times were more than 10 hours. In a), b), and c), isobutyric acid was used instead of the monomer methacrylic acid (MAA), because MAA with a double bond attached can homopolymerize at a temperature beyond 70 °C, while isobutyric acid, which has the similar structure to MAA, will not. In d), the heptanoic acid was used instead of isobutyric acid, because later in the study, higher reaction temperatures beyond 150 °C are required for a further investigation to the kinetics of this $COOH/NH_2$ chemical reaction. Heptanoic acid has a higher boiling point close to 230 °C than that of isobutyric acid, which is approximately 155 °C.

5.3.2 Analysis of the Chemical Kinetics in COOH/NH_2 Small Molecule Reaction

Two methods were applied to determine the reaction rate constant in the heptanoic acid/TMA small molecule reaction at various reaction temperatures. The activation energy of the reaction was calculated accordingly.

5.3.2.1 Second-Order Reaction

A typical acid and base reaction obeys the second order reaction law, so when the two reactants at comparable concentrations, it is reasonable to assume this COOH/NH_2 reaction is also a second order reaction with the reaction rate given by equation 5.3:

$$r = k_r[COOH]^1[NH_2]^1 \tag{5.3}$$

In this study, the ratio of [COOH]/[NH_2] = 2:1 was used, instead of 1:1 ratio, because heptanoic acid is more volatile than TMA, and one reactant in a little more excess can help the reaction equilibrium move to the product side.

Figure 5.4 presents typical ^{1}H NMR spectra showing the intensity evolution of the proton chemical shift in the vinyl group from the reactant TMA to the product amide. Based on these ^{1}H NMR results, the concentration of TMA remaining was plotted *vs.* reaction time at various temperatures (see Figure 5.5a). It is difficult to directly calculate the reaction rate constant from the reaction rate based on the second-order rate law, because this second order reaction is neither only first order in [COOH] nor only first order in [NH_2]. However, since the reaction rate constant is considered to be only temperature dependent, which means it remains the same from the very beginning to the

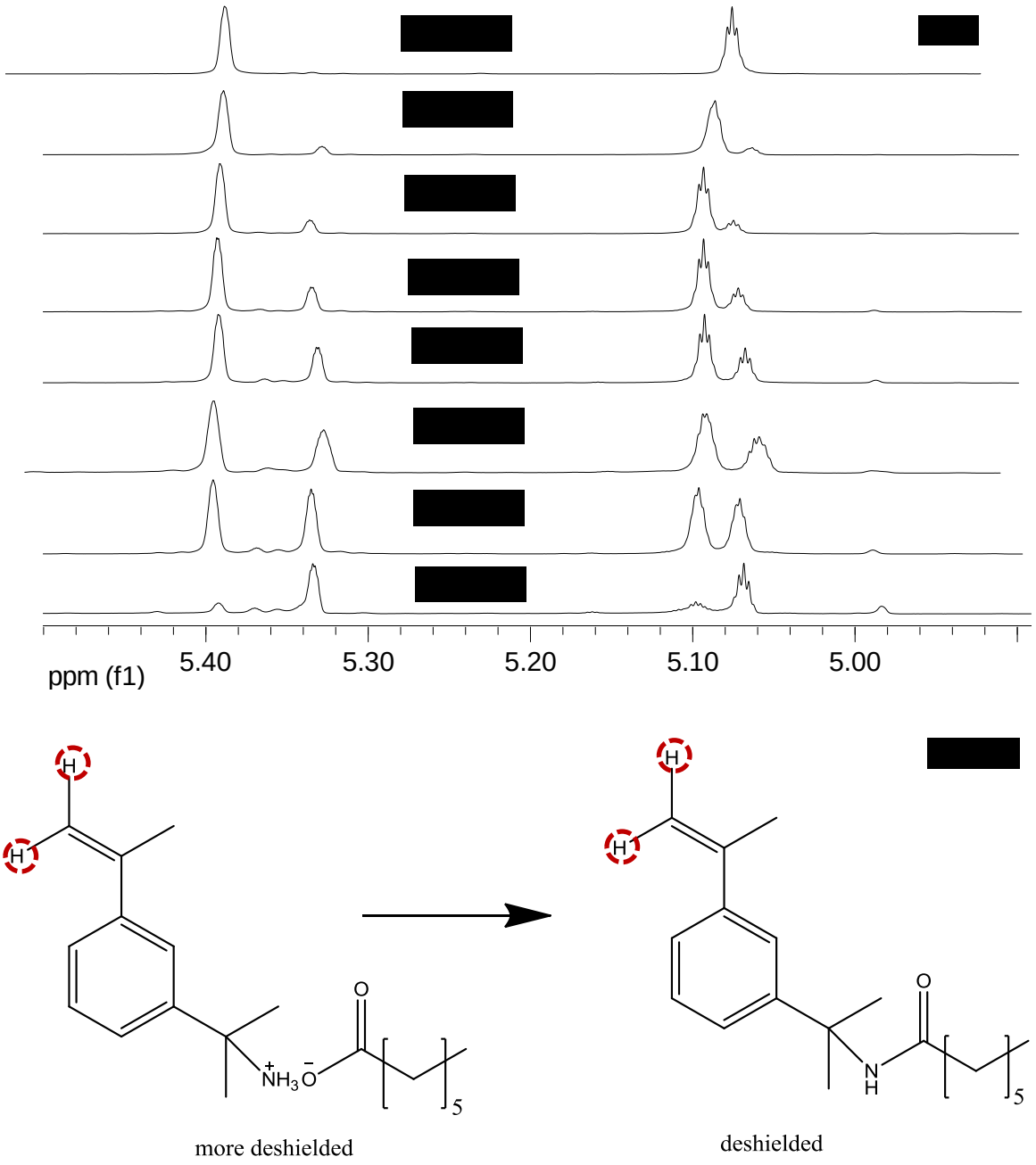

Figure 5.4: a) ^{1}H NMR spectra evolution showing the changes in the vinyl proton chemical shift intensity in the isopropenyl group attached to the benzene ring from the beginning of the reaction to the 25 h reaction time; b) illustration of the electronic environment change from the reactant to the product; the vinyl proton is more deshielded in the reactant salt than in the product with the amide covalent bond.

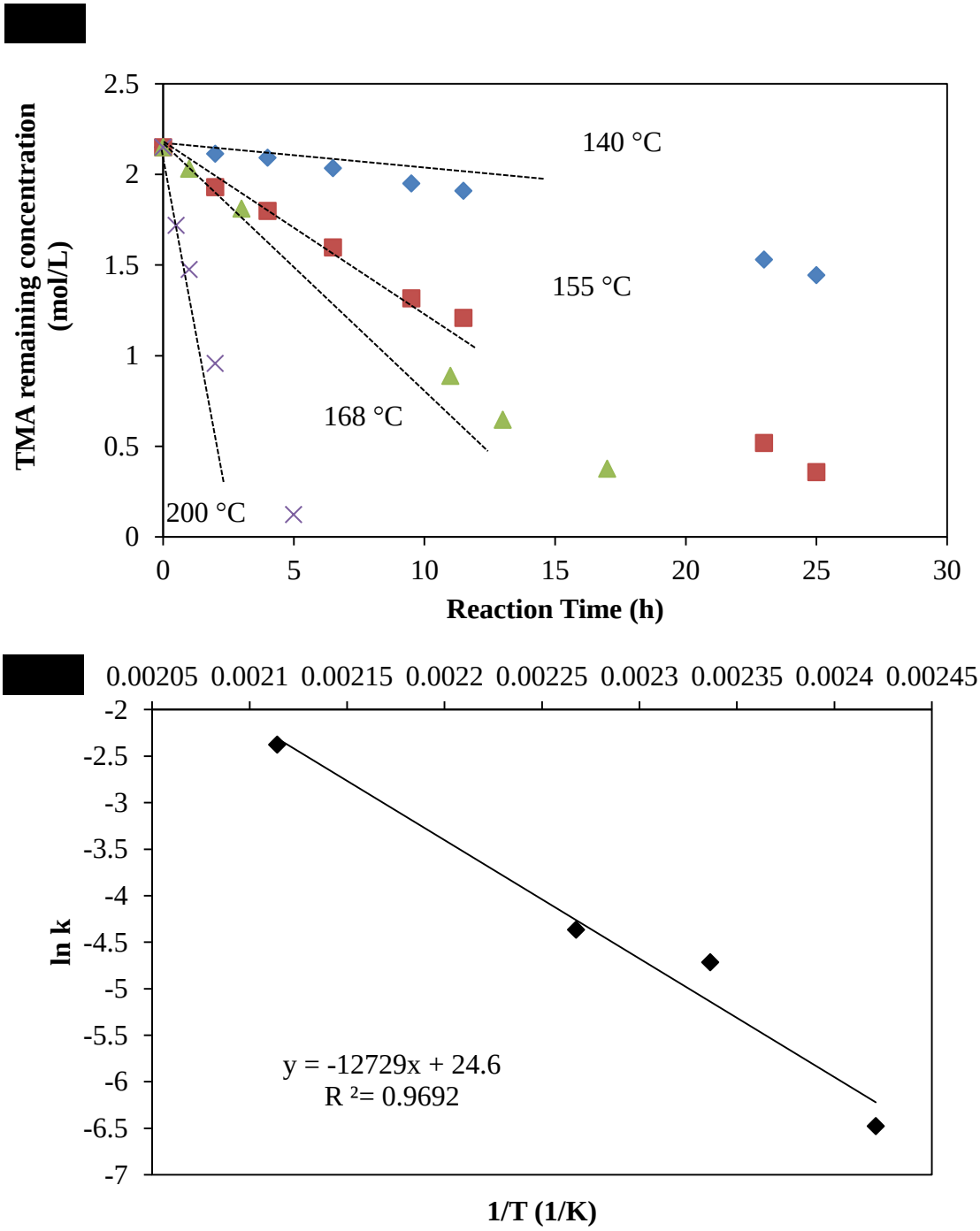

Figure 5.5: a) Amount of TMA remaining *vs.* reaction time at (◆) 140 °C; (■)155 °C; (▲) 168 °C; (×)200 °C; b) Arrhenius plot of natural logarithm of the reaction rate constant *vs.* the inverse temperature by monitoring the initial reaction rates.

end of the reaction, the reaction rate constant can be calculated based on the initial reaction rate and the initial reactant concentrations.

The reaction rate constants at different temperatures have been plotted *vs.* the reciprocal of absolute temperatures. According to the Arrhenius equation:

$$\ln k_r = -\frac{E_a}{R}\left(\frac{1}{T}\right) + \ln A \qquad (5.4)$$

in which k_r is the reaction rate constant, E_a is the activation energy, R is the gas constant, T is the temperature in Kelvin, and A is the pre-exponential factor.

The activation energy from the slope of the line in Figure 5.5b, was calculated to be 25.3 kcal mol^{-1}.

5.3.2.2 A Pseudo-first Order Reaction

Another way to check the reaction rate constant is to use the integrated first-order reaction rate law in a pseudo-first order reaction in TMA (in this case, $[COOH]/[NH_2]>20:1$). When the acid is in great excess, the concentration of the acid is assumed to be constant throughout the reaction. Thus, the reaction rate is given by:

$$r = k_r'[NH_2]^1 \qquad (5.5)$$

in which k_r' is equal to the real reaction rate constant k_r times the concentration of the acid.

Therefore, based on the integrated first-order rate law:

$$\ln[NH_2] = -kt + \ln[NH_2]_0 \qquad (5.6)$$

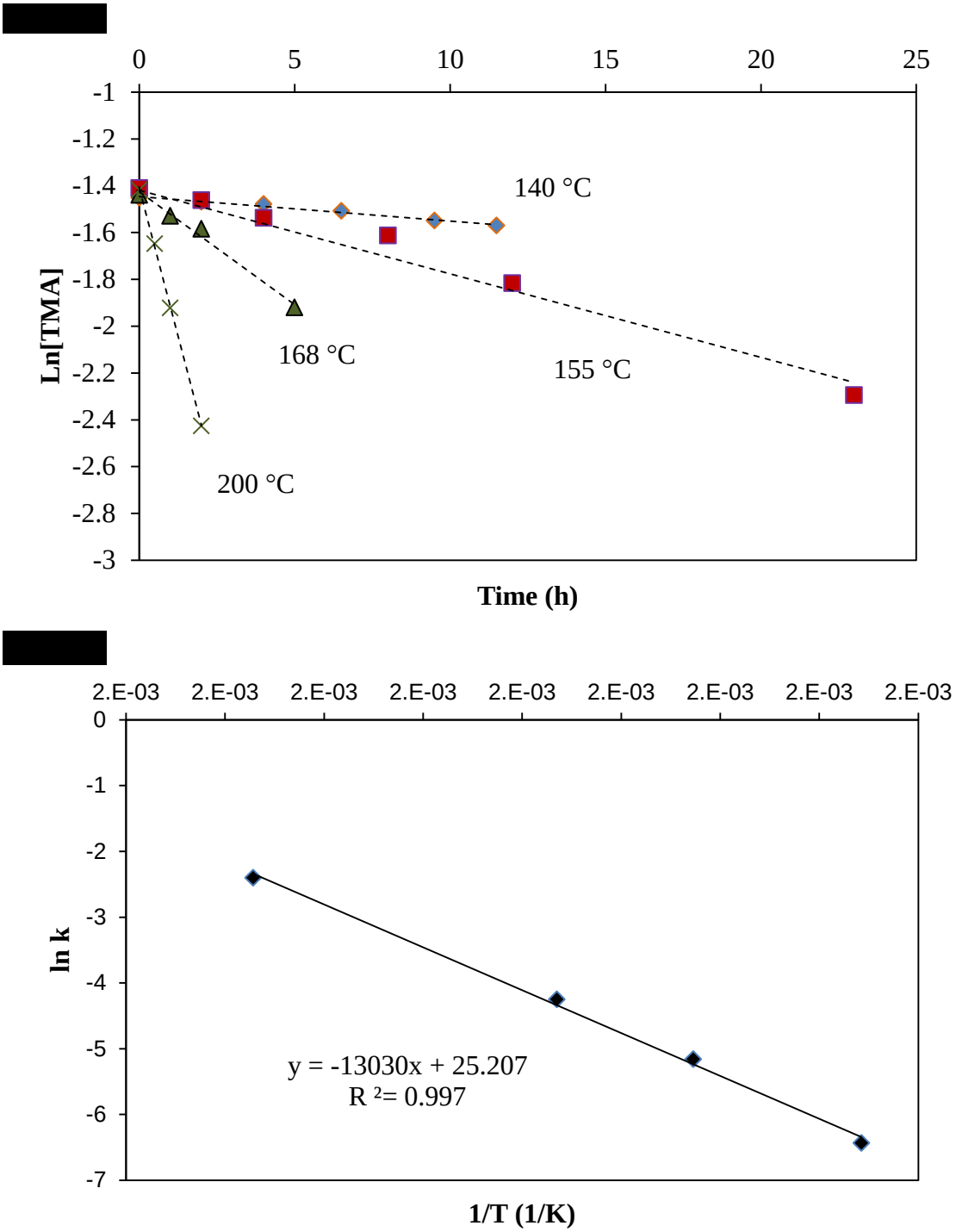

Figure 5.6: a) Natural logarithm of the amount of TMA remaining *vs.* reaction time at (◆) 140 °C; (■)155 °C; (▲) 168 °C; (×)200 °C; b) Arrhenius plot of natural logarithm of the reaction rate constant *vs.* the inverse temperature.

the natural logarithm of the concentration of TMA remaining (monitored by ^{1}H NMR) was plotted *vs.* reaction time at various temperatures (see Figure 5.6). Accordingly, the activation energy was calculated to be 25.9 kcal mol^{-1}, which is very close to the value obtained using the initial rates calculation (25.3 kcal mol^{-1}).

5.3.3 Analysis of the Chemical Kinetics in the Polymer Reaction

The polymer reaction here actually refers to the chemical reaction inside the latex films comprised of bimodal reactive latex blends. Different from the small molecules reaction, the chemical reaction generates the crosslinking between polymer macromolecules (see Figure 5.8b), which means the products can hardly be dissolved in any good solvent that can be used to dissolve the polymer itself. Therefore, the reaction rate in polymers cannot be monitored by liquid NMR. Neither can it be tracked by solid state NMR, because the amount of functional groups that are incorporated is very small (5 wt%) compared to that of the backbone polystyrene and the amount of carbonyl end groups is even smaller than that of the C-C chain in each individual polymer, which makes the change of the C=O carbonyl chemical shift very hard to be detected.

FTIR can overcome the solubility and sensitivity problem, but different from small molecules spectrum, in the IR spectrum of latex films, both carbonyl stretching bands at high and low frequency in the amide product are overlapped with the aromatic C=C bending band in the benzene ring of polystyrene (between 1700 cm^{-1} ~1500 cm^{-1}) which makes the reaction change difficult to detect.

Since the direct measurement is not available, de Gennes' scaling relationship is applied to back calculate the reaction rate constant, using equation 5.7:

$$t_{reaction} \cong \frac{N_c}{N} \frac{1}{QA_0^* b^3} \tag{5.7}$$

in which N_c is the number of monomers per crosslink (reached when the cross-linking reaction is completed), N is the total number of monomers per chain, and A_0^* is the initial volume concentration of the reactive sites in the system, which in this study is the concentration of the acid that takes part in the reaction. Q is the reaction probability and b is the capture distance, within which the reaction is able to occur.

Because Qb^3 in the physicochemical relation is considered to be equal to the reaction rate constant[3,4] k, the reaction rate constant can be calculated based on the reaction completion time t_{react}. Concerning the determination of the reaction conversion, the evolution of the crosslinking density in the system is used as the indicator. Basically, the more complete the reaction is, the tighter the gel network will be. Therefore, by using the swelling measurement (see details in Chapter 2), the extent of crosslinking in the system can be measured in terms of the molecular weight between crosslinks, M_c and crosslinking density, ρ_c. Figure 5.7a shows one of the typical M_c and ρ_c profiles *vs.* the reaction time. If precrosslinking density exists in the system, the relative reaction fractional conversion can be derived by subtracting the existing crosslinking density from the system (Figure 5.7b) using equation 5.8:

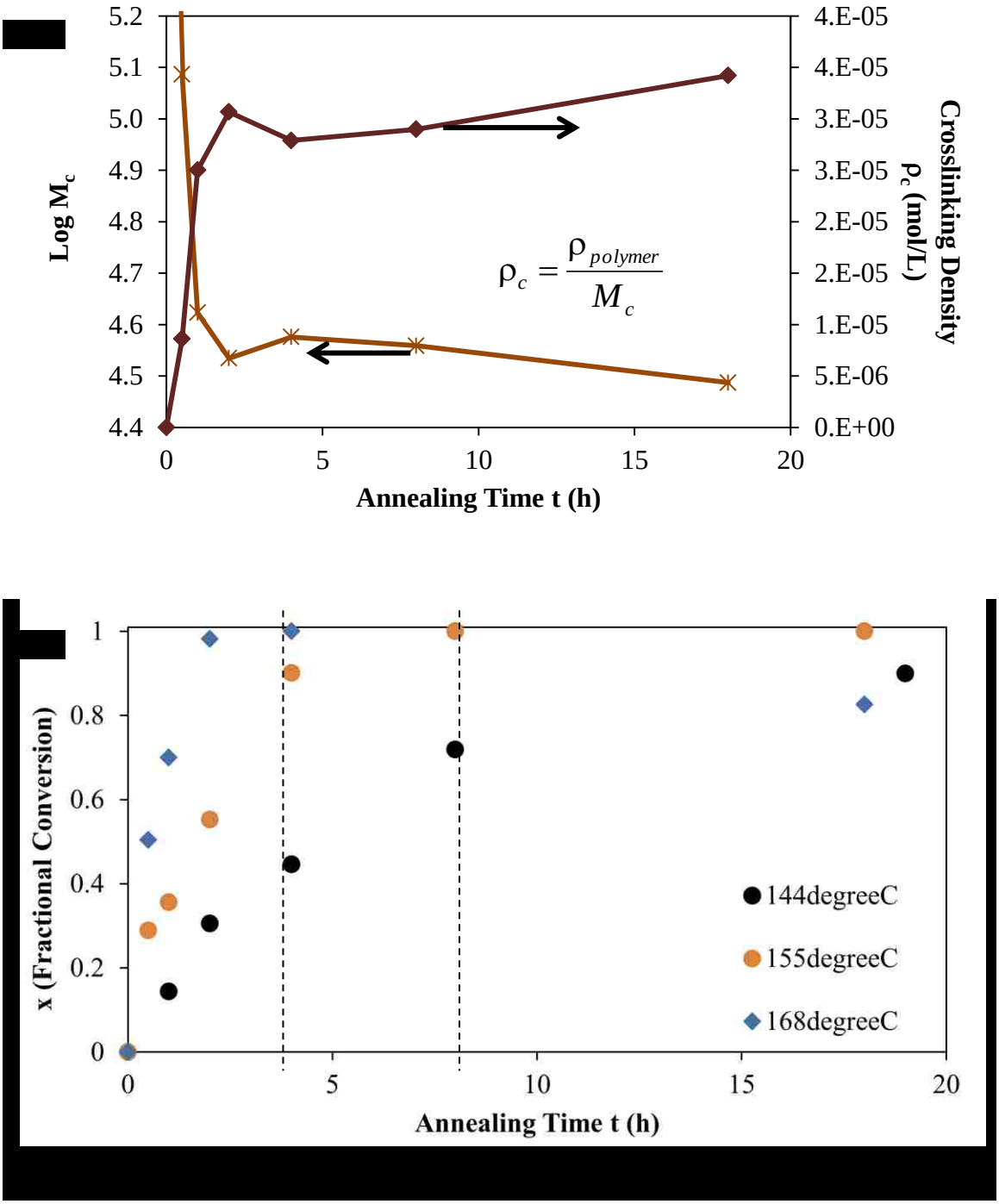

Figure 5.7: a) Evolution of crosslinking over time for films comprised of latex Blends II annealed at 165°C, in terms of the molecular weight between crosslinks (M_c) and crosslink density ρ_c. Because there is no crosslinking at t=0, M_c is supposed to be infinity; b) Calculated fractional conversion of the reaction considering the plateau of the crosslinking density is the final crosslinking density when the reaction is complete. The complete reaction time at 144 °C is beyond 24 hour, which is out of the x axis range.

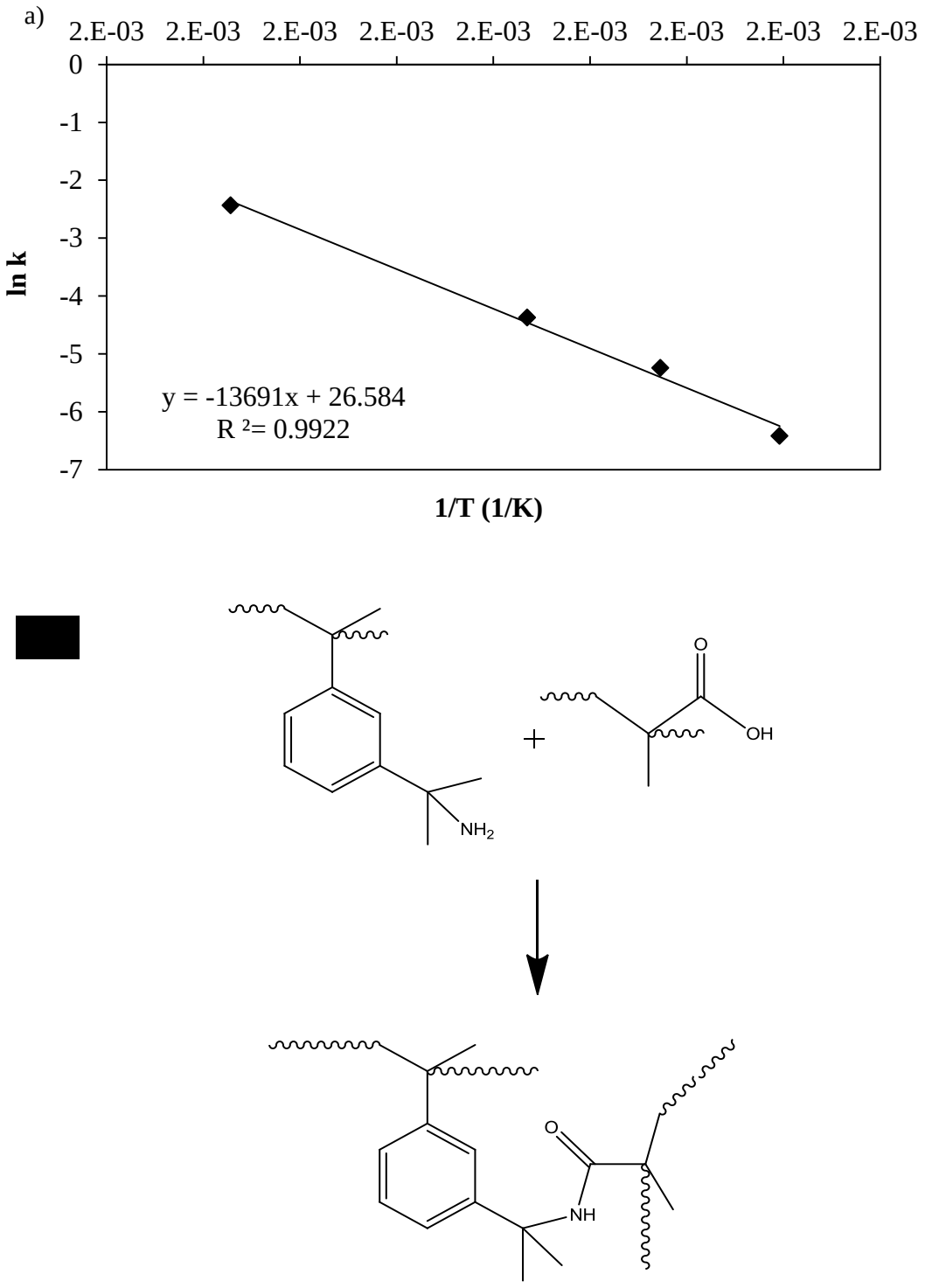

Figure 5.8: a) Arrhenius plot of natural logarithm of the reaction rate constant *vs.* the inverse temperature for the polymer reaction; b) Illustration of the crosslinking reaction between polymer chains.

$$x = \frac{n_t}{n_\infty} = \frac{\rho_t - \rho_0}{\rho_\infty - \rho_0} \tag{5.8}$$

in which n_t, n_∞, ρ_0, ρ_t, and ρ_∞ respectively represents the number of crosslinks at time t, final number of crosslinks, the initial crosslinking density, the crosslinking density at time t and final crosslinking density.

With measured reaction times t_{react} in hand, the reaction rate constants at various temperatures were calculated and the Arrhenius plot was made to determine the activation energy of the polymer reaction (see Figure 5.8a).

The activation energy of the polymer reaction was calculated to be 27.2 kcal mol^{-1}, which was comparable to the activation energy in the small molecule reaction. The difference (~1.5 kcal mol^{-1}) shows the additional difficulty for a chemical crosslinking reaction to occur in polymers due to the retardation of the macromolecules movements.

5.3.4 Analysis of the Control Parameter α

As mentioned before, there exists a competition between interdiffusion and chemical crosslinking reaction in a reactive film during the annealing process. According to de Gennes' scaling relationship, if the control parameter α, which is the ratio of the typical diffusion time to the typical reaction time, is less than 1, the reactive film is predicted to have a better mechanical performance in terms of the "interface-related" properties, such as film tensile strength.

By knowing the diffusion time in the absence of reaction and the reaction time without any diffusion taking place, the value of the control parameter can be experimentally calculated. As a result, a nonreactive and reactive film system pair needs to be prepared, which comprise of the crosslinked large particles (with similar crosslinking densities) and non-crosslinked small particles (with similar molecular weights of the linear polymer chains). The latex film made of latex blends I and the film comprised of latex blends III are the candidate systems used for comparison.

From the previous section, the complete reaction time can be estimated by measuring the evolution of crosslinking density inside the latex film. Similar to the determination of the typical reaction time, the typical diffusion time can be considered as the time to reach the plateau value in the tensile strength development profile. Based on the tensile strength profile of the latex film made of Blends I, the diffusion time is very short compared to the time needed for a complete reaction. The annealing temperature at 144 °C can be taken as an example. The diffusion time is less than 1 hour, while the typical reaction time is 24 hour. The control parameter α is, therefore, calculated to be far less than 1, which indicates the 144 °C annealing condition for the reactive film comprised of Blend III is reaction controlled. At 155 °C and 168 °C, the diffusion time is too short to be detected accurately (less than 5 minutes). Thus, the control parameter in these two cases is also less than 1, because the reaction time has the dimension of hours.

In the following sections, only 168 °C annealing temperature was chosen as representative to study the chemical crosslinking effect on the film strength. More discussion comparing different annealing conditions is found in Chapter 6.

5.3.5 Crosslinking Effect on Film Modulus *via* Dynamic Mechanical Analysis

Dynamic mechanical thermal analysis was performed on the films comprised of reactive latex Blend III (III_Blend) and films made of each individual component particles (crosslinked large particles (III_Large) and non-crosslinked small particles (III_Small)).

Figure 5.9 shows the temperature dependence of the storage modulus (G') and loss tangent (tan δ) for sintered films (sintered at 130 °C without annealing, which means the chemical reaction has not yet taken place in the films made of reactive latex blends). Only physical entanglements are responsible for the development of the mechanical integrity. It is observed that crosslinking broadens the transition region of the storage modulus G' and the peak width of tan δ. Compared to the non-crosslinked latex film, crosslinked films exhibit higher rubbery plateaus, G_0', and lower maximum values for tan δ. There is not much difference between the two pre-crosslinked films (III_Blend and III_Large), however, III_Blend presents a relatively broader tan δ than III_Large.

These results prove that crosslinking helps to improve the film modulus, which represents the stiffness of the film on a macroscopic level. The films made of blended latexes and films comprised of large size crosslinked latexes have similar storage moduli,

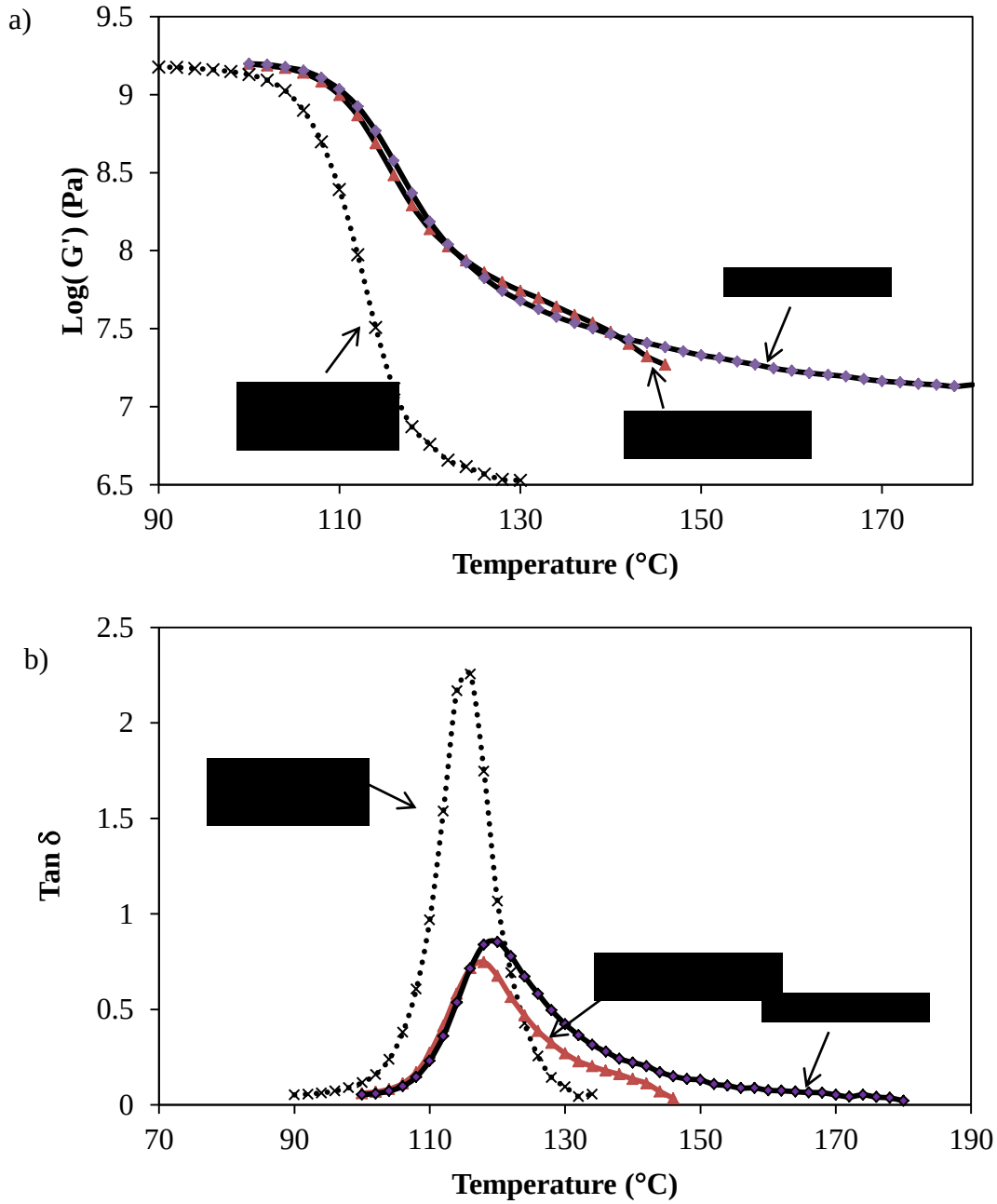

Figure 5.9: a) Storage modulus G' *vs.* temperature for sintered blended films (III_Blend) and films comprised of each individual particle (III_Large & III_Small). The film interface is only connected by physical entanglements; b) loss factor tan δ *vs.* temperature. The tan δ of crosslinked films is lower and has broader peak width than that of noncrosslinked films.

because they have similar crosslinking density right after the sintering process (both contributed by the crosslinked large particles). The tan δ peak is broader for the blended film compared to that of films made of large crosslinked latexes, because the sintered blended latex film is not a homogenous system. During the sintering process, there is not much polymer chain interpenetration between neighboring particles. A wide composition distribution leads to a broad range of transition temperatures.

The film modulus change was then investigated during the annealing process when the chemical crosslinking at the interface takes place. The comparison of storage moduli of blended films at various annealing times is shown in Figure 5.10. No change in tan δ (both the height and width) indicates that there is no significant phase separation during crosslinking, which means the blended film system is homogenous with most of the polymer chains already entangled in place when the chemical crosslinking reaction occurs. The rubbery plateau G_n^0 in the storage modulus G' increases with increasing annealing time, and the slope is more flattened as the crosslinking density increases.

However, a conclusion cannot be made that the rubbery plateau increases due to the contribution of the increased chemical crosslinking during the annealing process. Because the rubbery plateau in the profile of storage modulus is a viscosity-dependent bulk-related parameter, which is related to the molecular weight M_e' between entanglements or crosslinks[5] in the bulk system, by the equation 5.9:

$$M_e' = \frac{\rho RT}{G_n^0} \tag{5.9}$$

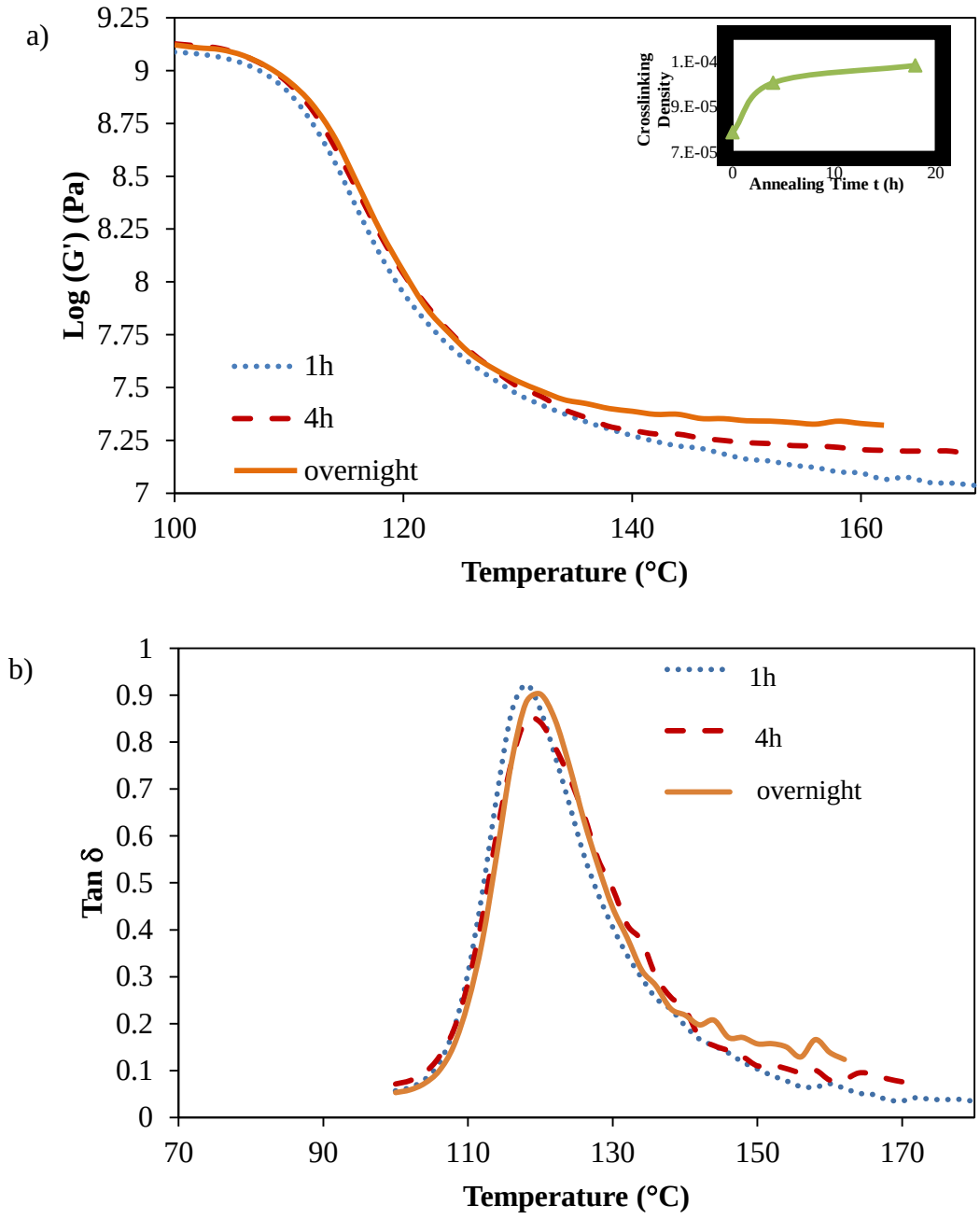

Figure 5.10: a) Storage modulus, G', *vs.* temperature for films comprised of III_Blend, annealed at 168 °C for various times; Inset is the evolution of crosslinking density as a function of annealing time; b) loss factor, tan δ, *vs.* temperature. The tan δ is almost the same for sample films III_Blend during annealing.

in which r is the density of the polymer, R is the gas constant, T is absolute temperature where G_n^0 is located, and G_n^0 is determined from the storage moduls G' at the onset of the rubbery region. For a crosslinked system, it is determined as the point of inflection in tan δ curve following the maximum point.

Therefore, the rubbery plateau value in Figure 5.10 actually reflects the contribution from both the physical entanglements and the crosslinking, but the dominant contribution is not sure. When the rubbery plateau value of the fully annealed films (physical entanglement completed as well as the chemical reaction completed) was compared, M_e' in the nonreactive film (III_Small) was decreased to 2.4 $\times 10^4$ g/mol (almost ten times decrease) from the original M_e' value of 1.04 $\times 10^5$ g/mol. However, M_e' in the fully annealed reactive film (III_Blend) was only decreased from 1.91×10^4 g/mol to 1.71×10^4 g/mol, which indicated fewer entanglements and less interpenetration took place at the particle-particle interface due to the additional chemical crosslinking.

Again, this is only an indication, and a sound conclusion cannot be made based on the DMA data. However, it proves that crosslinking helps to increase film modulus. To know the exact interpenetration distance in the reactive film, more direct characterization methods are needed, such as the measurements from small angle neutron scattering (SANS).

5.3.6 Crosslinking Effect on Film Tensile Strength

As mentioned before, in terms of crosslinking, there are pre-crosslinking (bulk or homogenous crosslinking) and post crosslinking (interface crosslinking). The film

strength can be built either by physical entanglements or chemical interlinkings at the interface in addition to the physical entanglement.

5.3.6.1 Pre-crosslinking Effect (Bulk Crosslinking)

If only physical entanglement plays a role in the film tensile strength build-up, the more effective the entanglements are at the interface, the higher the tensile strength that the film can achieve. Therefore, it is predicted that if crosslinked particles are introduced to the film system and the size of the crosslinked network is suitable for the linear polymer chains to be able to entangle with the microgel, the interfacial strength will be enhanced after fully entanglement of the chains with the network. From Figure 5.11a, it was found that the tensile strength of the precrosslinked film (comprised of Blend I) was higher than that of the noncrosslinked film comprised of only small particles. The plateau tensile strength of the Blend I film was similar to but did not exceed the upper limit of the polystyrene film tensile strength as mentioned in Chapter 4.

The result is understandable. If the crosslinked particle is assumed as a net and the polymer chains inside the noncrosslinked particle are like the threads made of the same material as the net, when the threads are short, they cannot form sufficient entanglements among themselves but they are able to form effective entanglements with the help of the net. On the other hand, if the threads are long enough, they are able to form sufficient entanglements within themselves and have no need for the net. Thus, there will be no difference at the breaking surface when the ultimate condition is achieved, in which all threads (including the net) are broken instead of threads being pulled out. Therefore, the

film made of Blend I had a higher tensile strength than the film made of its linear particle component, because the linear chains themselves cannot form effective entanglements, but with the help of the crosslinked network they will be able to create enough entanglements at the interface. The film, however, cannot exceed the maximum tensile strength that a polystyrene film can achieve, because the upper limit of the tensile strength is only dependent on the intrinsic properties of the polymer.

Predictably, the pre-crosslinking effect cannot be recognized if the linear polymer chains are long enough to achieve sufficient entanglements. Figure 5.11b shows that the tensile strength of the blended film (comprised of crosslinked particles and linear polymer particles with high polymer molecular weights) is the same as the strength of the unblended film made of linear particles only.

5.3.6.2 Post-crosslinking Effect (Interfacial Crosslinking)

When there is crosslinking at the particle-particle interface in addition to the physical entanglement, it is more complicated to determine the crosslinking effect on the film tensile strength. If there are only physical entanglements, the interfacial strength in a fully annealed film will be equal to the bulk strength of the film. However, when the interface is composed of both chemical bonding and physical entanglements, the structure of the interface has changed and the final interfacial strength is no longer equal to the bulk strength of the film (because in the bulk, there is seldom chemical bonding). The film strength is therefore dependent on the weaker part of the film, whether it is equal to the interfacial strength or the bulk strength.

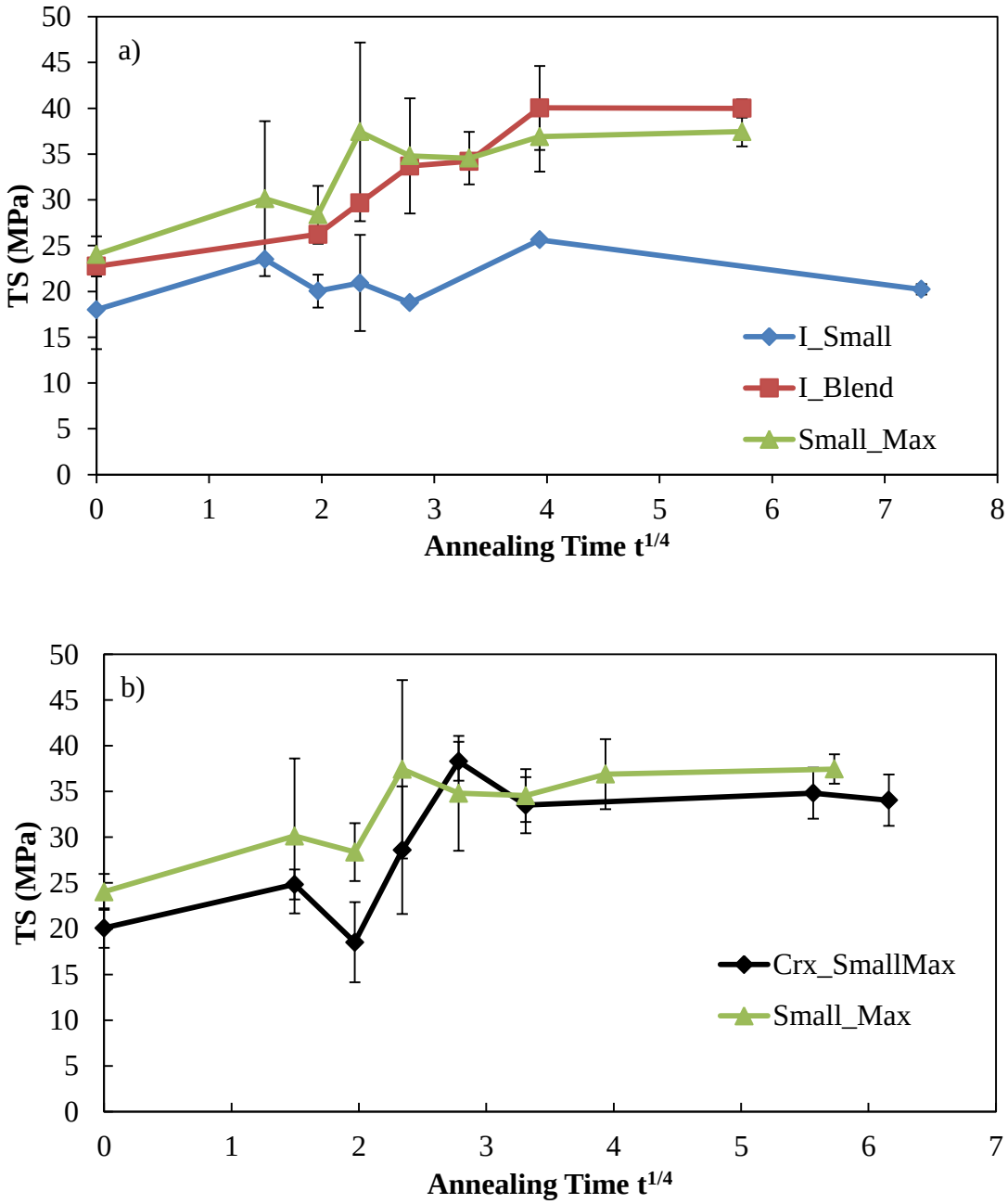

Figure 5.11: Tensile strength comparison *via* Instron at room temperature. a) 'Small_Max' represents the latex film that has the highest tensile strength if only physical entanglement plays a role in film strength, which is made of 74 nm PS particles with the weight-average molecular weight of 5.7×10^5 g/mol. The molecular weight of polymers in 'I_Small' and 'I_Blend' film is about 1.5×10^5 g/mol. b) 'Crx_SmallMax' represents the film made of crosslinked large particles (282 nm) with linear polymer particles (the same component as in the 'Small_Max' latex film). The V_c for blending is 25.9%.

To focus only on the crosslinking effect and avoid confusion later, here in this section, a modified tensile testing method *via* ARES was introduced instead of the universal tensile testing method *via* Instron (see the set up details in Chapter 2) to characterize latex film strength. The difference between the two methods is that ARES tensile test is taken at a higher testing temperature close to T_g of the polystyrene (the backbone polymer), while the Instron tensile test is normally done at room temperature.

For high T_g latex films, room temperature is far lower than the temperature needed for polymer chains to move around. The polymer chains are still frozen in their glassy state and there is little difference between breaking the non-crosslinked mobile chains and breaking the crosslinked polymer network. In other words, it is hard to differentiate the two contributions to the film strength: one is from physical entanglements and the other is from chemical crosslinking. To study the crosslinking effect, the testing temperature needs to be increased close to the T_g of the polymers, because the free volume of the polymer (which is related to the relaxation times) increases dramatically at about or beyond the glass transition temperature[6], which means almost all the non-crosslinked chains can move freely (see Figure 5.12 for various chain movements). Therefore, the non-crosslinked chains are able to disentangle and rearrange themselves in the direction of the applied stress. In this way, the contribution of the physical entanglements from the non-crosslinked chains can be reduced to a minimum (chain pull-out energy is much smaller than chain scission energy[7]), leaving only the entanglements that have been fixed by the chemical crosslinking to contribute to the strength of the film (see Figure 5.13 for proof).

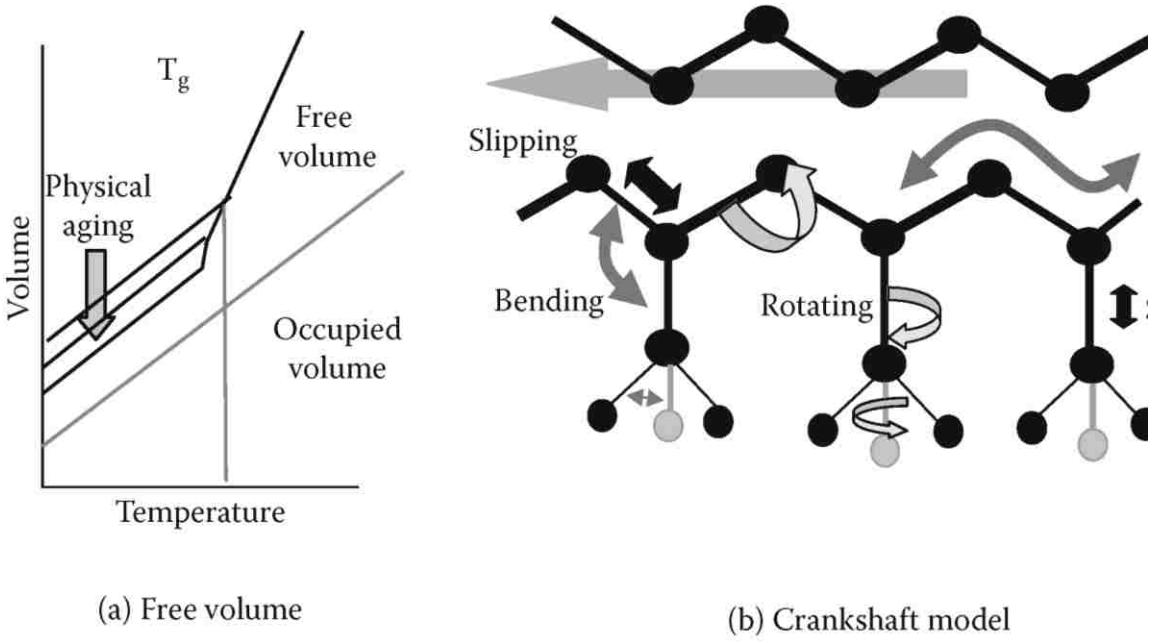

(a) Free volume

(b) Crankshaft model

Figure 5.12: Free volume in polymers. a) Relationship of free volume to transitions; b) The schematic example of free volume and the Crankshaft model.

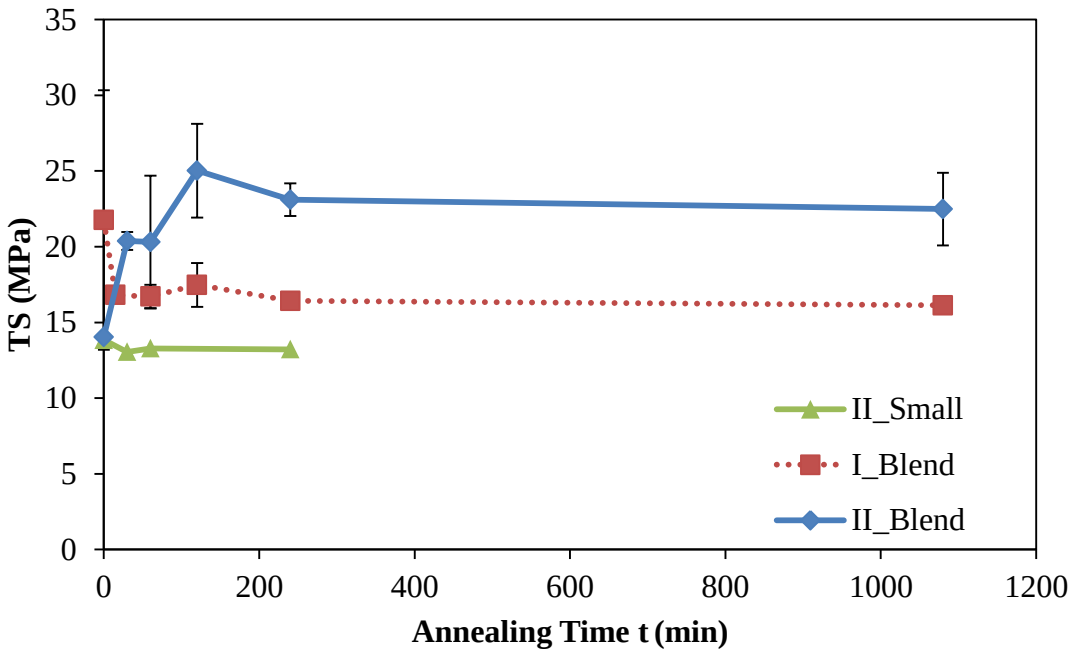

Figure 5.13: Tensile strength comparison *via* ARES at 105 °C. II_Small: film comprised of only linear polymer particles; I_Blend: film comprised of nonfunctionalized crosslinked large PS particles and non-functionalized non-crosslinked small PS particles; II_Blend: film comprised of carboxylated non-crosslinked large PS particles and amine functionalized non-crosslinked small PS particles. The parameter details are in Table 5.1.

Figure 5.13 shows that the increased tensile strength contributed by the physical entanglement of the polymer chains could not be observed at the 105 °C testing temperature, no matter whether the film had a pre-existing network (I_Blend) or not (II_Small). For the latex film made of Blend II latexes, although both component particles are non-crosslinked, the film strength increases with the annealing time due to the $COOH/NH_2$ chemical crosslinking at the interface.

This modified testing method makes this study of the crosslinking effect on high T_g polymer films analogous with the crosslinking effect on low T_g polymer films used in industrial coatings. Because room temperature is usually close to or above the T_g of most polymers used in coatings, when the tensile test is taken at room temperature, almost all the non-crosslinked chains are movable leaving the crosslinked chains in place to enhance the film strength in the macroscopic level.

Therefore, the crosslinking effect studied on the high T_g PS latex films at the higher testing temperature is comparable to the influence of chemical crosslinking on the low T_g latex films.

5.3.6.3 Pre-crosslinking Together with Post-crosslinking Effect

With this high-temperature tensile testing method in hand, the crosslinking effect on the film tensile strength was investigated when pre-crosslinking and post-crosslinking exist in the reactive film system simultaneously (see the schematic illustration in Figure 5.14a). In other words, the contributions to the film strength are both from the chemical crosslinking at the interface (chemical reactions between functional groups) and the

homogenous crosslinking in the bulk of the film (carboxyl functionalized crosslinked large particles). Figure 5.14b shows the film tensile strength comparison of the reactive film (III_Blend) with the unblended films comprised of each individual component particles (III_Small and III_Large).

The tensile strength of the films comprised of blended latexes was much higher than the film made of only small non-crosslinkined latex particles at any time regime during the annealing process. The blended film also had a higher strength than the film prepared from only large-size crosslinked latex particles, but this is not obvious in the early annealing time regime. This is because at the beginning of the annealing, the chemical reaction has not yet taken place. The film strength contributed by the pre-crosslinking density should be similar both in blended films (III_Blend) and films made of large-size crosslinked particles (III_Large). However, after the annealing process proceeds longer, the tensile strength of films made of large sized crosslinked particles decreases with time due to insufficient entanglements at the interface. Therefore, there can be phase separations between crosslinked network domains and linear polymer chain domains, which can be proved by comparing the stress-strain curves of the films.

Figure 5.15a shows that the Young's modulus (initial slopes) of the films made from the large crosslinked particles starts decreasing gradually upon annealing from 1.22 GPa to 0.78 GPa, which means the film stiffness decreases. Because of nonhomogeneity within films, films will break more easily at the interface where no crosslinking is present, which leads to the decrease of film strength. As a comparison, Figure 5.15b shows the stress-strain curves of blended films and films made of only small particles. In these two

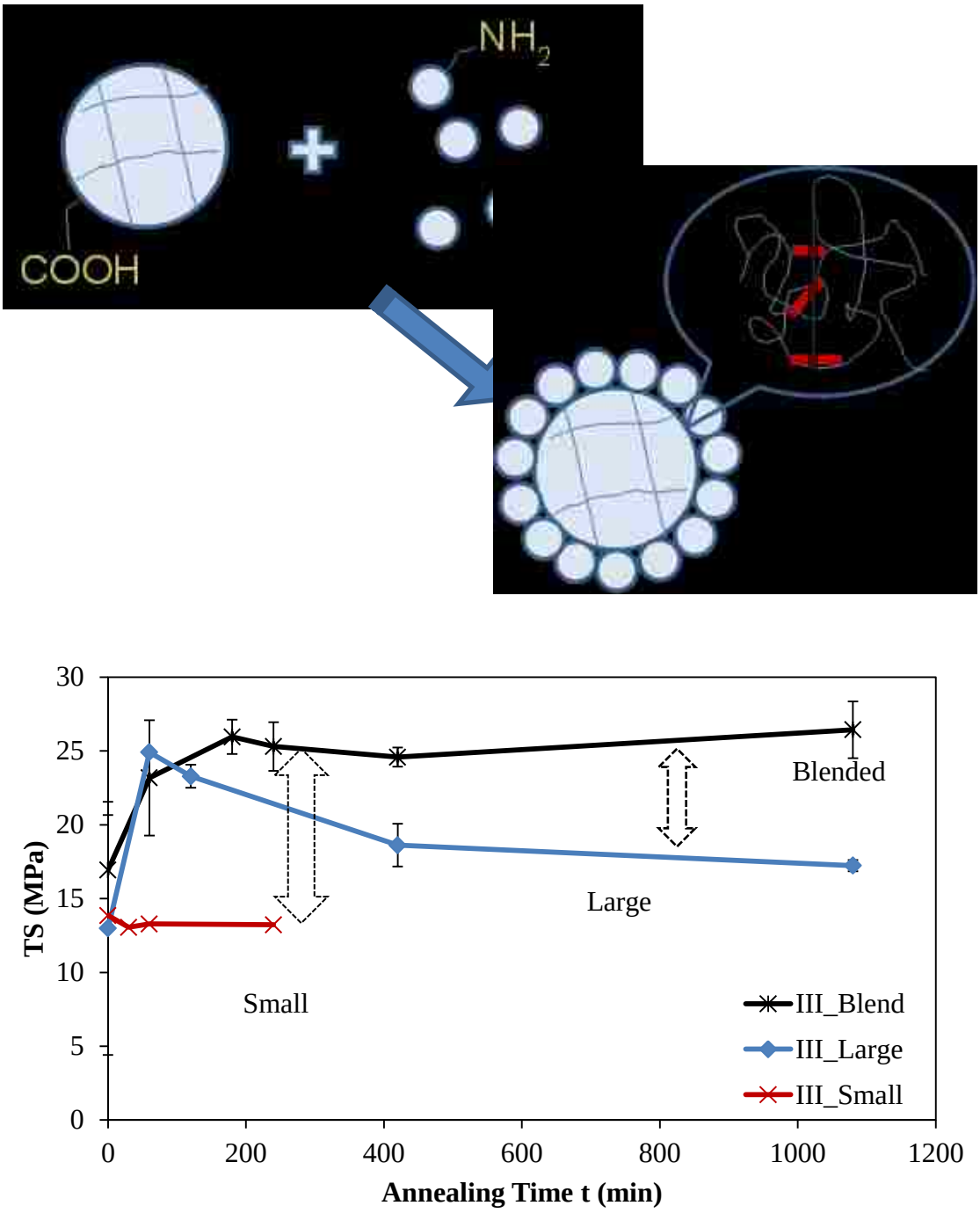

Figure 5.14: a) Scheme of the reactive film system that contains both bulk crosslinking and interface crosslinking; b) Tensile strength *vs.* annealing time for the films comprised of latex blends (III_Blend), large carboxylated crosslinked particles (III_Large), and small amine functionalized PS particles (III_Small) at tensile testing temperature of 105 °C. Films were all annealed at 168 °C.

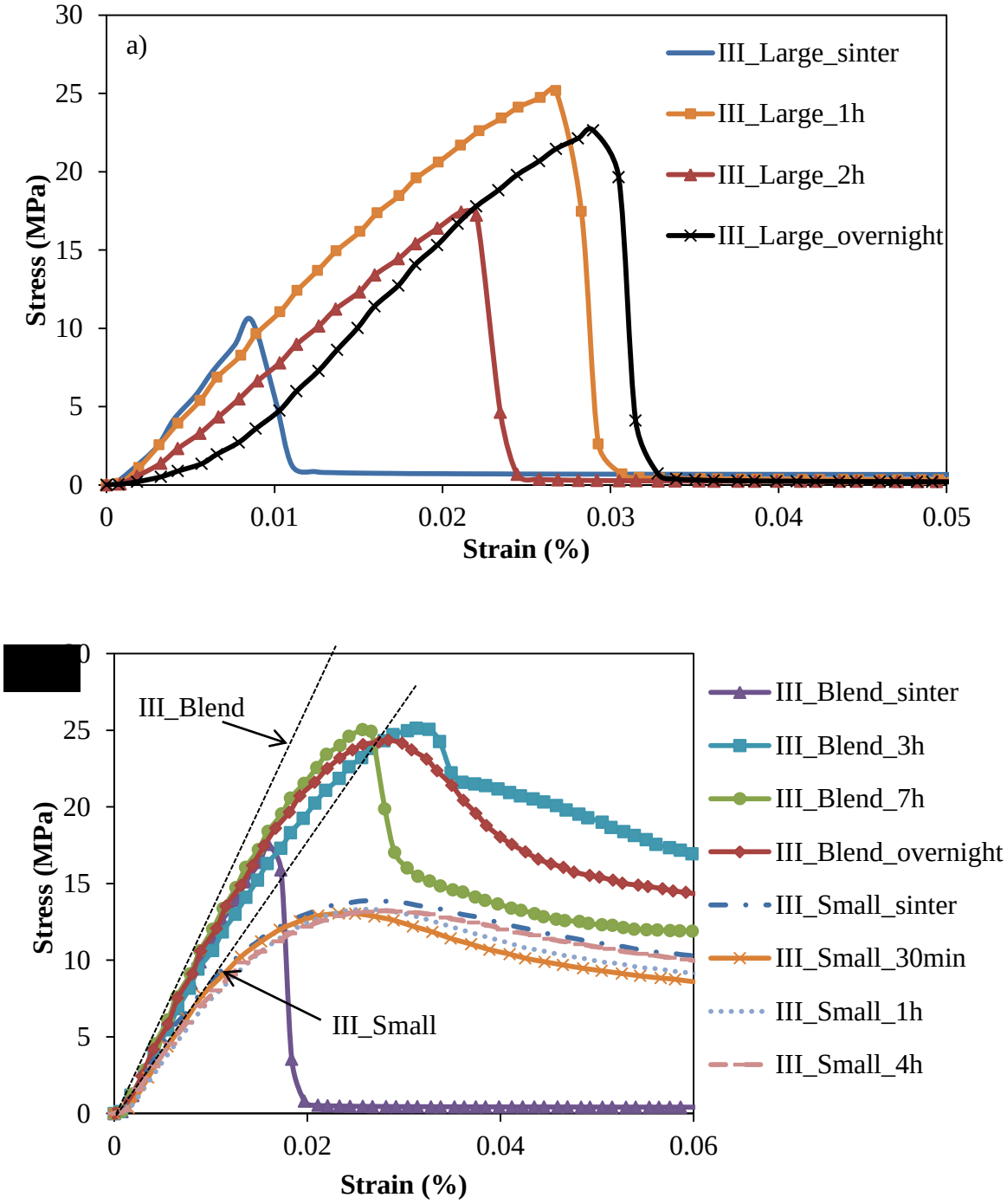

Figure 5.15: a) Stress-strain curves at 105°C for films made of only large size crosslinked particles (III_Large); b) stress *vs.* strain curves at 105 °C testing temperature for films comprised of large/small latex particles (III_Blend) and films made of only small size amine functionalized non-crosslinked latex particles (III_Small).

cases, Young's modulus does not change with time, which indicates homogeneity of the films. The films comprised of blended latexes have a higher Young's modulus and yield strength, which indicates an improved film stiffness and strength. Since the film toughness is the ability to absorb mechanical (or kinetic) energy up to failure and the area covered under stress-strain curve is related to the film toughness, the toughness of blended films (III_Blend) is improved accordingly due to the increase of both the yield strength and the elongation at break.

5.4 Conclusions

Bimodal particle packing can help the system to selectively arrange reactive particles into a state in which every large particle is surrounded by small particles, each containing the functional groups that can react with each other. In this way, the efficiency of the chemical reaction can be greatly increased, which provides a solid basis for the study of chemical crosslinking that occurs at the interface of two separate particles having different functional groups.

Introducing pre-crosslinked particles into the non-reactive blends system can increase the film mechanical strength only if the molecular weight of the linear polymer particles is smaller than the molecular weight needed to achieve maximum film strength.

Based on the investigation of the reaction kinetics for various small molecule reactions, the COOH and NH_2 functionalities were chosen to incorporate into separate latexes for use in a reactive blend. Because the minimum temperature to induce this

reaction is 30 °C higher than the glass transition temperature of polystyrene, this provides a possible temperature range to control separately the film formation process and the chemical crosslinking reaction. Thus, the experimental data can be compared with the theoretical model (de Gennes' Scaling relationship) in a more accurate way.

According to the scaling relationship, the control parameter α, which is defined as the ratio of the typical diffusion time to the typical reaction time, was calculated to be less than 1 under all annealing conditions (144 °C, 155 °C and 168 °C). The small α value predicts that under all annealing conditions, the film formation process is reaction controlled. Chemical crosslinking is the slow step comparing to polymer chain interdiffusion. Therefore, polymer chains have enough time to become nearly fully entangled at the particle-particle interface and then be fixed in position by chemical bonding. It is expected that the film interfacial strength will be enhanced.

The chemical crosslinking effect (post-crosslinking at the interface) on the film mechanical performance were studied based on the reactive blended film comprised of Blend III (carboxylated crosslinked large PS latex particles blended with amine functionalizd non-crosslinked small PS latex particles). The experiment results proved the theoretical prediction that in a reaction controlled film system, crosslinking at the interface not only enhances the film interfacial strength but also improves the other mechanical properties of the film, such as Young's modulus and film toughness.

The high temperature tensile strength measurements enable us to make a useful prediction, based on the study of crosslinking effect on high T_g PS latex films, for the

crosslinking effects on the low T_g latex films that have been widely used in the coatings industry.

5.5 References

1. Tobing, S.; Klein, A; Sperling, L. H.; Petrasko, B. *J. Appl. Poly. Sci.* **2001**, *81*, 2109-2117
2. Aradian, A., Raphael, E., deGennes, P.G. *Macromolecules*, **2000**, *33*. 9444.
3. Aradian, A., Raphael, E., deGennes, P.G. *Macromolecules*, **2002**, *35*. 4036.
4. O'Shaughnessy, B. *Macromolecules*, **1994**, *27*, 3875
5. Macosko, C. *Rheology*, VCH, New York, **1994**
6. Menard, K. *Dynamic Mechanical Analysis: A Practical Introduction*, Taylor & Francis Group LLC, **2008**

CHAPTER 6

Comparison of Shrinking-Core Model and Scaling Theory for the Competition Between Interdiffusion and Crosslinking

Abstract

In the formation of latex films, in which a chemical crosslinking reaction will take place, there always exists a competition between polymer chain interdiffusion and the crosslinking reaction at the polymer-polymer interfaces. The control parameter $\alpha=t_{diffuse}/t_{react}$, which adjusts the balance between these two processes and determines the final state of the polymer interface in deGennes' scaling theory was investigated by adjusting two different theoretical models to the experimental data: the Shrinking-Core Model and deGennes' scaling theory. Consistency was achieved when comparing the values of α obtained separately from these two models. In addition, this study showed a good agreement with the scaling theory in the slow reaction regime: when $\alpha<1$, the latex film formation is reaction controlled and the film interface can be therefore strengthened. The main focus of this study was to provide a practical guideline for the prediction and control of strengthening the 'interface-related' properties (such as film strength and toughness) in industrial latex coating applications.

6.1 Introduction

The investigation of the competition between the molecular interdiffusion and chemical crosslinking reaction during the latex film formation process is important both in theory and in industrial applications, such as polymer welding and healing, latex coatings and adhesives. One of the major objectives of this study is to model the film formation process in a reactive film in terms of polymer chain interdiffusion and crosslinking, during which these two processes occur simultaneously in competition and they both contribute to the final properties of the corresponding film. To improve the film strength, a fine balance is needed to maximize both contributions to the film performance. If the crosslinking happens too fast, it can greatly hinder the interdiffusion process and lead to less chain interpenetration at the polymer-polymer interface which will lower the film integrity and tenacity.

There are two basic models that take into account both the diffusion of polymer molecules and the chemical reactions between polymers: One is deGenns' scaling theory[1,2] and the other one is the shrinking-core model developed by Ishida and Wen[3]. These two models have been derived under different assumptions and have been used for describing different reaction models, yet they have relationships in common, which can be found later in this chapter.

i) The scaling relationship

de Gennes' scaling theory presents the approach to describe the situation in which both interdiffusion and chemical crosslinking occur at the homogenous and symmetric

polymer/polymer interface, and crosslinking happens by addition of an external crosslinker. They propose an important parameter α, named the control parameter, which is related to the physical-chemical properties of the polymer and the crosslinker and characterizes the final state of the polymer interface. α is defined as the ratio between the typical diffusion time in the absence of reaction $t_{\text{diffusion}}$ and the typical reaction time regardless of transportation processes, t_{reaction}:

$$\alpha = \frac{t_{diffusion}}{t_{reaction}} \tag{6.1}$$

Two limiting regimes are then determined by α: (1) when $\alpha \ll 1$, the reaction is so slow that the interface heals completely before the reaction takes place and 2) when $\alpha \gg 1$, the reaction goes much faster than interdiffusion such that the system is frozen before any significant coalescence occurs.

The diffusion time needed to heal the interface completely is considered to be equivalent to the chain reptation time (the time for a chain to move a distance comparable to its radius of gyration) based on deGennes' reptation theory by:

$$t_{diffusion} \cong t_{reptation} \cong \tau_0 \frac{N^3}{N_e} \tag{6.2}$$

in which N is the number of monomer units per chains, N_{e} is the number of monomer units between two entanglement points, and τ_0 is the typical microscopic time for molecule agitation.

The typical reaction time is assumed to be the time for one reaction per chain in the system, which means there will only be one interlink per chain after this time. The reaction time is derived as:

$$t_{reaction} \cong \frac{N_c}{N} \frac{1}{QA_0^* b^3} \tag{6.3}$$

in which N_c is the number of monomers per crosslink (reached when the cross-linking reaction is completed), N is the total number of monomers per chain, Qb^3 in the physicochemical relation equals to the reaction rate constant k, and A_0^* is the initial volume concentration of the reactive sites in the system.

The control parameter α is then derived as:

$$\alpha = \frac{t_{diffusion}}{t_{reaction}} \cong Q\tau_0 A_0^* b^3 \frac{N^4}{N_e N_c} \tag{6.4}$$

which can be experimentally measured as well as theoretically calculated. By determining the value of α, the timing of the chemical reaction can be predicted and controlled. Specifically, the practical interest is when $\alpha << 1$, *i.e.* in the slow reaction region, the diffusion time is much lower than the time needed to complete the reaction. In this case, the corresponding film can develop good mechanical properties due to these two processes giving synergistic contributions to the interfacial strength but with minimum influence on each other.

Because the scaling theory is based on a homogenous polymer system, to apply it to this current system, which is a mixture of carboxylated gel particles with amino-

functionalized linear polymer particles (COOH groups in the gel particles react with NH_2 sites on the linear polymers), several assumptions are needed as well as some adjustments of the parameters, for practically calculating the control parameter α in a reactive system.

1) As Aradian and co-workers proposed in their paper, the temperature is assumed to remain constant during the annealing process; the free linear polymer chains in the non-crosslinked particles are monodisperse, consisting of *N* mer units; only one reaction takes place per chain and crosslinked chains remain fixed in position in contrast to mobile chains.
2) The microscopic molecular agitation time, τ_0, should be temperature dependent. de Gennes assigns an approximate value on the order of 10^{-10} sec for the time τ_0 in polymer melts[4]. However, the agitation time should be very different for high T_g polymers (such as polystyrene) in their rubbery state compared to the melted state. To determine the exact value of τ_0 for polymers under various conditions, another expression of the reptation time can be applied[5]:

$$t_{diffusion} \cong t_{reptation} = \frac{r^2}{3\pi^2 D_e} \tag{6.5}$$

in which *r* is the end-to-end distance of a random polymer chain which is equal to $\sqrt{6}R_g$, R_g is the radius of gyration (Å) that is related to the weight-average molecular weight, M_w, in the relaxed state[6,7]:

$$R_g = 0.275 M_W^{1/2} \tag{6.6}$$

and the self-diffusion coefficient of the polymer chains, D_e, is temperature and molecular weight dependent. Therefore, the diffusion time can be written as:

$$t_{diffusion} \cong t_{reptation} = \frac{2 \times (0.275^2 M_W)}{10^{16} \pi^2 D_e} \tag{6.7}$$

Combining this with eq 6.2, the expression for τ_0 is:

$$\tau_0 = \frac{2 \times (0.275\sqrt{M_W})^2}{(10^{16})\pi^2 D_e} \times \frac{N_e}{N^3} = \frac{2 \times 0.275^2 (MW_m \times N)}{(10^{16})\pi^2} \times \frac{N_e}{N^3 D_e} = \frac{0.015 N_e}{(10^{16}) N^2 D_e} MW_m \tag{6.8}$$

in which MW_m is the monomer molecular weight, which for styrene, the value is 104 g/mol.

3) The N_c in eq 6.3 is the length in terms of the number of mer units between crosslinking points after the reaction is completed. In a polymer system with an existing amount of crosslinking density, N_c should then refer to the additional crosslinking that is newly created by chemical reactions, described in eq 6.9:

$$N_c = \frac{M_c}{MW_m} = \frac{\frac{\rho_{polymer}}{\rho_{c-total} - \rho_{c0}}}{MW_m} = \frac{\frac{\rho_{polymer}}{\frac{\rho_{polymer}}{M_{c-total}} - \frac{\rho_{polymer}}{M_{c0}}}}{MW_m} = \frac{N_{c-total} N_{c0}}{N_{c-total} - N_{c0}} \tag{6.9}$$

based on the relationship between crosslinking density and the molecular weight between crosslinks by:

$$\rho_c = \frac{\rho_{polymer}}{M_c} \tag{6.10}$$

in which $\rho_{c\text{-}total,}$ $\rho_{c0,}$ $M_{c\text{-}total,}$ $M_{c0,}$ $N_{c\text{-}total,}$ N_{c0} respectively represent the total crosslinking density after the reaction, the initial crosslinking density of the polymer network, final molecular weight between crosslinks, initial molecular weight between crosslinks, the final crosslink separation in terms of number of monomer units between crosslinks, the initial crosslink separation. $\rho_{polymer}$ is the density of polymer.

4) The A_o^* is the concentration of the reactive sites in the system. In the reactive blends system, the concentration of functional groups is not uniform throughout the particles due to the hydrophilic characteristics of the carboxyl and amine groups. Especially, in batch polymerized particles, more functional groups are concentrated on the surface and in the core area, while in between is a depletion area in which fewer functional groups are present (see conductometric titration results in Chapter 3 for evidence). Since only the surface and several layers beneath the surface are the regions that functional groups in different particles are able to most efficiently react with each other, A_o^* represents the concentration of functional groups within a thin layer of the particles.

   According to a statistical study of polymer aggregates in solution by molecular modeling[8], the hydrophilic chain ends prefer to concentrate in a "hairy" surface layer of 2-4 nm thickness. The surface concentrated area in this system is, therefore, assumed to have a 3 nm thickness and the functional groups are evenly distributed within this area. Through titration, the percent surface coverage of the functional groups is known and by dividing by the 3nm-thick ‘shell’ volume of

the particle, the value of A_0^* that takes part in the chemical reaction can be estimated.

On the other hand, the average interpenetration depth for polymer chains to reach full material strength is about 0.81 times the radius of gyration R_g[9]. Thus, for polystyrene chains with a molecular weight close to 10,000 g/mol, the interpenetration depth is about 7 nm in a noncrosslinked system. Considering that the linear polymer chain diffusing across the interface has to go through the gel network in the pre-crosslinked particle, the polymer chain will experience more diffusion resistance in the gel but have more efficient entanglements than in the polymer solution. Thus, the interpenetration depth needed to reach full film strength should be lower than 7 nm. As a result, the depth of the region in which the hydrophilic groups are concentrated is within this chain interpenetration depth.

5) Qb^3 is considered to be equivalent to the reaction rate constant k in the scaling theory, which can be acquired by monitoring the small molecules (monomers) reaction rates. Q is defined as the reaction probability and b is defined as the capture distance below which the reaction becomes possible. Often the capture radius b is assumed to be equal to the chain unit size a, which has the relationship with the chain end to end distance, r, in the relaxed state as follows:

$$a\sqrt{N} = r = \sqrt{6}R_g = \sqrt{6}\left(0.275\sqrt{M_W}\right) = \sqrt{6}\left(0.275\sqrt{N \times MW_m}\right) \qquad (6.11)$$

Therefore, for a typical polystyrene segment length in the relaxed state, a, is 6.8 Å. However, since the chain has more constraints in the rubbery state than it does in a θ solvent (ideal relaxed condition), it is reasonable to consider the chain unit

size is close to a monomer unit size. Here, the capture radius *b* is assumed to be 3 Å. Therefore, by knowing the reaction constant *k* and the capture distance *b*, the reaction probability *Q* is able to be estimated.

Taking the above considerations into account, the final modified analytical expression for the control parameter α in a reactive polystyrene system turns out to be:

$$\alpha \cong Qb^3\tau_0 A_0^* \frac{N^4}{N_e N_c} = k_r\left(\frac{1.56N_e}{(10^{16})N^2 D_e}\right)\frac{A_0^* N^4}{N_e N_c}$$

$$\therefore \alpha = (1.57\times10^{-16})\left(\frac{k_r}{D_e}\right)\left(\frac{A_0^* N^2}{N_c}\right) \qquad (6.12)$$

To calculate the numerical value of α, k_r ($Lmol^{-1}s^{-1}$), and N_c can be experimentally measured[i]. The diffusion coefficient D_e (cm^2s^{-1}) can also be directly measured by small-angle neutron scattering (SANS) and direct nonradiative energy transfer (DET) [10]. However, if none of the characterization equipment is available at hand, the simplest way is to either refer to literature data or acquire it from the Shrinking Core Model fit.

ii) The Shrinking Core Model (SCM)

The SCM is designed for solid-gas reactions occurring in a spherical particle, in which the reacting particle B is nonporous but the reaction product is a porous solid. Figure 6.1 shows the essence of the SCM, in which the unreacted core is shrinking with time. In this case, the gas molecule A initially can only react with the exterior surface of

[i] k_r can be measured by monitoring small molecule reaction and N_c can be measured by swelling measurements.

the particle, but then progressively diffuses through the porous product to reach a receding surface of the unreacted core particle. The density of solid B is either zero (completely reacted outer layer) or a constant value (unreacted core). There will be no reaction in the product layer where the gas molecule has to diffuse through, which means the diffusion of gas molecule A and the reaction between gas A and solid B at the surface of the core are in series (or in alternation). This is a very important assumption used in the SCM model, which differentiates the SCM from the scaling theory that considers the diffusion and reaction occur in parallel, which will be discussed again later in this chapter.

To apply this SCM model to this system, again, some assumptions need to be made as well as several adjustments to the parameters that govern the equation.

1) Shrinking core model assumes the chemical reaction is only a first order surface reaction in A (gas molecule). This assumption does not seem to be accurate for the COOH/NH_2 reaction in this film system. However, since the surface concentration of carboxyl groups in the crosslinked PS particle is measured to be more than 10 times higher than the surface concentration of amine groups in the non-crosslinked PS particles, the concentration of COOH groups can be estimated to remain the same compared to the change of concentration on the NH_2 groups and this second order reaction is then considered to be pseudo-first order in NH_2 in this system. Then the true reaction rate constant for the second order reaction can be back calculated out. Regarding the end point of the reaction, the time to reach plateau crosslink density as determined by swelling measurements is assumed to be the time to complete the reaction.

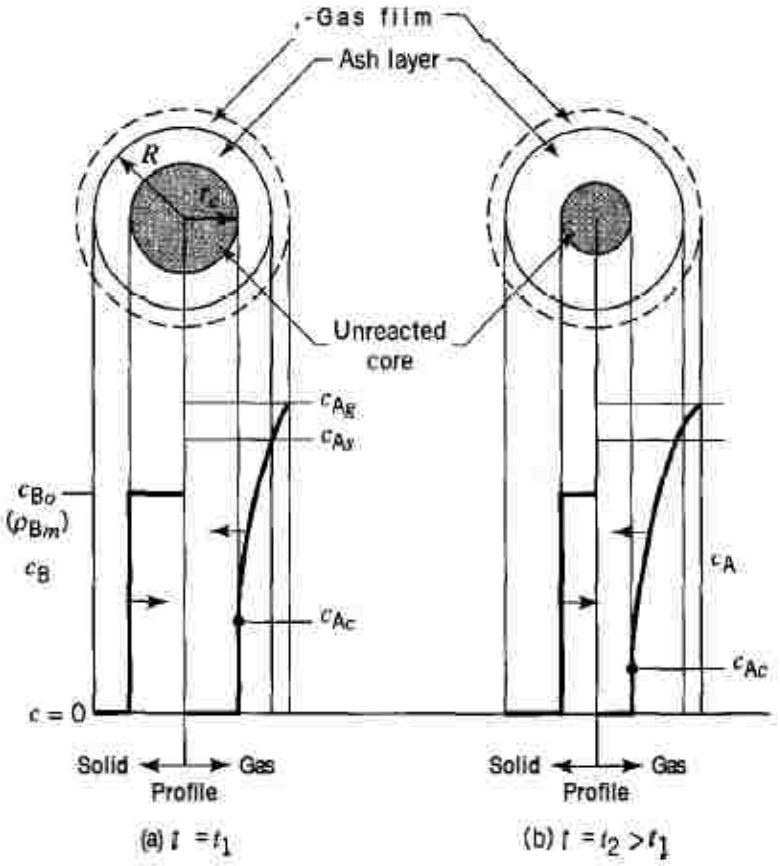

Figure 6.1: Reprint from the Chemical Reaction Engineering book of the scheme of shrinking core particle with increasing time t in the SCM. C_{B0} is the molar density of solid B, and C_{Ag}, C_{As}, and C_{Ac}, respectively represent the concentration of gas molecule A in the gas bulk layer, in the porous product layer, on the surface of the unreacted core.

2) Shrinking core model assumes the solid B particle size (including the ash layer) remains constant during reaction so that the integrity of the particle is maintained. This assumption holds in this system, because the precrosslinked network in the particle will help to maintain the original particle morphology and structure when linear polymer chains diffuse into and react with the gel network. The assumption that needed is the carboxylated crosslinked PS particles have a uniform particle size. Since by using surfactant free batch polymerization, it was already proved that the particle had a narrow size distribution (see Chapter 3 for evidence), and thus this assumption holds.
3) Shrinking core model is an idealized model, the boundary between the reacted and the unreacted zones is sharp and the diffusion coefficient is assumed to be constant within the reacted zone. This assumption is valid for a system with a slow crosslinking reaction rate. If the reaction was very fast, the diffusion rate would be significantly slower as the proceeding crosslinking hinders the interdiffusion process. However, it is not an issue in the system studied here because in all cases, the diffusion rate is slower than the reaction rate (see experimental results in this chapter for proof).
4) Shrinking core model assumes the solid B has a uniform density, which in this study means the functional groups are evenly distributed throughout the particle. Although for a conventional batch polymerization this assumption cannot be valid, it is still reasonable to consider that within the reaction zone, which is a thin shell

layer (3 nm) near the surface of the particle, the concentration of the functional groups remains the same.

5) Because the model is derived for a solid-gas reaction, it is considered that the solid is fully surrounded by the gas molecules. Thus, the last assumption is that every particle is surrounded by particles containing the opposite functional groups so that all the functional groups can play a role in the chemical reaction. This assumption becomes valid when the latex blends can self-arrange themselves. Chapter 4 gives the solution for the system self-assembly by mixing large and small particles at V_c (the volume percentage of small particles needed for film continuity) for a special close-packing.

Based on the analytical expression of the Shrinking Core Model and taking into account those assumptions discussed above, a modified equation was used to describe the overall reaction time in the reactive polystyrene latex blends (Appendix B has more derivation details):

$$t(x,K,Y) = K\left[1-(1-x)^{\frac{1}{3}}\right]\left\{1+\frac{Y}{6}\left[1+(1-x)^{\frac{1}{3}}-2(1-x)^{\frac{2}{3}}\right]\right\} \qquad (6.13)$$

$$K = \frac{3\rho_{Bm}}{k_r[NH_2][COOH]}, Y = \frac{k_r[COOH]R^2}{3D_e} \qquad (6.14)$$

in which ρ_{Bm}[ii] is the moles of unreacted COOH groups per volume of the crosslinked particle. k_r is the volume based reaction rate constant, $[NH_2]$ and [COOH] are the

[ii] The use of ρ_{Bm} follows the use of term in SCM model.

concentrations of NH_2 and COOH groups in the reaction zone, which is considered to be within a 3 nm thick thin layer near the surface of the latex particles. *R* is the radius of the large carboxylated crosslinked particles. D_e is the diffusion coefficient of linear polymer chains in amine functionalized particles. *t* is the time, and *x* is the fractional conversion of the reaction, which is determined using eq 6.15 considering the reaction is complete when the crosslinking density reaches the plateau value as determined *via* swelling measurements:

$$x = \frac{n_t}{n_\infty} = \frac{\rho_t}{\rho_\infty} \tag{6.15}$$

in which n_t, n_∞, ρ_t, ρ_∞ respectively represent the number of crosslinks at time t, final number of crosslinks, the crosslinking density at time t, and the final crosslinking density.

If there is a precrosslink density, ρ_0 (from the crosslinked gel particles), in the system, the initial number of crosslinks, n_0, needs to be subtracted from both n_t and n_∞. Therefore, eq 6.15 with the concern of initial crosslinks has the expression of:

$$x = \frac{n_t - n_0}{n_\infty - n_0} = \frac{\rho_t - \rho_0}{\rho_\infty - \rho_0} \tag{6.16}$$

The time required for complete conversion of the particle (x =1) is denoted by t^*, then eq 6.13 can be simplified into:

$$t^* = K + \frac{KY}{6} \tag{6.17}$$

If $t_{diffusion}$ is still defined as the typical diffusion time in the absence of reaction (k_r is infinity) and t_{react} as the typical reaction time regardless of diffusion (D_e is infinity), then another expression for the control parameter α described in the scaling relationship can be obtained by using this kinetics model (SCM):

$$\alpha = \frac{Y}{6} = \frac{1}{18}\left(\frac{k_r}{D_e}\right)[COOH]R^2 \qquad (6.18)$$

in which k_r is the reaction rate constant, D_e is the diffusion coefficient, [COOH] is the concentration of carboxyl groups within the particle 3 nm thick surface layers in which the reaction takes place, which is the same as A_0^* used in Eq 6.12. R is the radius of the large carboxylated crosslinked particle.

Eq 6.18 is very similar to Eq 6.12 in terms that the control parameter α is proportional to the ratio of the reaction rate constant to the diffusion coefficient, as well as the concentration of the reactive groups within the region in which the reaction occurs. D_e has the unit of cm^2s^{-1}, k_r has the unit of $Lmol^{-1}s^{-1}$, A_0^* and [COOH] have the units of $molL^{-1}$, and R has the unit of cm.

6.2 Experimental

Five sets of large/small latex blends were used in the film formation kinetics study. Table 6.1 gives the parameter details of each individual set. The latex blends were dried completely at 40-50 °C, sintered at 120-130 °C for 35 min and annealed at 144 °C,

155 °C and 168 °C for various times as described in Chapter 2. The crosslinking density curves determined by swelling measurements were analyzed by a non-linear regression fit of the Shrinking Core Model to determine the diffusion coefficients and the reaction rate constants for the system. Film tensile strength was tested at 105 °C *via* the modified ARES testing method (see Chapter 2 for details).

Table 6.1: Characteristics of Latex Blends

Blends / Parameters	IV-1	IV-2	IV-2H	IV-3	IV-4
D_L (nm)	351	330	330	293	302
PDI_L	1.003	1.002	1.002	1.005	1.007
D_S (nm)	86	63	72	63	63
PDI_s	1.03	1.07	1.05	1.07	1.07
V_c	24.5 %	20.1 %	22.5 %	22.0 %	21.5 %
M_{c0} (g/mol)	54,000	36,000	36,000	37,000	29,000
A_0^* or [COOH] (mol/L)	5.71	10.53	10.53	4.17	11.43
M_W (g/mol)	100,000	100,000	300,000	100,000	100,000
[NH_2] (g/mol)	0.50	0.50	0.59	0.50	0.50

D_L, D_S, PDI_L, PDI_S are the large and small number-average particle size and polydispersity (=D_w/D_N) *via* SEM; V_c is the volume percentage of small particles; M_{c0} is the molecular weight between crosslinks in the pre-crosslinked large particle; A_0^* is the concentration of COOH groups within the 3 nm surface layer of the crosslinked large

particles; M_W is the weight-average molecular weight of linear polymer chains in the small particles; [NH_2] is the concentration of NH_2 groups within the 3 nm surface layer of the non-crosslinked small particles.

6.3 Results and Discussion

6.3.1 Estimation of D_e and k_r using the Shrinking Core Model

Figure 6.2 shows fractional conversion of reaction for latex film samples comprised of Blends IV-1 and IV-2 with annealing time, based on the evolution of crosslinking density results as determined from the swelling measurements. By using the regression fit of the Shrinking Core Model Eq 6.13 to the curves in Figure 6.2, the reaction rate constant k_r and the diffusion coefficient D_e for each individual set of blend films at every annealing temperature can be determined. However, when performing a nonlinear least square fit with two adjustable parameters (K, Y), it is necessary to check the uniqueness of each solution. Checking the contour of residual sum of squares as a function of K-Y pairs can be used to determine whether or not a particular solution is the global minimum (depicted by a series of concentric closed curves) or a local minimum (depicted by open curves). In statistics, the residual sum of squares (RSS) is the sum of squared errors of prediction, which is a measure of the discrepancy between the data and an estimation model. A small RSS always indicates a tight fit of the model to the data.

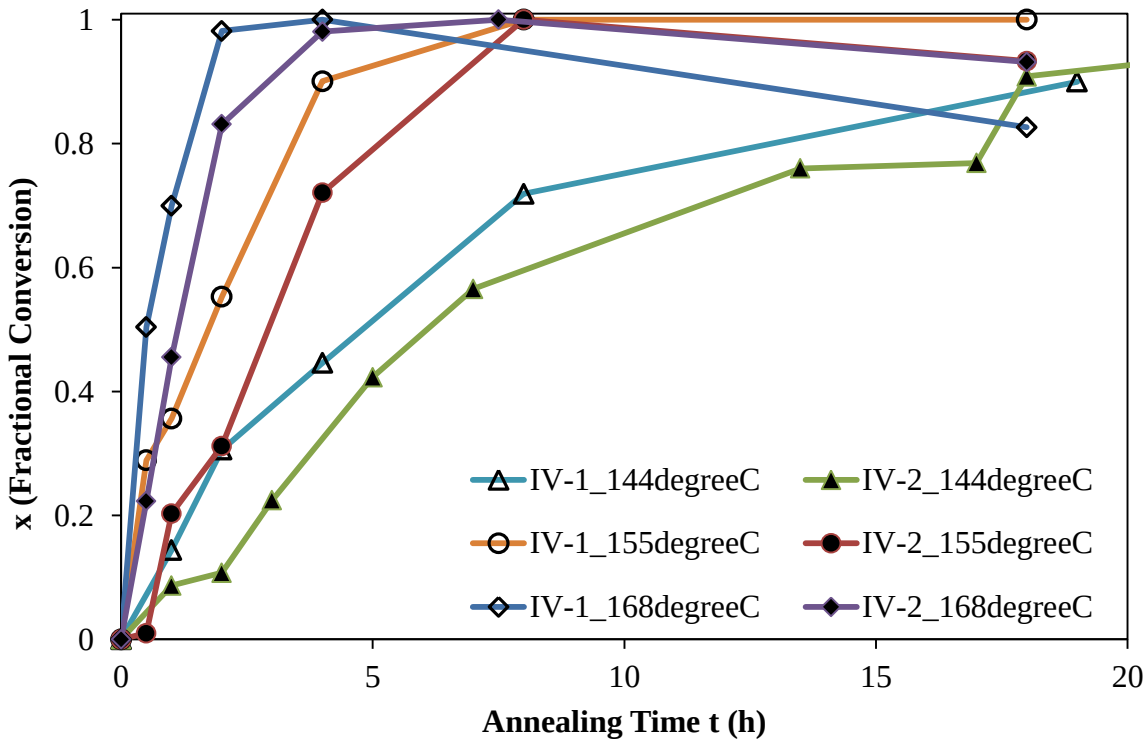

Figure 6.2: The fractional conversion (*x*) of the chemical reaction *vs*. annealing time for films made of Blends IV-1 and IV-2 at three different temperatures. The higher the crosslinking density in the film, the slower the reaction completes.

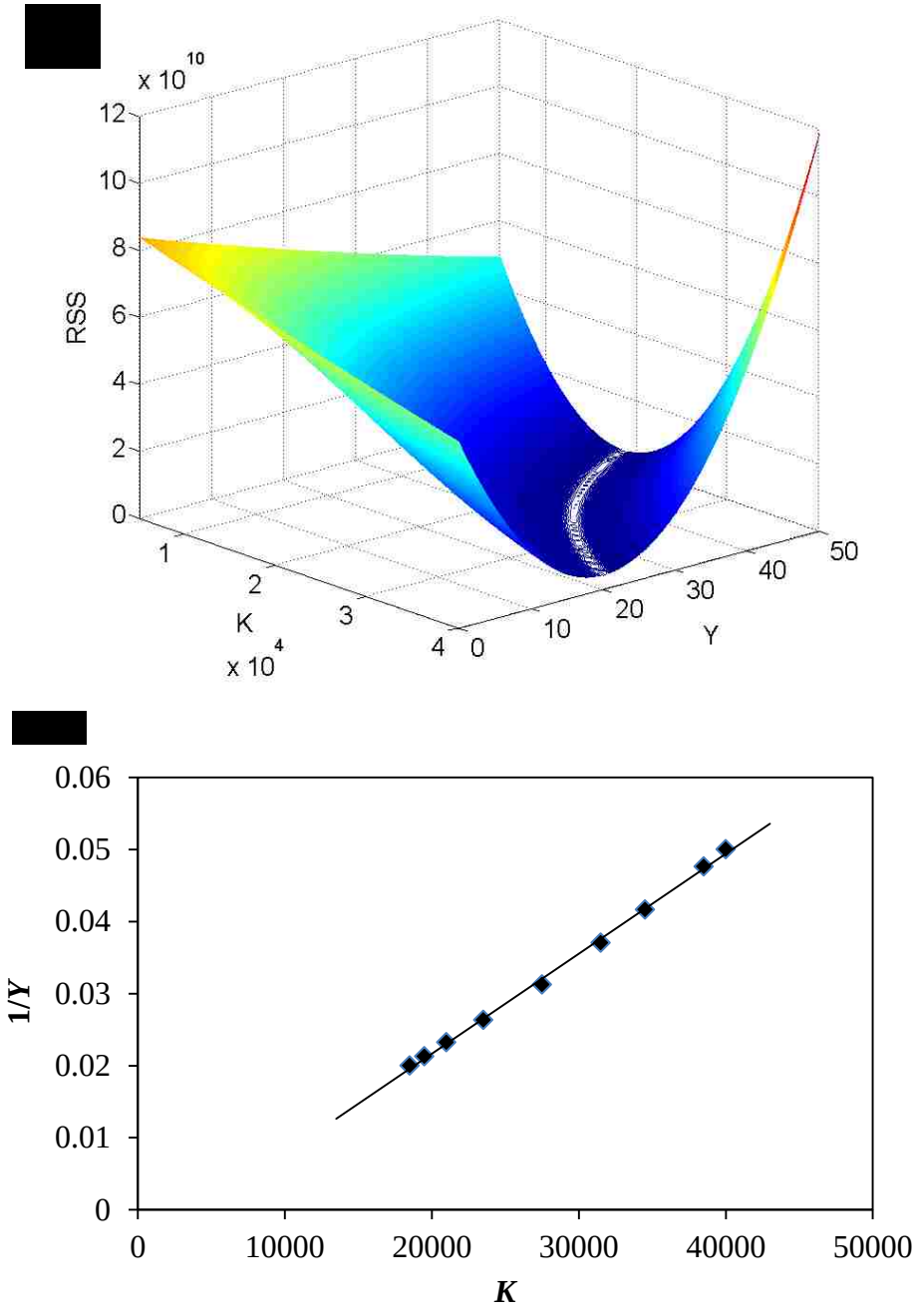

Figure 6.3: a) Residue sum square (RSS) contour plot based on SCM model fit to the fractional conversion of the chemical reaction in the film made of Blend IV-2 at 144 °C annealing temperature; b) the plot of 1/*Y vs. K* for the minimum RSS.

Figure 6.3a is one of the RSS contour plot obtained by varying the values of K and Y based on equation 6.19:

$$RSS = \sum_{i=1}^{n} \left(t_{i\,\mathrm{exp}} - t_i(K_i, Y_i) \right)^2 \tag{6.19}$$

The contour plot does not give a concentric closed curve, but instead, shows a valley of minimum RSS values within a certain range of K and Y, which indicates there is an infinite number of local minima and the K-Y value is not unique.

However, when the 3D RSS contour is read on the 2D K-Y plane, the K-Y pairs that correspond to the minimum RSS values actually fall into an asymptotic relationship. Within the range of K and Y that leads to the minimum RSS, the K *vs.* 1/Y plot shows a very good linear relationship (see Figure 6.3b). Since the D_e value is only related to the product of K and Y, with a general idea of the order of magnitude of D_e (which is 10^{-15} for a molecular weight near 100,000 g/mol), the value of D_e is able to be calculated, and then the value of Y can be estimated. Consequently, the reaction rate constant k_r in eq 6.14 can be solved. The reaction rate constant is considered to be only temperature dependent, which is important because it is another guideline to verify if the value of K-Y pair is a fit.

Figure 6.4 shows the Shrinking Core Model (SCM) curves fits to the experimental data. These curves fits prove that the regression of SCM to the experimental data is good in all cases. The resulting k_r and D_e values are shown in Table 6.2.

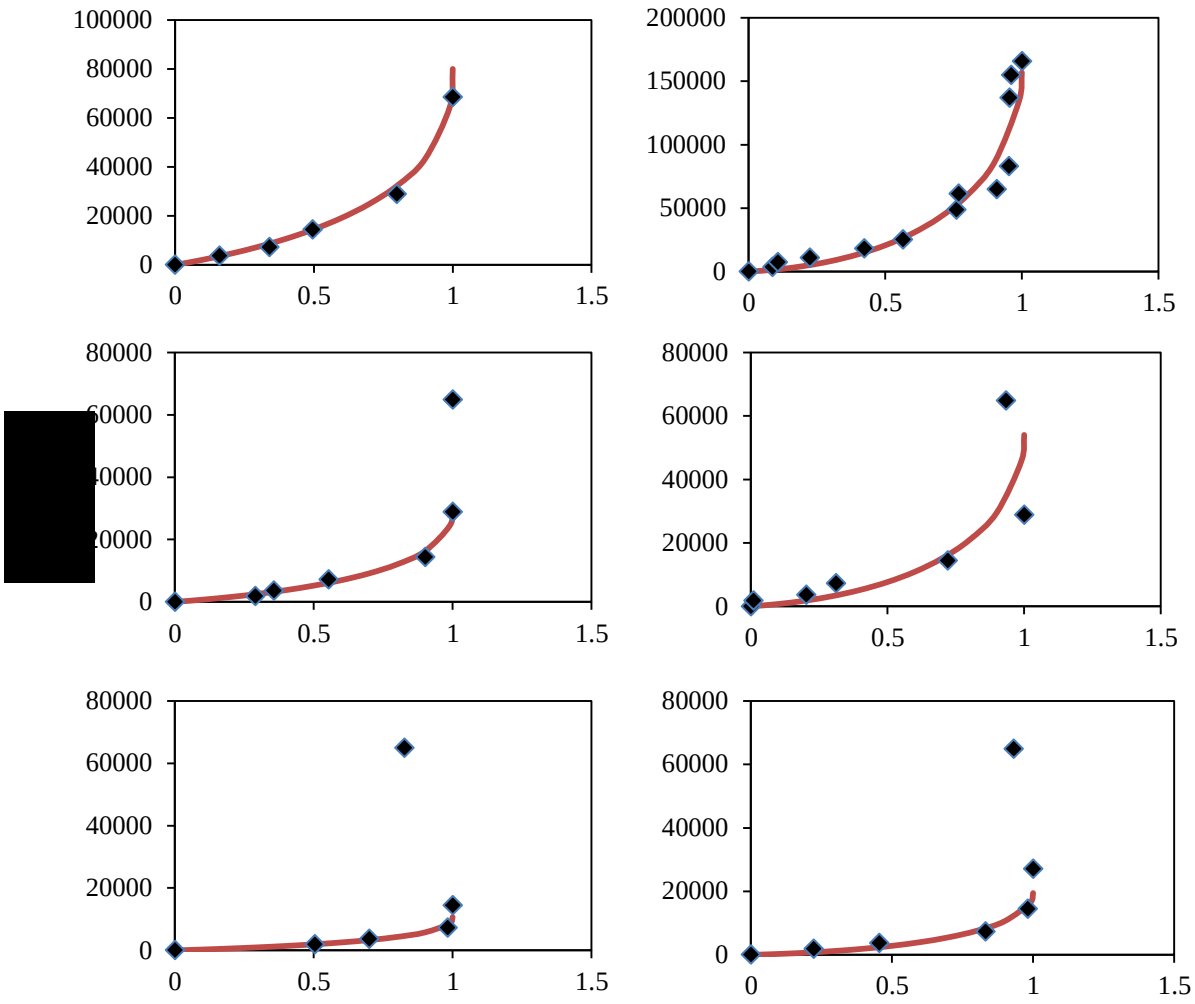

[redacted]

[redacted]

[redacted]

Table 6.2: The k_r and D_e Values for Blends IV-1 and IV-2 at Different Temperatures

Temperature (°C)	**k_r (10^{-6} Lmol^{-1}s^{-1})**	**D_e (10^{-15} cm^{2}s^{-1})**	
		IV-1	**IV-2**
144	7.58	3.54	1.70
155	15.2	11.8	5.71
168	37.9	44.2	16.9

To validate the usefulness of the Shrinking Core Model, on one hand, the estimated D_e values are compared with the previously published data directly measured by various analytical methods[9, 11] ; on the other hand, the estimated k_r values are compared with the k_r values obtained by monitoring the small molecules reaction rates (see Chapter 5 for more details), because no literature data is available for this k_r comparison.

Concerning the comparison of the estimated D_e values in this PS system with the literature data, an Arrhenius plot was made to see the relationship (all molecular weights were converted to the same molecular weight, 100,000 g/mol by using $D \propto M^{-2}$ relationship[12]). Figure 6.5 shows a good consistency of D_e values obtained in both current work and published work, which indicates that the SCM can correctly predict the value of the diffusion coefficient. However, the D_e values from Blend IV-2 are smaller compared to the values from Blend IV-1 and the values reported in the literature. This is expected, because the film from Blend IV-2 has a higher precrosslinking density than Blend IV-1.

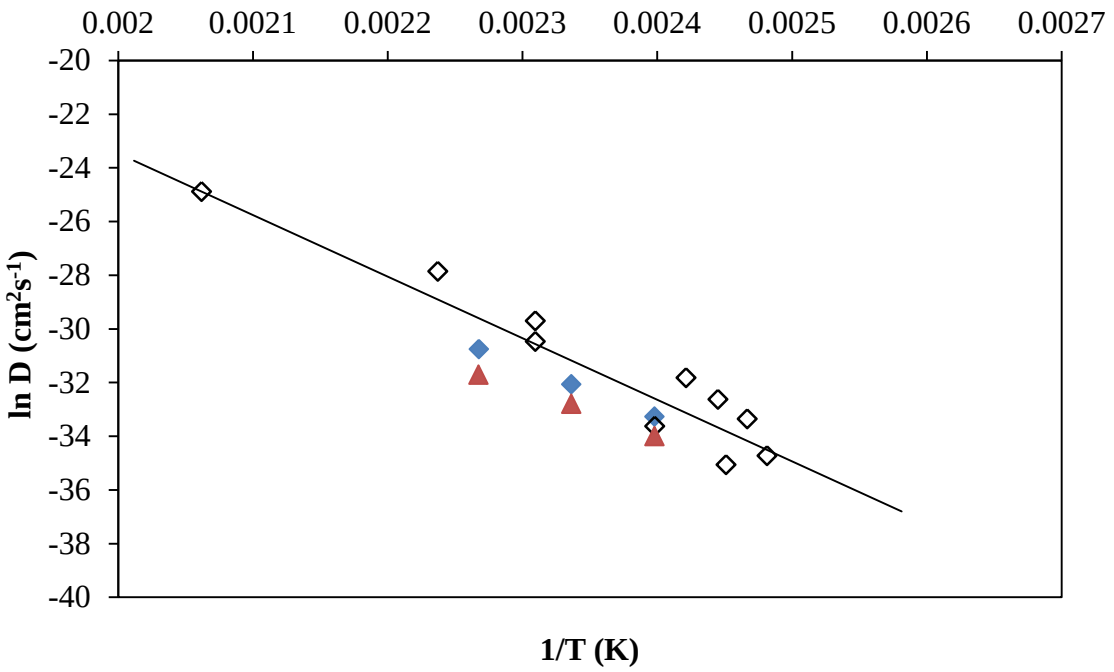

Figure 6.5: Arrhenius plot comparing the experimental data to the published diffusion data at various diffusion temperatures[12]. (◆) Blend IV-1, (▲) Blend IV-2, (◇) Published data were all converted to the same molecular weight (M_w= 100,000 g/mol) by using $D \propto M^{-2}$.

When the precrosslinked network is loose enough (like in the film of Blend IV-1), the polymer chain diffusion does not encounter significant resistance from the network and the rate of diffusion will be similar to the self-diffusion rate. When the precrosslinked network is tighter, the resistance effect from the gel network to the chain diffusion becomes significant and the corresponding diffusivity will be smaller than the self-diffusion coefficient. Therefore, it is reasonable to predict that for the extreme condition when the precrosslinked network is too tight, the diffusion coefficient will be close to zero which means that the polymer chains cannot diffuse in this very tight network.

It is worth mentioning that, the precrosslinking density does not affect the slopes in the Arrhenius plot in Figure 6.5. Based on the Arrhenius equation:

$$\ln D = \ln D^* - \frac{E_a}{RT} \tag{6.20}$$

in which E_a is the activation energy of diffusion, D^* is a pressure dependent constant, R and T represent the gas constant and temperature in Kelvin, the diffusion activation energy obtained from the slope of the plot is not affected by the pre-crosslinked gel network. It is because the diffusion activation energy reflects the energy barrier that polymer chains need to overcome to disengage themselves from their original position. It depends on the internal "chain-chain friction" (resistance to chain movement) within the material. As a result, it is the ability to move that matters to the activation energy not the movement speed. When the temperature is above the glass transition temperature, all chain segments gain the ability to move around. Therefore, the activation energy stays constant. Whether the activation energy increases or decreases most probably depends on

the intrinsic properties of the material, such as the difference between crystalline and amorphous polymers.

Comparing the estimated k_r values with the measured values by chemical reaction kinetics, the reaction rate constants from the model prediction at all three temperatures are larger by about an order of magnitude than the corresponding reaction rate constants directly measured in the small molecule reaction. This is due to one of the assumptions that mentioned previously in the introduction part. The complete reaction time is assumed to be the time that takes for the crosslinking density of the system to reach a plateau value. So when the fractional conversion of the reaction was calculated by swelling measurements, the 100% conversion was set to be the maximum crosslinking density that could be measured. Therefore, there was a difference between this relative conversion and the absolute conversion in the system. Because the SCM fit is based on the relative conversion, the predicted k_r value should be larger than the real k_r value.

However, by comparing these two k_r values, the real conversion of the chemical reaction that was achieved during the annealing processes in the latex blended system can be estimated. Table 6.3 gives the comparison details and the absolute conversion of the chemical reaction in polymers is calculated.

Table 6.3: Comparison of k_r Between the Estimated Values and Directly Measured Values

T	SCM Predicted k_r (10^{-6} Lmol^{-1}s^{-1})	Directly measured k_r (10^{-6} Lmol^{-1}s^{-1})	Absolute Conversion
144°C	7.58	0.662	8.73 %
155°C	15.2	1.59	10.49 %
168°C	37.9	3.96	10.44 %

Based on the calculation, only about 10% reactants have reacted during the annealing process of the latex films. There are two possibilities: first, the crosslinked network created by the chemical reaction greatly hinders further interdiffusion of the linear polymer chains, which makes the thickness of the reacted interface region even smaller than the estimated 3 nm and thus there are lots of reactive groups left unreacted; second, because the chain diffusion is quicker than the chemical reaction, some unreacted linear chains with amine reactive groups attached have the chance to diffuse into the COOH depletion region (deeper than 3nm beneath the particle surface), so that there are not enough carboxyl groups reacting with those reactive amine sites which makes the final conversion lower. It is not sure that which possibility is close to the reality, or maybe the two possibilities are both real but exist under different annealing conditions. For example, the first possibility more likely happens at a higher annealing temperature (such as 168 °C) under which condition the reaction rate and diffusion rate are comparable; while the second possibility will occur at a lower annealing temperature (such as 144 °C) under which condition the reaction is so slow that the polymer chains

are able to reach the maximum interpenetration depth before the crosslinking reaction can occur. Further investigations such as directly measuring the interpenetration depth *via* small angle neutron scattering can help to clarify this.

6.3.2 Comparison of Theoretical α with Experimental α

As mentioned in the introduction part, the control parameter α is the key to predicting if the reactive system is reaction controlled or diffusion controlled during the film formation process. A reaction controlled film formation is needed to gain better film mechanical performances.

Since the diffusion coefficients (D_e) were obtained from the fit to the Shrinking Core Model, and the reaction rate constant k_r was obtained from the kinetics study of the small molecule reactions, with all the parameters in hand, the theoretical value of α was able to be calculated using eq 6.12 and eq 6.18 derived from the scaling theory and the Shrinking Core Model and compared to the numerical value obtained in practice.

Table 6.4 shows the comparison of the experimental and theoretical control parameter α. From the table both the experimentally and theoretically obtained values prove that the $COOH/NH_2$ reaction in latex film formation is reaction controlled at all annealing temperatures used in the present study. More specifically, at 144 °C, the theoretical value calculated from the Shrinking Core Model is a better fit to the experimental result, while the experimental α is much closer to the calculated α value based on the scaling theory at 155 °C and 165 °C annealing temperatures. That is probably because at a lower annealing temperature, the reaction rate is much slower than

the chain self-diffusion so that the two processes can be considered to occur in series, which matches the basic idea for the design of the shrinking core model that assumes the gas molecule diffusion and the surface chemical reaction do not take place together but in successions. However, when the annealing temperature increases, the reaction rate becomes more comparable to the diffusion rate (although still α <1). Thus the two competitive processes more likely take place in parallel, which can be best described by the scaling theory that considers that the diffusion and chemical reaction both have an influence on each other. It is worth mentioning that although the α value is smaller at 155 °C and 165 °C than the value at 144 °C, this does not indicate that the reaction is slower at higher temperature, because the diffusion rate also needs to take into account as well as the amount of reaction that was completed during the annealing process.

Table 6.4: Comparison of Experimental α with Theoretical Calculated α

	Blend Film IV-1			Blend Film IV-2		
	144°C	155°C	168°C	144°C	155°C	168°C
Experimental t_{react} (h)	24	8	4	24	8	5
Experimental t_{diff} (h)	1	0.002	-(1)	2	0.008	-(1)
$R^{(2)}$ (nm)	350			330		
$N = \frac{M_W}{104}$	962			962		
$N_c = \frac{M_c}{104}$	224	241	283	168	164	150
A_0^* or [COOH]	5.71			10.5		
$k_r^{(3)}$ (10^{-6} Lmol^{-1}s^{-1})	0.662	1.59	3.96	0.662	1.59	3.96
D_e (10^{-15} cm^{2}s^{-1})	3.54	11.8	44.2	1.70	5.71	16.9
Experimental $\alpha = \frac{t_{diff}}{t_{react}}$	0.042	2.5 $\times 10^{-4}$	2.2 $\times 10^{-4}$	0.083	1.0 $\times 10^{-3}$	4.6 $\times 10^{-4}$
Scaling Theory Predicted $\alpha = (1.57\times10^{-16})\left(\frac{k_r}{D_e}\right)\left(\frac{A_0^* N^2}{N_c}\right)$	6.5 $\times 10^{-4}$	4.4 $\times 10^{-4}$	2.4 $\times 10^{-4}$	3.3 $\times 10^{-3}$	2.4 $\times 10^{-3}$	2.2 $\times 10^{-3}$
SCM Predicted $\alpha = \frac{Y}{6} = \frac{1}{18}\left(\frac{k_r}{D_e}\right)[COOH]R^2$	0.073	0.052	0.035	0.25	0.18	0.15
$\alpha_{exp}/\alpha_{scaling}$	65.1	0.574	1.036	25.1	0.411	0.234
$\alpha_{exp}/\alpha_{SCM}$	0.573	4.77 $\times 10^{-3}$	6.29 $\times 10^{-3}$	0.337	5.64 $\times 10^{-3}$	3.07 $\times 10^{-3}$

(1) Too small to be detected. Use theoretical $T_{diff} = T_{rep}$ for both cases at 165 °C.
(2) The large crosslinked particle size.
(3) Considering k_r is only temperature dependent, k_r is used in small molecule reactions for both cases, which is close to the 'diffusion-free' condition.

6.3.3 Estimation of Interfacial Energy G in the Slow Reaction Regime

When $\alpha < 1$, the film is expected to have better mechanical properties compared to the films made of each individual component particles, which was already proved in the case of the film made from Blend IV-1 annealed at 168 °C (the same composition as Blend III in Chapter 5). To further characterize the properties of these films, the maximum tensile strength was measured for various annealing conditions (all reaction controlled).

Since properties such as the film strength are more related to the state of the interface, in de Gennes' scaling relationship, they considered that the macroscopic tensile strength could be reflected by the interfacial energy *G* between two neighboring particles at the microscopic level. They presented a schematic plot of the interfacial energy *G* at the quasi-state[iii] as a function of the control parameter α (see Figure 6.6). When the system falls into the slow reaction regime ($\alpha < 1$), the interfacial energy *G* reaches a maximum value (the same as the material bulk strength) and remains constant no matter how the other molecular parameters in the system change.

The expression for *G* at fixed N_c in the slow reaction regime is given by:

$$G \cong \frac{U_0}{a^2}\sqrt{N_c} \cong G_{\max} \qquad (6.21)$$

[iii] Because of the visco-elastic dissipation, the interfacial energy depends on the rate of which the fracture is propagated. The quasi-state is the state with zero-detachment rate. Therefore, *G* at the quasi-state presents the lower bound of the observed energies.

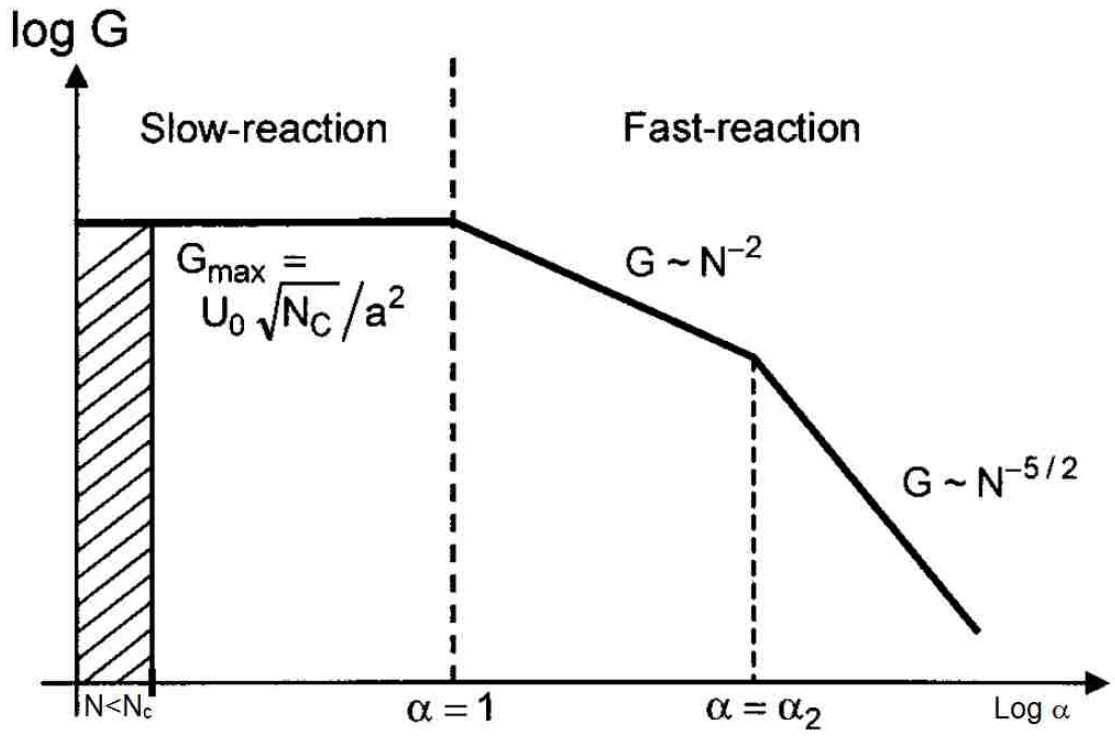

Figure 6.6: Reprints of schematic plot of the adhesion energy G *vs.* the control parameter[12] α. When $\alpha < 1$, the interfacial energy remains constant.

in which U_0 is of the order of the typical chemical bond energy, a is the monomer size and N_c is the final crosslinking density in the system.

Eq 6.21 is based on the prerequisite that the final N_c is fixed, which means that for a complete reaction, a fixed amount of chemical bonding must be achieved. The assumption is valid in their case, because their system is built on a mixture of linear polymer chains with the addition of an external crosslinker at a symmetric polymer-polymer interface. There is no initial crosslinking density in the system, so that given a fixed amount of crosslinker, the final crosslinking density will be the same if the reaction is complete (which is always the case in the slow reaction region).

However, in the studied system, this expression for G is no longer valid in the slow reaction regime. When the tensile strength is plotted as the function of ($Q\tau_0 A_0^* b^3$) and ($N^4/ N_e N_c$) based on the original expression for α (eq 6.4), the isocontour graph shows that the tensile strength is no longer a constant in the $\alpha < 1$ regime (Figure 6.7). Different from the model system in the theory, the present PS latex film system contains pre-existing crosslinks and the amount of functional groups varies from blend to blend. Therefore, the final N_c is no longer a constant value. The film strength apparently increases when the final crosslinking density increases (see Figure 6.8a). Figure 6.8b is a plot of film tensile strength *vs.* the reciprocal of the final N_c ($N_{c\text{-}tot}$) and it clearly shows an inverse proportionality between the two. The final crosslink separation is inversely proportional to the tensile strength, which indicates this final crosslink separation is also inversely proportional to interfacial energy G. This inverse relation is similar to the well-known classical theory of rubber elasticity:

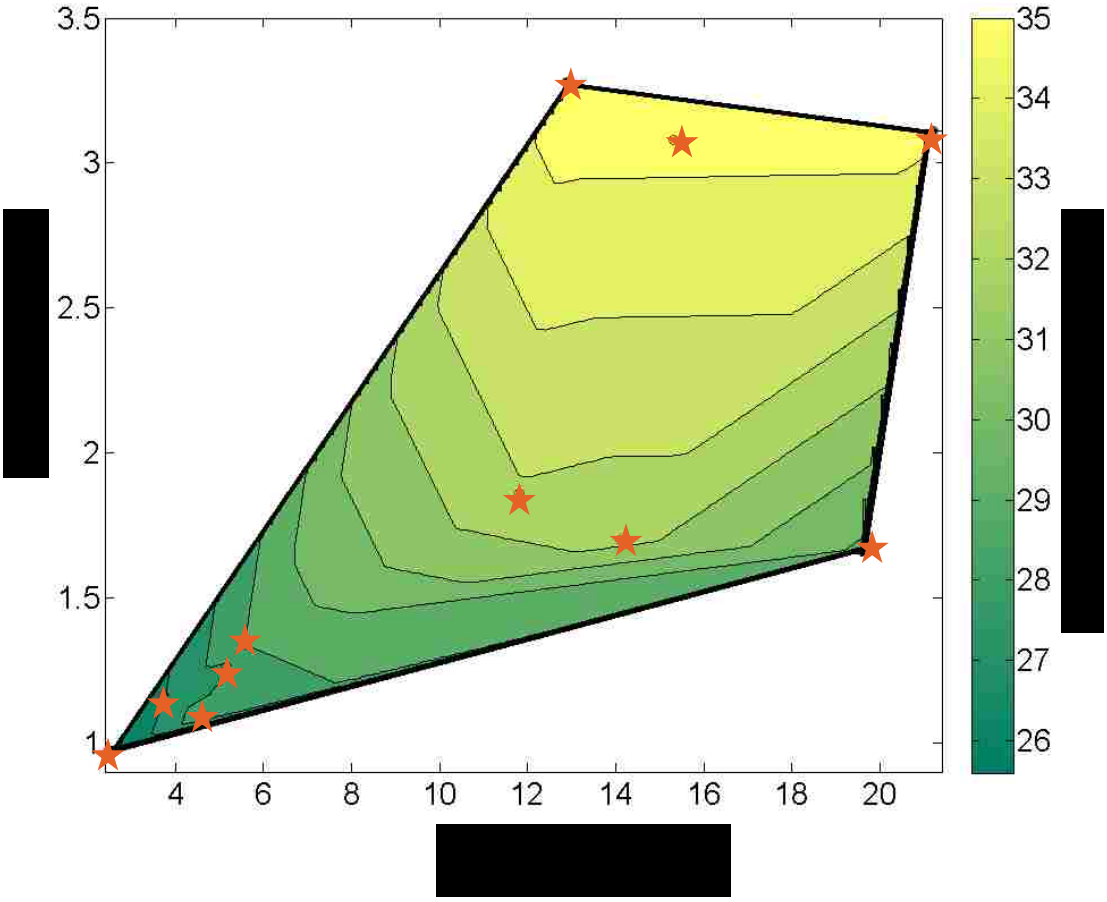

Figure 6.7: Isocontour profile of the film tensile strength as the function of various molecular parameters described in the scaling relationship. Only N_c has a slightly different definition, which is the number of units between crosslinks that has been created during reactions (see the introduction part in this chapter for explanation).

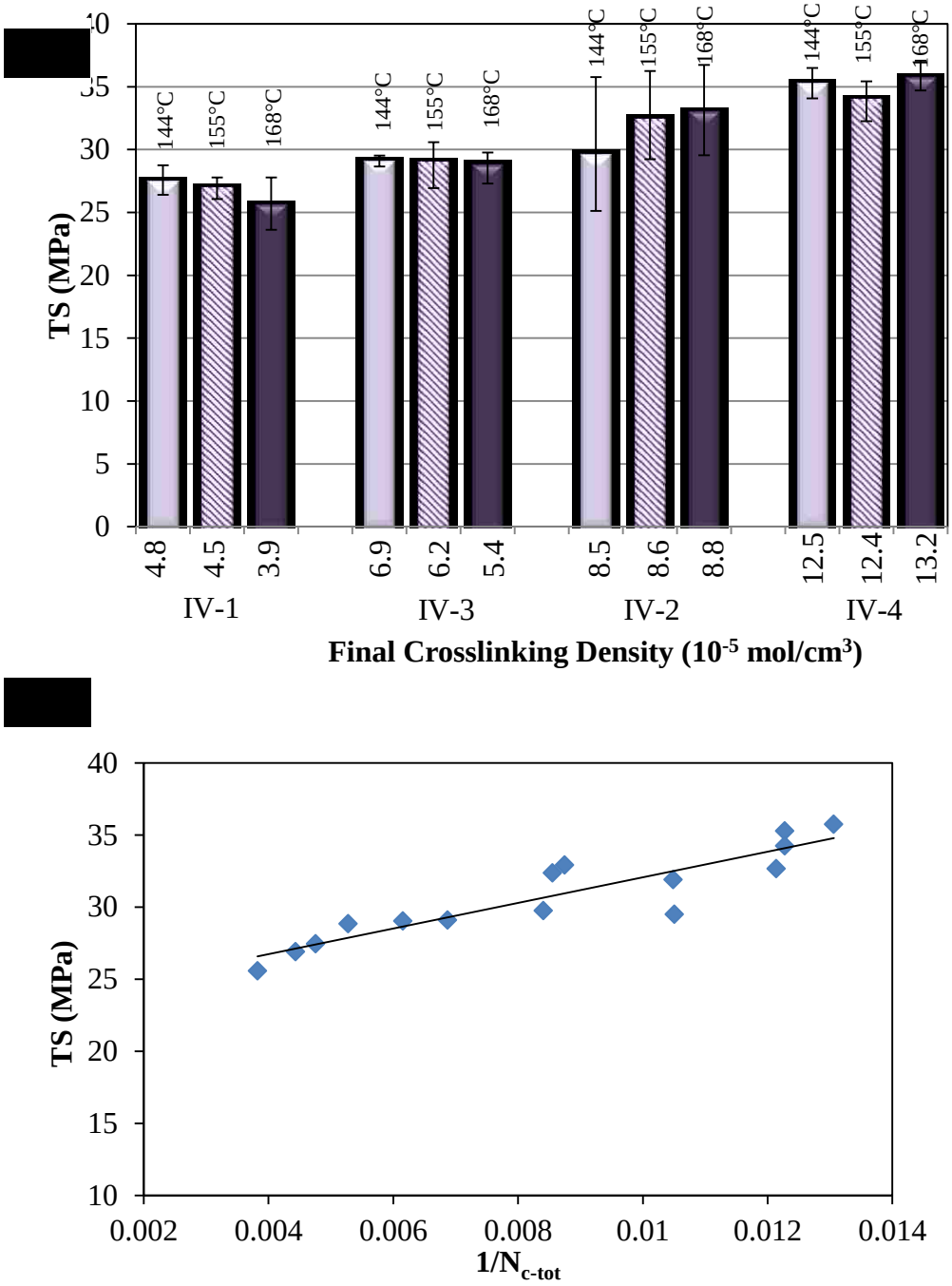

Figure 6.8: a) Film tensile strength *vs.* film final crosslinking density based on films comprised of Blends IV-1, IV-3, IV-2 and IV-4 (which have the same length for the mobile chains); b) TS *vs.* $1/N_{c\text{-}tot}$ based on films made from Blends IV-1, IV-2, IV-2H, IV-3 and IV-4.

$$E \sim \frac{kT}{N_c a^3} \tag{6.22}$$

in which the Young's modulus E is inversely proportional to the number of units between crosslinks N_c. The other parameters are constant: k is the Boltzmann constant, T is the temperature in degree Kelvin, and a is the monomer unit.

Young's modulus is a 'bulk-related' property, which is mainly determined by the density of crosslinks in the material. This similarity between the 'interface-related' tensile strength and the 'bulk-related' Young's modulus indicates that the interface really reaches close to the equilibrium state in the slow reaction region ($\alpha < 1$), the ideal condition under which there is no difference throughout the film no matter at the interface or inside the bulk of the material. Therefore, the interfacial energy becomes equivalent to the tear energy of the bulk. Similar to the relationship between Young's modulus and the network crosslink separation, N_c, the relationship of the interfacial energy G can be derived as a function of the final crosslink separation, $N_{c\text{-tot}}$, in the slow-reaction regime (see Appendix 3 for the derivation details), in which the chemical reaction is slower than the polymer chain interdiffusion, by:

$$G \cong \frac{U_0}{a^2 N_{c-tot}} \left(N_{c0}\right)^{\frac{3}{2}} \tag{6.23}$$

in which $N_{c\text{-tot}}$ is the number of monomer units between crosslinks in the final state. N_{c0} is the crosslink separation in the pre-existing network and it is considered to be fixed in the system if the amount of divinylbenzene used in preparing the large crosslinked particles remains the same. Although the pre-crosslinking density (of the large carboxylated

crosslinked particles) measured at room temperature *via* swelling measurements has contributions both from the chemical bonding of the divinylbenzene (DVB) crosslinker and the hydrogen bonding of the dimer between the carboxyl groups, the DVB contribution is the main focus, because the hydrogen bonding of the COOH dimers will be disassociated when the temperature increases[13]. Therefore, the hydrogen bonding will not contribute to the system crosslinking network that hinders the linear mobile chains interdiffusion process, and it is reasonable to consider N_{c0} in eq 6.23 to be the crosslinking density only contributed by the DVB crosslinkers. The value can be estimated as the crosslinking density of the pure crosslinked PS particles with the same amount of DVB incorporated but in the absence of the carboxyl functionalities.

If a fixed pre-crosslinking density exists in the system, based on the eq 6.23, the interfacial energy G will increase as the final crosslinking density increases ($N_{c\text{-}tot}$ decreases). However, a conclusion cannot be made for a changing precrosslinking density system yet. Take Blend Film IV-3 with Film IV-1 and IV-2 for comparison, Film IV-3 has a tighter precrosslinking density than both Film IV-1 and IV-2 (in terms of the amount of DVB used), but the tensile strength of Film IV-3 is higher than Film IV-1 and lower than Film IV-2 (see Figure 6.8a for evidence).

The influence of the precrosslinked network on the mobile chain diffusion is highly dependent on the dynamic size of the linear chains as well as the reactive sites present in the network. Tobing *et al.* in their study[14] mentioned that when the gel network size is at least the same or bigger than the dynamic diameter of the polymer chain, the mobile chains are able to diffuse into the gel network. However, when this prerequisite is

met (the chain is able to diffuse into the network), the effect of the existing network on the chain interdiffusion and on the corresponding interfacial strength in the presence of the chemical reaction becomes more complicated. Nevertheless, the maximum interfacial strength can still be able to be estimated based on Figure 6.8b with the consideration of Tobing's conclusion. Because in order for polymer chains to successfully diffuse into the preexisting network, the minimum molecular weight between crosslinking points of the network M_{c0} should be comparable to the entanglement molecular weight M_e. By using M_e as the initial crosslinking length and adding together the minimum crosslinking length (which presents the highest crosslinking density) that can be created by chemical reactions, M_c (based on the experimental data), the value of minimum final crosslink separation $M_{c\text{-}tot.}$, can be estimated by equation 6.24:

$$\frac{1}{M_{c-tot}} = \frac{1}{M_e} + \frac{1}{M_c} \tag{6.24}$$

As a result, the theoretical maximum tensile strength at the 105 °C testing temperature can be calculated using the linear relationship derived from Figure 6.8b. In this system, the theoretical value is calculated to be approximately 38 MPa.

6.4 Conclusions

In this chapter, two models: the scaling theory and the shrinking core model were utilized to investigate the competition between the polymer chain interdiffusion and the

carboxyl/amine chemical reaction during the film annealing process at various temperatures. The expression for the control parameter α was given in two ways:

$$\alpha = \left(1.57\times10^{-16}\right)\left(\frac{k_r}{D_e}\right)\left(\frac{A_0^* N^2}{N_c}\right) \tag{6.25}$$

$$\alpha = \frac{1}{18}\left(\frac{k_r}{D_e}\right)[COOH]R^2 \tag{6.26}$$

Both models show the control parameter α is proportional to the ratio of the reaction rate constant k_r to the diffusion coefficient D_e, as well as proportional to the concentration of the carboxyl groups (A_0^* or [*COOH*]) that take part in the reaction. There are, however, differences between the two models. The scaling theory focuses more on the molecular level of the polymer chains, such as the length of the chain N and the length of the crosslink separation N_c, because this theory is based on the kinetics of each individual chain and then is scaled up to predict the macroscopic level of the film performance. The shrinking core model is more concerned about the size of the 'solid' R, in this study is the size of the crosslinked large latex particles, D_L, because this model is based on the study of the solid-gas reaction and the whole solid particle is considered to be the reactor and the receding surface area of the solid is the key parameter to determine the reaction and diffusion rate. From a practical perspective, the reaction and diffusion occur simultaneously in most coating processes, thus eq 6.25 based on the scaling theory fits the model better.

Both experimental results and theoretical calculations have shown that the reactive latex film system comprised of carboxylated crosslinked large particles and amine functionalized non-crosslinked small particles was reaction-controlled during the annealing process, which was in the slow reaction regime expressed by the control parameter $\alpha < 1$. Further film tensile strength study shows that even within the slow reaction regime, the interfacial strength does not have a constant maximum value. Instead, the strength has an inverse relationship with $N_{\text{c-tot}}$, the number of monomer units between crosslinks at the final state of the film. As a result, an equation has been proposed to describe the relationship between interfacial energy G at zero-detachment rate and $N_{\text{c-tot}}$ in a fixed precrosslinked (N_{c0}) system in the slow reaction regime, which is shown as:

$$G \cong \frac{U_0}{a^2 N_{c-tot}} \left(N_{c0}\right)^{\frac{3}{2}} \tag{6.27}$$

Because $N_{\text{c-tot}}$ is highly dependent on the concentration of the reactive groups A_0^*, if the diffusion and the reaction rate are fixed for a specific system, within the range of $\alpha < 1$, the higher the concentration of reactive groups, the better the mechanical performance of the film will be.

6.5 References

1. Aradian, A., Raphael, E., deGennes, P.G. *Macromolecules*, **2000**, *33*. 9444.

2. Aradian, A., Raphael, E., deGennes, P.G. *Macromolecules*, **2002**, *35*. 4036.

3. Ishida, M., Wen, C.Y. *AIChE Journal*, **1968**, *14*. 311.

4. deGennes, P.G.,Leger, L. *Ann. Rev. Phys. Chem*, **1982**, *33*. 49.

5. Wool, R.P., Yuan, B.L., McGarel, O.J. *Polym. Eng. Sci*., **1989**, *29*. 1340.

6. Cotton, P.J., Decker, D. et al. *Macromolecules*, **1974**, *7*. 863.

7. Terao, K., Mays, J.M. *European Polymer Journal*, **2004**, *40*. 1623.

8. Evers, O.; Ley, G.; Hadicke, E. *Macromolecules* **1993**, *26*, 2885

9. Whitlow, S.J.; Wool, R.P. *Macromolecules* **1991**, *24*, 5926;

10. Kim, S.D.; Klein, A.; Sperling, L.H. *Polym.Adv. Technol.* **2002** *13* 403

11. a) Anderson, J.E; Jou, J.H. *Macromolecules* **1987**, *20*, 1544; b) Antonietti, M.; Coutandin, J.; Sillescu, H. *Macromolecules* **1986**, *19*, 793; c) Kim, K.; Sperling, L.H.; Klein, A.; Hammouda, B. *Macromolecules* **1994**, *27*, 6841; d) Whitlow, S.J.; Wool, R.P. *Macromolecules* **1991**, *24*, 5926; e) Brautmeier, D.; Stamm, M.; Linder, P.J. *J. Appl. Crystallogr.* **1991**, *24*, *665*; f) Mills, P.J.; Green, P.F.; Palmstrom, C.J.; Mayer, J.W.; Kramer, E.J. *J.Polym.Sci-Phys Ed* **1986**, *24*, 1.

12. de Gennes P.G. *J. Chem. Phys.***1971**, *55*, 572

13. Cleveland, C.S.; Fearnley, S.P.; Hu, Y.; Wagman, M.E.; Painter, P.C.; Coleman, M.M. *J. Macromol. Sci. Phys.* **2000**, *B39*, 197

14. Tobing, S.; Klein, A; Sperling, L.; Petrasko, B. *J. Appl. Poly. Sci.* **2001**, *81*, 2109

CHAPTER 7

Conclusions and Recommendations

7.1 Conclusions

The primary conclusion from this work is that by carefully controlling the molecular parameters of the polymer particles in latex blends, such as particle size and ratio, polymer molecular weights, bulk crosslinking as well as interfacial crosslinking, latex films with better mechanical performance can be designed. The detailed conclusions are drawn as follows:

1) Based on the theory of continuity, at the optimal blending ratio V_c, the bimodal latex blends can self-assemble into a close packing morphology during the film formation process, where every large particle is surrounded by small particles that form the continuous phase. This self-assembly greatly reduces the void content inside the latex film, resulting in a much shorter annealing time to reach film maximum strength.
2) Polymer molecular weight, and more precisely the weight-average molecular weight, is the dominant factor in determining film mechanical strength after full annealing. The film strength increases with increasing chain length, however, the strength plateaus after which no further increase in strength is seen. The optimal

molecular weight corresponds to the onset of the plateau in the film strength *vs*. chain length plot. For the polystyrene system studied in this research, the optimal molecular weight is close to 3.0×10^5 g/mol.

3) By introducing pre-crosslinked particles into blends, the film modulus can be increased. Film strength can also be improved if the linear component of the polymer particles has a molecular weight that is small enough to avoid entanglements. In this case, the pre-crosslinked network actually reduces the critical entanglement molecular weight of the films by creating a more efficient physical entanglement in the linear-gel network. However, if the particle with linear polymer chains has a molecular weight that is high enough, the pre-crosslinked network has either no effect or negative effect on the film strength.
4) Chemical crosslinking at the particle-particle interface can increase the film interfacial strength as well as the other mechanical performances (such as film toughness) if the film annealing process is reaction controlled, which means the chemical reaction is the slow step compared to the polymer chain diffusion across the interface.
5) To design a reaction controlled film system during the annealing process, the controlled parameter α that is defined as the ratio of typical diffusion time to the typical reaction time should be adjusted to be less than 1. By converting the de Genne's scaling theory and the Shrinking Core Model into two practical equations to calculate the control parameter α, it was found what both theories have in common is that the α value is related to the ratio of the reaction rate constant to

the diffusion coefficient of the polymer chains, as well as the concentration of the functional groups attached to the crosslinked gel particles that take part in the chemical reactions. It is suggested that if the diffusion rate and the reaction rate are fixed for a specific system, the higher the concentration of reactive groups, the better the mechanical performance of the film will be, as long as the value of the control parameter is less than 1.

7.2 Recommendations

In addition to this work, several branches of this research merit further investigations:

1) Direct measurement of void content

Particle packing was proved to be able to greatly reduce the voids content inside a latex film, but we only utilized a qualitative characterization method *via* SEM to check for visible voids on the surface and in the bulk. A more quantitative void content measurement could possibly be done *via* ellipsometry or optical transimission [1]. Ellipsometry measures the surface roughness and the concentration of nanovoids in latex films by determining the change of the state of polarization of light upon reflection from a surface or interface; while optical transimission usually measures the larger voids, like air voids inside the film.

Comparing the void content within the reactive latex films before and after the annealing process can also provide an assessment of the presence of any voids generated

in the bulk film, because water is one of the products of the COOH/ NH_2 chemical reaction that has to be released during the annealing process.

2) Drying effect on particle packing

Because the drying conditions that normally used to dry latex films (ambient, oven heating and vacuum) were of more interest in this study, a detailed study of the drying effect on latex particle packing was not carried out by accurately controlling the drying parameters, such as temperature, humidity, and pH. It would be important to see how drying conditions affect the close-packing morphology of bimodal latex blends. Hosokawa *et al.* in their nanoparticle technology handbook[2] mentions some conditions that are responsible for self-assembled structures, and that provides a good reference for this study.

3) Polymer chain interdiffusion via small angle neutron scattering

In the study of the competition between polymer chain interdiffusion and chemical reaction, a direct measurement of the polymer chain interpenetration depth at the particle-particle interface was not available. Because small angle neutron scattering (SANS) has been widely used for characterizing polymer chain diffusion[3,4,5], it will be very important to determine how the chemical crosslinking at the interface affects the film formation process by directly monitoring the polymer chain diffusion activities.

4) The negative effect of carboxyl groups on the pre-crosslinked films

When latex films comprised of carboxylated crosslinked large PS particles and non-functionalized non-crosslinked small PS particles were used for the study of pre-crosslinking effect, film strength decreased as annealing time increased, which is the opposite to the typical trend of the tensile strength development. To determine the negative effect of the carboxyl groups, a comparison experiment was prepared. Figure 7.1 shows the tensile strengths of four different latex blend films prepared from nonfunctionalized loosely (or tightly) crosslinked PS with nonfunctionalized linear PS particles (NF1 or NF2) and from carboxyl-functionalized loosely (or tightly) crosslinked PS with nonfunctionalized linear PS particles (FF1 or FF2). The parameters are shown in Table 7.1.

According to the results shown in Figure 7.1, two major trends are evident: one is that tensile strength (TS) increases with increasing annealing time, which is shown in the sample films NF1 and NF2; the other is that the tensile strength decreases as the annealing time increases, which is shown in the sample films FF1 and FF2. Nonfunctionalized sample films present the typical increasing trend. The longer the annealing time, the further the polymer chains diffuse and penetrate across the interface. The more entanglements, the stronger the polymer film will be. However, in the sample films FF1 and FF2, different TS trends are observed. The highest value of TS is reached immediately after the sintering process, but the value decreases as the annealing time increases. Especially in the sample FF2, more and more cracks were observed when the annealing time was increased. A possible explanation is that COOH groups undergo a

Table 7.1: Characteristics of Blended Latex Films

NF1 **V_c** = 25.9 %**	large Particle: 282 nm, $M_c >> 1 \times 10^5$ g/mol* Small Particle: 74 nm, $M_w = 5.8 \times 10^5$ g/mol
NF2 **V_c = 20.6 %**	large Particle: 413 nm, $M_c = 5.0 \times 10^4$ g/mol Small Particle: 81 nm, $M_w = 1.9 \times 10^5$ g/mol
FF1 **V_c = 25.21%**	large Particle: 292 nm, $M_c >> 1 \times 10^5$ g/mol* Small Particle: 74 nm, $M_w = 5.8 \times 10^5$ g/mol
FF2 **V_c = 26.14 %**	large Particle: 293 nm, $M_c = 2.9 \times 10^4$ g/mol $\approx M_e$ Small Particle: 78 nm, $M_w = 5.4 \times 10^5$ g/mol

* M_c was difficult to measure by swelling measurement due to the very loosely crosslinked network

** V_c is the volume percentage of small particles needed for integrity

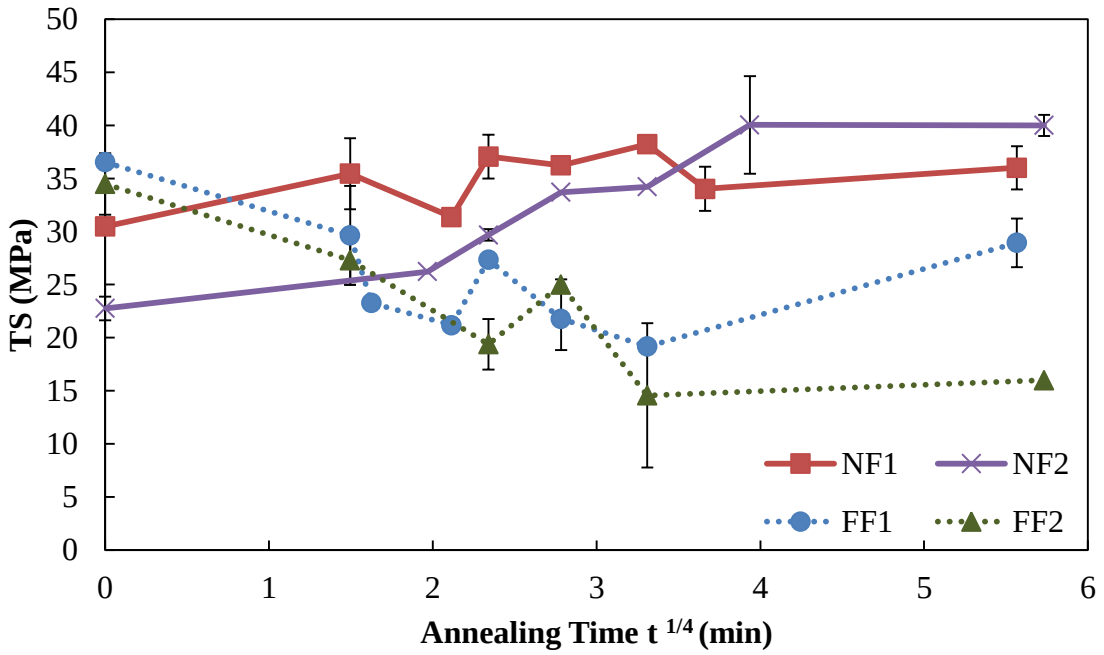

Figure 7.1: Film tensile strength development *vs.*one-quarter power of the annealing time

self-condensation reaction by forming anhydrides at high temperatures, so that the increasing crosslinking density on the surface hinders the polymer chain interdiffusion and leads to phase separation at the interface. Concerning sample FF1, because its initial crosslinking network was very loose, the hindrance caused by the additional surface crosslinking density could be overcome by further chain rearrangement and interpenetration during the annealing process. When the annealing time increased, the film strength of the sample FF1 rebounded. However, this statement is only our hypothesis. It would be a good supplemental work if the dehydration process could be clearly evident in the results, or if other possible reasons could be evaluated that explain this phenomenon.

5) Fast reaction regime

In our study, only reaction controlled film formation process was designed, because the practical interest is in the chemical crosslinking as the slow step compared to polymer chain diffusion, so that the polymer chain interdiffusion cannot be stopped by additional chemical crosslinking at the interface and thus a stronger film can be formed. However, for a fundamental study, it would be important to have comparative results when the film annealing process is diffusion controlled to see to what extent fast chemical crosslinking degrades film performance. Some preliminary results were obtained regarding this aspect of the fast reaction regime.

Since carboxyl and hydroxyl groups can react approximately 100 °C, when the COOH/OH reactive functional groups were introduced into the film system, the latex film increased the amount of crosslinking right after sintering at 130 °C. When the films

were then annealed at 168 °C for two hours, the molecular weight between crosslinking points was very small (approximately 6×10^3 g/mol). With this crosslinking density in the COOH/NH_2 system, the film tensile strength reached as high as 40 MPa, but in the COOH/OH system, the real film tensile strength was only 17.5 MPa. This result indicates that when a fast crosslinking reaction takes place during film formation, the crosslinking at the interface can greatly hinder or even stop the polymer chain interdiffusion, which leads to fewer effective entanglements at the particle-particle interface. Therefore, although the crosslinking density is higher in the diffusion controlled system, the resulting film interfacial strength is much lower due to insufficient polymer chain interpenetration.

If a more detailed study is carried out in this fast reaction regime and compared with the predictions based on our practical model, the study of the competition between diffusion and crosslinking processes in a reactive film system will be more complete.

6) Blends of small crosslinked and large noncrosslinked latex particles

In this system, large PS particles are crosslinked and carboxylated, and the small PS particles are noncrosslinked and amine functionalized. It would be interesting to see the film performance if the crosslinked carboxylated latexes are small sized particles and the noncrosslinked amino latexes are large sized particles.

7) Blends of hard and soft latex

To check if our practical guideline for the film-interface strengthening is universal and can be applied to low T_g reactive film systems, a further investigation of hard and

soft latex blends is desirable, which are much closer to the practical industrial application. Using the soft latex particles, the film is practically able to form at ambient temperatures in the absence of coalescing agents. As we mentioned in the introduction, the interfacial crosslinking is more important under conditions in which soft polymer chains need to diffuse into hard polymer particles, because fewer entanglements are expected at the interface and the film strength is more dependent on the crosslinking at the interface. Hopefully, our practical model developed in this research is able to provide useful guidelines for the design of a better hard/soft blended film systems.

7.3 References

1. Tzitzinou, A.; Keddie, J. L. *Macromolecules* **2000,** *33*, 2695
2. Hosokawa, M.; Nogi, K.; Naito, M.; Yokoyama, T. *Nanoparticle Technology Handbook,* Elsevier B.V. **2007**
3. Anderson, J.E.; Jou, J.H. *Macromolecules* **1987**, *20*, 1544
4. Kim, S.D.; Klein, A.; Sperling, L.H. *Macromolecules* **2002**, *13*, 403
5. Loppinet, B.; Fytas, G.; Vlassopoulos, D. *Macromolecular Chem. Phys.* **2005**, *206*, 163

APPENDIX A

Synthesis of 3-Isopropenyl-α,α- Dimethylbenzylamine (TMA)

In Chapter 3, the synthetic route[1] was used to produce amine functionality, as the chemical equation shown:

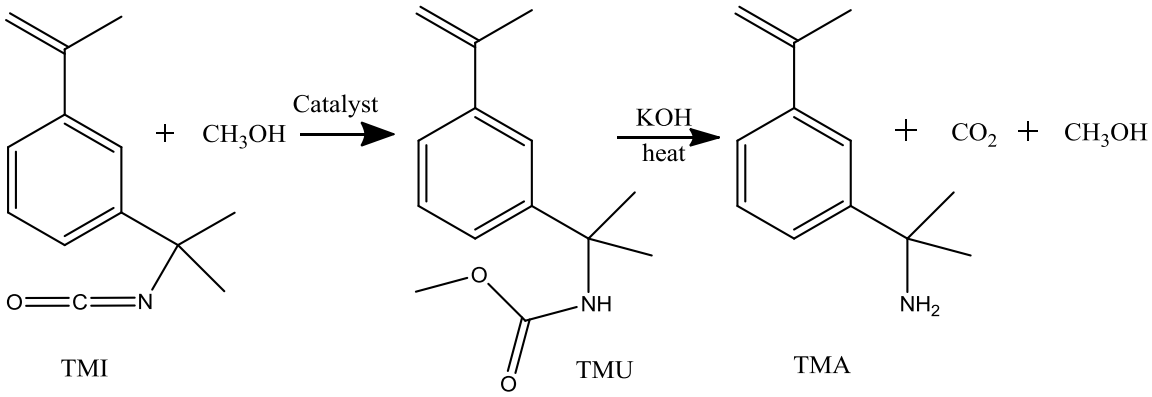

(A.1)

The purpose of this appendix is to show more details of the synthesis process, as well as several modifications to the original route and some precautions that are not reported in Trumbo *et al*'s paper[1].

The first step is to hydrolyze the isocyanate group to a carbamate group. The experimental set up is shown in Figure A.1.

[1] Trumbo, D. L.; Mote, B. E.; Trevino, A.S.; Van Den Brink, M. *J. Appl. Poly. Sci*, **2001**, *82*, 1030

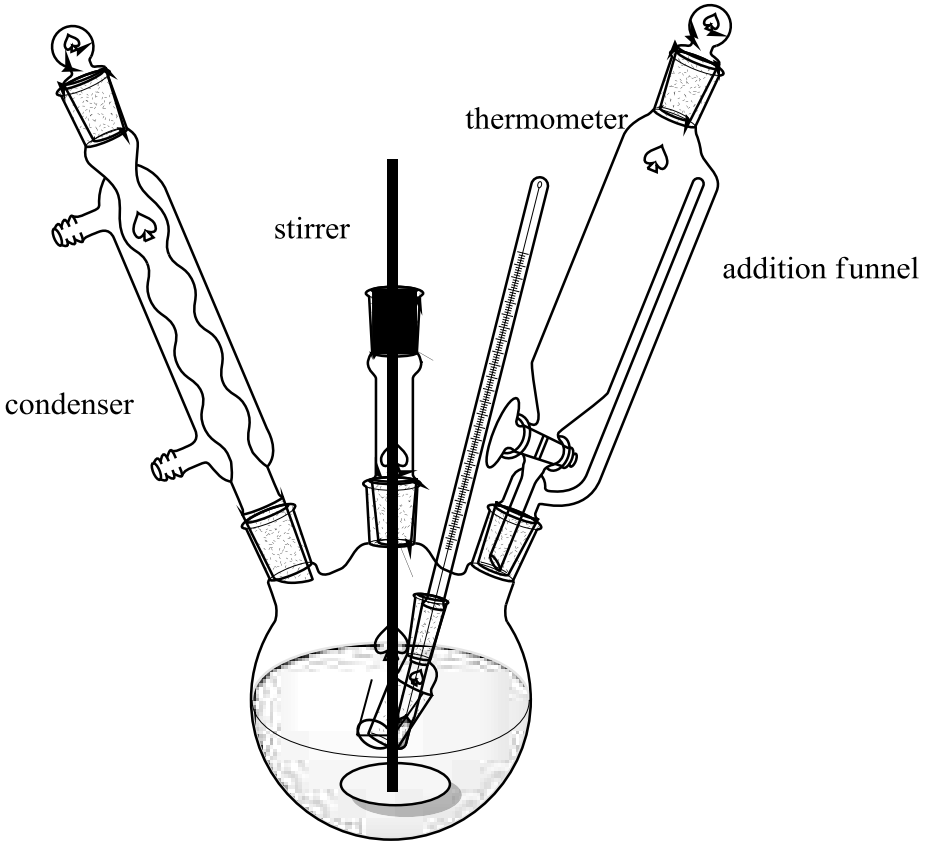

Figure A.1: Schematic of the reaction setup, which is suitable for both the first step and the second step of the reaction.

Isopropenyl dimethylbenzyl isocyanate 100.5 g (0.4994 mol) (TMI, without further purification) was added to a 500 mL four-neck round flask, together with 0.4 g dibutyltin dilaurate catalyst. Then through the addition funnel, 16.0 g methanol (0.471 mol) was added to the flask dropwise. Over half an hour during the addition of the methanol, the inner solution temperature increased from 25 °C to 34 °C. After cooling down for half an hour, the whole flask was then transferred to a preheated 60 °C water bath and allowed to react for 5 hours. After the reaction mixture cooled down to room temperature, the entire mixture did not solidify as Trumbo described. This first step in the reaction was repeated three times, but never yielded a solid product. The entire liquid mixture was tried to recrystallize in the freezer. However, after 3 to 4 days, the mixture was still liquid. Only after bubbling up the liquid mixture, the liquid started to crystallize within several hours in the freezer. And then within two days, the whole reaction mixture solidified.

For the second step, the intermediate product methyl urethane (TMU) was used both in its liquid form and in its crystallized solid form, and we found in both cases the final products could be made. The following details referred to the solid TMU reaction. TMU 30.0 g (0.129 mol) was dissolved in 30.0 g butyl cellosolve, and the solution was added to the 500 mL four-neck round bottom flask. The apparatus was the same as the first step, but instead of a water bath, a heating mantle was used. After adding the KOH solution (12.5 g KOH pellets in 60.0 g butyl cellosolve) to the flask, the contents were heated to boiling and refluxed for 4 hours. The voltage for the heating mantle was set at 120 V. The solution temperature when refluxing was only about 120 °C, less than the

pure butyl cellosolve boiling temperature of 170 °C. After the reaction, the mixture was cooled to room temperature. Then 60.0 g water and 100.0 g dichloroethane were added to the solution and the mixture was stirred at room temperature overnight. Later, the mixture was poured into an addition funnel and 200 mL (4 × 50 mL) water was used to wash the mixture. In the first separation, the oil layer was the upper layer. But later for the second to fourth separation, the oil layer remained at the bottom. After washing, the mixture was dried with anhydrous sodium sulfate.

Concerning the product purification, a two-step distillation was applied. For the first step, a rotary evaporator (Rotavap) was used for removing most of the dichloroethane out at 45 °C under reduced pressure. For the second step, a Schlenk line was used to provide a high vacuum condition. The heating temperature was 120 °C using a sand bath. Two fractions were collected. The first fraction was distilled at 23 °C under 560 millitorr pressure. The fraction was mostly the remaining dichlorethane and water. The second fraction was distilled at 68~70 °C under 510 millitorr. This fraction was the pure product TMA, as proved by the NMR spectrum in Chapter 3. The yield was 10.8 g of liquid.

APPENDIX B

Derivation of Shrinking Core Model Equations

In Chapter 6, the modified Shrinking Core Model was used to analyze the kinetics of film formation. The equation is as follows:

$$t(x,K,Y) = K\left[1-(1-x)^{\frac{1}{3}}\right]\left\{1+\frac{Y}{6}\left[1+(1-x)^{\frac{1}{3}}-2(1-x)^{\frac{2}{3}}\right]\right\} \qquad \text{(B.1)}$$

Eq B.1 is the derivation of the original Shrinking Core Model (SCM), which is designed to model gas-solid multiphase combustion reactions within one single particle (initially all solid substance B) reacting with gas molecules A. The standard reaction is:

$$A\,(\text{g}) + \text{b}B\,(\text{s}) \longrightarrow \textit{Products}\ (\text{s, g}) \qquad \text{(B.2)}$$

The basis for the analysis using SCM is that the three processes involving mass transfer of A, diffusion of A, and reaction of A with B at the surface of the core are in series. Therefore, by using the quasi-steady-state approximation, the continuity equation for steady-state diffusion of A is:

$$D_e\left(\frac{\partial^2 C_A}{\partial r^2}+\frac{2}{r}\frac{\partial C_A}{\partial r}\right)=\frac{\partial C_A}{\partial t}=0 \qquad \text{(B.3)}$$

in which D_e is the effective diffusivity of A through the porous product layer, C_A is the concentration of A, which is decreasing as reaction time increases.

By a two-step integration of eq B.3 using the boundary conditions (see Missen et al.'s chemical reaction engineering and kinetics book for more details[1]), the total reaction rate of A within the particle is:

$$-R_A = \frac{4\pi C_{Ag}}{\frac{1}{k_{Ag}R^2} + \frac{R - r_c}{D_e R r_c} + \frac{1}{k_{As}r_c^{\,2}}} \qquad \text{(B.4)}$$

in which C_{Ag} is the gas phase concentration of A, k_{Ag} is the mass transfer coefficient in the bulk gas layer or external diffusion resistance, k_{As} is the reaction rate constant for the first order surface reaction with the units in m s^{-1}, R is the radius of the particle B and r_c is the radius of the unreacted solid core.

In order to substitute the k_{As} with the volume based first order reaction rate constant k_{vol} (with units in s^{-1}), a relationship considering the whole particle as the reactor was derived:

$$-R_A = \frac{4\pi C_{Ag}}{\frac{1}{k_{Ag}R^2} + \frac{R - r_c}{D_e R r_c} + \frac{1}{k_{As}r_c^{\,2}}} = -Vk_{vol}C_A = \frac{4}{3}\pi R^3 k_{vol} C_A \qquad \text{(B.5)}$$

Because k_{vol} and k_{As} are considered to be constant throughout the reaction, a particular boundary condition can be applied to solve the equation. When the reaction just starts, r_c

[1] Missen, R.W.,Mims, C.A.,Saville, B.A. *Introduction to Chemical Reaction Engineering and Kinetics.* **1999**, John Wiely & Sons, Inc. p232.

is the same as R and the concentration of A is equal to gas phase concentration of A. Therefore, we can derive:

$$\frac{k_{As}}{k_{As}/k_{Ag}+1}=\frac{R}{3}k_{vol} \tag{B.6}$$

In the study of the polymer interface healing process, there is no external resistance to polymer chain diffusion, so the k_{Ag} can be treated as infinite. Then a simpler relationship is derived as:

$$k_{As}=\frac{R}{3}k_{vol} \tag{B.7}$$

The k_{vol} in the eq B.7 is the first order reaction rate constant. However, the COOH/NH_2 crosslinking reaction follows a second order reaction mechanism. Since the concentration of carboxyl groups (analogous to the solid B particle in the SCM model) is much higher than the concentration of NH_2 groups (analogous to the gas molecule A in the SCM model) where the reaction takes place, k_{vol} can be related to the rate constant in reaction that is pseudo-first order in NH_2 with the relationship of:

$$k_{vol}=k_r[COOH] \tag{B.8}$$

thus combining eq B.7 & B.8, a relationship was derived:

$$k_{As}=\frac{R}{3}k_r[COOH] \tag{B.9}$$

With the relationship between k_{vol} and k_r at hand and the consideration of an infinite value for k_{Ag}, the original final SCM equation

$$t = \frac{\rho_{Bm} R}{bC_{Ag}} \left\{ \frac{1}{3k_{Ag}} \left[1 - \left(\frac{r_c}{R} \right)^3 \right] + \frac{R}{6D_e} \left[1 - 3\left(\frac{r_c}{R} \right)^2 + 2\left(\frac{r_c}{R} \right)^3 \right] + \frac{1}{k_{As}} \left(1 - \frac{r_c}{R} \right) \right\} \quad \text{(B.10)}$$

can be modified into:

$$t = \frac{\rho_{Bm} R}{bC_{Ag}} \left\{ \frac{R}{6D_e} \left[1 - 3\left(\frac{r_c}{R} \right)^2 + 2\left(\frac{r_c}{R} \right)^3 \right] + \frac{3}{Rk_r[COOH]} \left(1 - \frac{r_c}{R} \right) \right\} \quad \text{(B.11)}$$

in which b is the stoichiometry number in reaction B.2. In the specific $COOH/NH_2$ reaction that studied, b=1; C_{Ag} is the concentration of A in the gas phase and in this polymer system, C_{Ag} can be considered as the concentration of NH_2 groups at the reaction site. ρ_{Bm} is defined to be the unreacted number of moles of B per unit volume of particle, which is an average value for integration purposes considering that the particle is uniform throughout. When r_c is close to 0, the total amount of B should be equal to $\rho_{Bm} V_{particle}$. However, in a batch polymerized particle, carboxyl functional groups are not evenly distributed due to its high hydrophilicity (see Chapter 3 for more details). The surface and core region have more concentrated functional groups, while in between there almost exists a depletion region. Therefore, ρ_{Bm} is not equivalent to the concentration of B where the reaction occurs.

Because the radius of the unreacted core is related to the fractional conversion of the chemical reaction by

$$x = 1 - \left(\frac{r_c}{R}\right)^3 \tag{B.12}$$

eq B.11 can be simplified as:

$$t = \frac{3\rho_{Bm}}{k_r[COOH][NH_2]}\left[1-(1-x)^{\frac{1}{3}}\right]\left\{\frac{k_r[COOH]R^2}{18D_e}\left[1+(1-x)^{\frac{1}{3}}-2(1-x)^{\frac{2}{3}}\right]+1\right\} \tag{B.13}$$

Define $$K = \frac{3\rho_{Bm}}{k_r[NH_2][COOH]}, Y = \frac{k_r[COOH]R^2}{3D_e} \tag{B.14}$$

and eq B.1 is derived.

APPENDIX C

Estimation of Interfacial Energy in the Slow Reaction Regime

In Chapter 6, a different version of interfacial energy was presented compared to the description published by Aradian et al.[1]:

$$G = \frac{U_0}{a^2 N_{c-tot}} \left(N_{c0}\right)^{\frac{3}{2}} \tag{C.1}$$

Eq C.1 is still based on the Lake and Thomas formula cited in Aradian et al.'s paper[1]:

$$G_{scission} \cong U_0 \tilde{\sigma} \tilde{n} \tag{C.2}$$

in which $G_{scission}$ is the interfacial energy contributed by chain scission at zero-detachment rate. Because of the visco-elastic dissipation, the interfacial energy generally depends on the rate at which the fracture is propagated. Therefore, at zero-detachment rate, the physically entangled chains have enough time to disentangle and then be pulled out and this quasi-static energy $G_{scission}$ only depends on chains that are chemically tethered on both sides of the interface. Thus, the calculated interfacial energy should be the lower limit of the observable energies. U_0 is of the order of the typical chemical bond energy, $\tilde{\sigma}$

[1] Aradian, A., Raphael, E., de Gennes, P.G. *Macromolecules*, **2002**, 35, 4036

is the density of connectors chains (crossing chains) per unit area of the interface, and $\tilde{n}$ is the number of monomers under load between two neighboring connector points.

Different from Aradian et al.'s model, this polystyrene system has a loosely crosslinked network instead of only free chains present at the interface. The interfacial strength is built by interlinking free chains with the existing polymer network. That is to say, the mobile chains that diffuse across the interface and entangle or react chemically with the polymer network contribute to the interfacial strength. However, because the energy contributed by chain extraction (chain pull-outs due only to physical entanglements with the network) is two orders of magnitude smaller than the energy contributed by chain scission, the interfacial energy G is often dominated by the chemical part:

$$G = G_{scission} + G_{extraction} \cong G_{scission} \qquad \text{(C.3)}$$

In the final state of the slow reaction regime (α<1, defined in deGennes' scaling relationship), the interface is allowed to reach the equilibrium state, and the ideal maximum interfacial energy is equivalent to the tear energy of the bulk after linear polymer chains become fully entangled with the network. For the pre-crosslinked network itself, the number of monomers under tension $\tilde{n}$ is around N_{c0} (the length between pre-crosslinking points) and the region thickness that effectively bridges the interface is $a\sqrt{N_{c0}}$ from the fracture (a is the monomer size). As the number of chains with length N_{c0} is 1/ (N_{c0}·a^3) per unit volume, the total broken connectors per unit area is

$\sigma \cong a\sqrt{N_{c0}} \times \frac{1}{N_{c0}a^3} \cong \frac{1}{\sqrt{N_{c0}}a^2}$. Due to the additional crosslinking contributed by the chemical bonding between linear chains and the polymer network, the effective broken connectors per unit area is increased by a factor of $\frac{N_{c0}}{N_{c-tot}}$ ($N_{\text{c-tot}}$ is the number of monomer units between crosslinks in the final state). Thus, the interfacial energy is:

$$G \cong U_0\left(\frac{1}{\sqrt{N_{c0}}a^2} \times \frac{N_{c0}}{N_{c-tot}}\right)N_{c0} \cong \frac{U_0}{a^2 N_{c-tot}}\left(N_{c0}\right)^{\frac{3}{2}} \qquad \text{(C.4)}$$

VITA

Lili Liu
Ph.D. in Chemistry

Emulsion Polymer Institute (EPI)
Lehigh University

1215A E Marks ST, APT 204
Allentown, PA 18109, USA
Cell Phone: +1 (610) 653-2450
Work Phone: +1 (610) 758-5571
Email: lil206@lehigh.edu

Summary

A hardworking and self-motivated researcher with a combination of background in chemistry and polymer engineering.

Education

Ph.D., Chemistry *May 2011*

Lehigh University, Bethlehem, PA
Dissertation: Aspects of film formation from bimodal latexes

Master of Science, Chemistry *May 2008*

Lehigh University, Bethlehem, PA
Thesis: Functionalization of metal-organic cages
Related courses:

- Advanced inorganic chemistry
- Chemical physics and bonding
- Analytical chemistry
- Instrumental analysis
- Crystallography and diffraction
- Surface chemistry
- Spectral analysis

Bachelor of Science, Polymer Science and Engineering *June 2006*

Zhejiang University, Hangzhou, China
Senior project: The influence of compression to polyelectrolyte multilayers on surface morphology, permeability and environmental responsiveness

Research Experience

Research Assistant, EPI, Lehigh University *August 2008 – May 2011*

Emulsion Polymerization and Latex Film Engineering

- Synthesize and characterize new functionalized styrene monomers, styrene-acrylic copolymers, and investigate chemical reactions between polymers with reactive functional groups.
- Synthesize and characterize polystyrene, functionalized polystyrene latexes with controllable particle size, molecular weight, crosslinking density via various polymerization techniques such as batch, semi-continuous, shot growth polymerizations.
- Study particle packing effect, molecular weight effect and crosslinking effect on film formation designed for bimodal latex particle systems.
- Sinter latex films via home-made vacuum compression molding and evaluate the mechanical properties (such as film strength, modulus and hardness, etc.) of the films after annealing process.

- Develop a model to describe the influence of molecular parameters (such as particle size, molecular weights, distribution of crosslinking density, etc.) on film mechanical properties based on the polystyrene system.
- Apply the model to polymers with low glass transition temperatures for the use of industrial coatings and adhesives.

Research Assistant, Chemistry, Lehigh University *August 2006 - June 2008*

Organic Synthesis of Metal Organic Cages and Functionalized Mesoporous Structure

- Synthesized silano functionalized ethylenediamine and bypyridine terminal ligands.
- Synthesized functionalized palladium nitrate/triflate clusters and cages.
- Self-assembled mesoporous silica frameworks via nonionic and ionic surfactants.

Research Assistant, Polymer Sci. and Eng., Zhejiang University *2003 - 2006*

Self-Assembly of Polyelectrolyte Multilayers (PEMs)

- Made polyelectrolyte multilayer thin films via layer-by-layer self-assembly.
- Loaded and released small dye molecules on compressed PEMs.
- Studied PEMs' responsibility to pH changes.

Teaching Experience

S.T.A.R Academy Summer Camp Science Instructor, Lehigh University *Summer 2010*

- Experiment creating and developing (in charge of every single detail)
- Instruction of science sections for kids aged between 10~13

Teaching Assistant, Chemistry, Lehigh University

General Chemistry *2006 - 2008*

- Assignment and exam grading
- Teaching in lab sections
- Preparation and instruction of student experiments
- Tutoring students

Organic and Advanced Organic Chemistry *Summer 2007*

- Assignment grading and preparation of experiments

Analysis Skills

Highly proficient with the hands-on operation of

AFM	Atomic Force Microscopy	**GPC**	Gel Permeation Chromatography
CHDF	Capillary Hydrodynamic Fractionation	**NMR**	Nuclear Magnetic Resonance
DLS	Dynamic Light Scattering	**SEM**	Scanning Electron Microscopy
DMA	Dynamic Mechanical Analysis	**TEM**	Transmission Electron Microscopy
DSC	Differential Scanning Calorimetry	**UV-Vis**	Ultraviolet-Visible Spectroscopy
FT-IR	Fourier Transform Infrared Spectroscopy	**XRD**	X-Ray Diffraction
GC	Gas Chromatography	**Instron**	
ARES	Advanced Rheometric Expansion System		

Computational Skills

Highly proficient with Excel, Origin, Chemdraw, MestReNova;

Familiar with MathCad, Matlab

Languages

- Mandarin Chinese
- English

Presentations

Annual Review Meeting *2009 - 2011*
Lehigh University, Bethlehem, PA

Advances in Emulsion Polymerization and Latex Technology *2009 & 2010*
Lehigh University, Bethlehem, PA

Chemistry Department Seminar Series *2008 & 2011*
Lehigh University, Bethlehem, PA

Publications

1. **Lili Liu**, Eric Daniels and Andrew Klein*, "Aspects of Film Formation from Bimodal Latexes". Emulsion Polymer Graduate Research Progress Reports, No. 73, July 2009
2. Bo Wang, **Lili Liu**, Ke Chen, Lin Chen, Jie Feng and Changyou Gao*, "Compression-Inhibited Pore Formation of Polyelectrolyte Multilayers Containing Weak Polyanions: A Scanning Force Microscopy Study." Chemphyschem, 2006, 7, 590.
3. Bo Wang, Changyou Gao*, Qinghe Zhao, **Lili Liu**, Kun Han, Junhu Zhang, Zheng Xiang and Bai Yang, "2D Chemically Tunable Patterns with Cellular Structures Fabricated via Thermal Pressing Method", Thin Solid Films, 2006, 500, 180.
4. Bo Wang, Changyou Gao* and **Lili Liu**, "Loading and Release Behaviors of Compressed Poly-electrolyte Multilayers for Small Dye Molecules", J. Phys.Chem. B 2005, 109, 4887.
5. Bo Wang, Tao He, **Lili Liu** and Changyou Gao*, "Poly(ethylene glycol) Micro-Patterns as Environmentally Sensitive Template for Selective or Non-Selective Adsorption", Colloid Surf. B-Biointerfaces, 2005, 46(3), 169.